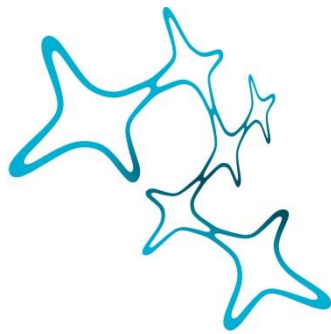

Brain-wide representation and integration of odor and taste in the adult fly

Paul Bandow



Graduate School of
Systemic Neurosciences
LMU Munich



Dissertation at the
Graduate School of Systemic Neurosciences
Ludwig-Maximilians-Universität München

October, 2023

Supervisor

Prof. Dr. Ilona Grunwald Kadow
Institut für Physiologie II
Universität Bonn

First Reviewer: Prof. Dr. Ilona Grunwald Kadow
Second Reviewer: Prof. Dr. Laura Busse
External Reviewer: Prof. Dr. Marion Silies

Date of Submission: 04.10.2023
Date of Defense: 09.02.2024

Abstract

Chemosensation, the sense of smell and taste, is an essential tool for most animals, including humans, for finding and evaluating possible food sources not only with respect to their edibility but also their nutritious value. Hence, odorants and tastants often have intrinsic valence which means that they are perceived as either positive or negative and can cause innate attraction or aversion.

The peripheral perception of these sensory inputs has been studied intensively, yet how these signals are encoded in and interpreted by higher brain centers, is still poorly understood, especially in gustation. How odor and taste signals together are integrated in the brain is even less known. Using in vivo whole brain light field imaging, I reconstructed a three-dimensional image of the adult fruit fly brain (*D. melanogaster*) and investigated how neurons respond to odor and taste of different valence on a global scale. Therefore, I expressed GCaMP, a genetically-encoded calcium indicator, pan-neuronally and recorded the Ca²⁺-dependent changes in fluorescence as a proxy for neuronal activity with high temporal resolution. Since it has been demonstrated that the valence of a stimulus can be modulated by the metabolic state of the animal, I also examined which brain regions are influenced in their responses by starvation.

Thus, I exposed fed and starved flies to different odor and taste substances and analyzed the peak responses in twelve major brain areas. Taste mainly activated the subesophageal zone (SEZ) and odor mainly the superior areas of the brain. Moreover, I found that starvation increases the global response to appetitive odor and in contrast reduces the global response to non-appetitive taste. This suggests that metabolic state modulates olfactory and gustatory circuits in different ways. When pairing a taste with an odor stimulus, both odor and taste regions were activated. I found that pairing an appetitive odor with a bitter taste resulted in higher responses brain-wide, especially in fed flies. This suggests that brain activity during multisensory integration of chemosensory stimuli is influenced by valence information and the

internal state. A principal component analysis on peak responses was able to find components that further subdivide and separate brain regions according to their chemosensory responses and between fed and starved flies. Moreover, peak responses could predict the stimulus modality, valence, and the internal state of the animals, using supervised machine learning classification algorithms. I used independent component analysis to plot spatial maps of functional components, small brain areas or putative single neurons, that show correlated activity with the stimulus. Most out of over 20 components responded specifically to odor and overlapped with anatomical structures of the fly olfactory pathway. One component in the SEZ that was only active during combined odor and taste stimulation overlapped with a set of neurons that connect the antennal lobe with the SEZ and could be involved in multisensory integration.

Graph analysis of the correlated activity among the brain regions showed that changes in the functional network between the rest and the stimulus phase differ between the modalities. During odor presentation, the existing connections are maintained and their weight increases, whereas during taste there seems to be a remapping of connections. The network tends to be the most stable during combined stimulation.

In this work, I was able to show that whole brain imaging can be used to study neuronal activity upon chemosensory stimulation in adult *Drosophila melanogaster*. I found that neural signals were highly region-specific, depending on the sensory modality. Unimodal stimuli of different valence elicited different responses, which were in turn influenced by the internal state of the animal. Furthermore, I discovered that a valence-mismatch of combined odor and taste presentation caused higher global activity. In addition, I found an area in the ventral brain that is only responding during bimodal stimulation. Which neurons reside in this area and if they truly integrate multisensory information into a circuit that is relevant for food search, food choice or food intake remains an open question.

List of abbreviations

AC	Adenylyl cyclase
AgRP	agouti-related peptide
AL	Antennal lobe
ANOVA	Analysis of variance
ATP	Adenosine triphosphate
Benz	Benzaldehyde
BOLD	Blood-oxygenation-level dependent
cAMP	Cyclic adenosine monophosphate
CX	Central complex
EM	Electron microscope
FAFB	Full adult fly brain
GNG	Gnathal ganglia
GRN	Gustatory receptor neurons
GUI	Graphical user interface
ICA	Independent component analysis
INP	Inferior neuropils
KNN	K-nearest neighbor
LDM	Linear discriminant model
LFM	Light field microscope
LH	Lateral horn
LX	Lateral complex
MB	Mushroom body
MRI	Magnetic resonance imaging
NNM	Neural network model
OFC	Orbito-frontal cortex
OL	Optic lobe
ORN	Olfactory receptor neuron
OSN	Olfactory sensory neuron
PCA	Principal component analysis
PENP	Periesophageal neuropils
POMC	pro-opiomelanocortin
Qui	Quinine
ROI	Region of interest
SEZ	Subesophageal zone
SNP	Superior neuropils
Sta	Starved
Suc	Sucrose
TRC	Taste receptor cell
Vin	Vinegar
VLNP	Ventrolateral neuropils
VMNP	Ventromedial neuropils

List of figures

Figure 1	Mammalian chemosensory organs	13
Figure 2	The chemosensory system of <i>Drosophila melanogaster</i>	18
Figure 3	Molecular mechanisms behind genetically encoded calcium indicators	23
Figure 4	Illustration of light field microscopy setup	24
Figure 5	Whole-brain light field imaging of chemosensory responses	35
Figure 6	Average unimodal response towards the first stimulation	38
Figure 7	Average multisensory response towards the first stimulation	39
Figure 8	Whole brain median responses for three repeated stimulations	40
Figure 9	Standardized peak responses	41
Figure 10	Peak responses to chemosensory stimulation mapped onto neuropil supercategories	43
Figure 11	Direct comparison of peak responses per region and whole brain response	45
Figure 12	Principal component analysis for peak responses of all groups	53
Figure 13	Principal component analysis for peak responses of odor groups	54
Figure 14	Principal component analysis for peak responses of taste groups	55
Figure 15	Principal component analysis for peak responses of multisensory groups	56
Figure 16	Principal component analysis for peak responses of all groups with the brain regions as variables	57
Figure 17	Linear discriminant classification model predicts stimulus type	61
Figure 18	Neural network classification model predicts stimulus type	62
Figure 19	Classification models predicting valence and internal state	63
Figure 20	Classification models predicting the stimulus substance	64
Figure 21	Neural network classification model predicts internal state and valence from odor data	66
Figure 22	Neural network classification model predicts internal state and valence from taste data	67
Figure 23	Neural network classification model predicts internal state and valence from multisensory data	68
Figure 24	Linear discriminant classification model fails to predict internal state from multisensory datasets	70
Figure 25	Neural network classification model predicts valence from multisensory data sets	71
Figure 26	Functional component frequency and peak response	76

Figure 27	Most relevant functional components derived from ICA	77
Figure 28	Neurons and expression pattern with similarity to GNG (paired)	79
Figure 29	Brain-wide correlation during resting phase	83
Figure 30	Brain-wide correlation during stimulus phase	84
Figure 31	Correlation ratio and connectivity change between rest and stimulus phase	85

List of tables

Table 1	Fly strains, reagents and software	25
Table 2	Tastants and odorants used for chemosensory stimulation	28
Table 3	Classification model parameters	31
Table 4	Results for 3-way ANOVA on odor responses	47
Table 5	Results for 3-way ANOVA on taste responses	47
Table 6	Results for 3-way ANOVA on multisensory responses in fed flies	48
Table 7	Results for 3-way ANOVA on multisensory responses in starved flies	48
Table 8	Ordinary 1-way ANOVA Whole Brain Median for multisensory stimulation (Fed). $F=7.57$, $p=0.0001$, $R^2=0.37$	50
Table 9	Ordinary 1-way ANOVA Whole Brain Median for multisensory stimulation (Starved). $F=4.76$, $p=0.01$, $R^2=0.28$	50
Table 10	Classification model accuracy in percent	60
Table 11	Classification model total cost	60
Table 12	Classification model accuracy for predicting stimulus type from different datasets in percent	60
Table 13	Accuracy for the best classification models (responses from OL, VLNP, VMNP and LX excluded)	65
Table 14	Accuracy for LD and NN classification models predicting internal state in percent (models include responses from all regions)	65
Table 15	Accuracy for LD and NN classification models predicting valence in percent (models include responses from all regions)	69
Table 16	Finding neural correlates for GNG (paired) component	78

Contents

Abstract	2
List of abbreviations	4
List of figures	5
List of tables	6
Introduction	9
The chemical senses	9
The insect as a model organism	14
The fly’s olfactory system	14
The fly’s gustatory system	16
The influence of the metabolic state	19
Whole brain calcium imaging	21
Aims and hypotheses	23
Material and methods	25
Fly husbandry	25
Fly preparation and light field calcium imaging	25
Experimental paradigm	27
Image processing	29
Statistics	29
Principal component analysis	30
Classification models	31
Functional Component Analysis	32
Graph Analysis	32
Results	34
Chemosensory stimulation activates different areas of the brain depending on the modality	34
Valence and metabolic state influence chemosensory responses	44
Principal component analysis separates between brain regions and internal state	51
Classification models can accurately predict the stimulus type from peak responses	58
Chemosensory-specific functional components can be obtained from spatial ICA	72
Comparing global brain connectivity during resting and stimulus phase	80
Discussion	86
Global effect of metabolic state	87
Finding candidate neurons	88
Localizing sites of chemosensory integration	90

Inferring functional connectivity	92
The dichotomous view of odor and taste	94
Valence of chemosensory cues	95
Specificity and resolution of whole brain imaging	98
Pros and cons of light field microscopy	99
Establishing the experimental protocol	101
Conclusion and outlook	104
Publication bibliography	106
Appendix	120
List of appendix figures	121
List of appendix tables	175
Curriculum vitae	189
List of publications	190
Declaration of author contributions	191

Introduction

The chemical senses

In order to perceive the outside world and to navigate within their environment, animals have evolved a diversity of sensory systems. Two of the most common senses are smell and taste, which can be categorized as chemical senses and therefore are sometimes summarized under the term chemosensation. They have the function of detecting a wide array of volatile or soluble molecules. Recognition of these molecules is crucial for finding and evaluating food, avoiding danger and toxic substances, or facilitating reproductive behavior. This is mediated via chemosensory receptors, which make up the most widespread and diverse receptor family among the animal kingdom and can even be found in bacteria (Nei et al. 2008).

In terrestrial mammals, air-borne chemicals are recognized by odorant receptors. They are G-protein coupled receptors with highly variable transmembrane domains, which are encoded by a large number of genes (~1100 in the mouse and ~400 in humans; Barnum and Hong 2022) and serve as the binding site for the large variety of existing odorants (Mombaerts 1999). Notably, the odorant receptors are not selective for a single molecule but rather a range of ligands with common structural features. This enables the olfactory system to recognize thousands of compounds (Araneda et al. 2000). Upon binding of the odor molecule, often short-chained or cyclic carbohydrates, the transmembrane domains undergo a conformational shift, which activates the G-protein on the intracellular side (Fleischer et al. 2009). This protein activates adenylyl cyclase (AC) which catalyzes the transformation from ATP to cyclic AMP that acts as a second messenger by opening non-selective cation channels (Breer et al. 1990). In turn, the chemosensory neuron which houses the odorant receptor undergoes a change in membrane potential. The depolarization is increased by the subsequent opening of Ca^{2+} -activated chloride channels (Kleene 2008). When a certain voltage threshold is reached, one or multiple action potentials are generated which travel along the neuron's axon. Hereby the

chemical information is transduced and transmitted as electrical information from the periphery to the central nervous system.

In mammals, these olfactory sensory neurons (OSNs) can be found in the olfactory epithelium in the nose, where their apical part, which is covered with tiny cilia, extends into the mucus within the nasal cavity (Figure 1 A). Their axons terminate in the olfactory bulb, where they are organized into spatial subunits, called glomeruli. One glomerulus only contains axons from those OSNs which express the same odorant receptor (Murthy 2011). This creates a stereotyped sensory map of the odor environment. The OSN axons directly synapse onto second order neurons, called mitral cells which project to the olfactory tubercle, the entorhinal cortex and the primary olfactory (piriform) cortex which includes the anterior olfactory nucleus (Binder 2009). The neurons in the piriform cortex encode for the intensity and identity of odors (Rolls 2019).

In addition, some mammals also possess the so-called vomeronasal organ (VNO), which is located in the skull, above the oral cavity. It is innervated by two types of sensory neurons, which project to accessory olfactory bulb, from where the information is transmitted to the hypothalamus. The sensory neurons express either one of two vomeronasal type receptors (V1R, V2R) that also are G-protein coupled. The VNOs main function is detecting pheromones and thereby contributing to reproductive behaviors (Døving and Trotier 1998). However, its existence and function in humans is still debated (Stoyanov et al. 2018).

When we talk about smell we usually think of what is called orthonasal olfaction, which occurs during inhalation. However, there is also retronasal olfaction which typically happens during chewing and after swallowing (Buettner et al. 2001; Burdach and Doty 1987). This pathway strongly contributes to our perception of flavors and highlights the connection of food consumption and odor perception (Rozin 1982; Shepherd 2004). It was shown that retronasal odor delivery elicits differential neural responses than orthonasal delivery in humans (Small et al. 2005). Furthermore, rodents require the taste cortex for processing of retronasal information during olfactory learning (Blankenship et al. 2019).

The gustatory system primarily distinguishes between five major tastes: sweet, salty, bitter, sour and umami. The sensation of sweetness is detected by two heterodimeric G-protein coupled receptors (T1R2, T1R3; Nelson et al. 2001). Natural sugars, like sucrose bind to the receptor, which then triggers cAMP increase via AC that activates the protein kinase A, which then inhibits a potassium channel and causes depolarization of the cell. Upon binding of non-caloric sweeteners, like aspartame, a phospholipase C on the intracellular side is activated that mediates the release of Ca^{2+} ions from the endoplasmic reticulum into the cytoplasm via inositol-3-phosphate. Ca^{2+} activates the TRPM5 sodium ion channel leading to depolarization of the cell (Molitor et al. 2021). The same pathway is also involved in the detection of bitter compounds by T2R receptors that exist in over 30 variations and the sensation of umami taste. Umami is a Japanese word that translates to “savory” and is for example used to describe the taste of chicken broth, mushrooms or ripe tomatoes, all of which contain high amounts of glutamate that functions as a ligand for the T1R1/T1R3 heterodimer (Kinnamon 2009). Sour taste is evoked by low pH when protons are conducted into the cell by the OTO1 channel. The positive charged ions can alone depolarize the cell, however also acidification of the cytoplasm can cause a blockade of the potassium channel KIR2.1, causing an increase in membrane potential (Liman and Kinnamon 2021). Salty taste is evidence for the presence of sodium chloride. Na^+ ions enter the taste cells through ENaC channels, causing depolarization and generation of action potentials. This results in CALHM1/3-mediated ATP release and activation of the afferent nerve fiber (Liman 2020).

The salt-sensitive taste cells belong to the type III taste receptor cells (TRCs), together with the ones that detect acid. Type II TRCs are sensitive to sweet, bitter or umami ligands. At least fifty or more taste receptor cells from type II and III are grouped together in a taste bud. They are supported by the glia-like type I cells (Finger 2005). The apical end of the TRCs are located at the taste pore, a small well-like structure within the epithelium of the tongue (Figure 1 B). The taste buds can be found within the so-called papillae, which come in different shapes and sizes. Circumvallate papillae are found at the very back of the tongue. Foliate papillae are

present at the posterior lateral edge of the tongue, whereas fungiform papillae are found in the anterior two-thirds (Chandrashekar et al. 2006). Recently, “fatty” has emerged as a sixth taste, signaling an energy-rich food source. A current working model suggests that fatty acids mediate depolarization of type II TRCs via the CD36 receptor and the DRK channel, leading to the release of ATP (Besnard et al. 2016). All TRCs are secondary sensory cells, this means that they synapse onto neurons that relay the information from the tongue to the brain via the facial and glossopharyngeal nerve. At the nucleus solitarius they connect with secondary fibers that ascend to the thalamus. From here, third-order neurons travel to the primary taste cortex, consisting of the frontal operculum and the anterior insula (Gibbons and Sadiq 2023). The neurons in this region encode for the identity and intensity of taste, as well the texture and temperature of an oral stimulus (Rolls 2019). In contrast, the sensation of spiciness is mediated by the heat-sensitive ion channel TRPV1, which is also activated by the alkaloid capsaicin that can be found in red peppers. The trigeminal nerve relays the information to the brain and causes a burning, pain-like feeling (Caterina et al. 1997; Bevan and Szolcsányi 1990).

While the peripheral coding of odor and taste stimuli is relatively well described, there is still ongoing research how these sensory cues are integrated in the central brain and used to direct behavior. The orbitofrontal cortex (OFC) is thought to be the secondary chemosensory cortex, since it receives gustatory and olfactory information and therefore might be responsible for the perception of flavors, which depends on multiple sensory inputs (Spence 2015). Neural activity in this area was found to correlate with reward value and pleasantness or unpleasantness of tastes and odors. In addition, the neural activity towards chemosensory stimuli is reduced when the subjects were fed to satiety. Hence the OFC might also be involved in influencing feeding decisions based on nutrient needs (Rolls 2019). Odor and taste projections also innervate the amygdala, which has been shown to be involved in reward- and motivation-related learning, as well as taste-odor conditioning. Therefore, it is believed to be important for storage of flavor memory (Miranda 2012).

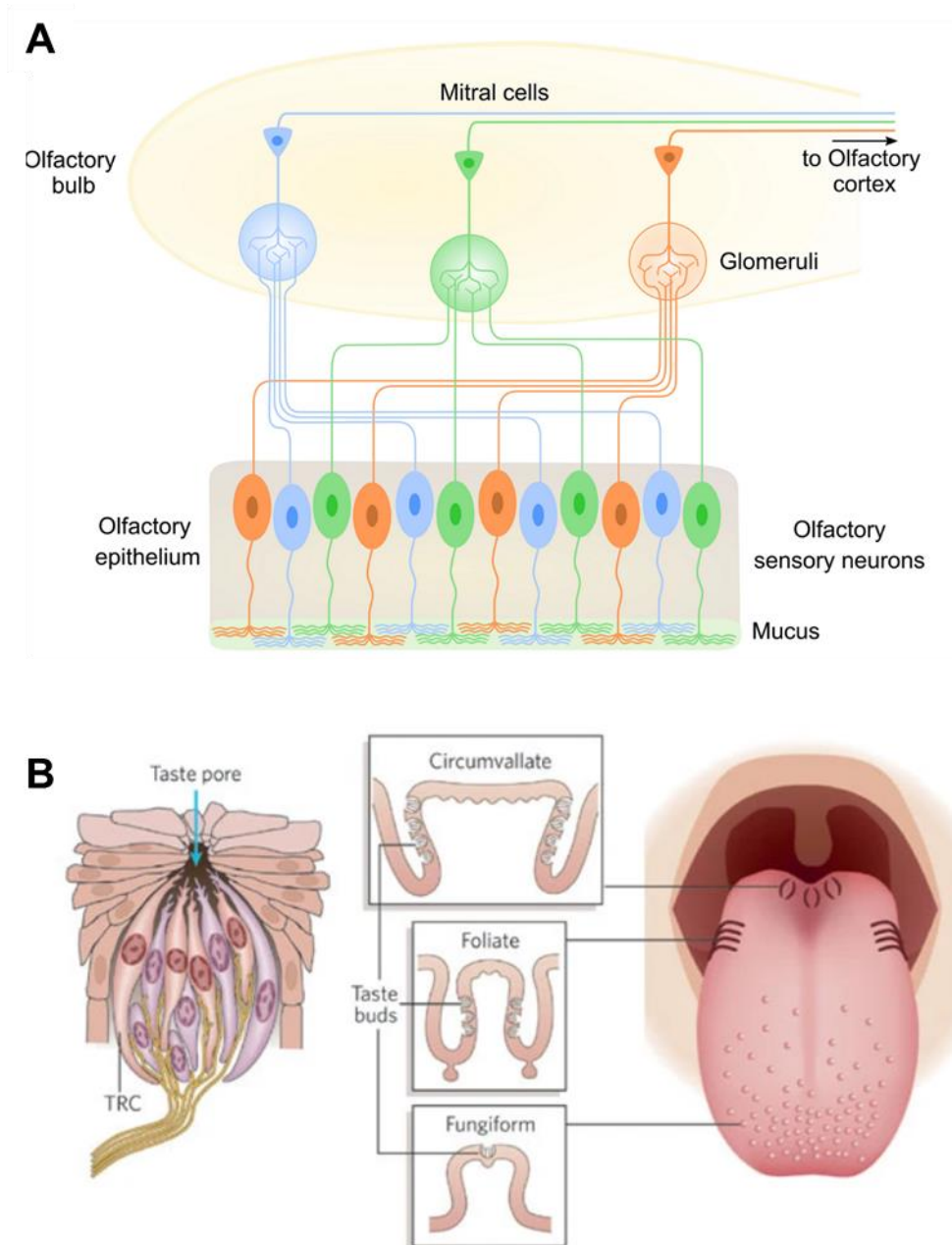


Figure 1: Mammalian chemosensory organs

A Functional organization of the peripheral olfactory system. The olfactory epithelium contains the bipolar olfactory sensory neurons (OSNs), which extends their dendrites into the mucus. The OSNs that express the same olfactory receptor project their axons to the same glomerulus in in the olfactory bulb (schematically shown by the color code). Here they synapse onto the mitral cells which relay the information to the olfactory cortex. (Boccaccio et al. 2021) © Cell and Tissue Research, licensed via Copyright Clearance Center Inc., 25.08.2023, order number 5615780926399) **B** Functional organization of the peripheral gustatory system. The taste buds (left) contain 50-150 taste receptor cells (TRCs) which extend their apical part into the taste pore. Taste buds can be found in different types of taste papillae (middle), distributed across the tongue (right). The large circumvallate papillae are found at the very back, while the foliate papillae are present at the posterior lateral edge. The small fungiform papillae are found in the anterior two-thirds of the tongue. (Chandrashekar et al. 2006) © Nature, licensed via Copyright Clearance Center Inc., 25.08.2023, order number 5615790588666)

The insect as a model organism

In order to investigate fundamental biological principles on a smaller scale, scientists have turned to invertebrates more than hundred years ago. The fruit fly *Drosophila melanogaster* is a commonly used model organism and has already led to groundbreaking discoveries in genetics and embryogenesis (T. H. Morgan et al. 1915; St Johnston and Nüsslein-Volhard 1992). Since then, it has been studied extensively, with the advantage that it is relatively easy and inexpensive to breed and produces a lot of offspring within a short generation time. Its genome was sequenced in the year 2000 (Adams et al. 2000) and over the years an ever-growing genetic toolset has been developed. One of the most commonly used genetic tools is the GAL4/UAS system (Brand and Perrimon 1993). It uses the gene for the galactose-responsive transcription factor (GAL4), which is inserted into the genome, downstream of a tissue-specific genomic enhancer. The GAL4 protein will bind to the upstream activating sequence (UAS), which functions as a promoter of the target gene (Figure 3 A). Hence, the respective gene will only be expressed in the designated cells. This has been particularly useful for investigating neuronal circuits because it allows to target specific subsets or even individual neurons, manipulate their function to influence behavior or record their activity in vivo. The brain of adult *Drosophila* only contains about 130.000 neurons and its anatomy is well-described (Ito et al. 2014). Very recently a full connectome has been published as a preprint, containing the wiring diagram of the entire brain at synaptic resolution which can help to understand the network of the brain on a global scale (Dorkenwald et al. 2023).

The fly's olfactory system

Over a century ago, it was first described that *Drosophila* flies detect and respond to odorants (Barrows 1907). It took a number of decades until the responsible receptors were found, which can be divided into two main classes: odorant receptors (ORs, Clyne et al. 1999) and ionotropic receptors (IRs, Benton et al. 2009). Unlike vertebrate olfactory receptors, they function as odorant-gated ion channels (Wicher et al. 2008; Sato et al. 2008). The seven-

transmembrane-structure of ORs assembles into two types of subunits. One is the highly conserved odorant receptor coreceptor (ORCO) and the other functions as “tuning receptor” and is highly variable, allowing for the structural diversity needed, to bind a large number of odor molecules. There are 60 genes that encode for OR proteins (Robertson et al. 2003). The IRs have evolved from ionotropic glutamate receptors and are encoded by 66 genes. Out of those, four likely act as co-receptors (IR25, IR8a, IR76b and IR93a) together with one of the other ligand-specific IRs to form a functional complex (Abuin et al. 2011).

In most cases, olfactory receptor neurons (ORNs) express only one olfactory receptor type. About 2-4 ORNs are located on tiny hairs that cover the antennae (and the maxillary palps, Figure 2 A, B), called sensilla (Vosshall and Stocker 2007). According to their morphology, the sensilla are grouped into four main classes: basiconic, trichoid, intermediate and coeloconic. The sensilla have pores in the cuticle that allow the diffusion of odorant molecules into the lymph, where they come into contact with the dendrites of the ORNs with the help of odorant binding proteins (Shanbhag et al. 1999; Shanbhag et al. 2001). On either side, about 1200 ORNs send axons to the brain via the antennal nerve and terminate in the antennal lobe (AL, Figure 2 C). Each ORN expresses only one out of 62 types of ORs (Robertson et al. 2003). All ORNs that express the same receptor converge in the same glomerulus in the AL (Couto et al. 2005). Over 40 glomeruli form a stereotyped spatial map of the OR repertoire in the AL. This organization has developed analogously to the vertebrate system (Barnum and Hong 2022). The glomeruli are activated in distinct patterns according to the presented odor (Fishilevich and Vosshall 2005). At the glomeruli, the ORNs synapse onto about 150 projection neurons (PNs, analogs to the vertebrate mitral cells), which extend their axons to the lateral horn (LH). Hereby, they pass the mushroom body (MB) calyx, where they form en-passant synapses with the dendrites of the MB Kenyon cells (KCs, Tanaka et al. 2004). All KCs (~2000) extend their axons through the peduncle to form the three characteristically shaped MB lobes. Twenty-one types of MB output neurons (MBONs) form dendritic arbors in specific areas of the lobes, segregating the MB into different compartments. Each compartment is almost

exclusively innervated by one specific type of dopaminergic neurons, which come from two clusters (PAM and PPL1) and convey information about punishment and reward. This enables the MB to function as a center for olfactory learning and memory (Aso et al. 2014a; Aso and Rubin 2016). The LH contains about 1400 neurons (LHNs), 40 percent of which are local neurons (LHLNs) and the remaining are output neurons (LHONs). The LHNs receive stereotyped input from the PNs and show stereotyped responses to certain odors (Frechter et al. 2019; Dolan et al. 2019). Therefore, the LH is thought to mediate innate odor responses although this strict distinction has been questioned over the last years with studies suggesting that the MB is involved in mediating innate attraction and aversion (Bräcker et al. 2013; Lewis et al. 2015). Conversely, the LH was shown to be involved in olfactory memory formation and more recent data even suggests neuronal plasticity in LH neurons upon learning (Dolan et al. 2018; Das Chakraborty et al. 2022). LHONs and MBONs both converge in the superior lateral protocerebrum (SLP) and the neighboring neuropils, which are believed to represent a third-order olfactory center. There are also further connections between the MB and the LH, which suggest a more complex form of functional interaction (Das Chakraborty and Sachse 2021).

The fly's gustatory system

Even though, flies can distinguish between similar taste qualities as humans, they use a different set of receptors. The majority belong to the protein superfamily of gustatory receptors (GRs), which has 68 members and is related to the *Drosophila* OR family (Scott et al. 2001). Most of those ligand-gated ion channels are sensitive to bitter substances. Five of them (Gr32a, Gr33a, Gr66a, Gr89a and Gr39a) have been suggested as the most important and might function as obligatory co-receptors, similar to ORCO in the olfactory transduction (Weiss et al. 2011). The main sweet receptors are Gr5a, Gr64a, and Gr64f (Dahanukar et al. 2007; Jiao et al. 2008). Gr5a is needed for detecting trehalose, while Gr64a is activated by sucrose and maltose. Gr64f might function as a co-receptor, since it is required for the response to all tested sugars except fructose, which is only detected by Gr43a (Miyamoto et al. 2012).

Although most of the IRs are only expressed in the antennae, some are also present in taste tissue. One of them, IR76b, has been implicated in salt detection, polyamine and amino acid sensing (Zhang et al. 2013; Hussain et al. 2016b; Ganguly et al. 2017). In addition, IR64a which is however expressed in OSNs is responsible for acid sensing (Ai et al. 2010). Furthermore, flies can taste water via a specialized channel called PPK28 (Cameron et al. 2010) and electrophiles like allylisothiocyanate (found in wasabi) with the help of dTRPA1 (Kang et al. 2011).

Drosophila gustatory receptor neurons (GRNs) can express multiple types of gustatory receptors. Hereby, a particular cell is usually sensitive to either aversive or appetitive stimuli. For example, one GRN that can be activated by sugars or low salt, would promote feeding, whereas a GRN that is activated by different bitter compounds inhibits feeding (Wang et al. 2004; Thorne et al. 2004). The GRNs are located in the taste bristles, which can be found on the proboscis, the legs and the wing margins (Figure 2 A). Female flies even have some on the vaginal plate, which are probably relevant during egg-laying (Stocker 1994). The tips of the proboscis, called labella, each contain 31 taste bristles, which house 2-4 GRNs, as well as 30 taste pegs with one GRN each (Vosshall and Stocker 2007). Additionally, the pharynx has three internal taste organs (LSO, VCSO, DCSO), which contain a low number of taste sensilla, that likely help the fly evaluate the food, after it has been swallowed (Nayak and Singh 1983; Gendre et al. 2004; Chen et al. 2019b). The axons of the GRNs from all body parts project to the subesophageal zone (SEZ, Figure 2 C), where they connect to motor neurons that drive feeding responses via local circuits (Shiu et al. 2022; Miyazaki and Ito 2010). Arborization of GRNs in the SEZ shows segregation based on the two main taste categories (bitter and sweet), which translates into a functional map (Engert et al. 2022; Harris et al. 2015; Marella et al. 2006). There is only little evidence of secondary taste projections. Three neurons are known to transmit taste signals to higher brain centers and the ventral nerve cord. They have been found to influence a stereotyped feeding behavior, called proboscis extension reflex (PER; Dethier 1976) and being essential for conditioned taste aversion by acting

upstream of the MB (Kim et al. 2017a). Another neuron relays taste information from sweet GRNs to the antennal mechanosensory and motor center (AMMC, Kain and Dahanukar 2015). Whether other areas of the fly brain are involved in taste processing remains unknown.

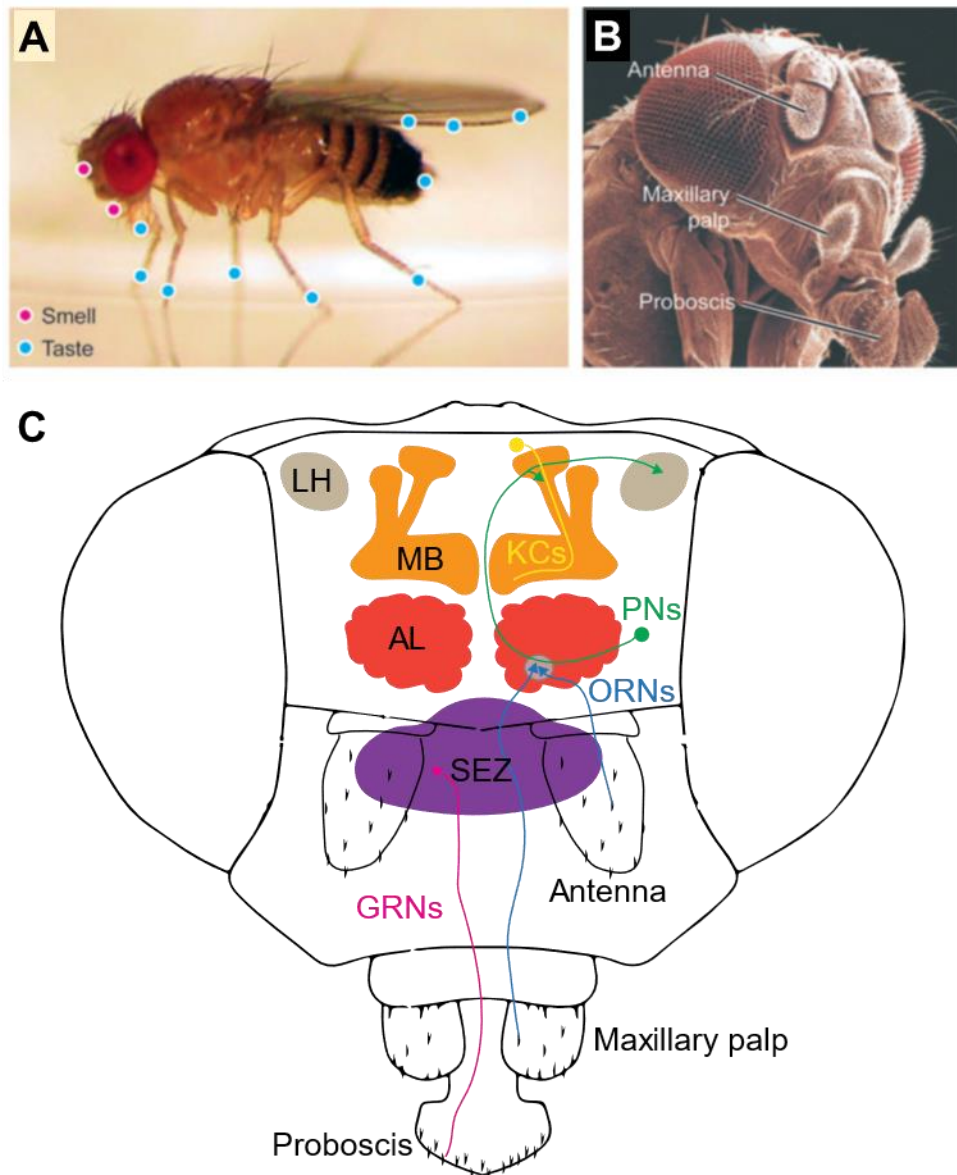


Figure 2: The chemosensory system of *Drosophila melanogaster*

A Schematic indicating the position of the olfactory (pink) and gustatory (blue) neurons on the body of the fly. **B** Scanning electron micrograph of a fly head, indicating the major chemosensory organs. SEM image courtesy of J. Berger, MPI-Developmental Biology, Tübingen. (Vosshall and Stocker, © 2007 Annual Reviews, licensed via Copyright Clearance Center, Inc, 17.07.2023, order number 1376227). **C** Illustration of the chemosensory pathways. Gustatory receptor neurons (GRNs, pink), project from the tip of the proboscis to the subesophageal zone (SEZ, purple). Olfactory receptor neurons (ORNs, blue) project from the maxillary palps and the antenna to the antennal lobe (AL, red). At the level of the glomerulus (grey), they synapse onto olfactory projection neurons (PNs, green) which project to the lateral horn (LH, beige). On the way they form en-passant synapses with the Kenyon cells (KCs, yellow) at the level of the mushroom body (MB, orange).

The influence of the metabolic state

Animals need a supply of nutrients and energy in order to survive and reproduce. In the past it has been discussed whether blood glucose levels or signals released by fat tissue control feeding behavior. It was believed that two major hormones, insulin and leptin, regulate food intake by influencing neural signaling in the hypothalamus (Niswender and Schwartz 2003; Elmquist et al. 1999). In recent years, other evidence has been gathered that is challenging this theory (Levitsky et al. 2022). Nevertheless, the hypothalamus is crucially involved in regulating feeding behavior, receiving afferent inputs about mechanical and chemical stimuli from the gastrointestinal tract via the vagal nerve (Schwartz 2000). Two populations of neurons in the hypothalamus (AgRP and POMC) have been found to either drive or inhibit feeding in rodents (Aponte et al. 2011). Sensory detection of food inhibits AgRP neurons and activates POMC neurons (Chen et al. 2015). Although this occurs before any food is ingested, AgRP neurons still drive feeding by positive reinforcement through food reward and modulation by neuropeptide Y (Chen et al. 2016; Chen et al. 2019a). AgRP neurons innervate the insular cortex, which regulates attention towards relevant sensory cues based on the physiological state (Livneh et al. 2017; Livneh et al. 2020). The insular cortex is involved in the hedonic aspects of food. It responds to food cues of different modalities, encodes for reward and is believed to be involved in eating disorders (Frank et al. 2013).

The sensation of odorants and tastants is often linked with food searching or food intake. Hungry mice can use their sense of smell to find buried food pellets (Machado et al. 2018). Many food-related chemical cues have intrinsic valence. Appetitive substances are perceived as positive, whereas non-appetitive or noxious substances have negative valence. The olfactory tubercle in the ventral striatum has been reported to encode for odor valence in behaving mice (Gadziola et al. 2015). In humans, odor valence perception is associated with activity in the olfactory bulb. Negative odors are linked to neural responses in the motor cortex that correlate with avoidance behavior (Iravani et al. 2021). Another study found that the olfactory sensitivity was increased in hungry individuals, as compared to satiated ones.

Furthermore, subjects with low blood sugar levels showed increased sensitivity towards sweet, sour and salty taste but decreased sensitivity to bitter substances (Hanci and Altun 2016). A similar pattern in hunger-dependent taste modification in mice was found to be regulated by AgRP neurons. They connect with glutamatergic neurons in the lateral hypothalamus which innervate the lateral septum and lateral habenula. This down-stream pathways regulate the modulation between appetitive and aversive taste, respectively (Fu et al. 2019).

Drosophila melanogaster flies are attracted to vinegar odor because it represents a cue for fermenting fruit, their main food source (Budick and Dickinson 2006; Zhu et al. 2003). On the other hand, flies are repulsed by elevated levels of CO₂ (Suh et al. 2004). Further research has shown that the responses towards chemosensory stimuli are modulated by the metabolic state of the fly. This is regulated by internal nutrient sensors and a number of different neuropeptides (Lin et al. 2019). For example, satiated flies avoid high concentrations of vinegar, which they no longer do, when they are deprived of food (Simmelhack and Wang 2009). This behavior can be attributed to the activity of specific glomeruli in the AL that in turn are influenced by two neuromodulators, short neuropeptide F (sNPF) and tachykinin (DTK, (Root et al. 2011; Ko et al. 2015). Notably, both sNPF and DTK expression levels are regulated by insulin signaling. Starved flies also overcome their aversion of carbon dioxide in the presence of vinegar odor (Bräcker et al. 2013). This context-dependent switch requires a dopamine-gated shift of activity in the underlying MB circuits (Lewis et al. 2015). The gustatory receptor Gr43a, which is also expressed in the gut and the central brain has been found to act as internal nutrient sensor by detecting changes in hemolymph fructose levels (Miyamoto et al. 2012). Hungry flies also show increased sensitivity to sweet taste but decreased sensitivity towards bitter substances (Inagaki et al. 2014). The release of the adipokinetic hormone (insect analogue of glucagon) inhibits the activity of bitter-sensing GRNs via sNPF and GABAergic cells, while NPF activates a dopaminergic neuron in the SEZ, which increases the activity of sugar-sensing neurons and causes increase in PER (Marella et al. 2012).

Similarly, starved flies begin to like acetic acid taste, which they normally avoid, when they are fed (Devineni et al. 2019). Here, both sugar- and bitter-sensitive neurons are involved and the balance between the two pathways seems to shift the behavioral response. In mammals, the orbitofrontal cortex, is thought to integrate signals of hunger and reward while receiving olfactory and gustatory input (Rolls 2012). Nonetheless, the sensory interaction of odor and taste has been understudied, although we know that both senses together form our perception of flavor (Spence 2015; Small and Prescott 2005). Evidence of such chemosensory integration in the fly is scarce. One study has found that yeast odor can enhance the appetitive response to sugar stimulation but the neurophysiological mechanism behind this, remains unknown (Oh et al. 2021).

Whole brain calcium imaging

To understand physiological processes in the brain it is important to monitor the activity of neurons in vivo. This can be achieved, with the help of calcium-sensitive fluorescent proteins. One of the most common is GCaMP, a genetically encoded calcium indicator (Tian et al. 2009). This molecule consists of a green fluorescent protein (GFP) that is circularly permuted and fused with two other peptides: calmodulin which functions as a calcium-binding domain and M13 (Figure 3 B). During depolarization, neurons exhibit a temporary Ca^{2+} ion influx (Baker et al. 1971; Tank et al. 1988). The ions bind to the GCaMP which undergoes a conformational change that results in an increase of green fluorescence (Akerboom et al. 2009; Wang et al. 2008). This ultimately means that firing neurons appear brighter, when viewed under a microscope that uses blue light to excite the GFP fluorophore. Recording the changes in light emission over time can be used to quantify neuronal activity under the given conditions.

Calcium imaging has been used for years to study the activity of neurons in *Drosophila*. While most work was focused on particular region of interest or small neuronal subpopulations, one recent study recorded spontaneous whole-brain activity to reveal intrinsic functional networks

in resting flies. Among other things, they found that functional connectivity is strong among regions of the olfactory pathway, even in the absence of odor input (Mann et al. 2017).

Light field microscopy (LFM) is a technique that can be utilized to record calcium activity in large samples with high temporal resolution. It uses a wide-field, epifluorescence setup, where the blue excitation light is delivered through the same objective that is capturing the green fluorescence and magnifying the sample. An optic filter separates the two channels. However, a microlens array is positioned at the image plane of the objective and the sensor of digital camera that is recording the scene is moved to the image plane of the array (Aimon et al. 2019; Levoy et al. 2006). The image information received from the microlens array allows to reconstruct a three-dimensional image from all light rays that are emitted by the specimen, even if they come from outside of the focal plane, using deconvolution (Broxton et al. 2013). It means that a volumetric image of the entire fly brain can be obtained from a single snapshot, which limits the temporal resolution for recording Ca^{2+} transients only to the acquisition speed of the microscope camera. Modern high-end scientific cameras can record with over 100 frames per second, which makes this approach faster than other, more common methods, which are based on recording the depth of the sample plane by plane.

This method has already been used to investigate global brain activity during behavior (Aimon et al. 2019). Here it was shown that whole brain activity was increased when the flies were walking compared to when they were grooming. Furthermore, they found different patterns of activation across the brain when the flies were stimulated with odor puffs in comparison with light flashes. A subsequent study showed that excitatory and inhibitory neurons were recruited during walking as well as neuromodulatory neurons that express dopamine or octopamine (Aimon et al. 2023). In contrast, serotonergic neurons were inhibited during walking.

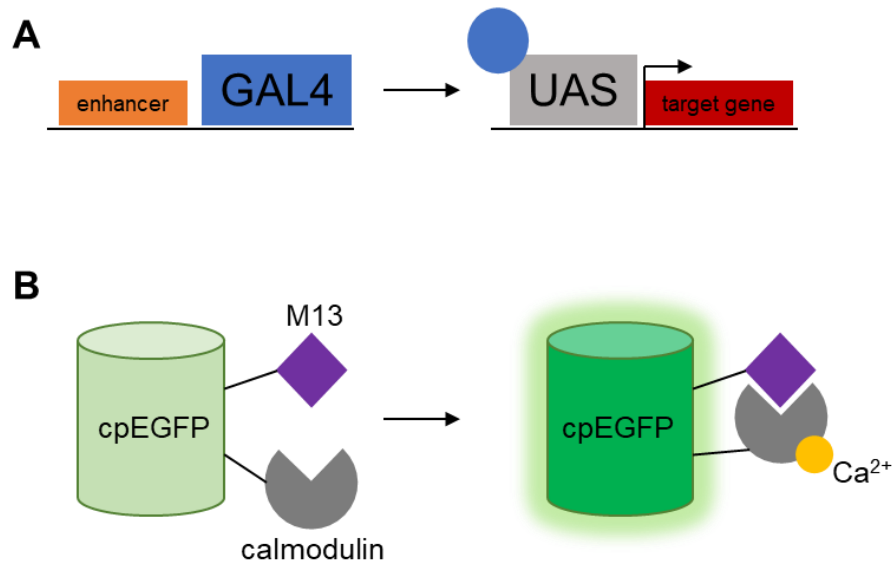


Figure 3: Molecular mechanisms behind genetically encoded calcium indicators

A Illustration of GAL4/UAS system. The GAL4 gene (blue) is expressed by activation of a tissue-specific genomic enhancer (orange). The GAL4 protein binds to the UAS promoter sequence (grey) and leads to expression of the target gene (red). **B** Illustration of GCaMP fluorescence change. GCaMP consists of a circularly permuted cpEGFP protein (green), fused to a calmodulin domain (grey) and the M13 peptide (purple). When calmodulin binds Ca^{2+} ions (yellow) it wraps around M13 which stabilizes cpEGFP in an ionized and highly fluorescent state.

Aims and hypotheses

The processes of chemosensation on a molecular level are relatively well understood. We also understand how identity of chemical cues is represented in the neural architecture of primary sensory centers. There is even increasing evidence on the function of sensory learning and memory, how reward and punishment are encoded and even how this can be modulated by internal state of the animal. However, most of these studies focus on a very narrow population of cells, sometimes neglecting the dense network of neurons that they are embedded in. In this study, I aimed to unravel how the central nervous system as a complex unit integrates gustatory and olfactory signals. To that end, I recorded the calcium activity of the whole brain upon chemosensory stimulation in the model organism *Drosophila melanogaster* with light field microscopy.

I was interested in where the brain processes odor and taste information. I hypothesized that the activity between the two modalities would diverge on the level of the primary sensory

areas. Odor would activate the AL, whereas taste would activate the SEZ. In addition, I expected responses in the MB and the LH towards odor cues, which are known secondary olfactory centers. Also, I hypothesized there would be some convergence between odor and taste responses in superior brain areas, as they also receive some taste projections (Kim et al. 2017a). I was hoping to discover taste-evoked activity in areas that were previously not indicated but might function as secondary taste centers.

Odors and tastes can be inherently attractive or aversive since they often signal the presence of nutritious or harmful substances. I wanted to know if valence is represented in specific areas of the brain or encoded in different levels of activity. So, I used different attractive and aversive cues to compare the responses.

Furthermore, I wanted to investigate how the presentation of two cues at the same time is integrated in the central brain. Therefore, I combined olfactory and gustatory stimulation, to see whether the activity would show an overlap of the unimodal responses or if some areas show more signal, which would implicate them as regions of multisensory integration. I was also curious if there would be an effect by pairing substances of matching or opposing valence, to see how the brain deals with conflicting sensory information.

Since odor and taste are closely linked with feeding behaviors, I asked whether changes in the metabolic state would modulate neuronal activity during chemosensory processing and whether fed flies show a different brain activity than starved flies. Therefore, I tested satiated, as well as food deprived flies under the same paradigm. I hypothesized that the response to cues of different valence, which normally lead to opposing behavior, would be modulated by starvation.

Material and methods

Table 1: Fly strains, reagents and software

Experimental organisms		
Strain	Source	Stock Number
<i>D.mel/UAS-jGCaMP7s</i>	Bloomington DSC	BDSC_79032
<i>D.mel/nSyb-GAL4</i>	Bloomington DSC	BDSC_51635
Chemicals		
Name	Formula	Product/Manufacturer
Sucrose	C ₁₂ H ₂₂ O ₁₁	PanReac AppliChem
Quinine	C ₂₀ H ₂₄ N ₂ O ₂	Sigma-Aldrich
Benzaldehyde	C ₇ H ₆ O	Sigma-Aldrich
Water	H ₂ O	Ampuwa/Fresenius Kabi or MilliQ filtered/Merck
Vinegar	-	Aceto Balsamico, Alnatura
Software		
Product	Version	Distributor
Python	3.1	Python Software Foundation
MATLAB	R2022a	Mathworks Inc.
GraphPad Prism	9.5	GraphPad Software LLC
FIJI (ImageJ)	1.53	Wayne Rasband, NIH

Fly husbandry

Flies were reared on standard cornmeal medium at 25°C and 60% humidity with a day/night cycle of 12 h. For wet starvation, flies were anesthetized with CO₂ and transferred to a vial with moistened tissue paper. Flies were starved overnight until the experiment (approx. 18-24 h).

Fly preparation and light field calcium imaging

Female flies (*nSyb-GAL4;UAS-jGCaMP7s*) were collected at eclosion and kept with males for 6 to 8 days at 25°C until the experiment. The females were prepared for whole brain imaging,

as previously described in (Woller et al. 2021). Hereby, the flies were attached at the neck to a 3D-printed holder. The head was positioned at an angle while the body is pushed down, to allow access to the brain from the posterior side.

For the taste and multisensory experiments, the proboscis was pulled out, with vacuum from a mouth pipette that was positioned with a mechanical micromanipulator (Narshige MMN-1). Then the rostrum and maxillary palps were cured with UV-glue (Fotoplast Gel, Dreve Otoplastik GmbH), so the haustellum and the labella would stick out. For taste-only experiments, the third antennal segment was removed and the rest was covered with UV-glue. For odor-only experiments, the proboscis was pushed back and completely covered with UV-glue. The legs of the flies were removed to avoid interference with the taste delivery and to minimize movement. After sealing all spaces between head, body and holder with glue and grease, the prep was covered with extra-cellular saline (103 mM NaCl, 3 mM KCl, 5 mM TES, 8 mM trehalose·2 H₂O, 10 mM glucose, 26 mM NaHCO₃, 1 mM NaH₂PO₄, 2.5 mM CaCl₂·2 H₂O, 4 mM MgCl₂·6 H₂O) and a cuticle window was cut using fine forceps. Air sacks and fat bodies were carefully removed to allow free visual access to the neural tissue and muscle 16 was cut to prevent the rhythmic pumping motion it performs that would otherwise cause serious motion artifacts in the image.

The light field microscope was set up according to Aimon et al. (2019; Figure 4). The system was based on a Thorlabs Cerna with a Leica HC FLUOTAR L 25x/0.95 objective and MLA-S125-f12 microlens array (RPC photonics). The microlens array was placed on the image plane, while the camera imaged the microlens array through 50mmf/1.4 NIKKOR-S Nikon relay lenses. A 470 nm LED lamp (Thorlabs M470L3) was used for excitation at roughly 20% of the full intensity. The light field images were recorded at 10 Hz with a scientific CMOS camera (Hamamatsu ORCA-Flash 4.0).

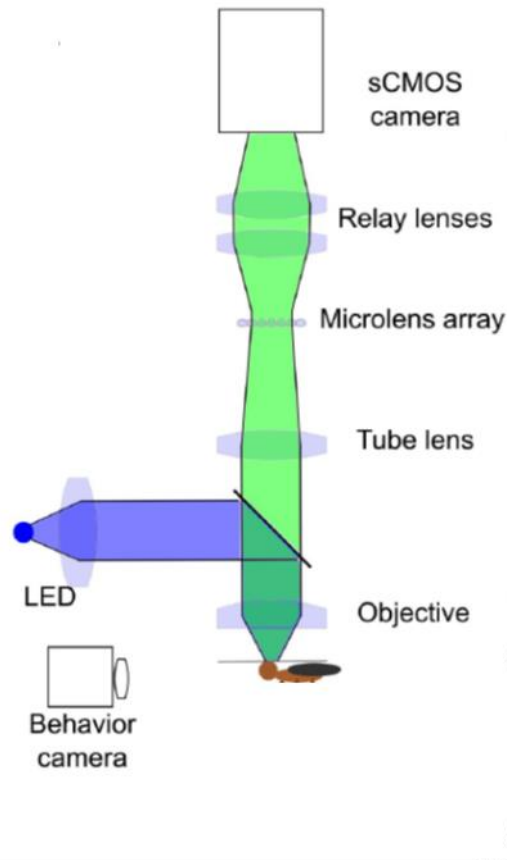


Figure 4: Illustration of light field microscopy setup

The fly's head was fixed and positioned under the objective and monitored via two behavior cameras. A blue LED (470 nm) was used to excite the GCaMP fluorophore. The green fluorescent light emitted from the brain passes the dichroic mirror and travels through the tube lens to the microlens array. The raw image was then recorded by a scientific CMOS camera (sCMOS) via two relay lenses. (© Aimon et al., 2019, CC BY 4.0 license)

Experimental paradigm

Each recording was 2 minutes long. Within that time the fly was stimulated repeatedly three times with either one taste, one odor or a combination of a taste and an odor substance (Table 2). For taste delivery, a glass capillary (1.5 mm diameter) was sealed at one end with UV-glue to produce a small cavity and positioned vertically on a movable stage under the microscope. The cavity was filled with approx. 1 μ l of taste solution, which resulted in a droplet on top of the capillary (Figure 5 A). A different capillary was used for every substance. The capillary was positioned underneath the fly. In order to deliver the stimulus, the capillary was moved upwards using a mechanical micromanipulator until the drop touched the labella of the fly and then moved back down after approx. 5 seconds. To ensure delivery of the stimulus,

the fly was illuminated with infrared LEDs and monitored by digital cameras (Firefly MV-03M2M, Point Grey Research) from two angles. Each fly was stimulated three times for 5 sec with 25 sec interstimulus intervals.

For odor delivery, a Syntech Stimulus Controller (CSS-55) was connected to a 4 mm PVC tube that was placed under the microscope, about 5 mm in front of the fly's head and delivered a constant air stream of 1000 ml/min. Flies were stimulated by redirecting 30% of main air flow for 1 sec through a head-space glass vial filled with odor solution by a manual trigger (foot pedal). Each fly was stimulated three times with 29 sec interstimulus intervals (at 30, 60, and 90 sec). Every fly was recorded three times and stimulated with two taste or odor substances with a ten-minute break between recordings. In between, during the second recording, the flies were always stimulated with water taste or water odor.

For multisensory recordings a taste substance was delivered for 5 sec. As soon as the droplet touched the labella, the foot pedal was pushed down to deliver an odor stimulus for 1 sec. This was repeated three times with a 25 sec interval. Each fly was recorded three times and given two combinations of taste and odor substances and a combination of water taste and water odor on the second recording. Each individual either received stimulations only with pairs of matching valence or only conflicting valence.

Table 2: Tastants and odorants used for chemosensory stimulation

Experiment	Positive Valence	Negative Valence	Solvent
Taste	500 mM Sucrose	4 mM Quinine	H ₂ O
Odor	1% Vinegar (5 ml)	1% Benzaldehyde (1 ml)	H ₂ O
Multisensory (Matching Valence Pair)	500 mM Sucrose + 1% Vinegar	4 mM Quinine + 1% Benzaldehyde	H ₂ O
Multisensory (Conflicting Valence Pair)	500 mM Sucrose + 1% Benzaldehyde	4 mM Quinine + 1% Vinegar	H ₂ O

Image processing

The imaging data was processed similarly as described in Siju et al. (2020) and Boehm et al. (2022). Volumes were reconstructed using a Python program developed by Broxton et al. (2013) and available on github (github.com/sophie63/FlyLFM). The resulting images were cropped in FIJI (ImageJ, version 1.53, NIH) and the last 3-6 slices in Z were removed because they usually only contained image information posterior of the actual brain tissue.

The movement artifacts were removed by 3D registration using the 3dvolreg routine from AFNI. The following steps were performed with MATLAB (version R2022a, MathWorks Inc.) unless stated otherwise (code available at <https://drive.google.com/drive/folders/19hquVbGaagNCIuL09KIFTDCxWDIdGtXi?usp=sharing>). The voxel time series were transformed to dF/F by subtracting and normalizing with a moving average over 60 s and noise was reduced, using Kalman filtering. Functional regions were then extracted using principal component analysis and independent component analysis. These were then used as landmarks to register the recordings to an anatomical template based on the JFRC2018 template from Bogovic et al. (2020) in FIJI. Masks were created to extract and average dF/F time series for the voxels in twelve major brain regions (neuropil supercategories). Peak responses to chemosensory stimulations were obtained by extracting maximum dF/F value in a 4 sec window after the stimulus onset. The stimulus onset of the taste and multisensory experiment was determined by reviewing the videos recorded on the Firefly cameras and noting the time frame where the drop first touched the labellum. Example recordings are available at <https://drive.google.com/drive/folders/1yhKOpbjeuuNuNnJ6ZeFF5trKiS-WCySc?usp=sharing>.

Statistics

Statistical analysis was performed with GraphPad Prism (version 9.5, GraphPad Software

LLC). Peak responses were first averaged across three repeated stimulations in each animal. Then average peak responses for odor and taste stimulation were analyzed separately in a 3-way ANOVA (with Tukey's multiple comparison) with the factors: Odor or taste substance (i.e. Vin vs Benz or Suc vs Qui), internal state (i.e. fed vs starved) and brain regions (i.e. 12 neuropil supercategories). For the multisensory stimulation the dataset for fed and starved animals were analyzed separately in 3-way ANOVA (with Tukey's multiple comparison) with the factors: Odor-taste combinations (i.e. matching valence vs conflicting valence), odor substance (i.e. Vin vs Benz) and brain regions. To analyze whole brain response, the median across all brain regions was calculated within each animal. Whole brain median responses for odor or taste were compared with paired, two-tailed t-test (within the same group, fed or starved) and with an unpaired, two-tailed t-test (between the groups). Whole brain median responses for multisensory experiments were analyzed separately in fed and starved groups with an ordinary 1-way ANOVA with Tukey's multiple comparison.

Principal component analysis

PCA was performed on a dataset of average peak responses that contained the observations for each region in every fly in the rows and all experimental groups as variables in the columns. Respectively, the transposed dataset contained the experimental groups in the rows and the brain regions in the columns. Before using the transposed dataset, rows with NaN values were removed, to have an even number of 10 observations per group. The `pca` function in MATLAB was used with default parameters to calculate component coefficients (i.e. loadings), component score and the variance explained by each component.

Classification models

Classification models were created with the Classification Learner App in MATLAB. The average peak response for the 12 major neuropils was used to predict each of the following response classes separately: Stimulus type, valence, internal state and substance. Five different models were first trained on the full data set with 5-fold cross validation. The model parameters are listed in Table 3. Then predictor variables were subsequently excluded to optimize the two best performing models. The optimized models were then trained with 70% of the data and tested on the remaining 30%.

Table 3: Classification model parameters

Parameter	Fine Tree	Linear Discriminant	Quadratic Discriminant	Medium KNN	Medium Neural Network
Max. number of splits	100	-	-	-	-
Split Criterion	Gini's diversity index	-	-	-	-
Covariance structure	-	Full	Full	-	-
Number of neighbours	-	-	-	10	-
Distance metric	-	-	-	Euclidean	-
Distance weight	-	-	-	equal	-
Number of fully connected layers	-	-	-	-	1
First layer size	-	-	-	-	25
Activation	-	-	-	-	ReLU
Iteration Limit	-	-	-	-	1000
Lambda	-	-	-	-	0
Misclassification cost	Default	Default	Default	Default	Default

Functional Component Analysis

The functional components were derived from an algorithm used by Aimon et al. (2019) which detects voxels with highly correlated intensity over time and plots them as spatial maps. The algorithm applies two steps of melodic single value decomposition (based on the FSL package), followed by independent component analysis using FastICA. The components were sorted with a custom-made Python GUI, programmed by Subhadarshini Parhi, based on the correlation of their time series with the stimulus and annotated according to their shape and position. Independent components that did not correlate with the stimulus or could not be annotated were discarded from further analysis. The remaining components were compiled into a list and sorted according to their frequency in each experimental group. The time series and the peak response for the first stimulus phase were extracted with MATLAB. Within the same individual, most components consisted of two bilaterally symmetric parts, so the time series were averaged for both hemispheres. The component relevance score was calculated by multiplying frequency with the average peak response across animals. An image-based search with FlyCircuit 1.2 (www.flycircuit.tw) was conducted to find neurons that show similarity with the relevant functional components. In addition, Virtual Fly Brain (www.virtualflybrain.org) was used to find Gal-4 lines that show a similar expression pattern as the functional components.

Graph Analysis

Graphs analysis was performed in MATLAB. Pearson correlation between all of the 12 brain regions was calculated on the dF/F time series for two different time intervals. The “rest” interval was specified as the first 25 seconds of each recording. The “stim” interval was defined for 15 second after the onset of the first stimulus. Pearson correlation was averaged across animals within each group and the Fisher-Z-transformation (atanh function) was applied to give the values a normal distribution. Then values were thresholded with the `threshold_proportional` function of the Brain Connectivity Toolbox (Rubinov and Sporns, 2010,

brain-connectivity-toolbox.net) to retain only 40 (and 20) percent of the strongest correlations. To obtain binary connections the `weight_conversion` function from the same toolbox was applied. The correlation ratio was calculated by dividing the correlation during stimulus phase with the correlation during the rest phase. Connectivity change was calculated by subtracting the binary connectivity during the resting phase from the binary connectivity during the stimulus phase. Adjacency matrices were plotted using `pcolor`. The graphs were created using the `graph` function.

Results

Chemosensory stimulation activates different areas of the brain depending on the modality

Since the central nervous system is a highly dynamic and complex network of cells that communicate with each other simultaneously, the aim of this project was, to measure the global neuronal activity upon odor and taste stimulation, in order to unravel the functional dynamics during chemosensory processing. To that end, I used transgenic flies, that express a calcium-sensitive fluorescent protein (jGCaMP7s; Dana et al. 2019) in all neuronal cells with neural synaptobrevin (nSyb) as the GAL4 driver, which encodes for a protein involved in synaptic vesicle fusion (Broadie et al. 1995). After exposing fed and starved flies to different odor and taste cues (or a combination of both) and recording the GCaMP fluorescence with the light field microscope (LFM), a volume of the fly brain was reconstructed from the microlens raw image (Figure 5 B, C). Then the volume was registered to an anatomical template (Figure 5 D). Afterwards the fluorescence timeseries (dF/F) for the voxels in twelve of the major brain regions (neuropil supercategories, Figure 5 F, Ito et al. 2014) was extracted and averaged across both hemispheres. Figure 5 E shows an example time series for a fly that was stimulated with vinegar odor. I averaged the fluorescence time series for the first stimulation across individuals for each experimental group.

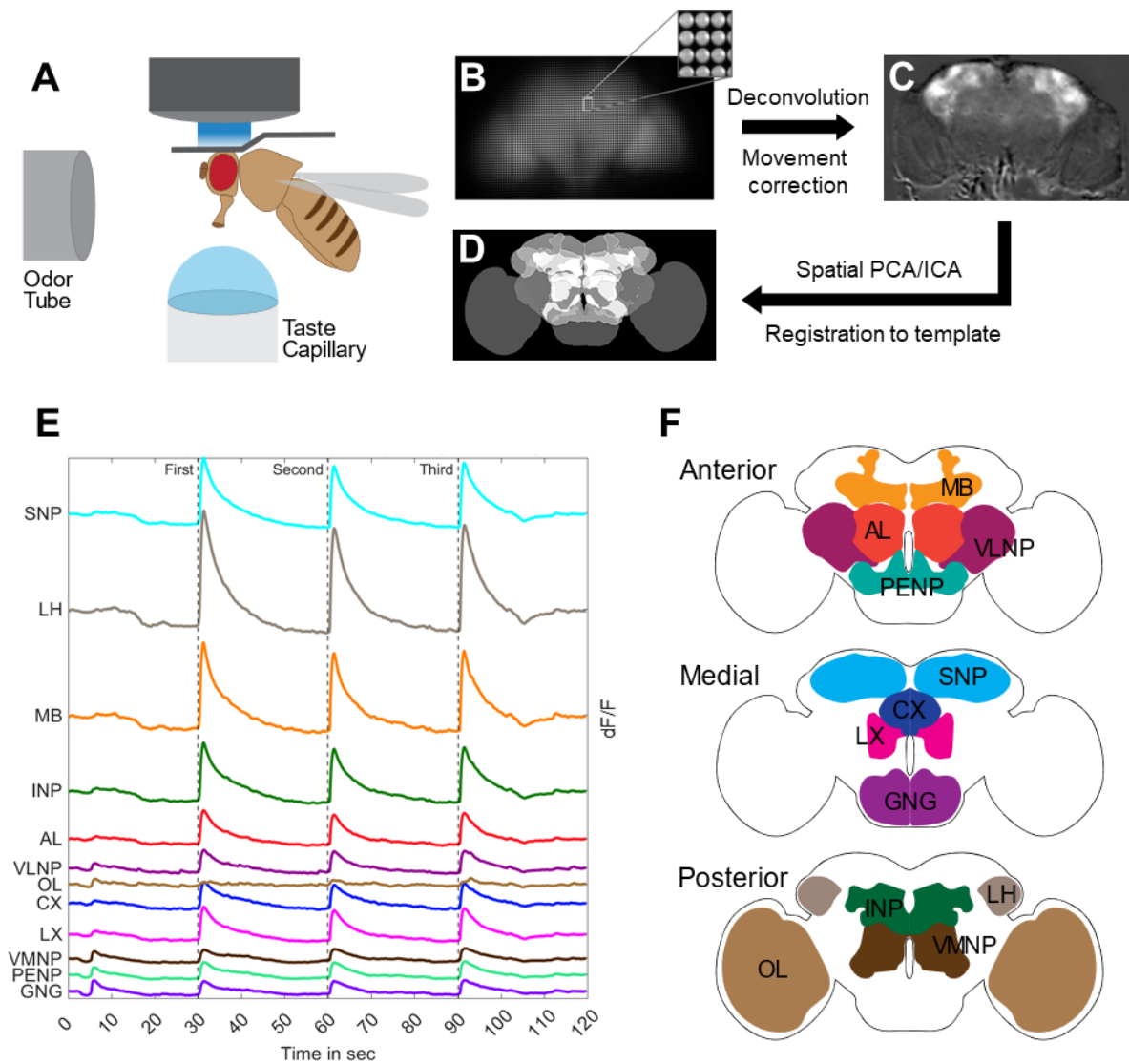


Figure 5: Whole-brain light field imaging of chemosensory responses

A Illustration of the experimental setup. **B** Raw image of the microlens array (adapted from Aimon et al., 2019, CC BY 4.0 license) **C** Example image after light field reconstruction. Shows a Z-plane just dorsal of the focal plane during combined odor and taste stimulation. **D** Anatomical template used for registration (JFR2018 template, © Bogovic et al., 2020, CC BY 4.0 license). **E** Example recording of a fly stimulated with vinegar odor. Traces show dF/F time series averaged for the neuropil supercategories in both hemispheres. **F** Illustration of neuropil supercategories. Anterior: Antennal lobe (AL), mushroom body (MB), periesophageal neuropils (PENP), ventrolateral neuropils (VLNP). Medial: Central complex (CX), gnathal ganglia (GNG), lateral complex (LX), superior neuropils (SNP). Posterior: Inferior neuropils (INP), lateral horn (LH), optic lobe (OL), ventromedial neuropils (VMNP).

Figure 6 shows the mean response for stimulation with one chemosensory modality. Odor stimulation caused the highest activity in the lateral horn (LH), whereas taste stimulation yielded the strongest response in the gnathal ganglia (GNG). The GNG receives direct input from gustatory receptor neurons in the labella (Miyazaki and Ito 2010). The LH receives secondary odor input from projection neurons that originate in the antennal lobe (AL, (Jefferis et al. 2007). Surprisingly, the AL itself, where the axons of the olfactory receptor neurons (ORNs) terminate (Jefferis 2005), was not strongly activated by the odor stimulus. The AL is organized into a large number of glomeruli and each only responds to specific odors (Stocker et al. 1990; Grabe et al. 2016). This could explain, why I only saw a low response in the AL, since I am averaging across the whole neuropil but the signal itself is spatially very sparse. The odor response reached its maximum shortly after the onset of the 1 s long stimulus and then went back to baseline after another 5 seconds. Because the taste stimulation was given for an extended time of 5 seconds, the maximum was found just at the end of stimulus. However, the scale of the taste response was different. The maximum dF/F of the taste response was only about half as high as the maximum odor response. This makes it difficult to directly compare both modalities and that becomes even more obvious in Figure 7. It shows the responses towards the combined stimulation with odor and taste. Here again, the region with the highest calcium activity was the LH. There was also activation in the GNG but it appeared small in comparison. However, the response profile was clearly different from odor alone. Overall, there was increased activity in most brain regions, except for the optic lobe (OL) which did not respond at all. There were also subtle differences in the response timing. The signal in the GNG and periesophageal neuropil (PENP), which also showed taste response (Figure 6 B), started ramping earlier than in other regions. This can be explained by the experimental paradigm, where the taste stimulus was given first. After approximately 0.5 s the odor stimulus was applied and the other regions, like the mushroom body (MB) and superior neuropils (SNP) were activated (Figure 7). Interestingly, the LH answered even earlier after the odor onset than those regions, because there was already a low increase in calcium signal due to the taste stimulation before. Additional figures showing the individual traces for

every animal or the average traces with standard deviation can found in the appendix (Figure A11 - A18.2).

I calculated the peak responses after stimulation and averaged across repeated stimulation. Overall, the responses declined over repeated stimulation. This effect was relatively consistent across groups (Figure 8). The standardized peak responses in Figure 9 show high positive Z-scores for odor in the LH, MB and SNP, which means they exhibited higher peak responses compared to the average across all regions. In taste, mainly the GNG shows strong activation (Z-score: \sim 2). The multisensory stimulation produced Z-scores similar to the odor alone. However, here the GNG does not have a negative score. This relatively low score could be explained by the fact, that the overall dF/F signal in the GNG, caused by taste-stimulation is lower than the signal in the superior regions that are caused by odor. Most other regions scored around 0 (i.e. average), except for the OL, which always scored negative. Since the OL is a prominent part of the visual pathway (Bausenwein et al. 1992; Zhu 2013), it accordingly showed very little activity during processing of chemosensory inputs. Figure 9 also illustrates that the variance of the taste responses was higher in comparison with odor or combined stimulation. This is probably also due to the fact that the calcium activity during the taste presentation was overall lower and therefore only yielded low signal-to-noise ratio (see also Figure A13 - A14, A13.2 - A14.2).

Together, this data suggests that odor presentation caused robust and high neural activity in specific areas of the brain, like the LH, SNP and MB. Taste however activated different areas like the GNG and the PENP, although with lower signal, relative to odor stimulation. Consequently, combined presentation elicited activity in all the regions mentioned above for the duration of the stimulus. In contrast to those chemosensory regions, other areas like the OL, which deals with visual stimuli remained inactive.

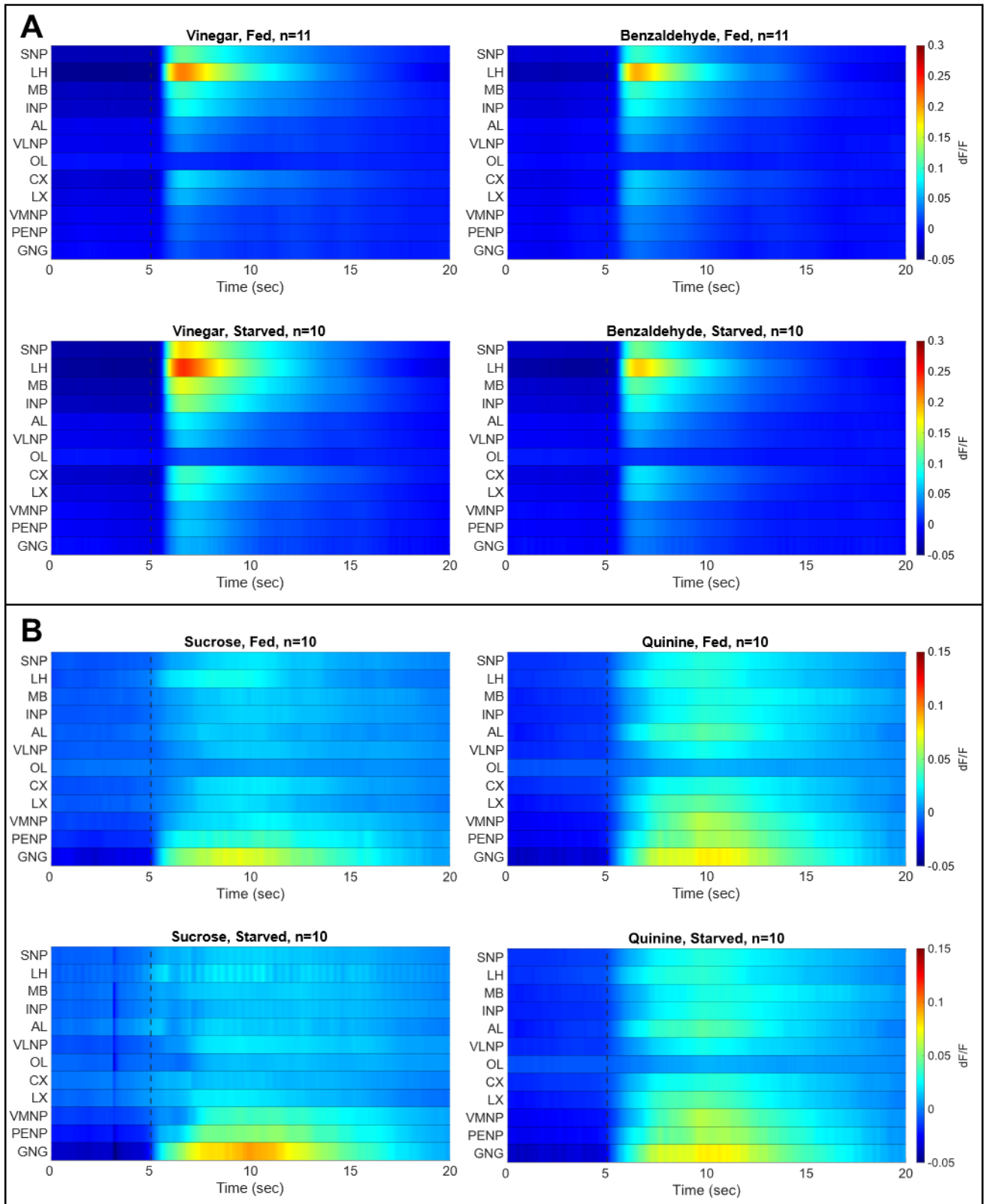


Figure 6: Average unimodal response towards the first stimulation

A Average dF/F time series for odor stimulation. N(Fed: 11/11), N(Starved: 10/10). **B** Average dF/F time series for taste stimulation. N(Fed: 10/10), N(Starved: 10/10). Stimulus onset indicated by dashed vertical line at 5 seconds.

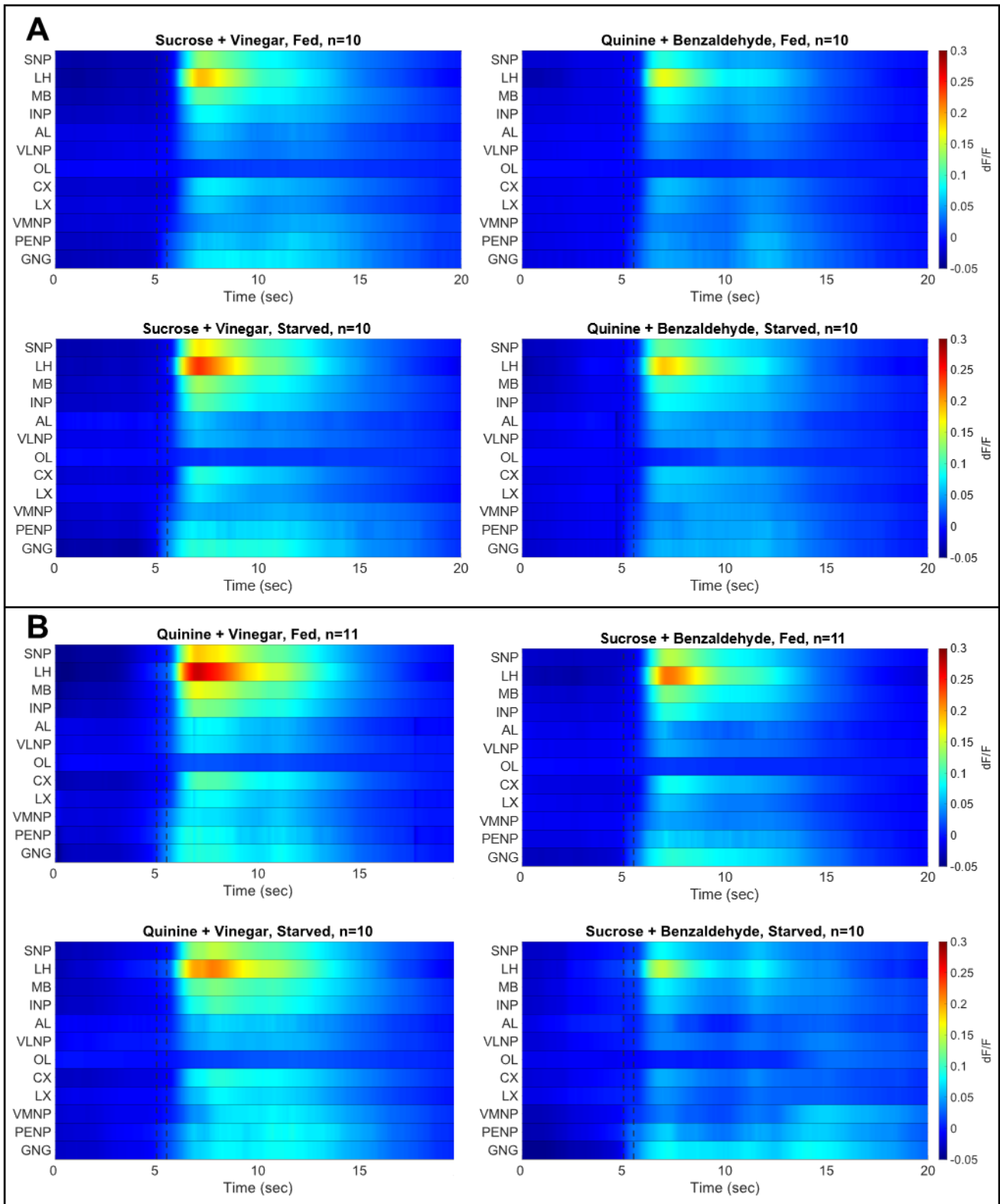


Figure 7: Average multisensory response towards the first stimulation

A Average dF/F time series for taste + odor stimulation with matching valence pairs. N(Fed: 10/10), N(Starved: 10/10). **B** Average dF/F time series for taste + odor stimulation with contradicting valence pairs. N(Fed: 11/11), N(Starved: 10/10). Taste stimulus onset indicated by dashed vertical line at 5 seconds. Estimated odor stimulus onset indicated by dashed line at 5.5 seconds.

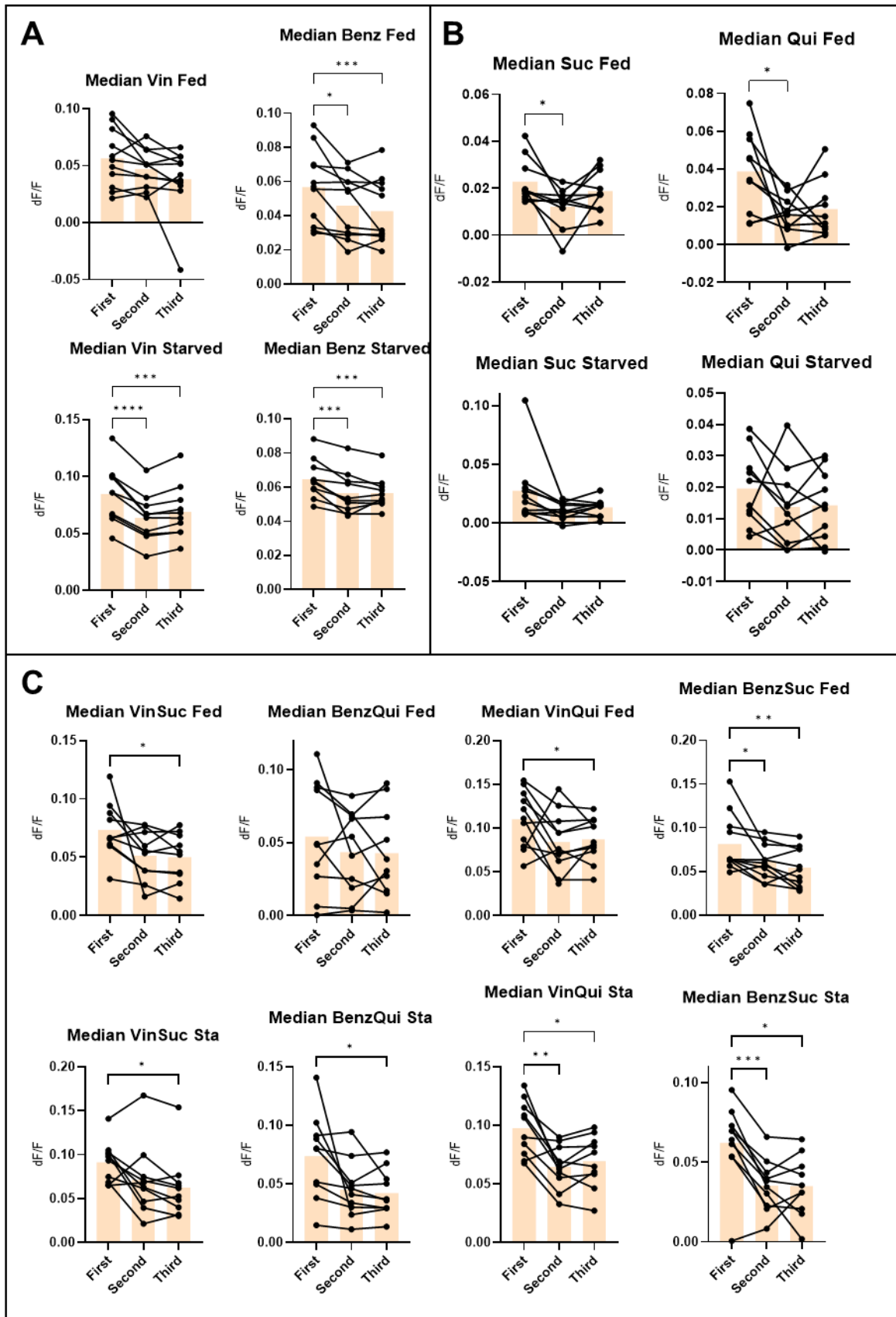


Figure 8: Whole brain median responses for three repeated stimulations

A Median peak dF/F for odor stimulation. B Median peak dF/F for taste stimulation. C Median peak dF/F for multisensory stimulation. The * indicates $p < 0.05$, ** indicates $p < 0.01$, *** indicates $p < 0.001$ (Dunnett's multiple comparison test within repeated measures 1-way ANOVA).

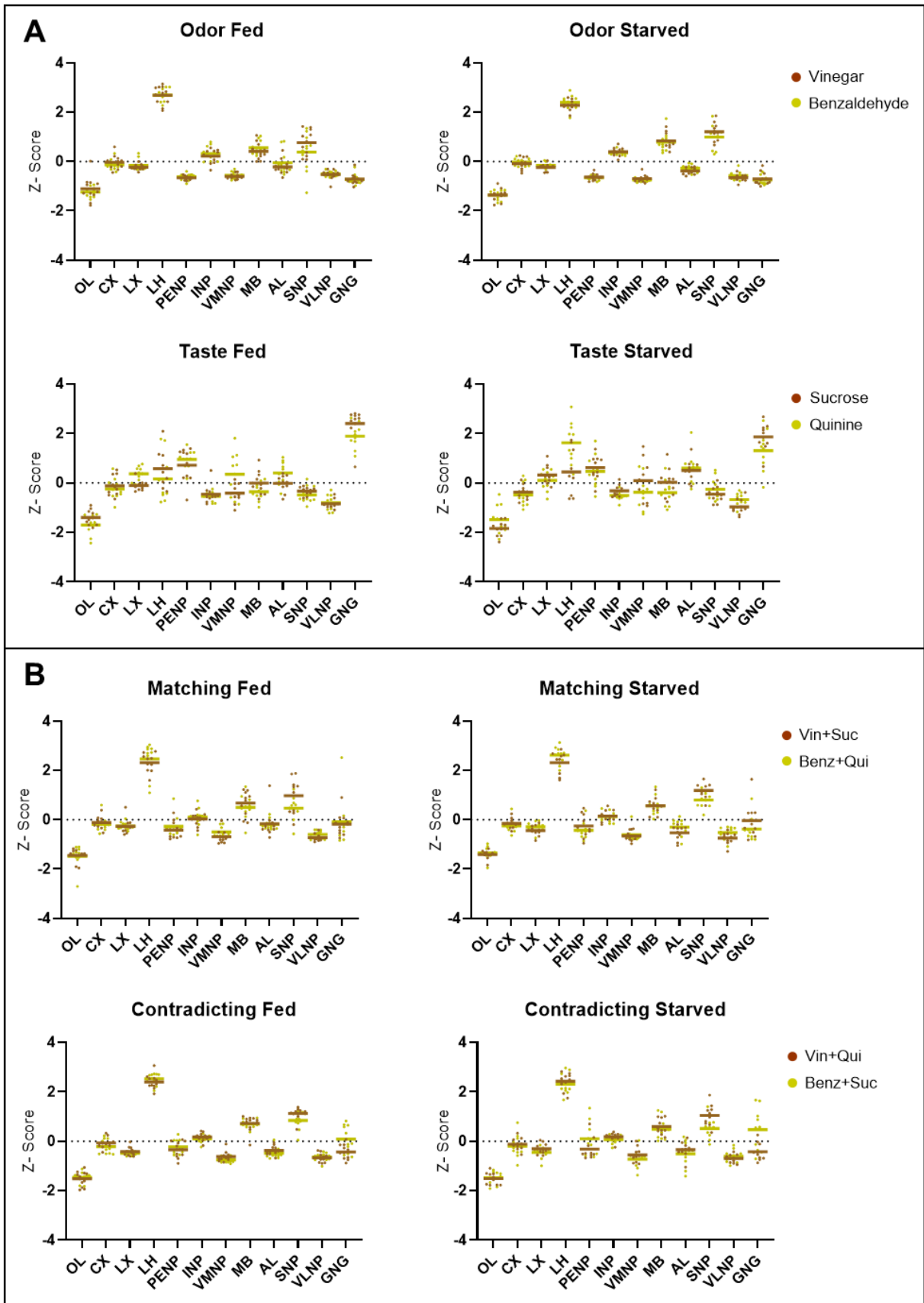


Figure 9: Standardized peak responses

A Z-Score of average peak dF/F for odor and taste stimulation. **B** Z-Score of average peak dF/F for multisensory stimulation. Horizontal lines indicate mean Z-score across animals. Dashed line at 0 indicates mean across all regions.

Next, I plotted the average peak response as gray scale values back onto the anatomical map to illustrate the brainwide distribution of the stimulus-induced neuronal activity (Figure 10). Here it becomes obvious that odor stimulation mainly activated the superior areas of the brain, whereas taste only activated the inferior parts. The maps for multisensory stimulation show activity in the superior as well as the inferior regions. This division along the dorso-ventral axis between of olfactory and gustatory activity can be understood from the anatomical organization of the fly brain. The inferior part mostly consists of the GNG and the PENP (Figure 5 F). The GNG and parts of the PENP, which are located below the esophagus, together form the subesophageal zone (SEZ, Ito et al. 2014). It is a center of sensorimotor integration, as it receives gustatory and mechanosensory input (Miyazaki and Ito 2010) but also contains a number of motor neurons and descending neurons (DNs; Namiki et al. 2018). Gustatory receptor neurons (GRNs) connect to the motor neurons that drive feeding behavior via a local circuit of interneurons and pre-motor neurons (Shiu et al. 2022). DNs send axons to the ventral nerve cord (VNC), the insect analog to the vertebrate spinal cord. DNs from the SEZ mainly innervate the leg neuromeres and therefore help control ground locomotion (Namiki et al. 2018). The LH and the MB however are located in the superior part of the brain and are considered secondary olfactory centers as they obtain significant input from AL projection neurons (PNs; Jefferis et al. 2007; Fişek and Wilson 2014). The LH is involved in mediating innate odor responses (Schultzhaus et al. 2017; Das Chakraborty and Sachse 2021). However, it was also found to integrate gustatory signals (Snell et al. 2022), which would explain the small responses during taste stimulation and the accelerated ramping of the signal during combined stimulation. The MB has been termed the center of olfactory learning and memory of the insect brain (Aso et al. 2014a; Heisenberg et al. 1985), hence there was strong activation upon odor presentation and little during taste application, although the MB was also reported to respond to gustatory cues (Kirkhart and Scott 2015). The most superior area of the brain is occupied by the SNP (Ito et al. 2014). The SNP is strongly connected with the LH and the MB which project to it via so-called output neurons. The SNP functions as a third order center in olfactory processing but its role is not well understood (Das Chakraborty and Sachse

2021). However, it explains why I measured strong calcium activity in that part of the brain after odor presentation.

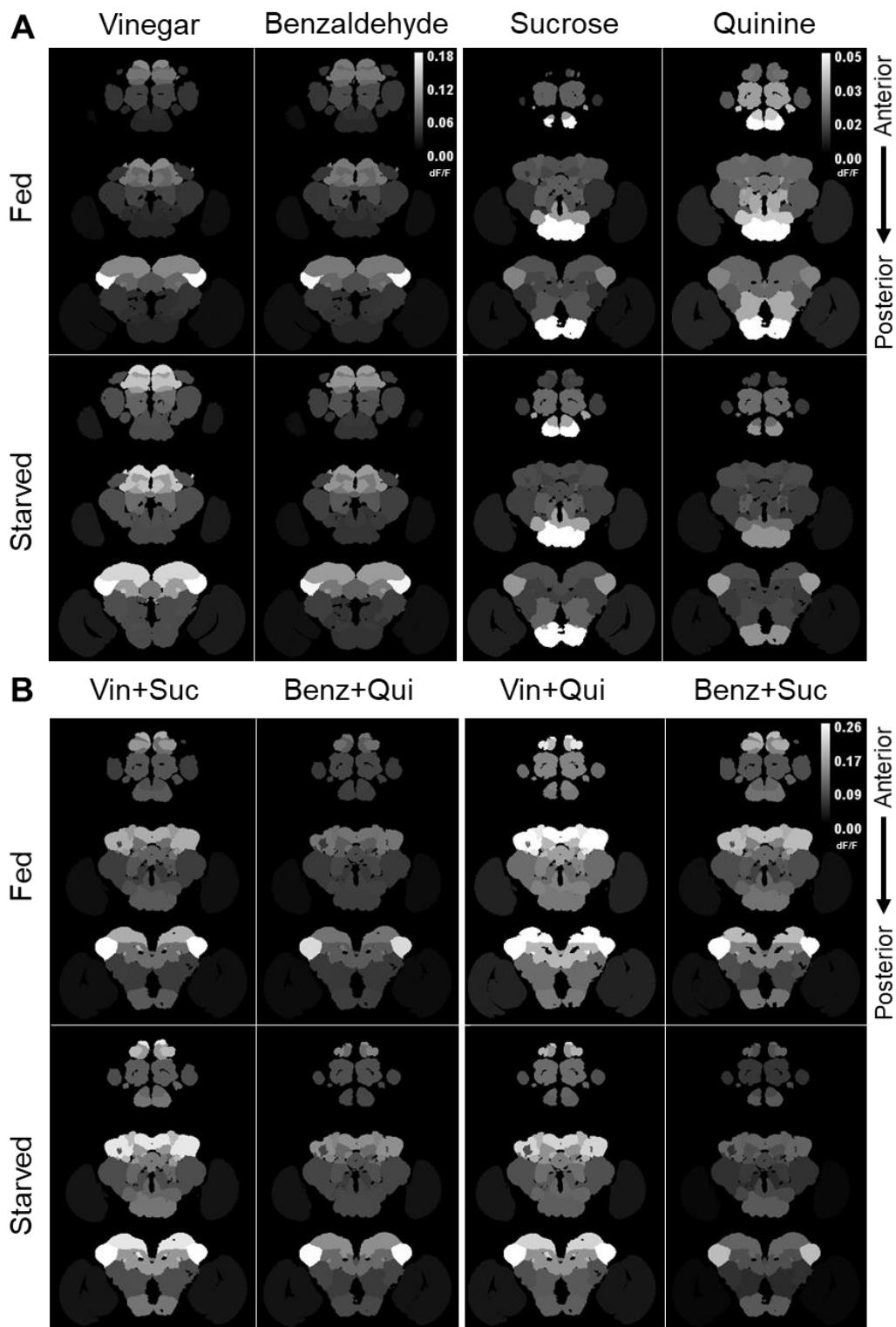


Figure 10: Peak responses to chemosensory stimulation mapped onto neuropil supercategories
A Peak dF/F for odor (left) and taste stimulation (right). Averaged across 3 repeated stimulations and individuals. N(Fed: 11/11//10/10). N(Starved: 10/10//10/10). **B** Peak dF/F for multisensory stimulation. Pairs of matching valence (left) and pairs of contradicting valence (right). N(Fed: 10/10//11/11). N(Starved: 10/10//10/10).

Valence and metabolic state influence chemosensory responses

Since the senses of smell and taste are intrinsically linked to feeding behavior, I recorded the brain activity in satiated as well as flies that were deprived of food for 18-24 hours before the experiment, to investigate the effect of metabolic state on whole brain activity. The hypothesis was that starved flies would respond more to appetitive stimuli than fed flies and less to the aversive stimuli. To compare between the groups, I performed a 3-way ANOVA on the average peak responses to odor and taste (Table 4 and 5). There was a significant effect between the brain regions for both modalities ($p < 0.0001$), indicating that not all regions showed the same peak activity. Figure 11 A and B highlight the differences. For odor, there were strong responses in the LH, SNP, MB and INP, whereas for taste most of the activity was confined to the GNG and PENP. There was no significant effect of vinegar vs benzaldehyde (Table 4, $p = 0.06$) or sucrose vs quinine (Table 5, $p = 0.65$), which suggests that valence of a stimulus alone did not lead to a change in brain-wide activity and brain state. However, there was significant interaction effect between regions and valence (odor $p = 0.0006$, taste $p < 0.0001$), indicating that the difference in peak activity towards cues of opposing valence was different among the regions. Tukey's multiple comparison test showed that for odor there was only a significant difference between stimuli of different valence in the LH (only in starved animals) and the SNP (in starved and fed, Table A5). For taste, the multiple comparison only showed a significant difference between sweet and bitter in the GNG (only in starved animals, Table A6). These are the same regions that showed the highest response to the appetitive cue after starvation. For odor there was also a significant interaction effect of region and internal state (Table 4, $p = 0.04$), which indicates that a difference in the response between fed and starved flies could only be detected in certain brain areas. The multiple comparison points to the MB and the SNP, where the difference of peak activity towards vinegar was different among the fed and the starved group (Table A5). This effect was not observed in the taste group, however here all three factors showed a significant interaction (Table 5, $p = 0.0001$). Surprisingly, there was no interaction effect of valence and internal state in either modality, implying that the

activity towards stimulation with positive or negative substances was not influenced by the metabolic state of the animal.

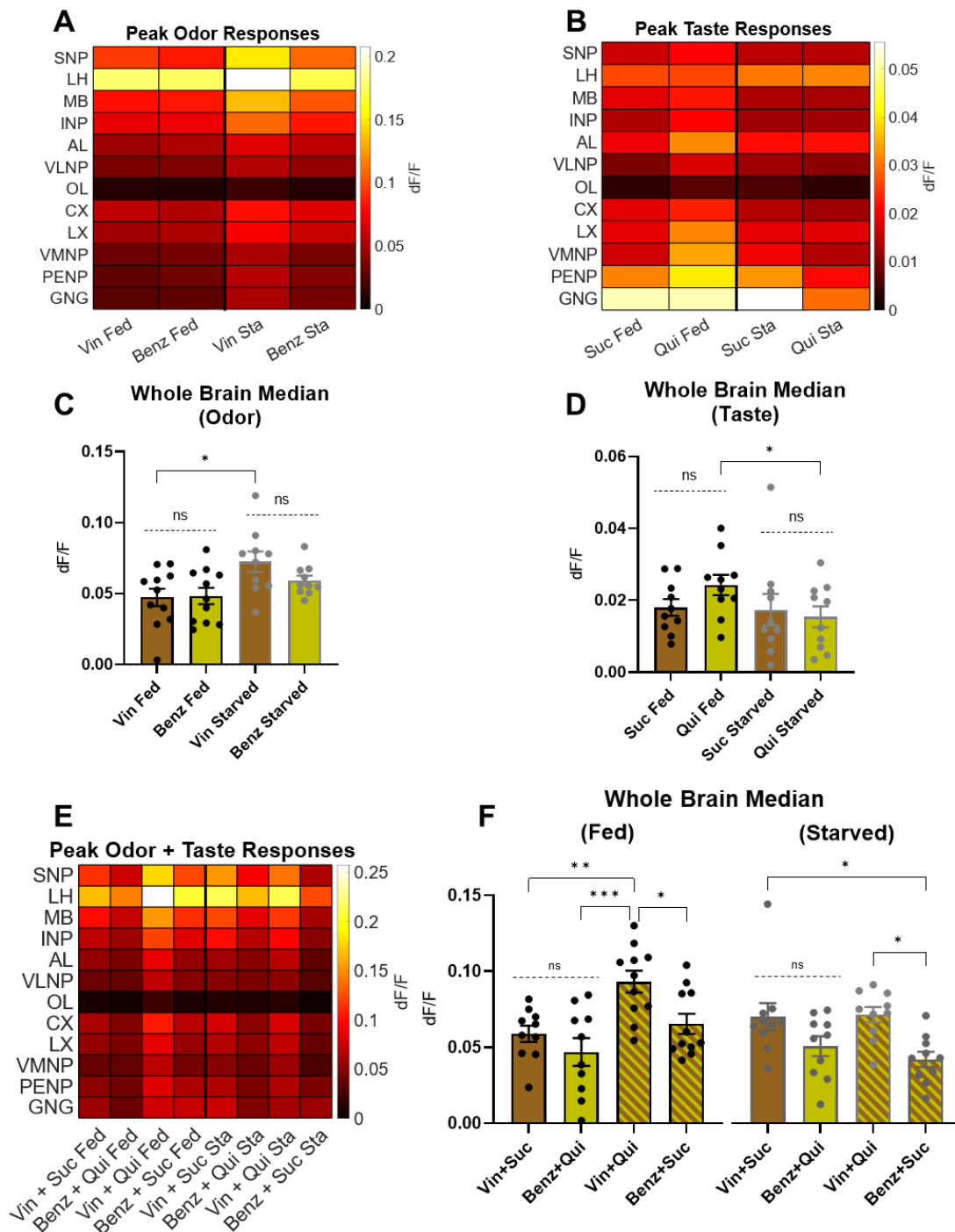


Figure 11: Direct comparison of peak responses per region and whole brain response
A Peak dF/F for odor responses. N(Fed: 11/11), N(Starved: 10/10). **B** Peak dF/F for taste responses. N(Fed: 10/10), N(Starved: 10/10). **C** Whole brain median across brain regions for peak odor responses. **D** Whole brain median across brain regions for peak taste responses. Bars show mean with SEM. The * indicate $p < 0.05$ (unpaired, two-tailed t-test). The ns indicate $p > 0.05$ (paired, two-tailed t-test). **E** Peak dF/F for multisensory responses. N(Fed: 10/10/11/11), N(Starved: 10/10/10/10). **F** Whole brain median across brain regions for peak multisensory responses. Bars show mean with SEM. The * indicates $p < 0.05$, ** indicates $p < 0.01$ and *** indicates $p < 0.001$ (Ordinary 1-way ANOVA with Tukey's multiple comparison). ANOVA results for A, B and E are shown in Table 4 to 7.

Since these results painted a complex picture of chemosensory input on local circuits and how they are influenced by the internal state, I wondered if there was also global effect. Hence, I calculated the median response across all brain areas and compared between the groups. I found that the whole brain response to vinegar odor was increased in starved compared to satiated flies (Figure 11 C, $p=0.02$, unpaired t-test). In contrast, the global response to quinine taste was reduced in starved animals (Figure 11 D, $p=0.04$). This illustrates that changes in internal state can have a global effect on brain activity during sensory integration and ultimately cause changes in behavior (Sayin et al. 2018; Dethier 1976). Furthermore, these results highlight similarities and differences between these two closely related senses. Locally, there was an increase of activity towards appetitive cues in hungry individuals. In gustation, this was only observed in primary sensory center, the GNG, but for olfaction these differences became apparent in second or third order centers like the LH and the SNP. Vinegar is produced during fermentation, in the presence of yeast and sugar (Zhu et al. 2003), both of which serve as food for the fly (or its offspring). Hence, they use the vinegar smell as a long-distance cue during foraging (Jung et al. 2015; Budick and Dickinson 2006; van Breugel and Dickinson 2014). They integrate the sensory information with other cues for orientation towards a potential food source (Matheson et al. 2022; Mamiya et al. 2008; Budick et al. 2007) and even might require some form of learned experience or contextual memory (Aso et al. 2014b; Tsao et al. 2018). All of this depends on activity in higher brain centers. On the other hand, taste is a near-field sense which is used when the fly is right on top of a substrate, probing with its leg or actively feeding. Here, only the local circuits in the SEZ are active, that translate sensory information of nutritious food vs. potentially noxious substance into motor action (i.e. extension or retraction of the proboscis, (Yapici et al. 2016; Shiu et al. 2022)). I also found this duality to be reflected in the influence of the internal state on the whole brain. When the fly is hungry the activity towards vinegar odor is increased, as the primary objective is finding a food source. Once at the destination, the activity towards bitter taste is reduced, as food intake, even in the presence of potentially harmful substance is prioritized to increase the chance of survival (LeDue et al. 2016; Devineni et al. 2019; Inagaki et al. 2014).

Table 4: Results for 3-way ANOVA on odor responses

Source of Variation	% of total variation	P value	P value summary
Region	67,52	<0,0001	****
Vinegar v Benz	0,8307	0,0616	ns
Fed v Starved	3,013	0,0358	*
Region x Vinegar v Benz	0,4105	0,0006	***
Region x Fed v Starved	0,9013	0,0365	*
Vinegar v Benz x Fed v Starved	0,9107	0,0513	ns
Region x Vinegar v Benz x Fed v Starved	0,1518	0,3166	ns

Table 5: Results for 3-way ANOVA on taste responses

Source of Variation	% of total variation	P value	P value summary
Region	34,88	<0,0001	****
Sucrose v Quinine	0,1617	0,6510	ns
Fed v Starved	1,843	0,2479	ns
Region x Sucrose v Quinine	2,076	<0,0001	****
Region x Fed v Starved	1,235	0,0603	ns
Sucrose v Quinine x Fed v Starved	2,444	0,0905	ns
Region x Sucrose v Quinine x Fed v Starved	1,308	0,0001	***

Table 6: Results for 3-way ANOVA on multisensory responses in fed flies

Source of Variation	% of total variation	P value	P value summary
Region	42,60	<0,0001	****
Matching v Conflicting	8,146	0,0092	**
Vinegar v Benzaldehyde	3,134	0,0191	*
Region x Matching vs Conflicting	2,477	<0,0001	****
Region x Vinegar v Benzaldehyde	0,3982	0,0377	*
Matching v Conflicting x Vinegar v Benzaldehyde	1,768	0,0695	ns
Region x Matching vs Conflicting x Vinegar v Benzaldehyde	0,3400	0,0885	ns

Table 7: Results for 3-way ANOVA on multisensory responses in starved flies

Source of Variation	% of total variation	P value	P value summary
Region	41,24	<0,0001	****
Matching v Conflicting	1,091	0,3167	ns
Vinegar v Benzaldehyde	5,706	0,0061	**
Region x Matching v Conflicting	0,1229	0,9977	ns
Region x Vinegar v Benzaldehyde	1,819	<0,0001	****
Matching v Conflicting x Vinegar v Benzaldehyde	0,5023	0,3685	ns
Region x Matching v Conflicting x Vinegar v Benzaldehyde	0,6551	0,1781	ns

Multisensory responses were analyzed separately in the fed and starved groups. Here, I compared the factors 'brain regions', 'stimulus pair' (matching vs conflicting valence) and 'odor identity' (vinegar vs benzaldehyde) in a 3-way ANOVA (Table 6 and 7). Both datasets show a significant effect of regions ($p < 0.0001$), which can be attributed to the superior brain regions showing higher overall activity (Figure 11 E). Both groups also show a significant difference between vinegar and benzaldehyde (fed: $p = 0.02$, starved: $p = 0.01$). This suggests that tastants paired with vinegar odor caused higher responses than those paired with benzaldehyde. In addition, the identity of the paired odor showed significant interaction with the regions (fed: $p = 0.04$, starved: $p < 0.0001$). Tukey's multiple comparison test shows significant differences mainly in the LH and the SNP (Table A7 and A8). In fed flies there was also a significant increase of the response to stimulus pairs of conflicting valence compared to pairs of matching valence (Table 6, $p = 0.01$). This factor shows significant interaction with the regions ($p < 0.0001$). The multiple comparison shows differences only in the LH, MB and SNP (Table A7). Comparison of the whole brain median is illustrated in Figure 11 F. It shows that in fed flies the combination of vinegar and quinine caused significantly higher global activity than the other combinations (ordinary 1-way ANOVA with Tukey's multiple comparison, Table 8). This mismatch of sensory information only seemed to lead to an increase in response, when an appetitive odor was paired with bitter taste, but not when an aversive odor was paired with a sweet taste. Furthermore, this could only be observed in satiated flies. In starved animals, the combination of benzaldehyde and sucrose was significantly lower than both tastes combined with vinegar (Table 9). It seems like the context of vinegar odor facilitated a strong response towards quinine in the fed state but also in the starved state, where the quinine response alone was reduced. As explained in the introduction, the sensory interaction of smell and taste in the fly is not well studied. However, some evidence suggests that yeast odor can enhance feeding responses towards sucrose solution (Oh et al. 2021).

**Table 8: Ordinary 1-way ANOVA Whole Brain Median for multisensory stimulation (Fed).
F=7.57, p=0.0001, R²=0.37**

Tukey's multiple comparisons test	Mean Diff,	95,00% CI of diff,	Summary	Adjusted P Value
Vin+Suc vs. Benz+Qui	0,01201	-0,01592 to 0,03995	ns	0,6581
Vin+Suc vs. Vin+Qui	-0,03430	-0,06160 to -0,007009	**	0,0089
Vin+Suc vs. Benz+Suc	-0,006513	-0,03381 to 0,02078	ns	0,9180
Benz+Qui vs. Vin+Qui	-0,04632	-0,07361 to -0,01902	***	0,0003
Benz+Qui vs. Benz+Suc	-0,01853	-0,04582 to 0,008767	ns	0,2783
Vin+Qui vs. Benz+Suc	0,02779	0,001154 to 0,05443	*	0,0380

**Table 9: Ordinary 1-way ANOVA Whole Brain Median for multisensory stimulation (Starved).
F=4.76, p=0.01, R²=0.28**

Tukey's multiple comparisons test	Mean Diff,	95,00% CI of diff,	Summary	Adjusted P Value
Vin+Suc vs. Benz+Qui	0,02054	-0,006413 to 0,04749	ns	0,1883
Vin+Suc vs. Vin+Qui	-0,001543	-0,02850 to 0,02541	ns	0,9987
Vin+Suc vs. Benz+Suc	0,02976	0,002804 to 0,05671	*	0,0257
Benz+Qui vs. Vin+Qui	-0,02208	-0,04904 to 0,004869	ns	0,1408
Benz+Qui vs. Benz+Suc	0,009216	-0,01774 to 0,03617	ns	0,7939
Vin+Qui vs. Benz+Suc	0,03130	0,004347 to 0,05825	*	0,0175

Principal component analysis separates between brain regions and internal state

The previous results have shown that stimulus valence and internal state have complex effects on the neural activity in each region among the different groups. To analyze whether this is true over all tested conditions, I performed principal component analysis (PCA) on the peak responses in all regions over all 16 experimental groups (odor only, taste only, odor + taste). PCA is a useful method to reduce dimensionality in multivariate data. Figure 12 A shows that component scores in the OL cluster at negative x-values and at y-values around zero in the PCA plot. On the other hand, the LH, SNP and MB have positive scores in the first component. All other regions group around the origin, slightly skewed to the left. This implies that the first principal component, that explains almost 70 % of the variance (Figure 12 C) separates between low odor responsive regions (like the OL) and high odor responsive regions (like the LH). Intermediate odor responsive regions and taste responsive regions (like the GNG) are distributed between those extremes. Figure 12 B shows that all groups have positive coefficients in the 1st component, however the 2nd component distinguishes between odor responses (and Vin + Qui Fed), and all other groups. It also shows that taste responses contribute very little to the first two components, since the coefficient vectors are quite small. I wondered whether PCA can distinguish between stimulus valence or internal state within each stimulus group. Therefore, I performed PCA on the data for odor, taste and odor + taste, separately. Figure 13 A shows again, that the 1st component separates between low and high odor responsive brain regions. Figure 13 B illustrates that the 2nd component separates the coefficients of the starved and fed groups. Both components together account for over 90 % of the variance (Figure 13 C). In Figure 14 A, the first component differentiates between low taste responsive regions (OL, VLNP) and strong taste responsive regions (GNG, PENP). Component 2 distinguishes between fed and starved groups (Figure 14 B). The scatter plot in Figure 15 A, which displays the odor + taste data looks similar to the one in Figure 13 A, with negative scores of the OL and positive scores of the LH on the horizontal axis. Figure 15 B

shows positive coefficients in component 2 for matching pairs in starved animals and negative coefficients for contradicting pairs in fed animals. The coefficient vectors of other groups are almost parallel to the x-axis. Altogether, this shows that PCA on peak responses can recapitulate the spatial differences in chemosensory activity. Furthermore, it shows that within each modality the second-most relevant component clearly separates between fed and starved flies, which implies that global brain activity is modulated by the metabolic state.

I also tested the results of a PCA where I used the brain regions as variables instead of the groups (transposed dataset). Figure 16 A shows that component scores for taste responses cluster together, but odor and odor + taste responses are more or less randomly distributed. This implies that odor activity and paired activity are very similar but still can be clearly distinguished from taste activity. Figure 16 B illustrates that the LH coefficient vector is clearly separated from the other regions, potentially because it shows the largest difference in activation out of all regions during odor and combined stimulation as compared to taste presentation (Figure 9).

In summary, the PCA suggests that differences in regional activity best explain the variability in the data. However, if you separate the data according to the modality, the 2nd principal component separates between fed and starved individuals, which suggest that chemosensory-evoked brain activity is modulated by the internal state.

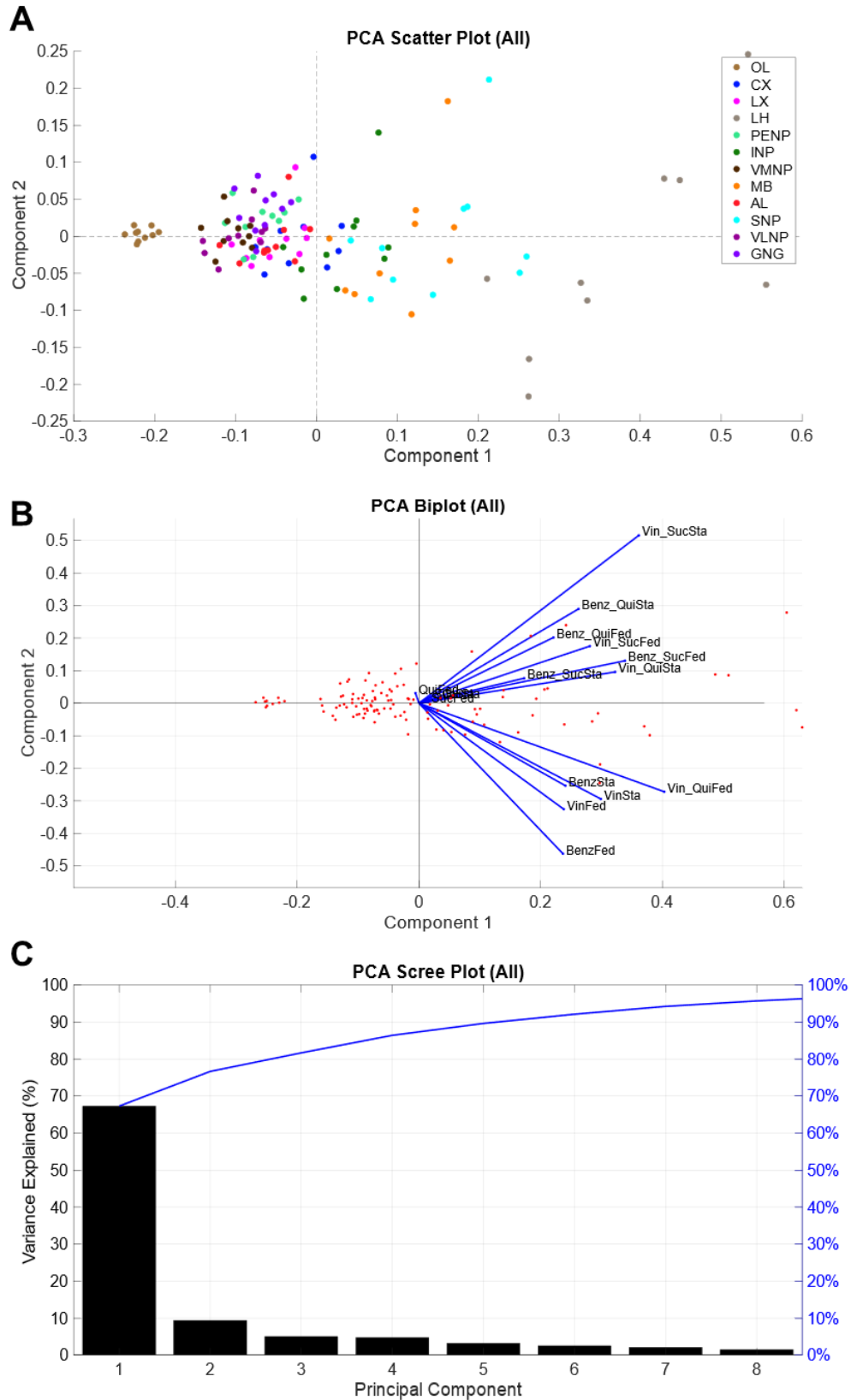


Figure 12: Principal component analysis for peak responses of all groups

A Scatterplot for the scores of the 1st and 2nd principal component. Colors indicate the brain regions.

B Biplot for the 1st and 2nd principal component. Red dots indicate component scores (as seen in A).

Blue lines indicate component coefficients for each group. **C** Scree plot of principal components. Bars indicate the variance that is explained by each component. Blue line indicates cumulative variance.

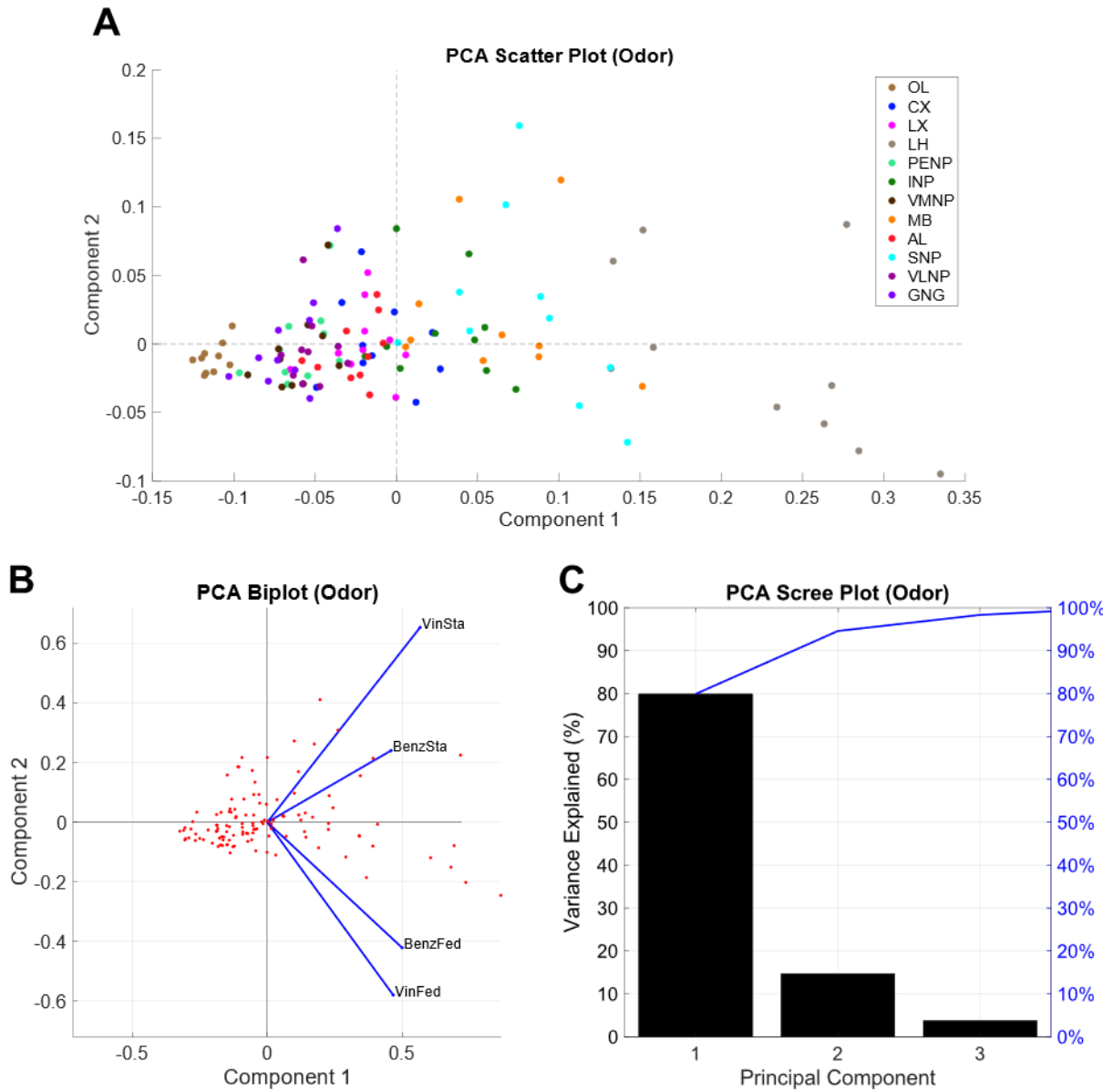


Figure 13: Principal component analysis for peak responses of odor groups

A Scatterplot for the scores of the 1st and 2nd principal component. Colors indicate the brain regions. **B** Biplot for the 1st and 2nd principal component. Red dots indicate component scores (as seen in A). Blue lines indicate component coefficients for each odor group. **C** Scree plot of principal components. Bars indicate the variance that is explained by each component. Blue line indicates cumulative variance.

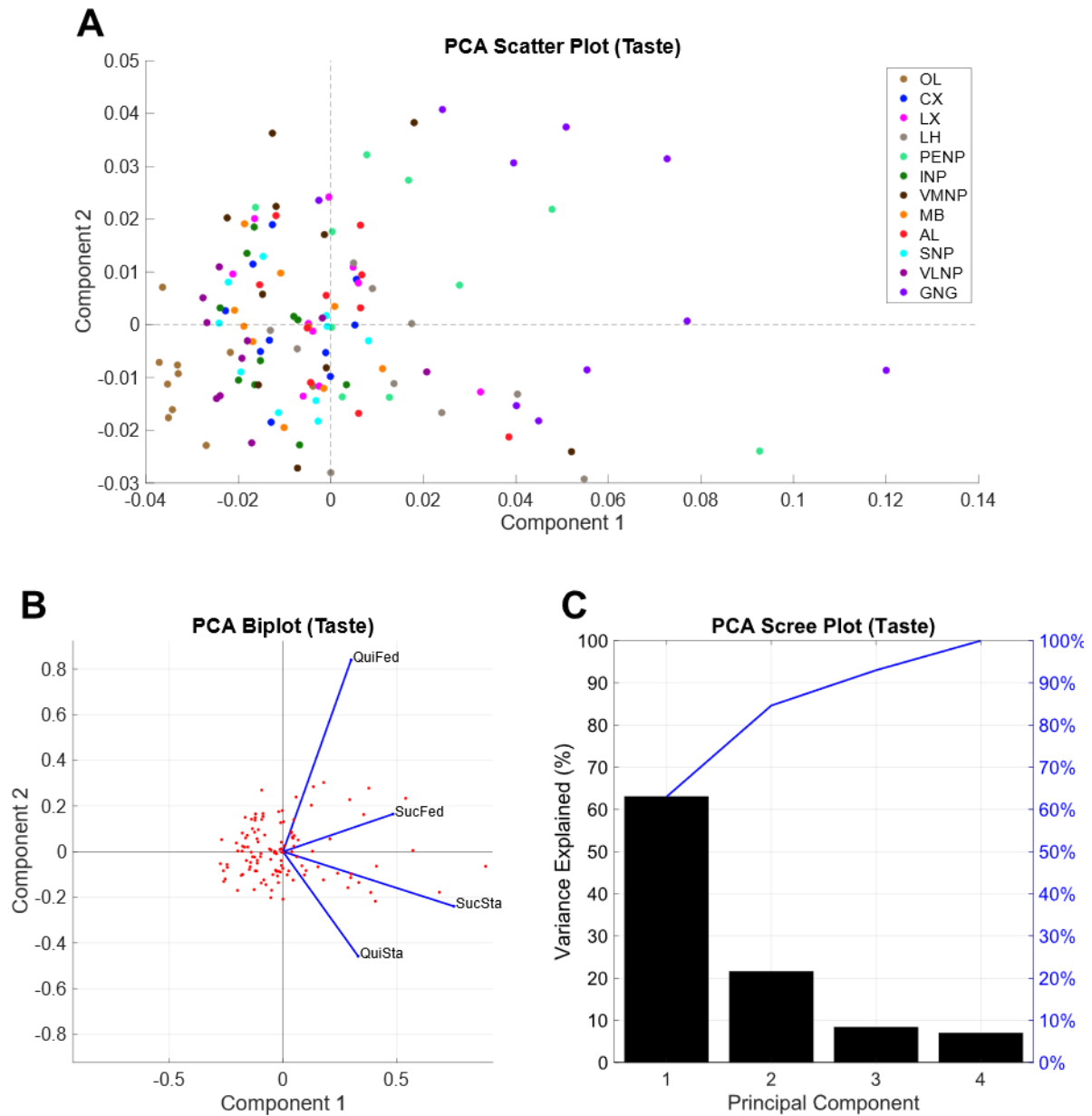


Figure 14: Principal component analysis for peak responses of taste groups

A Scatterplot for the scores of the 1st and 2nd principal component. Colors indicate the brain regions.

B Biplot for the 1st and 2nd principal component. Red dots indicate component scores (as seen in A). Blue lines indicate component coefficients for each taste group.

C Scree plot of principal components. Bars indicate the variance that is explained by each component. Blue line indicates cumulative variance.

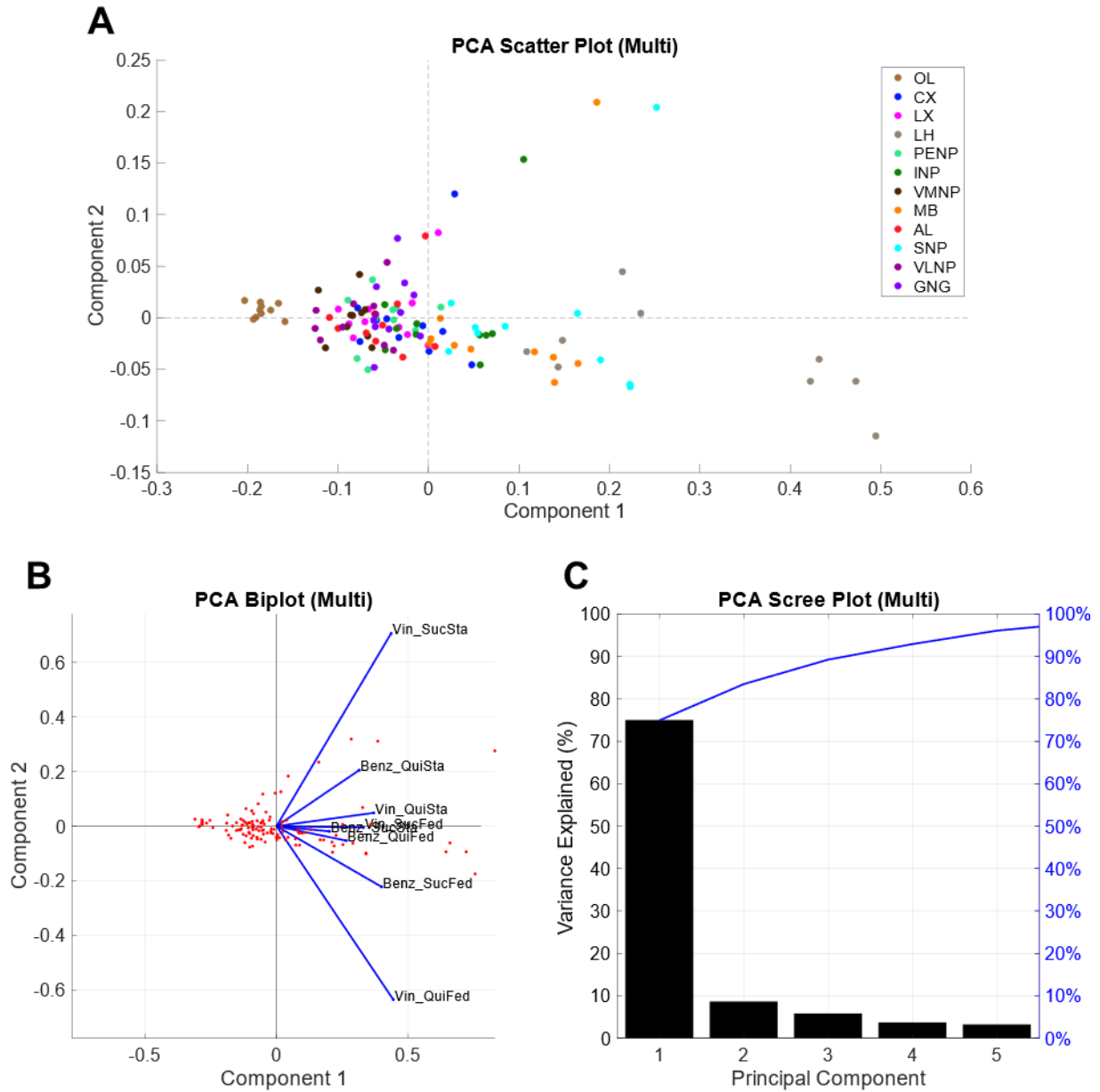
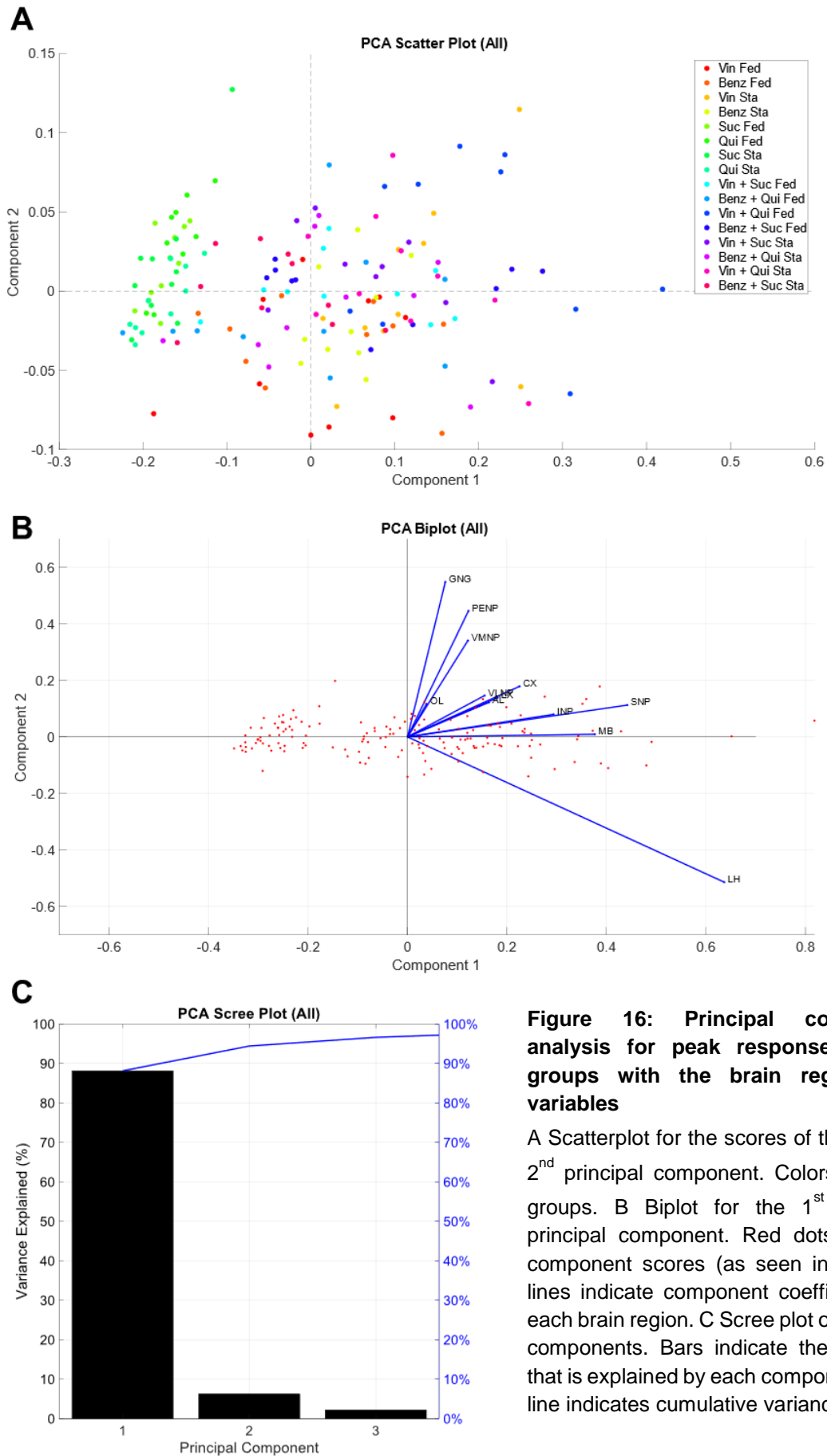


Figure 15: Principal component analysis for peak responses of multisensory groups

A Scatterplot for the scores of the 1st and 2nd principal component. Colors indicate the brain regions. **B** Biplot for the 1st and 2nd principal component. Red dots indicate component scores (as seen in A). Blue lines indicate component coefficients for each multisensory group. **C** Scree plot of principal components. Bars indicate the variance that is explained by each component. Blue line indicates cumulative variance.



Classification models can accurately predict the stimulus type from peak responses

The PCA indicated that brain regions and internal state account for the majority variance in my whole brain imaging data. Next, I wanted to test, whether I could use the same data to train supervised machine learning models to identify the classes of experimental variables. Therefore, I applied the Classification Learner App in MATLAB. I used the average peak responses in the 12 major neuropils as predictors to predict the following response variables: Stimulus type, valence, internal state, and stimulus substance. I used five different machine learning models, with different levels of complexity. Accuracy and total cost of each model are summarized in Table 10 and 11. All models performed well in predicting the stimulus type. However, they failed at the classification of the other variables such as metabolic state and only performed at or below chance level. The linear discriminant model (LDM) assumes that different classes generate data based on different Gaussian distributions. To train a classifier, the fitting function estimates the parameters of a Gaussian distribution for each class with linear boundaries between the classes (see MATLAB documentation). The LDM exhibited highest overall accuracy at the lowest total misclassification cost (i.e. sum of all false classifications with a penalty of 1). The second-best model was the medium neural network (NNM) which is a feedforward network with 25 layers, where the first fully connected layer receives input in form of the predictor data. Each subsequent layer has a connection from the previous layer. Each layer multiplies the input by a weight matrix and then adds a bias vector. An activation function follows each layer. The final layer and the subsequent softmax activation function produce classification scores and predicted classes (see MATLAB documentation). Both could correctly predict taste stimuli at 90% accuracy or above (Figure 17 A and 18 A). However, they performed less well in discriminating between odor and odor + taste. Consequently, both models predicted sucrose or quinine responses but could only poorly detected benzaldehyde or vinegar (Figure 20). Interestingly, the LDM could distinguish negative from positive or conflicting valence at relatively high rate, whereas the NNM could

not (Figure 19 A, B). I hypothesized, that not all regions are equally important as predictors, since some of them were not activated by chemosensory stimulation. Therefore, I subsequently excluded the responses from particular regions and trained the LDM and the NNM again to predict the stimulus type. The models performed best, when the responses of the OL, VLNP, VMNP and LX are excluded (Table 12). Even when the LH and the SNP were excluded as well the accuracy was still increased. However, when I also excluded the GNG and PENP the performance dropped below 70%.

When I only included the AL responses, the models could no longer identify odor (Figure A1). Vice versa, when only the GNG was used as a predictor, the models failed to predict taste (Figure A2). Interestingly, they could still predict odor + taste reasonably well in both cases.

In order to test the two models with the reduced set of predictors (OL, VLNP, VMNP and LX excluded), they were trained again on 70 percent of the data. The validation showed an average accuracy of 75% (Table 13) and both showed highest true positive rate for predicting taste class (Figure 17 B and 18 B). When testing the models on the remaining 30 percent of the data, the NNM performed better than the LDM with over 95% accuracy (Table 13). Both perfectly predicted taste, however the LDM still confused odor with odor + taste in one out of four cases (Figure 17 C and 18 C).

These results indicate that it is possible to predict stimulus type from the peak activity in major brain regions. However, mainly the responses in relevant chemosensory regions contain the necessary information, whereas responses in other regions contain are noisier and therefore reduce the accuracy of the classification models.

Table 10: Classification model accuracy in percent

Class	Fine Tree	Linear Discriminant	Quadratic Discriminant	Medium KNN	Medium Neural Network
Stimulus Type	76,8	76,8	82,3	78,7	78
Internal State	50	51,2	56,7	51,2	53
Valence	44,5	55,5	54,9	53,7	53,7
Substance	35,4	47,6	28,7	38,4	41,5
Average	51,675	57,775	55,65	55,5	56,55

Table 11: Classification model total cost

Class	Fine Tree	Linear Discriminant	Quadratic Discriminant	Medium KNN	Medium Neural Network
Stimulus Type	38	38	29	35	-
Internal State	82	80	71	80	-
Valence	91	73	74	76	-
Substance	106	86	117	101	-
Average	79,25	69,25	72,75	73	-

Table 12: Model accuracy for predicting stimulus type from different datasets in percent

Excluded Responses	Linear Discriminant	Medium Neural Network	Average	Included Responses
OL, VLNP, VMNP, LX	81,7	83,5	82,6	AL, MB, LH, SNP, INP, CX, PENP, GNG
OL, VLNP, VMNP, LX, CX	82,3	79,3	80,8	AL, MB, LH, SNP, INP, PENP, GNG
OL, VLNP, VMNP, LX, AL	80,5	79,3	79,9	MB, LH, SNP, INP, CX, PENP, GNG
OL, VLNP	78,7	78,7	78,7	AL, MB, LH, SNP, INP, CX, PENP, GNG, VMNP, LX
OL, VLNP, VMNP, LX, LH, SNP	79,3	78	78,65	AL, MB, INP, CX, PENP, GNG
None	76,8	78	77,4	All
OL, VLNP, VMNP, LX, INP, MB	76,2	75	75,6	AL, MB, LH, SNP, PENP, GNG
OL, VLNP, VMNP, LX, CX, INP	75,6	74,4	75	AL, MB, LH, SNP, INP, PENP, GNG
OL, VLNP, VMNP, LX, GNG, PENP	68,3	69,5	68,9	AL, MB, LH, SNP, INP, CX
OL, VLNP, VMNP, LX, CX, INP, GNG, PENP, LH, SNP	67,7	66,5	67,1	AL, MB
OL, VLNP, VMNP, LX, CX, INP, GNG, PENP	67,1	66,5	66,8	AL, MB, LH, SNP
OL, VLNP, VMNP, LX, CX, INP, GNG, PENP, LH, SNP, MB	62,2	59,8	61	AL
OL, VLNP, VMNP, LX, CX, INP, PENP, LH, SNP, MB, AL	55,5	46,3	50,9	GNG

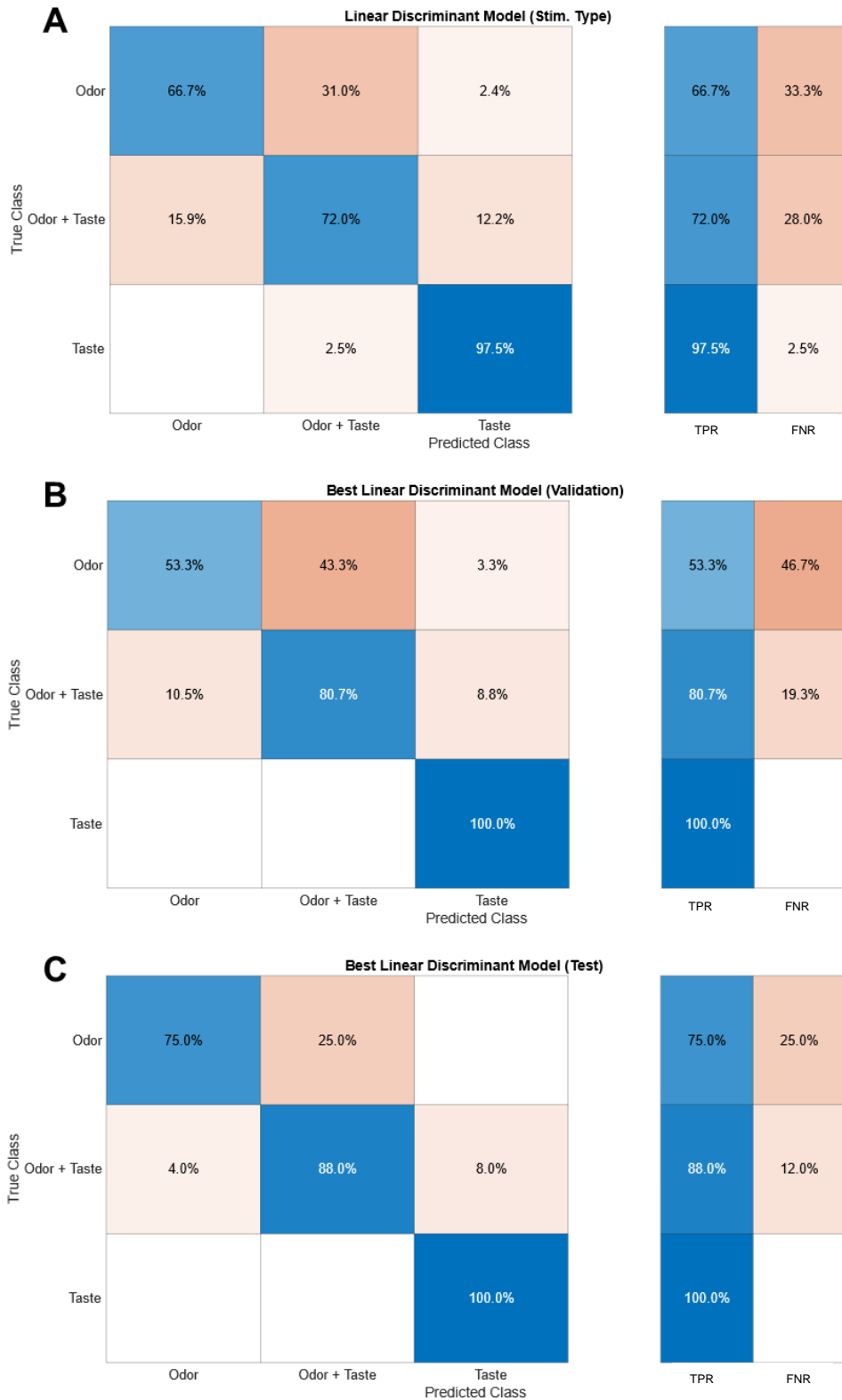


Figure 17: Linear discriminant classification model predicts stimulus type

A Confusion matrix for the linear discriminant model (LDM) predicting the stimulus type from the full data set. **B** Confusion matrix for validation the best LDM (responses from the OL, VLNP, VMNP and LX excluded) on a training dataset (70% all observations). **C** Confusion matrix for the performance of the best LDM on a test dataset (30% of all observations). TPR=true positive rate, FNR=false negative rate.

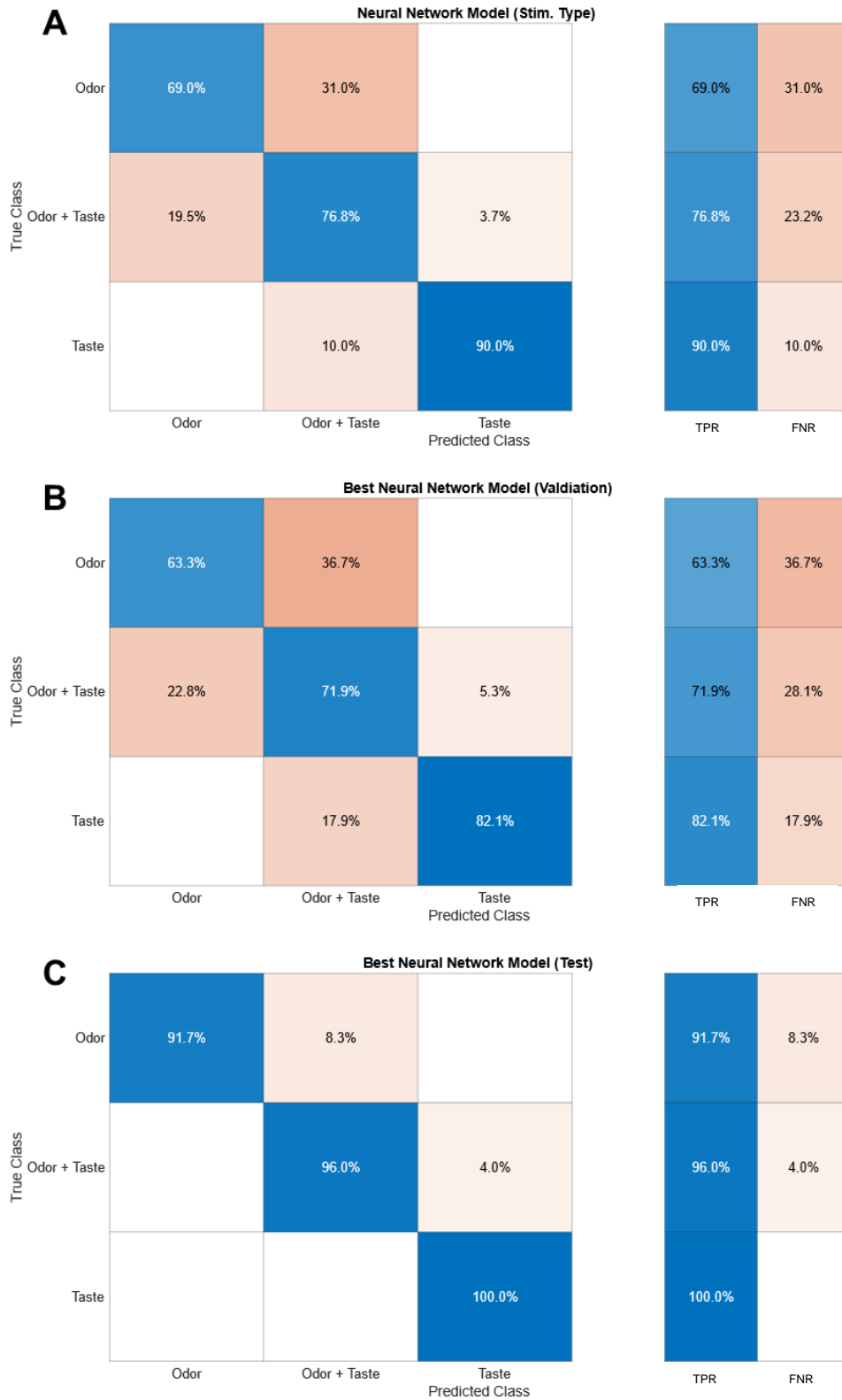


Figure 18: Neural network classification model predicts stimulus type

A Confusion matrix for the neural network model (NNM) predicting the stimulus type from the full data set. **B** Confusion matrix for validation the best NNM (responses from the OL, VLNP, VMNP and LX excluded) on a training dataset (70% all observations). **C** Confusion matrix for the performance of the best NNM on a test dataset (30% of all observations). TPR=true positive rate, FNR=false negative rate.

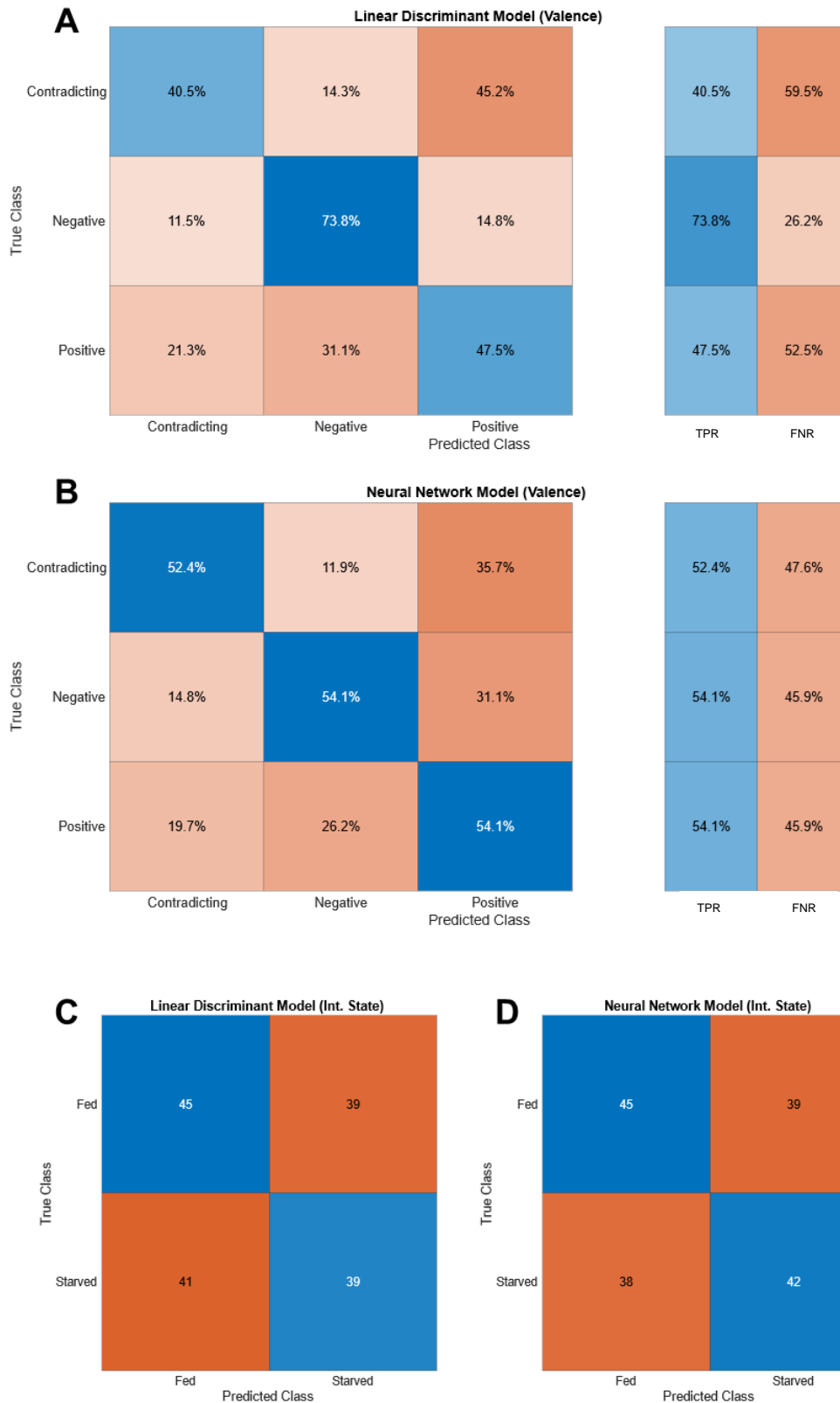


Figure 19: Classification models predicting valence and internal state

Confusion matrices for (A) the linear discriminant model and (B) the neural network model predicting the valence of the stimulus. Confusion matrices for (C) the linear discriminant model and (D) the neural network model predicting the internal state of the animal. TPR=true positive rate, FNR=false negative rate. C and D show total observations.

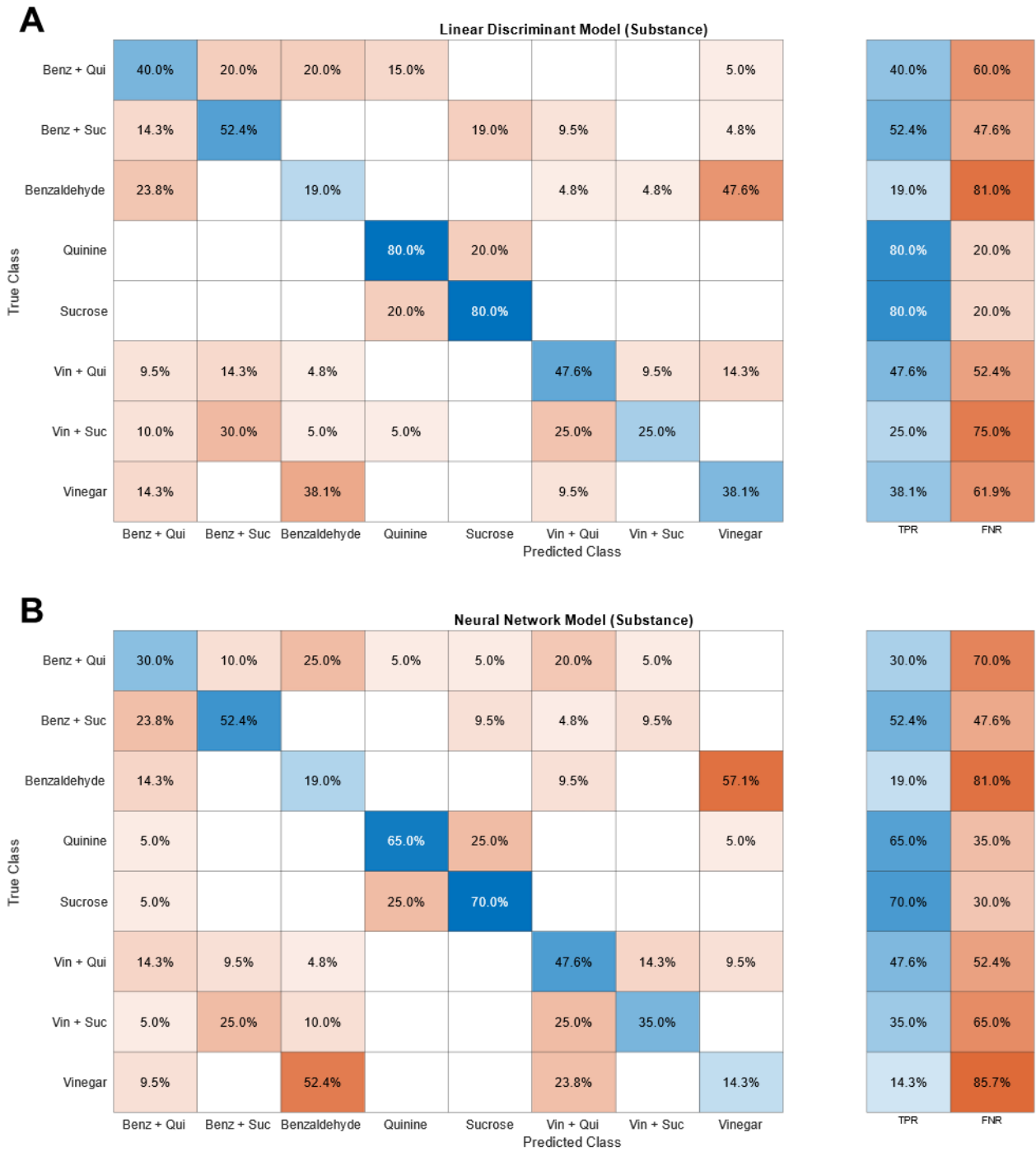


Figure 20: Classification models predicting the stimulus substance
 Confusion matrices for (A) the linear discriminant model and (B) the neural network model predicting the stimulus substance. TPR=true positive rate, FNR=false negative rate.

Given that stimuli of different valence had opposing effects in fed and starved flies, depending on the internal state (see Figure 11 C, D), I asked whether the internal state and stimulus valence can be predicted from a dataset that only includes odor or taste (or multisensory) responses. Therefore, I trained the NNM and the LDM again and tested the performance. Indeed, I found that both models could classify the metabolic state with an average accuracy of 75 percent, when trained with just odor or taste responses. However, the accuracy dropped to chance level when the multisensory dataset was used (Table 14). Notably, the stimulus valence could also be predicted with high accuracy in the taste responses, but less precise in the odor and multisensory responses (Table 15). Overall, the NNM seemed to do a better job in predicting the variables than the LDM (Figure 21-23, Figure A3-A5). Interestingly, both models were better at predicting the fed state than the starved state. This suggests that metabolic state and to some degree also the stimulus valence are represented by whole brain neuronal activity but the machine learning algorithms could only classify the variables from odor and taste responses alone, but not from combined stimulation.

Table 13: Accuracy for the best classification models (responses from OL, VLNP, VMNP and LX excluded)

Dataset	Linear Discriminant	Medium Neural Network	Average
Training (70%)	78,3	72,2	75,25
Test (30%)	87,8	95,9	91,85

Table 14: Accuracy for LD and NN classification models predicting internal state in percent (models include responses from all regions)

Stimulus Type	Dataset	Linear Discriminant	Medium Neural Network	Average
Odor	Training (70%)	66,7	70	68,35
	Test (30%)	66,7	83,3	75
Taste	Training (70%)	46,4	64,3	55,35
	Test (30%)	75	75	75
Odor + Taste	Training (70%)	48,3	53,4	50,85
	Test (30%)	41,7	50	45,85
O + T Matching	Training (70%)	50	60,7	55,35
	Test (30%)	58,3	41,7	50
O + T Contra	Training (70%)	53,3	46,7	50
	Test (30%)	58,3	50	54,15

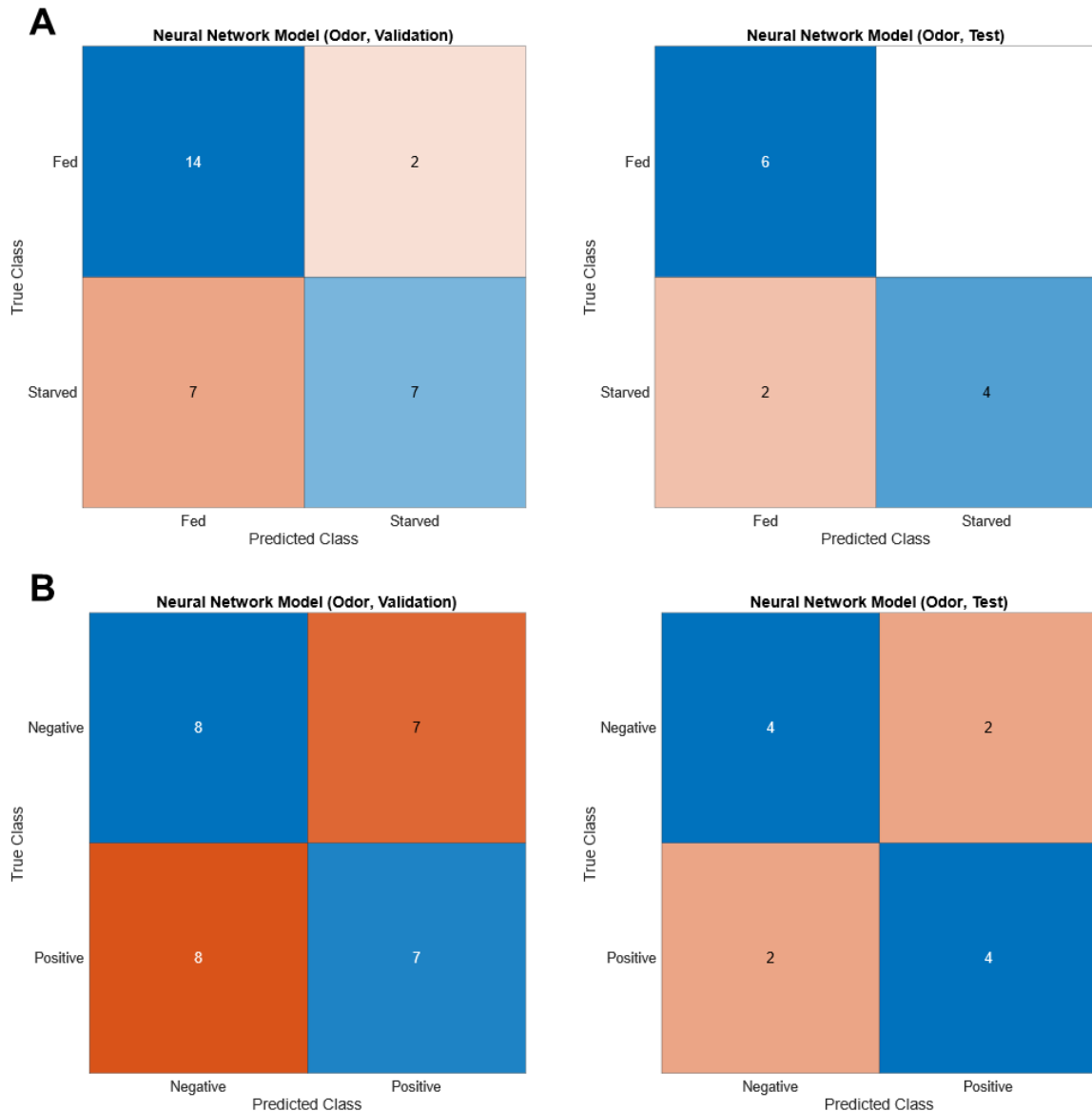


Figure 21: Neural network classification model predicts internal state and valence from odor data

A Confusion matrices for the neural network model (NNM) predicting the internal state of the flies from the odor data set. Left: Model validation for the training dataset (70% of all odor observations). Right: Model performance on the test dataset (30% of all odor observations). **B** Confusion matrices for the neural network model (NNM) predicting the valence of the stimulus from the odor data set. Left: Model validation for the training dataset (70% of all odor observations). Right: Model performance on the test dataset (30% of all odor observations). Numbers indicate total observations.

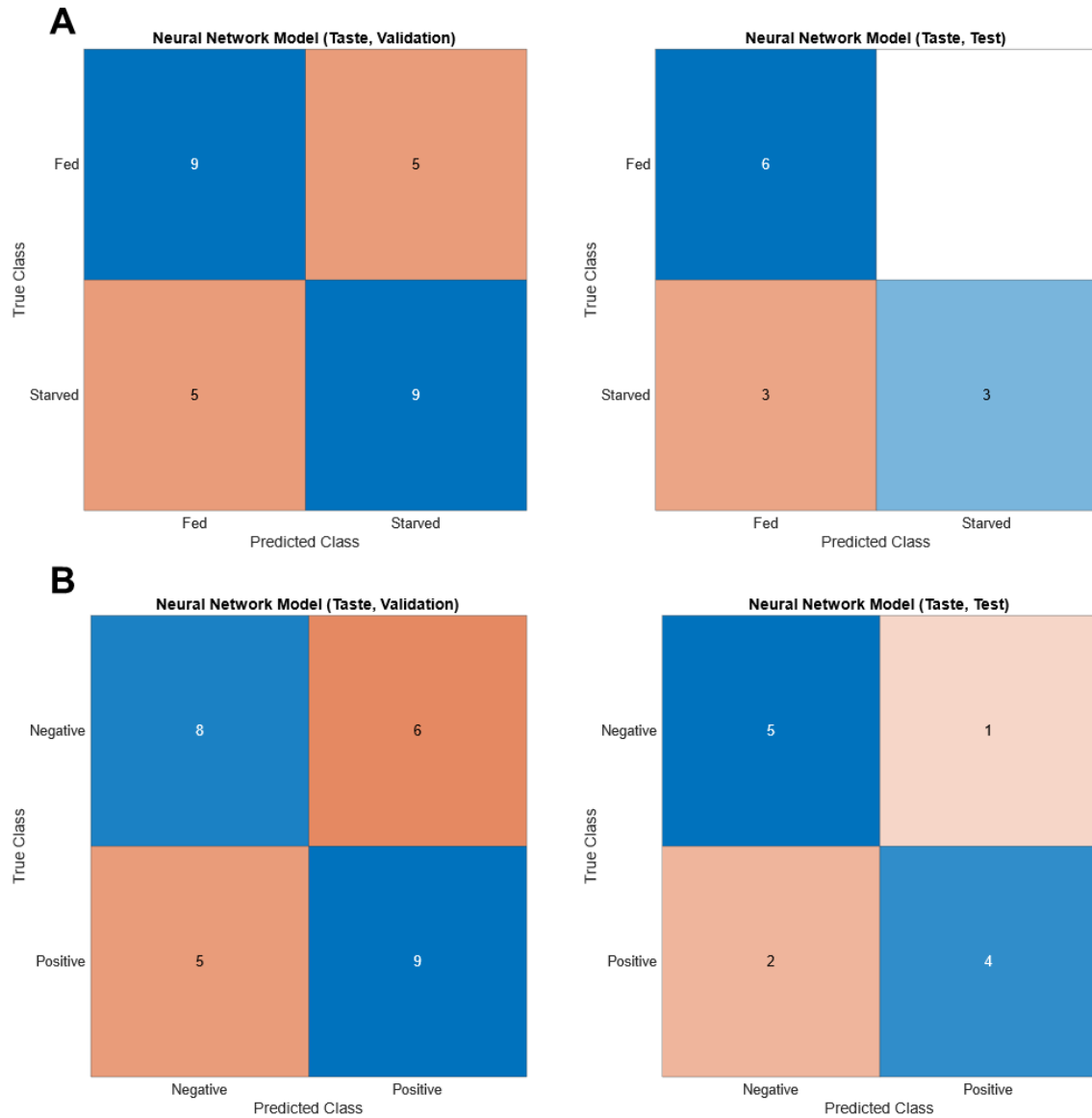


Figure 22: Neural network classification model predicts internal state and valence from taste data

A Confusion matrices for the neural network model (NNM) predicting the internal state of the flies from the taste data set. Left: Model validation for the training dataset (70% of all taste observations). Right: Model performance on the test dataset (30% of all taste observations). **B** Confusion matrices for the neural network model (NNM) predicting the valence of the stimulus from the taste data set. Left: Model validation for the training dataset (70% of all taste observations). Right: Model performance on the test dataset (30% of all taste observations). Numbers indicate total observations.

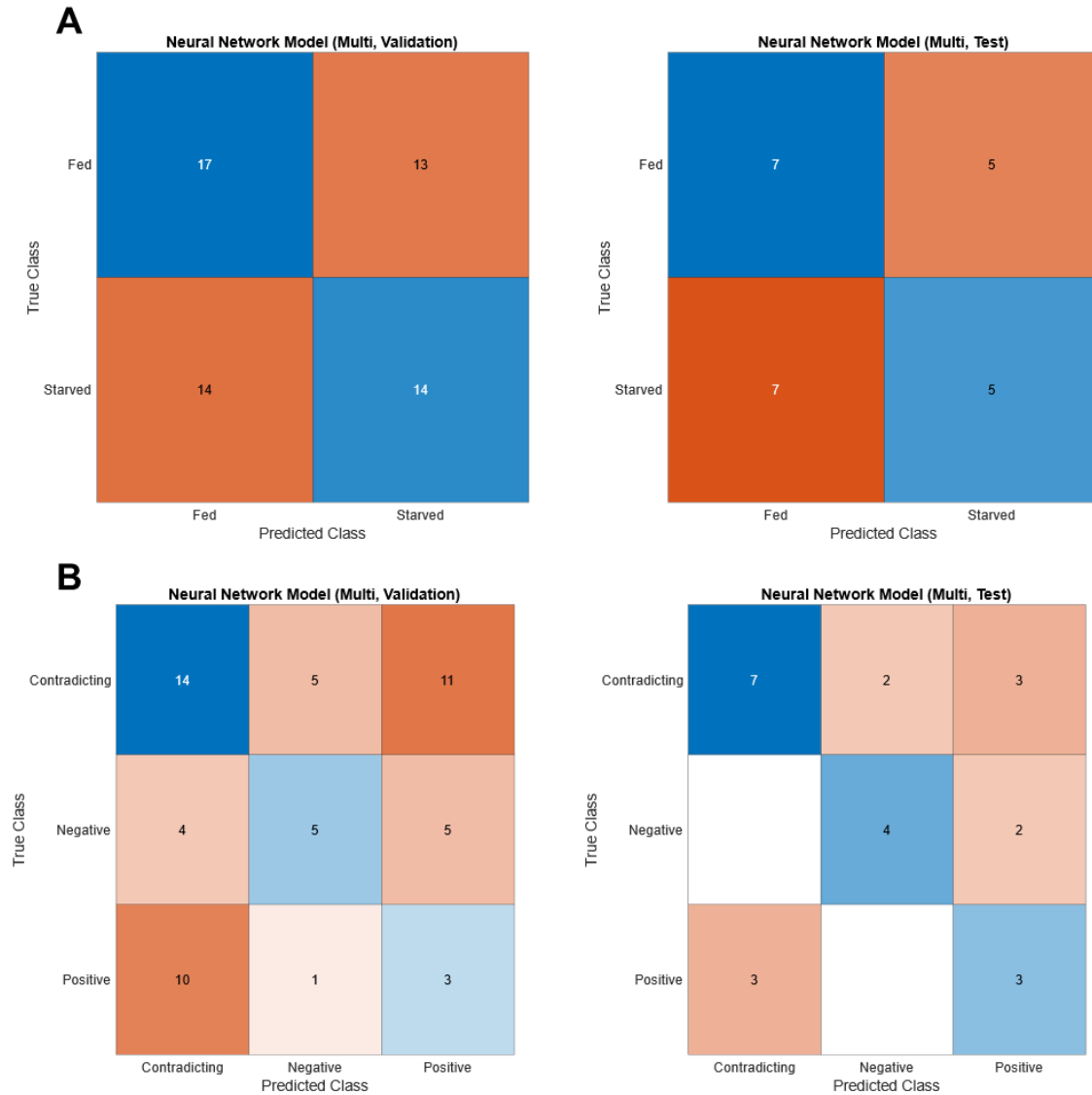


Figure 23: Neural network classification model predicts internal state and valence from multisensory data

A Confusion matrices for the neural network model (NNM) predicting the internal state of the flies from the multisensory data set. Left: Model validation for the training dataset (70% of all multisensory observations). Right: Model performance on the test dataset (30% of all multisensory observations). **B** Confusion matrices for the neural network model (NNM) predicting the valence of the stimulus from the multisensory data set. Left: Model validation for the training dataset (70% of all multisensory observations). Right: Model performance on the test dataset (30% of all multisensory observations). Numbers indicate total observations.

Since the models were unreliable in predicting valence and state from multisensory responses, I wondered whether this was due the effect of the difference between matching and contradicting pairs of stimuli rather than stimulus modality. Therefore, I separated both data sets and trained the classification models again. The analysis indicated that both models fail to predict internal state, even if I separated the two datasets (Table 14). The LDM performed slightly better than the NNM (Figure 24, Figure A6), but only with an accuracy of 58 % during testing. This shows that in contrast to unimodal stimulation, the global activity caused by matching or conflicting combinations of stimuli did not differ between fed and starved flies. Interestingly, both models could predict the valence of the stimulus pairs with 75 percent or higher (Table 15). The NNM did a slightly better job at classifying the contradicting combinations than the LDM (Figure 25, Figure A7). This suggests that whole brain activity towards multimodal chemosensory stimulation can encode for valence of the stimulus pairs, however they can only be correctly classified when the responses to matching and conflicting valence pairs are separately used as inputs, since I would expect an overlap of activity between both groups that cannot be resolved. For example, it might not be possible to detect whether vinegar was paired with sucrose or quinine taste, because the response profiles are too similar.

Table 15: Accuracy for LD and NN classification models predicting valence in percent (models include responses from all regions)

Stimulus Type	Dataset	Linear Discriminant	Medium Neural Network	Average
Odor	Training (70%)	40	50	45
	Test (30%)	66,7	66,7	66,7
Taste	Training (70%)	60,7	60,7	60,7
	Test (30%)	75	75	75
Odor + Taste	Training (70%)	46,6	37,9	42,25
	Test (30%)	54,2	58,3	56,25
O + T Matching	Training (70%)	71,4	71,4	71,4
	Test (30%)	75	75	75
O + T Contra	Training (70%)	66,7	76,7	71,7
	Test (30%)	75	83,3	79,15

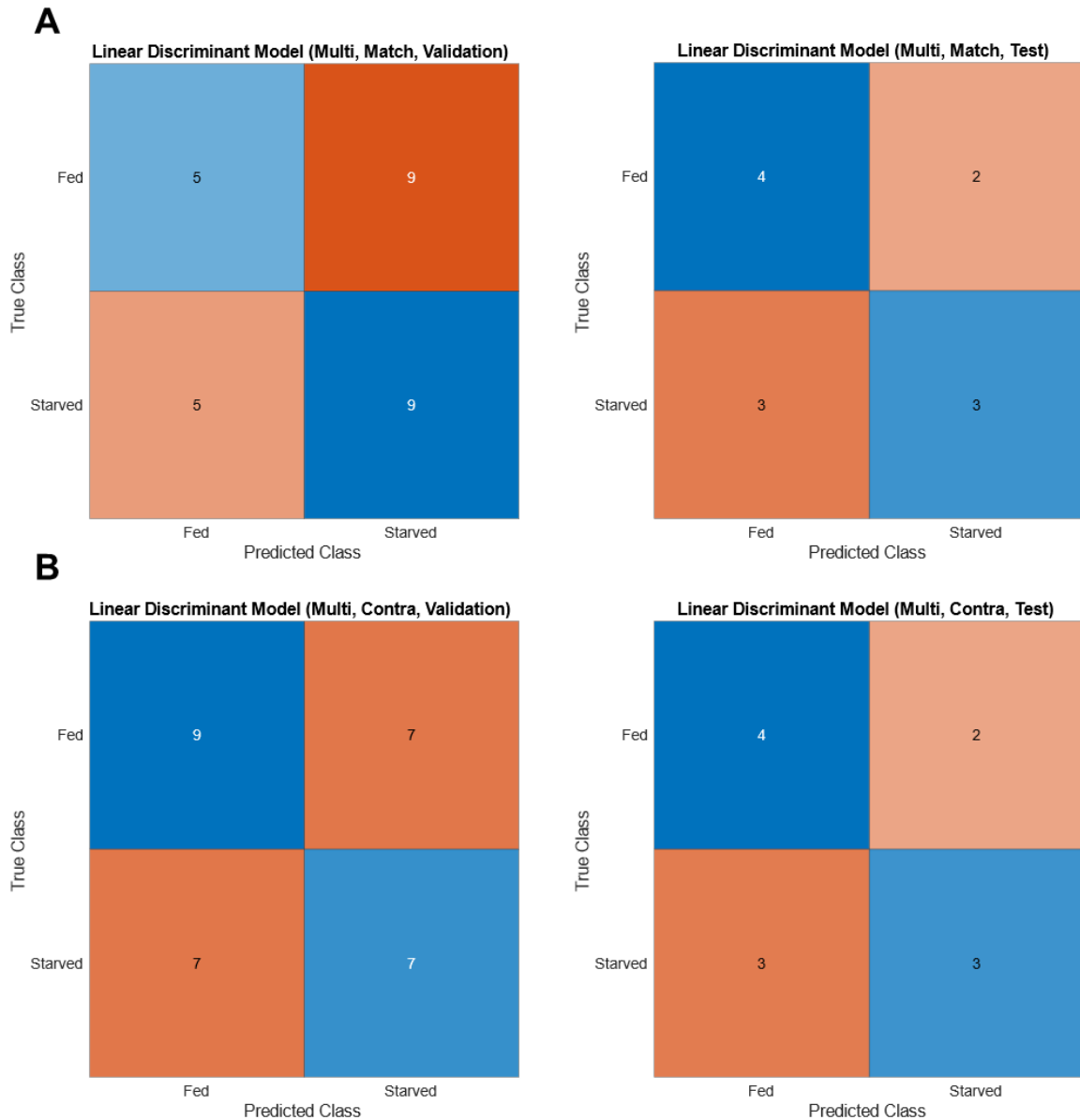


Figure 24: Linear discriminant classification model fails to predict internal state from multisensory datasets

A Confusion matrices for the linear discriminant model (LDM) predicting the internal state of the flies from the multisensory data with stimuli of matching valence. Left: Model validation for the training dataset (70% of all multisensory observations). Right: Model performance on the test dataset (30% of all multisensory observations). **B** Confusion matrices for the linear discriminant model (LDM) predicting the valence of the stimulus from the multisensory data with stimuli of contradicting valence. Left: Model validation for the training dataset (70% of all multisensory observations). Right: Model performance on the test dataset (30% of all multisensory observations). Numbers indicate total observations.

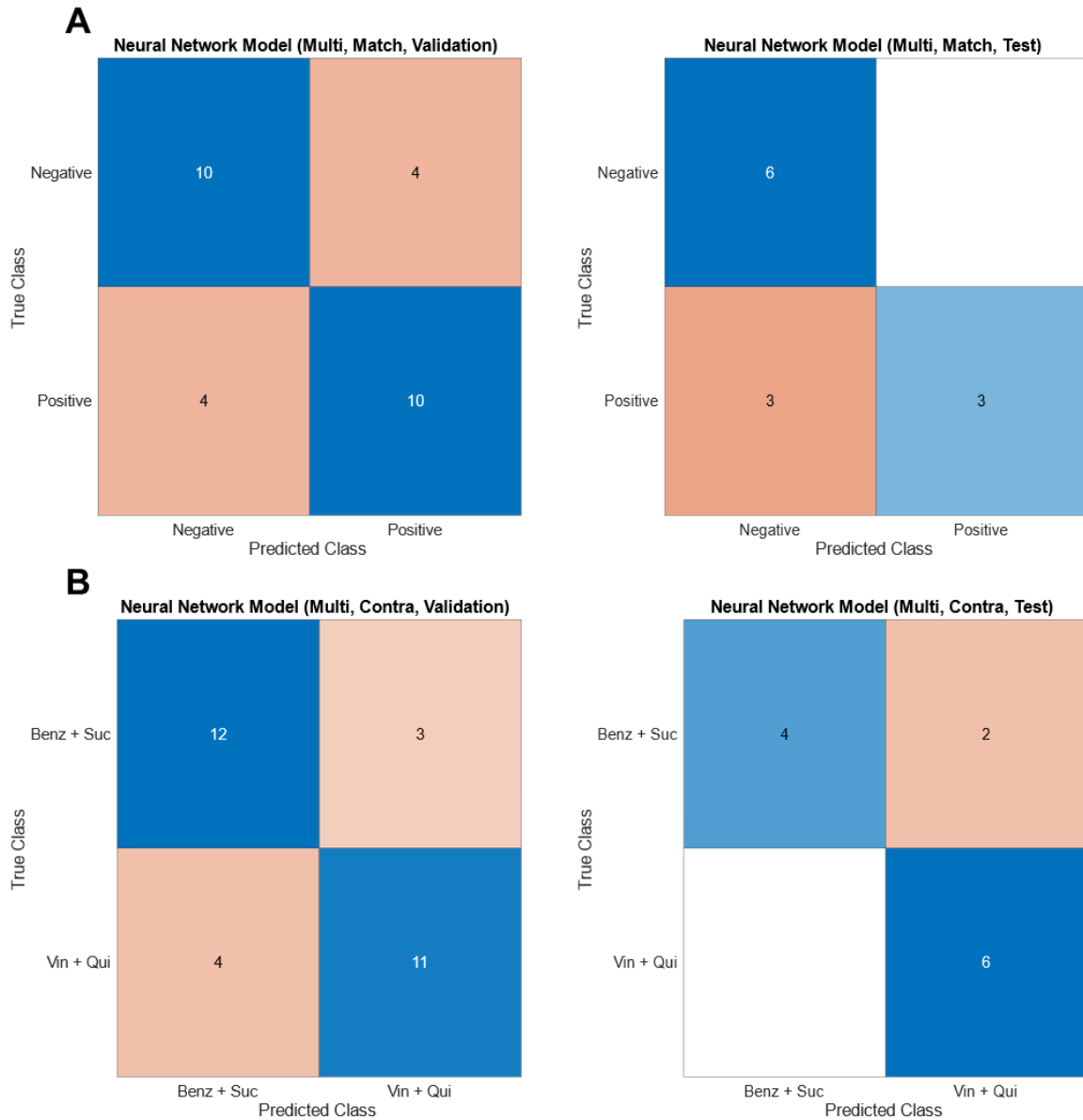


Figure 25: Neural network classification model predicts valence from multisensory data sets

A Confusion matrices for the neural network model (NNM) predicting valence of the stimulus pair from the multisensory data with stimuli of matching valence (Positive: Vinegar + Sucrose, negative: Benzaldehyde + Quinine). Left: Model validation for the training dataset (70% of all multisensory observations). Right: Model performance on the test dataset (30% of all multisensory observations). **B** Confusion matrices for the neural network model (NNM) predicting the valence of the stimulus from the multisensory data with stimuli of contradicting valence. Left: Model validation for the training dataset (70% of all multisensory observations). Right: Model performance on the test dataset (30% of all multisensory observations). Numbers indicate total observations.

Chemosensory-specific functional components can be obtained from spatial ICA

In order to reduce the dimensionality of the data and gain spatial resolution, independent components for each recording were extracted as described previously by (Aimon et al. 2019; Aimon et al. 2022). The algorithm plots voxels that show highly correlated activity over time as spatial maps, which are termed components. However, the functional components that resemble neuronal ensembles and show correlated activity with the actual stimulus needed to be sorted and annotated by eye in every recording. Afterwards, I compiled a list of 10-30 components for each fly and matched them among the groups. I excluded those components that did not appear consistently (i.e. at least three times or more in one group). In the end, I found 26 functional components that showed correlated activity during chemosensory stimulation. For each component and every fly, I extracted the dF/F time series (Figure A19-A31), calculated the peak response to the first stimulation and averaged the result for every group (Figure 26 C). I multiplied the average peak response with the frequency of each component (Figure 26 A) to estimate the relevance of each component (Figure 27 A). This way, components that appeared often and had a high peak response were assigned a high relevance score, whereas rare components with low response scored low, which made the resulting heat map clearer. Most components were odor-related, as they appeared in the odor or the odor + taste groups. Especially, components in the superior part of the brain were very prominent. I found three components that are most likely “LH-PNs” (lateral horn-projection neurons), that project from the AL to different parts of the LH (Figure 27 B). The other three components label parts of the SNP and might overlap with LH output neurons (“SLP”, “LH-SIP”) or MB output neurons (“SMP-SIP”, Dolan et al. 2019; Das Chakraborty and Sachse 2021). Interestingly, “LH-SIP” consistently showed higher scores in the presence of vinegar and was also found in taste-only experiments (Figure 26 A). I found three components that overlapped with the MB calyx and the MB peduncle, which I named “PN-KC”, because they are likely to label projection neurons that synapse onto the Kenyon cells (KCs) at the level of

the calyx (Masse et al. 2009). Consequently, I also found four components that anatomically match the KCs in different MB compartments (“gamma”, “beta”, “alpha-beta” and “alpha KCs”). The “alpha-beta KC” component was also found in some of taste recordings, although the response was only low (Figure 26 C). I also found a component that matched the AL. This likely labels the AL hub, which consists of a dense network of local neurons (Ito et al. 2014). Interestingly, this component also could be found during taste stimulation. Even though, I did not find components that consistently label individual AL glomeruli, the spatial ICA on the functional imaging was able to recapitulate every other step in the olfactory pathway (Stocker 2009).

However, the algorithm also detected functional components that were not part of the canonical olfactory pathway in the central complex (CX) that relatively consistently responded to odor cues but less frequent to multisensory stimulation (Figure 26 A). The fan-shaped body (“FB”), for example is known to be involved in nociceptive avoidance (Hu et al. 2018), promotes arousal (Kato et al. 2022) or encodes airflow direction (Currier et al. 2020). It closely interacts with the ellipsoid body (“EB”) in visual pattern memory (Pan et al. 2009), whereas the protocerebral bridge (“PB”) regulates sleep (Tomita et al. 2021). Since these neuropils seem to be involved in a number of functions, it is not that surprising that they were also active during chemosensation. One of the most frequent components, I named “PLP” after the posterior-lateral protocerebrum as this component anatomically matched this brain region. This region receives many visual projections (Ito et al. 2014) but in this case it showed robust odor responses and was also present during taste-only conditions. The spatial maps suggest that neurites originate in a more inferior part of the brain (Figure 27 B), where I found two rare components in the wedge (“WED”, “WED-PN”). These components looked very similar and were hard to distinguish. In most animals they appeared as one component, but in some animals, they appeared separately. The wedge is anatomically closely connected with the antennal mechanosensory and motor center (AMMC, Ito et al. 2014). The “AMMC” showed up as components on its own, but oddly only in multisensory recordings. The signal for this

component was ramping already before the onset of the stimulus (Figure A19 B), during the phase where the taste drop is brought closer to the head of the fly. The signal might represent a stimulation of humidity sensing receptors on the antennae that respond to an increase of water vapor as the drop is approaching the fly's head (Enjin et al. 2016; Li et al. 2022). On the other hand, the AMMC also receives mechanosensory input via the antennae (Patella and Wilson 2018). In the taste-only experiments, I did not detect this signal because the antennae were removed (see methods). The least frequent component was the flange ("FLA"), which was only found in fed flies stimulated with taste. This structure lies very close to the esophagus and showed some activity that could be attributed to the residual motion of the feeding apparatus (Figure A21 B).

The most prominent taste components were the prow ("PRW") and the gnathal ganglia ("GNG"). Both showed high scores in taste and multisensory experiments (Figure 27 A). The PRW was even more frequent than the GNG and showed small responses in a few odor-only flies (Figure A29 B). The PRW is the most anterior part of the SEZ and lies above the GNG (Ito et al. 2014). As mentioned previously, the GNG is the primary gustatory center of the fly brain. Within the GNG the axons of sweet and bitter GRNs project in distinct patterns (Wang et al. 2004; Marella et al. 2006). However, the ICA approach was not able to separate those patterns. Similar to the AL glomeruli, imaging at higher magnification would likely be necessary. In addition, the position of the head is not ideal for imaging the GNG, as it is located far from the focal plane. Hence other studies use a different angle, although this requires to fully remove the antennae (e.g. Münch et al. 2022). There was another component located at the level of the SEZ, which I termed "GNG (paired)", because the algorithm separated this component into two symmetric parts on each hemisphere. This was actually true for most of the other components but not for the "PRW" or the "GNG". It also labels the most ventral part of the GNG as well as some parts near the AL. Interestingly, "GNG (paired)" was only observed when odor and taste were presented in combination and therefore could be a site of multisensory integration. Since the SEZ is a relatively large region and contains very little

anatomical landmarks, it is difficult to estimate what neural correlates “GNG (paired)” might depict. I browsed through “FlyCircuit”, in order to find a neuron that looks similar to the component. I found VGlut-F-800026 (Figure 28 B, Chiang et al. 2011), which has significant overlap with 9 other neurons that form a cluster (cluster 942), according to their NBLAST scores (Costa et al. 2016, Table 16, Figure 28 D). Those neurons show dendritic arborization in the SEZ as well as the inferior part of the AL. This could mean that they relay or receive information between or from, the primary odor and taste centers, respectively and play a role in chemosensory integration. Then, I used the NBLAST feature on “Virtual Fly Brain” to find GAL4-driver lines, which expression patterns overlap with VGlut-F-800026. Unfortunately, I did not find GAL4-lines that label neuronal subsets showing high anatomical similarity with VGlut-F-800026. The highest overlay was detected with SS01576 (Figure 28 C), a line that is labeling two descending neurons (DNs, Namiki et al. 2018). Even though, the measured congruence is relatively small, it could be worth investigating the role of these neurons in chemosensory integration. A list of potential candidate neurons for most of the other functional components can be found in the appendix (Table A9).

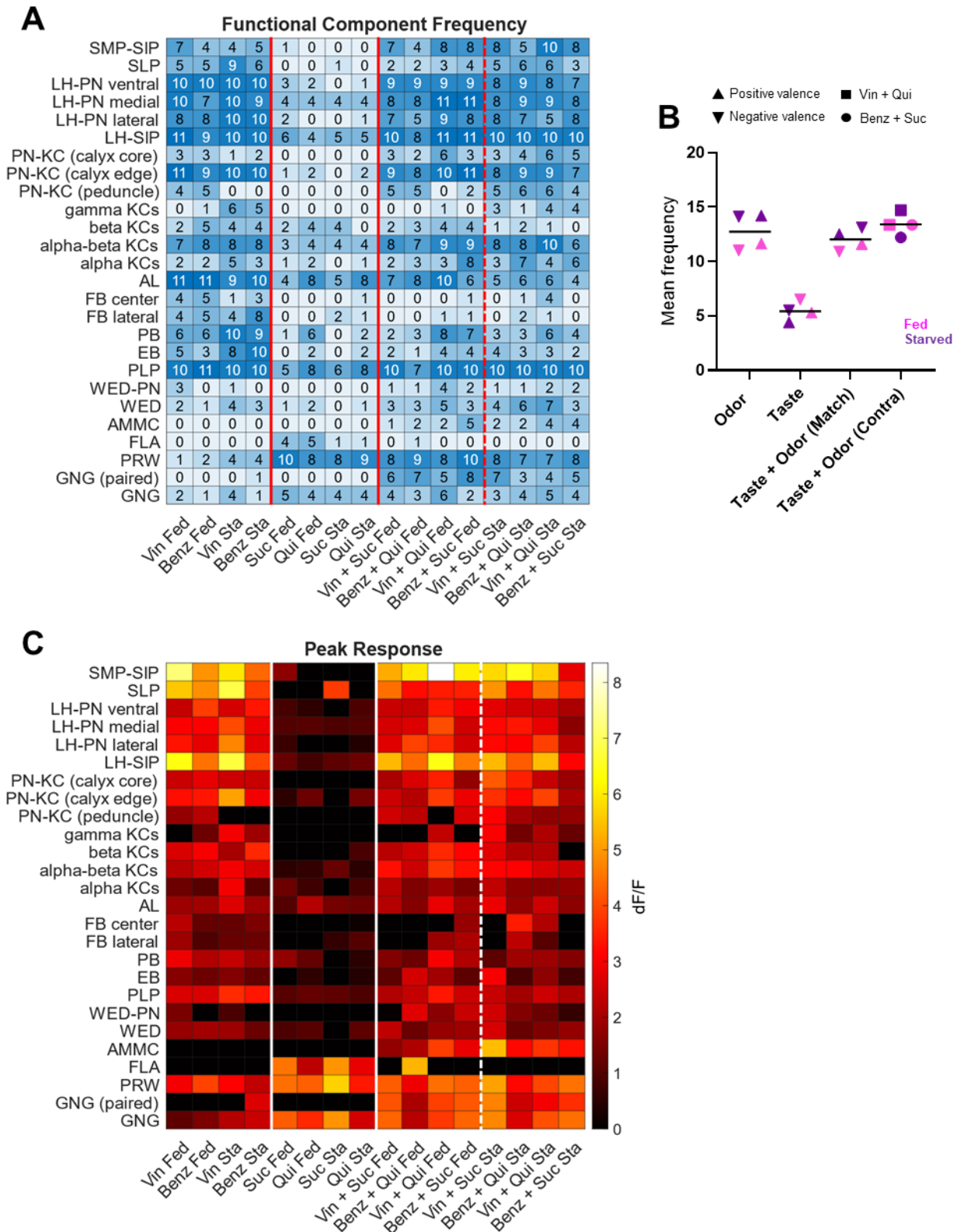


Figure 26: Functional component frequency and peak response

A Frequency of each functional component per group (i.e. How many individuals in this group showed this particular component?) **B** Component frequency averaged across animals per group. Horizontal line indicates mean across groups. **C** Mean peak response of each functional component to the first stimulation per group. Average traces for each component can be found in the appendix (Figure A9 to A20).

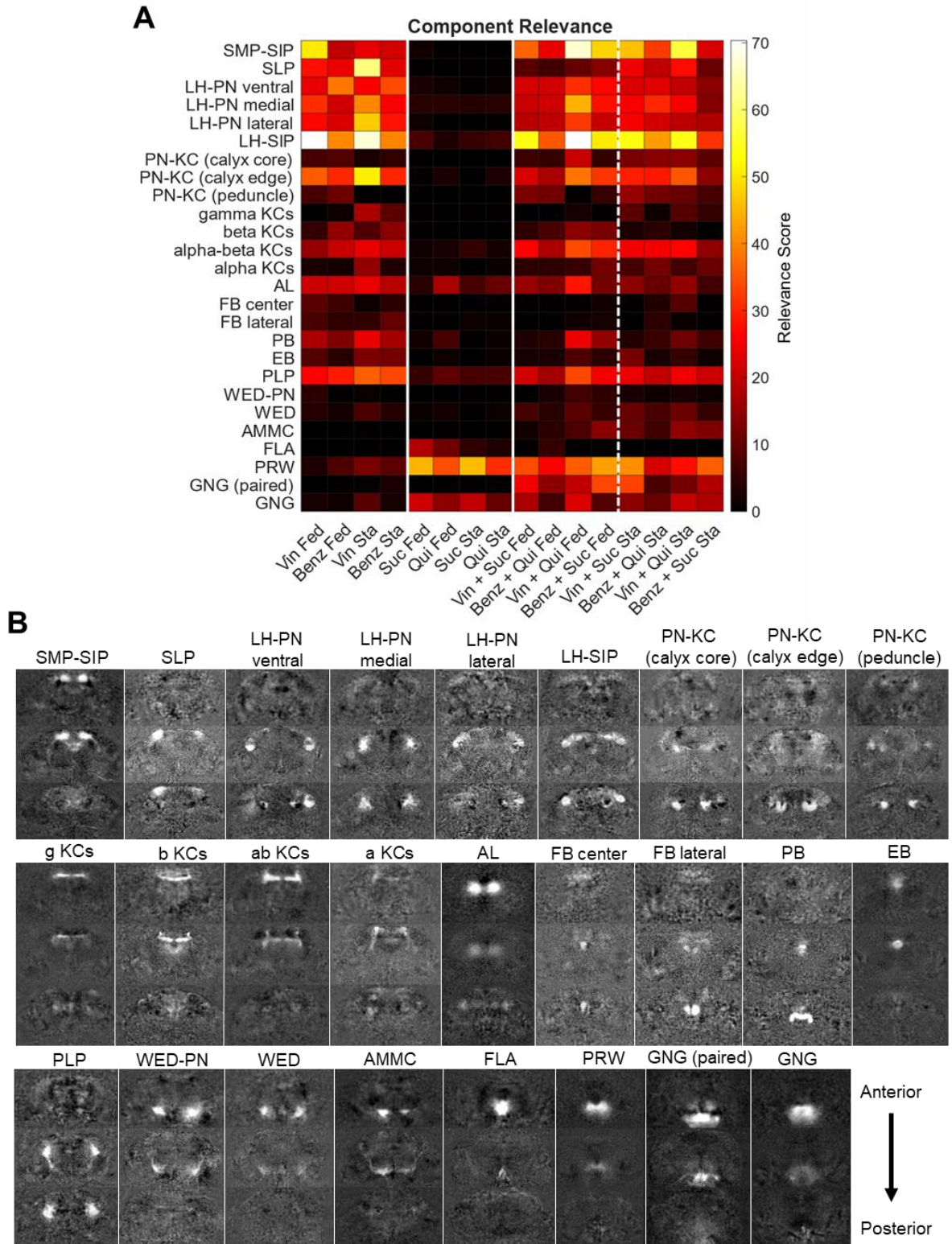


Figure 27: Most relevant functional components derived from ICA

A Heatmap of relevance score for each component in each group. The relevance score is calculated by multiplication of the component frequency and its mean peak response to the first stimulation per group. **B** Example images for each of the most relevant components which were derived from ICA and show high correlation with the stimulus.

Table 16: Finding neural correlates for GNG (paired) component

Starting neuron found in FlyCircuit:	VGlut-F-800026	NBLAST score	Labelled cell types (FlyLight)
Neurons with similar morphology (NBLAST):	VGlut-F-000195	0,77	
	VGlut-F-000004	0,72	
	VGlut-F-000346	0,69	
	VGlut-F-200236	0,57	
	VGlut-F-000418	0,52	
	Cha-F-600003	0,49	
	Cha-F-100061	0,57	
	fru-M-300037	0,59	
	fru-F-000087	0,55	
Expression patterns with similar morph (VFB):	SS01576	0,36	DNd02, DNd03
	SS01570	0,35	DNd02, DNd03
	SS01569	0,31	DNd02, DNd03
	SS01545	0,27	DNd02, DNd03

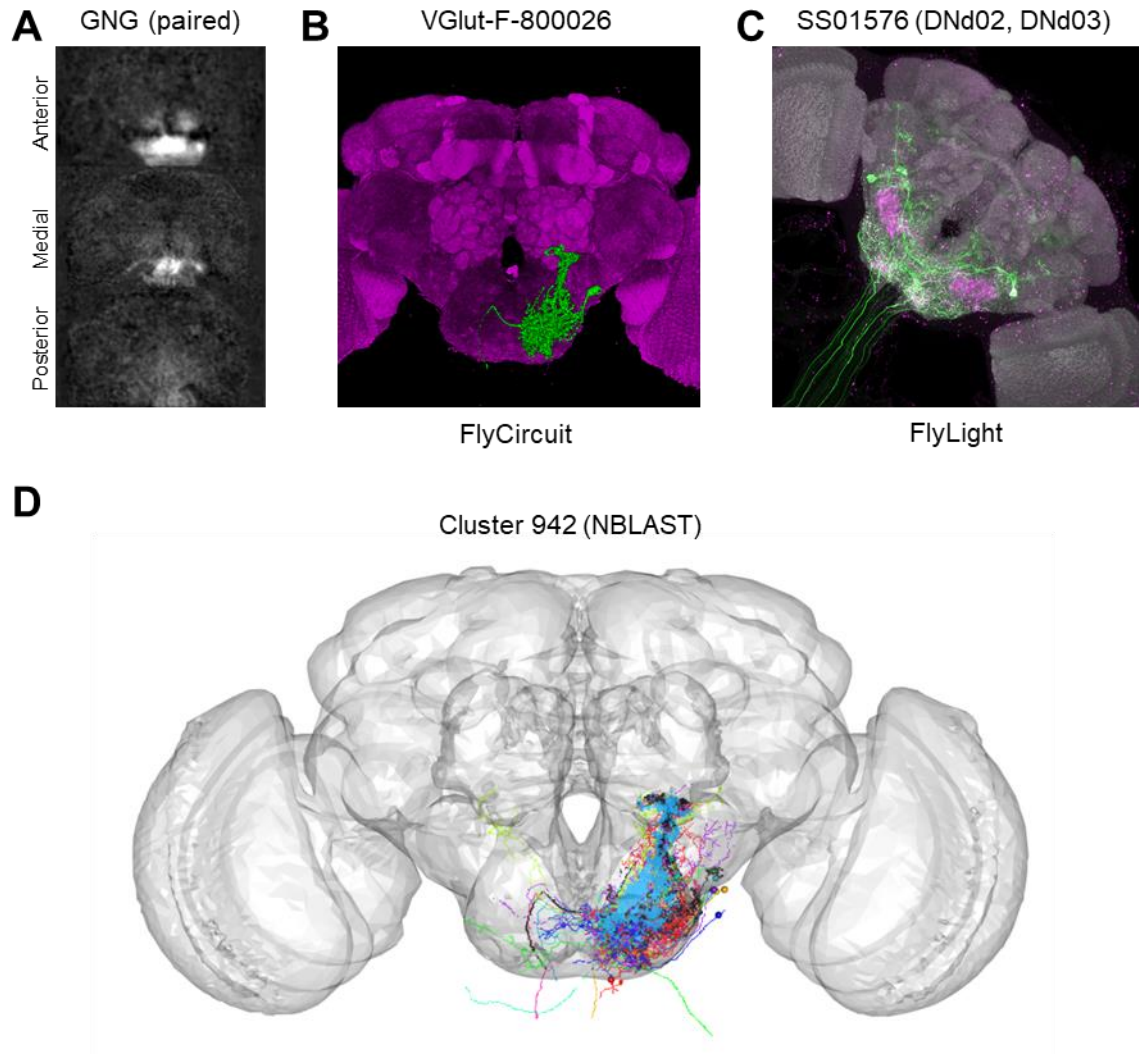


Figure 28: Neurons and expression pattern with similarity to GNG (paired)

A Example image of GNG (paired). **B** Image of Vglut-F-800026 taken from www.flycircuit.tw (Chiang et al., 2011, © NCHC & BRC/NTHU, 2009, licensed via Elsevier RightsLink, license number 5567591362885). **C** Image of SS01576 taken from FlyLight Split-Gal4 Driver Collection (www.splitgal4.janelia.org/cgi-bin/splitgal4.cgi, Namiki et al., 2018, © 2012-2023 Howard Hughes Medical Institute Janelia Research Campus, CC BY 4.0 license). **D** 3D-rendering of neurons in the cluster 942 that contains 10 neurons with high similarity to VGlut-F-800026 (black) according to the NBLAST scores (© Costa et al. 2014, CC BY 4.0 license).

Comparing global brain connectivity during resting and stimulus phase

In order to investigate complex brain dynamics, graph theory can be applied. This method is widely used in structural and functional MRI (Bullmore and Sporns 2009) but a similar approach can also be used to analyze functional imaging data in flies (Aimon and Grunwald Kadow 2019). The underlying assumption is that highly correlated activity of two brain regions over time infers high connectivity between those two regions. Therefore, I calculated the Fisher-Z-transformed Pearson correlation between the average fluorescence time series of the twelve neuropil supercategories for the pooled data of odor, taste and odor + taste conditions. The resulting weighted adjacency matrix were thresholded to retain only 40 percent of the highest correlated pairs (i.e. strongest connections), in order to make the networks sparser. I defined the time period before the first stimulus as “rest” (Figure 29). Here, in the absence of any salient stimulus, the brain connectivity among the given groups looked relatively similar. Also, the weights of the connections were evenly distributed as they were potentially driven by spontaneous activation. However, there were subtle differences between the taste cohort and the other two groups. These could potentially be caused by the ablation of the antennae, which is a major sensory organ of the fly and the lack of input could cause a shift in resting state connectivity. In the odor and multisensory group, the central complex (CX), lateral complex (LX) exhibited a high node degree, which means they were well connected with other regions and could be classified as hubs (Bullmore and Sporns 2009). In a recent study on resting state functional connectivity in *Drosophila* using whole brain metabolic imaging, the FB and EB (as parts of the CX, which is located at the midline), were found to play a major role in inter-hemispheric communication (Mann et al. 2017). In the taste cohort, the inferior neuropil (INP) had the highest node degree (Figure 29 B). Interestingly, in the other two groups, the INP showed a strong weighted connection to the MB. This can be explained by the anatomical location of the two regions, as parts of the INP basically wrap around the MB lobes (Ito et al. 2014). Mann et al also highlighted the olfactory pathway as an important cluster of recurrent connections. I also found that the MB, LH and SNP show high

correlation in the odor and multisensory group. This was even the case when the threshold is lowered to 20 percent of the most correlated pairs (Figure A8). Surprisingly, the AL was not directly connected to the LH and in the multisensory group not even to the MB. It is also noticeable that the GNG was not directly connected to the rest of the brain, but only indirectly through the PENP and the ventromedial neuropil (VMNP). The optic lobe (OL) was not functionally connected to any other brain region.

The functional connectivity changed dramatically when a stimulus was applied (Figure 30). In odor, the “SEZ cluster” of GNG, PENP and VMNP were uncoupled from the rest of the brain, where, in turn, a strong increase of interconnectivity (increase of node degree) and connection weight could be observed in almost all regions. Only the ventrolateral neuropil (VLNP) did not change a lot, probably because it is a region that mainly receives visual input (Ito et al. 2014). During multisensory stimulation, the weight of the connections (i.e. the strength of the correlation) did not increase as strongly (Figure 30 C). Here, the GNG and PENP still appeared to be connected to the rest of the brain via the VMNP, possibly because of the presence of the taste stimulus. During taste-only, the weights actually appeared to be reduced as compared to resting state, however the connectivity itself seemed to change (Figure 30 B). In order to clarify this, I calculated the correlation ratio between rest and stimulus phase (Figure 31 A). For odor, the ratio was clearly above one for most connections, which means that the weight of the connections increased during the stimulus period in comparison to the resting period. The strongest increase could be found in the connections of LH to the LX and AL. Also, the connections between those regions were only seen during the stimulus phase as depicted in Figure 31 B, which shows the binary connectivity changes. For odor + taste, the ratio was slightly above one in most cases and the connectivity change was rare (e.g. between AL to MB and INP). In contrast, the correlation ratios for taste were around one or even below one in most cases (Figure 31 A). That means, pairwise correlations stayed the same or became weaker. However, I saw an increase in connectivity change (Figure 31 B), as more connections were lost or gained from rest to stim phase, which can be interpreted as a remapping of functional connectivity during gustatory tasks. In comparison, during odor and

multisensory task, the existing connections were maintained but the strength between them was increased.

Overall, this analysis suggests that during resting phase neural connectivity was evenly distributed across the network with a high number of connections with similar weights. During stimulus phase there was a shift towards increased connectivity in the superior and central regions of the brain when the flies were presented with odor or odor + taste, as the correlated activity among those regions increased. However, during taste stimulation there was a decrease of correlated activity compared to the resting state and an increase of connectivity change.

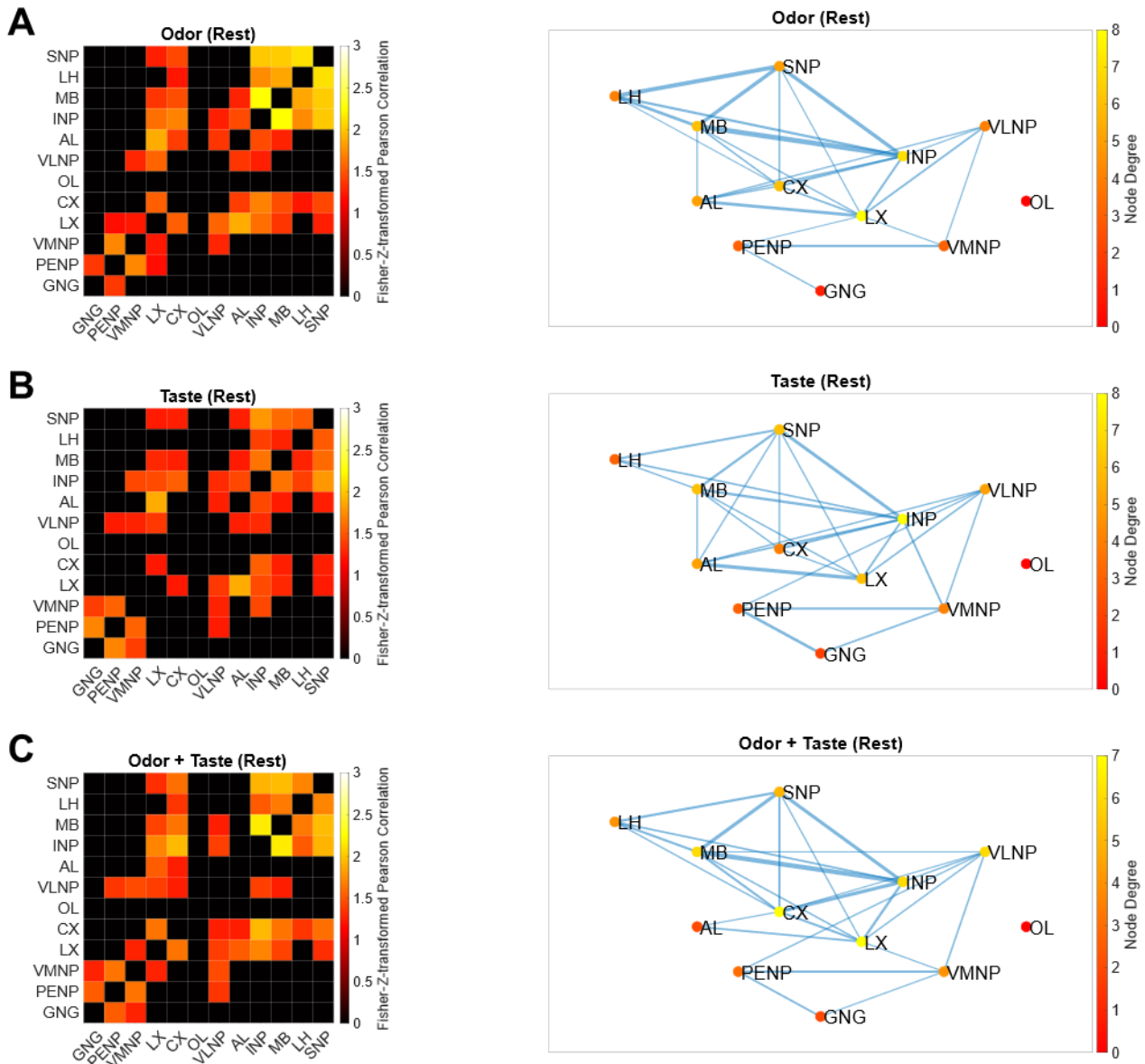


Figure 29: Brain-wide correlation during resting phase

A Adjacency matrix and resulting graph of the activity correlation of the odor group. **B** Adjacency matrix and resulting graph of the activity correlation of the taste group. **C** Adjacency matrix and resulting graph of the activity correlation of the multisensory group. Data for fed and starved groups was pooled. The resting phase was defined as the first 25 seconds of every recording before the first stimulus was applied. Correlation was thresholded proportionally to retain only 40 percent of the strongest connections. The width of the edges (blue lines) scales proportionally with weight of the connection between the nodes.

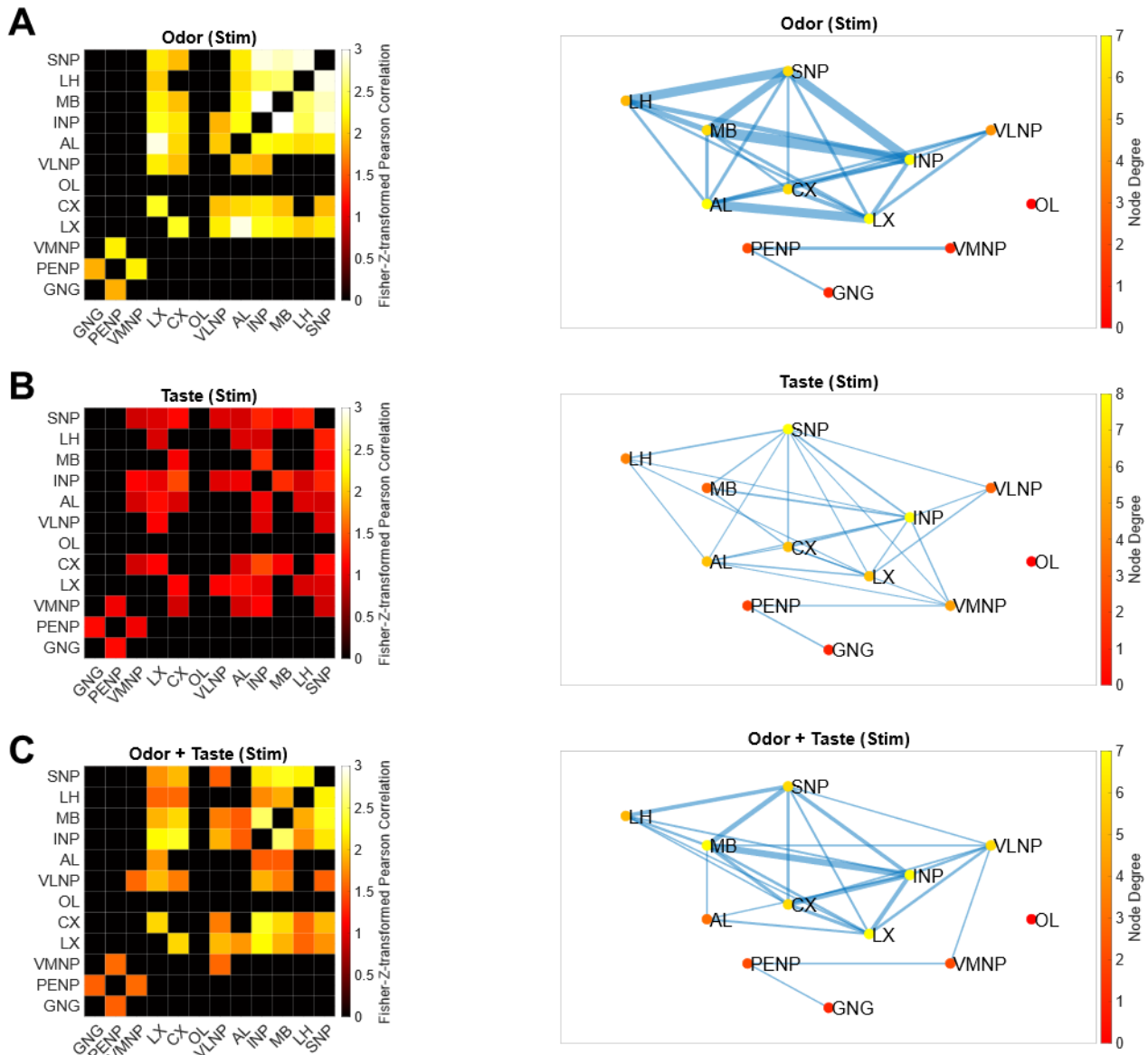


Figure 30: Brain-wide correlation during stimulus phase

A Adjacency matrix and resulting graph of the activity correlation of the odor group. **B** Adjacency matrix and resulting graph of the activity correlation of the taste group. **C** Adjacency matrix and resulting graph of the activity correlation of the multisensory group. Data for fed and starved groups was pooled. The stimulus phase was defined as the first 15 seconds after the onset of the first stimulus. Correlation was thresholded proportionally to retain only 40 percent of the strongest connections. The width of the edges (blue lines) scales proportionally with weight of the connection between the nodes.

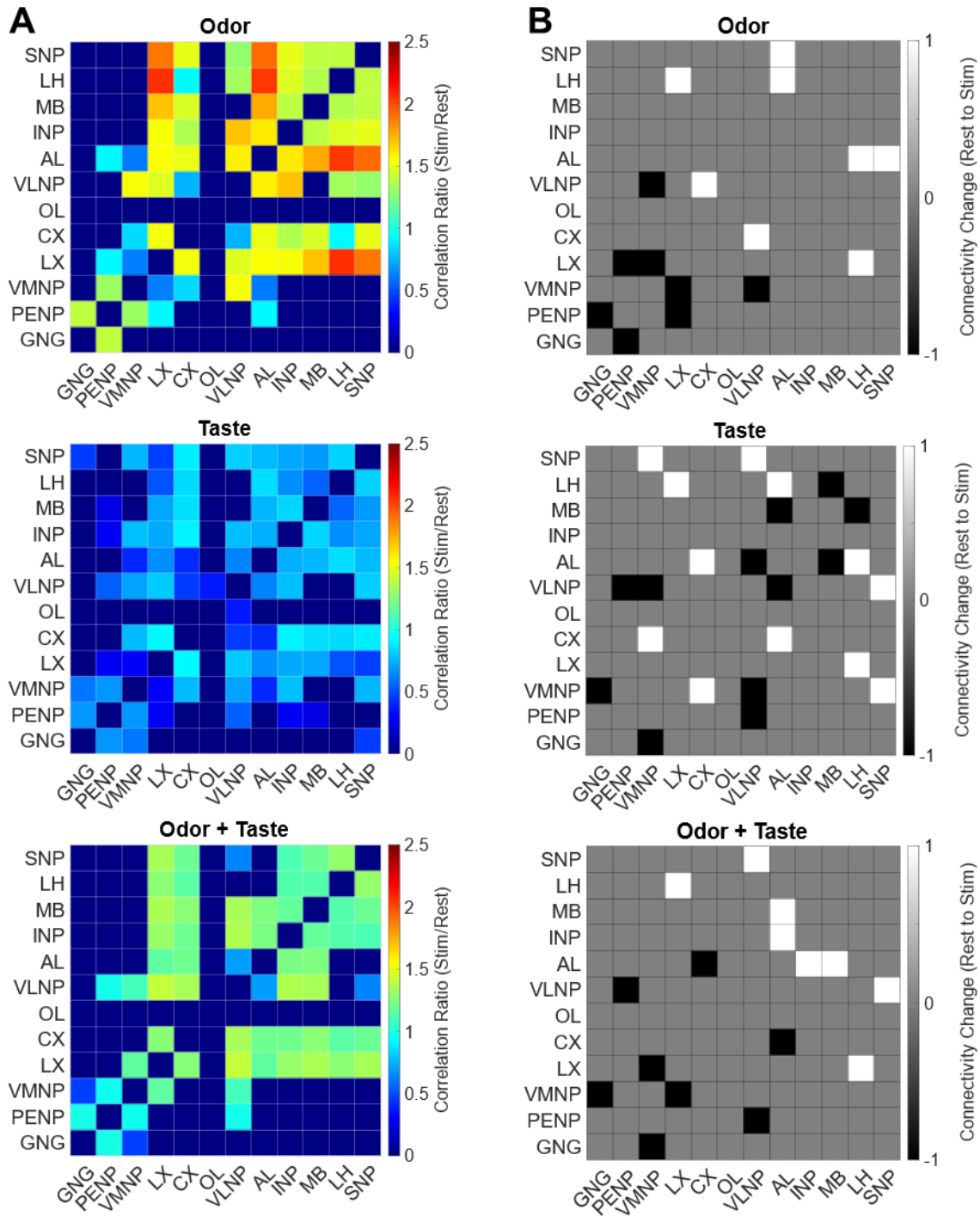


Figure 31: Correlation ratio and connectivity change between rest and stimulus phase

A Correlation ratio matrices for the all stimulus groups. Correlation ratio was calculated by dividing the correlation during stim with the correlation during rest. Correlation was thresholded proportionally to retain only 40 percent of the strongest connections. **B** Connectivity matrices for all stimulus groups. Connectivity change was calculated by subtracting the binary connectivity during rest from the binary connectivity during stim. Black: connection is lost, white: connection is gained, grey: connection remains unchanged.

Discussion

In order to investigate the global neuronal activity evoked by chemosensory stimulation, I exposed fed and starved flies to different odor and taste substances and analyzed the peak responses in twelve major brain areas. Taste mainly activated the SEZ and odor mainly the superior areas of the brain. This suggests that chemosensory activation is regionally specific, depending on the modality and is in accordance with the neural projections from the sensory periphery. In addition, a PCA on peak responses was able to find components that further subdivide and separate brain regions according to their chemosensory responses and between fed and starved flies. Moreover, I found that starvation increases the global response to appetitive odor and in contrast reduces the global response to non-appetitive taste. This suggests that metabolic state modulates olfactory and gustatory circuits in different ways. By using supervised machine learning classification algorithms, I found that peak responses could predict the stimulus modality, valence, and the internal state of the animals, suggesting that global brain activity exhibits measurable differences between those conditions. When pairing a taste with an odor stimulus, both odor and taste regions were activated. I found that pairing an appetitive odor with a bitter taste resulted in higher responses brain-wide, especially in fed flies. This suggests that brain activity during integration of chemosensory stimuli is influenced by valence information and the internal state.

I used ICA to plot spatial maps of functional components, small brain areas or putative single neurons, that show correlated activity with the stimulus. Most components responded specifically to odor and label all stages of the fly olfactory pathway. A component, which I named "GNG (paired)" only responded during combined odor and taste stimulation. It overlapped with a set of neurons that connect the AL with the SEZ and might be involved in multisensory integration.

Graph analysis of the correlated activity among the brain regions showed that changes in the functional network between the rest and the stimulus phase differ between the modalities.

During odor presentation, the existing connections are maintained and their weight increases, whereas during taste there seems to be a remapping of connections. The network tends to be the most stable during combined stimulation. This suggests that global neuronal connectivity is changing upon chemosensory stimulation but effect differs between the modalities.

Global effect of metabolic state

Notably, the valence-effect on the brain activity was depending on the metabolic state and even detectable on a global scale (Figure 11). In fed flies, there was no difference in peak dF/F between positive and negative odorants or tastants (Figure 11 C, D). The odor responses across the regions were almost identical (Figure 11 A). When the flies were starved there was a strong increase in the responses of the SNP, LH and MB towards vinegar. It was reported that calcium activity of dopaminergic neurons in the MB can be modulated by the internal state (Siju et al. 2020) and that this circuit integrates hunger and satiety signals to control innate food seeking behavior (Tsao et al. 2018; Perisse et al. 2016). Whether the neurons in the LH or the SNP are directly modulated by hunger is not known, however they receive direct input from MBONs and therefore might be indirectly effected in their activity. The whole brain median across all regions was also significantly increased in starved flies exposed to vinegar compared with fed flies. On the other hand, the sucrose response did only increase locally in the GNG and the PENP in starved flies, whereas the global response did not change (Figure 11 B, C). Surprisingly, the median response towards quinine was significantly decreased in hungry flies. Here, the activity in the GNG and PENP is lowered. Münch et al (2022) have also shown that taste processing in the SEZ can be modulated by hunger by using pan-neuronal calcium imaging. They even showed that yeast taste is more likely to elicit responses in protein-deprived flies than sucrose, suggesting that this is specific and based on the nutrient needs of the animal. Other findings support the notion that integration of taste and hunger signals is confined to local circuits in SEZ (Yapici et al. 2016; Shiu et al. 2022). However, here I could show that starvation also had a global effect on brain activity towards chemosensory

cues and that it had opposite effects on olfaction and gustation, depending on the valence of the stimulus. Furthermore, when I combined odor and taste, there was a global increase in brain activity when a positive odor was paired with an aversive taste. This effect however was only found in satiated flies. A set of conflicting sensory information did seem to put the brain in a more active state. Surprisingly, this was not the case when an aversive odor was paired with a positive taste. This suggests that interactions of multimodal sensory signals are complex and that brain activity not just represents the sum of all unimodal responses. My results suggest that starvation has an effect on local circuits involved chemosensory information as well as throughout the entire brain. This indicates that the metabolic state of the animal influences neuronal activity on a global scale and thereby influences behavioral outcome of sensorimotor processing based on the nutrient needs.

Finding candidate neurons

Analysis of the functional components derived from spatial ICA was done by eye, for every recording separately, which was very time-consuming. It also bears the risk of bias towards those components that were easier to identify and annotate. Using automated image-segmentation would have been a great way to speed up the process and to make it more reproducible. This is relatively widespread in medical diagnostics but implementing and validating such algorithms for the LFM data would potentially have been the same amount of work than reviewing them manually. Nevertheless, future work should try to find a more unbiased approach to component annotation. The functional components I found, displayed some overlap with those published by Aimon et al. (2019, 2022) that show correlation with walking. However, I found a lower number of components overall, because the activation during chemosensation was less global than during walking. Furthermore, I discovered that most components are odor-specific. Many of these were found in the superior part of the brain, whereas the few the taste-exclusive components were located in the SEZ. Walking components on the other hand, were distributed widely across the brain.

There was one component in the GNG (“GNG (paired)”) that only showed activity when odor and taste were combined (Figure 28). I found that this component looks similar to a cluster of neurons that have dendrites in the SEZ and the inferior AL. Unfortunately, I could only find GAL4-lines with similar expression patterns for a line that label two descending neurons (DN02 and DN03, Namiki et al. 2018, Figure 28 C). It is still conceivable, that these neurons integrate the coincidence of odor and taste, but unlikely. Since those DNs project to all neuromeres of the VNC, they might play an important role during movement control. Therefore, it could be useful to confirm, if these neurons receive input from odor or taste input by checking synaptic connection in the FAFB EM volume (Zheng et al. 2018). However, so far there has only been effort in tracing the GRNs in the SEZ, which means there is only limited connectomic information in that region (Engert et al. 2022). Anyway, if this was to rule out the DNs, one would need to look for other driver lines with high matches to VGlut-F-800026. I checked a study that has created split-GAL4 lines which label 510 neurons in the SEZ but I could not find any obvious matches. However, this set only represent about one third of all cells found in that region (Sterne et al. 2021). A functional map of the SEZ has been created by Münch et al. (2022), but this has been focused on the taste valence and neuronal anatomy from light or EM microscopy was not used as a basis or for comparison. Also, it does not show individual neurons but functional areas that correlate with taste or motor activity. There is no information, whether there is also multisensory integration.

Another option could be the Color-depth MIP dataset (www.janelia.org/open-science/color-depth-mip), however during completion of this thesis (August 2023) the respective files were not available for download. In the end, it might be necessary to create and screen split-GAL4 lines in the SEZ to find the candidate neurons. If this was to be successful, further experiments could be conducted. One could express GCaMP in the respective neurons and perform functional imaging upon combined chemosensory stimulation. For this, the LFM would probably be unsuitable, because the signal would be too low. Multiphoton imaging would be more sensible. However, it would be more difficult to deliver a taste stimulus under those

conditions. The taste delivery system would need to be remote controlled or automated. The next step would be to investigate the effect of the candidate neurons on feeding related behavior. A common way to test this would be the FlyPad (Itskov et al. 2014) or the OptoPad, (Moreira et al. 2019). Here, it is possible to measure single sips of an individual fly, while simultaneously manipulating neuronal activity in open- or closed-loop paradigms with thermo- or optogenetics (Bernstein et al. 2012).

Although being performed in rudimentary way, the analysis of functional components suggested that certain neuronal ensembles are robustly activated by chemical cues, across a number of flies. However, this technique needs to be improved to make it faster, more reliable and less susceptible to bias, in order to use it as a standard and high-throughput technique. Then, it might potentially be a powerful tool to assign functional relevance to previously poorly described brain regions.

Localizing sites of chemosensory integration

Multisensory integration is thought to shape the perception of flavor in humans (Spence 2015). It does not only involve the interaction of smell and taste, where the perception threshold of a positive smell is lowered by sweet taste (Dalton et al. 2000). Even the texture of a bite can influence the perceived odor intensity (Roudnitzky et al. 2011). It can also involve vision. An orange-flavored drink is more likely to be identified as such, if it is also colored orange, instead of another color (Zampini et al. 2007). Furthermore, the sensation of crispness is reduced, when the associated auditory cue is omitted (Demattè et al. 2014). While this is potentially of great interest to the food industry and surely already applied, we still lack knowledge of the underlying neurophysiological principles. There is some evidence that a combination of odor and taste signal converges in the orbitofrontal cortex (OFC). Activity in this area is also associated with ratings of pleasantness of food cues which in turn can be modulated by satiety (Rolls 2006). But also the insular taste cortex has been found to be coding for quality of food odors (Veldhuizen et al. 2010). Furthermore, single neurons in the gustatory cortex of rats

show bimodal activation and code for palatability better than unimodal taste neurons (Samuelsen and Fontanini 2017). On the other hand, the posterior piriform cortex, which receives direct input from the olfactory bulb (Scott et al. 1980), contains a significant number of neurons that are taste-selective (Maier et al. 2012). These findings highlight the importance of neurophysiological studies to understand the complexity of interaction between olfaction and taste.

Targets of second-order gustatory neurons in the fly have been reported in different parts of the SNP by transsynaptic labeling of sweet GRNs (Talay et al. 2017). Interestingly, they were also found to project to the VNC. Similar pathways of taste projection neurons, which also include the LH have been identified independently (Kim et al. 2017a). These neurons were involved in aversive taste conditioning by activation or inhibition of MB extrinsic dopaminergic neurons. Olfactory projections are much better understood (Wong et al. 2002; Marin et al. 2002) and suggest that innate responses are mediated via the LH (Varela et al. 2019) and learned responses via the MB (Bräcker et al. 2013). Since both modalities converge in the SNP, an interaction in this area would be likely. However, I did not find this to be reflected in the whole brain activity. The SNP was mainly activated by odor signals, but I recorded some taste signal in the LH. The LH has diverse functions in coding for odor quality, intensity and valence (Strutz et al. 2014; Dolan et al. 2019). It is therefore not surprising, that the LH showed the strongest response towards odor stimulation. If it also integrates gustatory cues remains unknown. It has been reported that the LH has some intrinsic spatial organization. For example, activity in the anterior-lateral part correlates with negative odor valence, whereas the posterior-medial part correlates with positive valence (Strutz et al. 2014). The spatial functional component analysis could find multiple components in the lateral horn, however none of them showed obvious correlation with odor valence. The same was true for the MB lobes. Even though, the algorithm segregated the different MB lobes, they did not correlate with odor valence. It actually seemed like the algorithm always found the same component under both conditions in one fly, whereas in another fly it failed to detect it completely.

Furthermore, the MB showed very little taste response. Even though it is known to be involved during gustatory learning (Kirkhart and Scott 2015; Jelen et al. 2021), it does not seem to be directly activated by taste input. There was one functional component that exhibited some valence-specific activity. The “LH-SIP” had a higher relevance score when the flies are exposed to vinegar odor (Figure 27). This was due to increased peak dF/F in comparison to benzaldehyde stimulation (Figure A26 B). The component appears consistently in almost all odor-stimulated flies (Figure 26 A). It labels the whole LH and the SIP. Therefore, it might represent a cluster of LH output neurons that are tuned to innate odor valence. They could potentially signal approach behavior towards an appetitive cue. Interestingly, “LH-SIP” is also found in almost every second the taste-only flies. However, there was no valence-specific difference in the activity. The “PRW”, on the other hand showed a higher score upon sucrose presentation. The prow is the most anterior and superior region of the SEZ. Here, the pharyngeal nerve, which consists of the axons of the pharyngeal GRNs forms extensive terminals (Miyazaki and Ito 2010; Ito et al. 2014).

This is the first study in *Drosophila* that compares global neural activity upon unimodal odor or taste stimulation with bimodal activation of both sensory circuits. The data suggests that the activation patterns do not overlap much between the two modalities. During stimulation of both senses the olfactory activity seems to be overrepresented in comparison, by eliciting strong signal in the superior brain, suggesting that has a larger impact on higher brain functions.

Inferring functional connectivity

To describe the brain activity on the global scale, I used graph theory. Although being widely used in the field of human neuroimaging it has some limitations. First of all, it infers connectivity based on correlated activity over time (Bullmore and Sporns 2009). The result depends strongly on the threshold that is applied, which is arbitrary. I have used a density threshold of 40 and 20 percent and the results differ strongly. For example, at 20 percent there was no

more connectivity between the GNG and PENP during multisensory stimulation (Figure A9 C), even though a taste stimulus was presented, which caused visible activity in the SEZ. If I had used a global instead of relative threshold, then it would have been difficult to compare taste and odor data because of the difference in signal. In human studies, which rely on BOLD signal, usually much lower thresholds are used. Furthermore, most graphs use a much higher number of regions of interest (ROIs, Rubinov and Sporns 2010). Although, there is no standard approach in flies, Mann et al (2017) used 61 ROIs and displayed their results on resting-state connectivity with a cut-off of 3 percent. I only use twelve ROIs, which could be an oversimplification. Even so, the results are difficult to interpret. I tried to compare the “resting state” network with the “stimulus effected” network. Even though, it nicely displayed the changes in connections, there are other, more sophisticated approaches to functional connectivity. For example, task-related fMRI studies use a measure called PPI (psychophysical-interaction) in which the signal of a seed-ROI is convolved with a stimulus time series and then used as a regressor to calculate the correlation to all other ROIs (Friston et al. 1997). Of course, the result of this is heavily influenced by the choice of seed region. In my case, I could have chosen the primary sensory centers like the AL or the GNG, but how can I then compare the resulting networks? They would look completely different. Overall, it is difficult to deduce functional connectivity from large-scale recordings, since the actual communication happens on a cellular level.

Therefore, it would be much more exact to have single cell resolution. Attempts to achieve this have been made in the nematode *C. elegans*, where they even could compare their results with the actual connectome (Randi et al. 2022). They expressed and excited a light-sensitive ion channel in each of the neurons and recorded simultaneously from all other neurons. However, *C. elegans* only has a total of 302 nerve cells (White et al. 1986), which means that this is not yet feasible to achieve for more complex brains like *Drosophila* with about 130.000 neurons. Nevertheless, there are interesting advances in this direction, with the recent innovations in ultrafast single-cell optogenetics (Faini et al. 2023; McRaven et al. 2020). Of

course, it will be also helpful, that we will soon have access to the full connectome of the fly brain, which maps all neural connections at synaptic resolution (Scheffer et al. 2020; Dorkenwald et al. 2023). This can be used to investigate specific neural circuits in more detail and study their role in sensorimotor integration and complex behaviors in the fly, like it has already been done in the worm (Flavell and Gordus 2022).

Here, I show how large-scale functional connectivity changes upon chemosensory stimulation. The graph analysis approach can be refined in different ways to make statements about the global brain network. While the type of data I have collected is suitable for this kind of investigation, most of the tools were developed for human MRI data and need to be adapted and validated accordingly. This is a difficult task that requires deep knowledge of the underlying principles as well as computational skills. However, it can be a great advantage and help bridge the gap from the anatomical to the functional connectome in the fly.

The dichotomous view of odor and taste

Recently, it has been debated whether our view of olfaction and gustation as two separate senses might be biased towards terrestrial animals and vertebrates. Under a broader perspective, the chemical senses could be considered as two sides of the same coin (Mollo et al. 2022). This notion seems to be supported by the fact that the chemosensory receptors in *Drosophila* belong the same gene superfamily (Scott et al. 2001). Furthermore, GRNs that ectopically expressed ORs still mediate the correct appetitive or aversive responses, when odors of positive or negative valence are presented (Hiroi et al. 2008). Interestingly, the projections of the GRNs do not change. Million years of evolution have created highly specified chemosensory organs in the fly that each integrate into specific neuronal circuits (Vosshall and Stocker 2007). My work suggests that the functional segregation of smell and taste is also represented in the global neuronal activity. Gustatory cues mainly elicit responses in the SEZ, whereas olfactory stimuli activate superior regions of the brain, with very little overlap. Principal component analysis, revealed not only that brain regions can be separated according to their

chemosensory responses, but also fed flies are distinguishable from starved flies. However, this was only possible when the data was sorted by modality. This suggests that starvation has global effect on neuronal activity but it cannot be generalized across chemical senses. In support, I trained classification models on the functional data that could successfully distinguish between the modalities and even a combination of both. These models could even predict valence of the given stimuli or the internal state of the animal, when trained with data from one modality only. Notably, prediction from multimodal data was only possible when I separated responses of matching and conflicting valence pairs, which implies that overlapping activity prevents correct classification. Using spatial ICA, I discovered only one functional component in the GNG that is only present when odor and taste were presented together, while all others were mostly modality-specific.

The neuronal correlates of this component still need to be characterized and could help understand the way of how multimodal stimuli are integrated in the brain. All in all, these findings support the dichotomous view of olfaction and gustation, since the separation on the peripheral level seems to carry over into the central nervous system. Nonetheless, further research is needed to clarify how the two senses interact and shape the perception of the chemical environment.

Valence of chemosensory cues

For the chemosensory cues, I used substances that are widely used in *Drosophila* research and well described as either appetitive or aversive (Semmelhack and Wang 2009; Störtkuhl et al. 2005; Fujii et al. 2015; Apostolopoulou et al. 2014). However, it is not clear whether the respective substances also elicit olfactory responses, when they are presented as tastants. Or simply speaking, I cannot be sure if flies can also smell sucrose or quinine. To minimize the potential stimulation of odor receptors by the taste solutions, the antennae were removed. I also had to remove the legs during the experiments, because the flies would try to grab the taste capillary. This also minimized movement artifacts and noise due to movement related

brain activity. Unfortunately, it meant the input from the taste receptors on the legs was lost. This could explain the low signal during the taste stimulation of the labella. Normally, one would expect the signal from the legs (or the wings) and the proboscis to coincide in the SEZ, where all GRNs project to (Amrein and Thorne 2005), which could in turn cause a higher overall signal. The taste response from the legs is also ethologically relevant, because the flies might use the legs to probe the substrate and only if it is considered nutritious and safe to eat, they would start extending the proboscis (Shiraiwa and Carlson 2007). Since I glued the proboscis, the flies could neither extend nor retract it anymore and I basically forced them to taste whatever they were presented. Furthermore, I could not assess whether the flies actually ingested parts of the sucrose solution, although sometimes there was some movement of the esophagus visible in the LFM recordings. For odor experiments I glued the proboscis in a retracted position and removed the legs, to minimize taste responses during odor stimulation. Obviously, during multisensory stimulation both sensory organs (antennae and labella) had to be intact. Unfortunately, I still had to fix the proboscis. It was not possible to achieve this, without also covering the maxillary palps with glue. These also express odor receptors and were found to be involved in multisensory integration (Shiraiwa 2008).

During the experiment, I also stimulated the flies with water only. Initially, the aim was, to wash the labella of the fly and neutralize any remaining tastants before proceeding with the next substance. To keep the protocol consistent, I also stimulated flies during the odor experiments with “water odor”. I also recorded the brain activity during those trials and detected responses. This is not surprising, since the sensory perception of water is mediated by specific receptor pathways (Cameron et al. 2010; Enjin et al. 2016). However, the data is not shown here for a few reasons.

First of all, if the water responses would have been included, the presence of another variable would have complicated all further analysis. Second, because it is difficult to assign any clear valence to a water stimulus. It is definitely not a neutral stimulus, especially to a thirsty animal it can be rewarding and it has been shown that thirsty flies can even track a water plume,

whereas water-satiated flies tend to avoid it (Limbania et al. 2023; Lin et al. 2014). Furthermore, a specific circuit is known to regulate the prioritization of water consumption in thirsty flies over food intake (Landayan et al. 2021). Even though, the flies that I used, were fed or wet-starved, the true valence of a water stimulus cannot be assessed. Therefore, it would have been difficult to compare water responses with the other stimuli. Since all substances were diluted with water, I assumed water responses act as a uniform baseline. It still might be interesting to record water responses and see if they are modulated by thirst.

I used the same substances during the paired stimulation and assumed that vinegar and sucrose (respectively benzaldehyde and quinine) have the same valence, and therefore represent matching pairs. If the substances are exchanged, it will result in conflicting valence information. However, one could argue that the smell of vinegar and the taste of sugar also represents a conflicting signal. Because, why would something that smells like vinegar would not taste sour but sweet? It might have been more naturalistic to use vinegar smell and taste at the same time. However, here the valence changes with the metabolic state, because fed flies avoid sour solutions, whereas starved flies seem to like it (Devineni et al. 2019). Another possibility would have been to use yeast as an appetitive cue. It has already been found that the smell can enhance feeding responses (Oh et al. 2021). Yet, it would have been difficult to compare these results with the unimodal experiments. Also vinegar and yeast can be considered a blend of different substances, which means that they can activate multiple odor or taste receptors at the same time (Scheidler et al. 2015; Zhu et al. 2003). I tried to use simple cues that have described responses in the fly, at least on peripheral level and the first order center. Unfortunately, I could not identify responses in single glomeruli of the AL or the distinct projection patterns for sweet and bitter GRNs in the GNG (Marella et al. 2006). Both neuropils are located in the anterior part of the brain. However, the resolution of the reconstructed LFM volumes decreases further away from the focal plane (Aimon et al. 2019). Whereas the activity recorded in the GNG upon taste stimulation was still high, the activity measured in the AL upon odor presentation was lower than expected. This can be explained by the fact, that I

averaged the signal across the whole structure but the response is spatially sparse, since only a small number of glomeruli actually respond to a given odor. Interestingly, the AL also showed some activity to taste stimulation. Furthermore, I found a functional component that is labelling the AL in odor as well as in taste recordings. This component displays the entire AL and therefore I suspect it to be the AL hub, which lies below the glomerular layer and contains local interneurons, which are often inhibitory (Seki et al. 2010).

The stimuli I used were sufficient to answer the initial research questions. They elicited activity in brain areas associated with chemosensory processing. The responses of appetitive and aversive cues were modulated by starvation. It would be interesting to see if these results can be reproduced by using different sets of chemical cues, either mono-molecular or more naturalistic blends.

Specificity and resolution of whole brain imaging

Because the flies expressed GCaMP under the *nsyb-Gal4* driver, it is not possible to know, whether the recorded activity comes from excitatory or inhibitory neurons. Aimon et al. (2023) have shown that glutamate, GABA and acetylcholine releasing neurons all show correlated activity with walking bouts on the whole brain level. This work followed up on a first study which showed a global increase in calcium activity under a pan-neuronal driver during walking in comparison with grooming (Aimon et al. 2019). Further experiments would be needed to investigate, if this is also the case during chemosensation. It would also be interesting, to record the activity of aminergic neurons during odor and taste stimulation. Peptidergic cells can have neuromodulatory function and can mediate changes in the internal state and regulate innate behavior (Kim et al. 2017b; Sayin et al. 2018). Aimon et al. (2023) found that activity of serotonergic neurons during walk is reduced compared to dopamine or octopamine releasing cells. Activity of dopaminergic cells in the MB encode for odor and taste valence and hunger-state (Siju et al. 2020). Dopamine signaling is also required in the MB for olfactory and gustatory memory (Masek et al. 2015; Aso and Rubin 2016). A dopaminergic interneuron in

the SEZ also regulates the feeding behavior and is modulated by the internal state (Marella et al. 2012). Serotonergic neurons in the GNG were found to be activated by taste signals and trigger insulin release and gastric motility in anticipation of food intake (Yao and Scott 2022). Serotonin is also involved in fine tuning of olfactory coding on the level of the AL (Dacks et al. 2009). Octopamine can promote feeding or influence odor choice decision making (Youn et al. 2018; Claßen and Scholz 2018). Since neuromodulatory neurons appear closely linked with chemosensory circuits, it could be worth studying their whole brain activity by expressing GCaMP in neuronal subsets and recording them with LFM while presenting olfactory and gustatory cues to the flies. Instead of using GCaMP, one could also use GRAB sensors, that exhibit changes in fluorescence in the presence of specific neurotransmitters. So far this genetically encoded indicators have been used to record dopamine, acetylcholine, and norepinephrine dynamics in vivo (Sun et al. 2018, 2018; Jing et al. 2018; Feng et al. 2019) and potentially more will be available in the near future (Deng et al. 2023).

The goal of this study was to investigate neuronal activity under a broad scope and hereby revealed global patterns. In order to gain more detailed insight on large circuits it could be useful to increase specificity and look at certain neuronal subtypes, either by focusing on certain areas of interest or neuronal subpopulations. Since neuropeptidergic cells are involved in modulating state-dependent processing, they might be promising target.

Pros and cons of light field microscopy

Usually functional imaging in the fly is confined to a certain region of interest like the AL, MB or SEZ (Siju et al. 2020; Münch et al. 2022; Strube-Bloss et al. 2017). Most in vivo techniques like confocal or light sheet microscopy rely on some form of optical sectioning to scan the tissue and then stitch the image together in the process (Yang and Yuste 2017). This increases spatial resolution in thick samples (especially when multiphoton lasers are used as a light source), but it comes with a loss of temporal resolution. Therefore, most applications are unsuitable to record large volumes, like the entire brain of small model organisms fast

enough to still resolve the kinetics of the calcium response (Bai et al. 2022). LFM, which was introduced in *Drosophila* by Aimon et al. in 2019, is a good compromise because it offers high temporal precision, at decent spatial resolution. The spatial resolution can be further increased by using higher magnification and zooming in on smaller areas such as the central brain or the optic or antennal lobes. Together with the mounting technique published by Woller et al. (2021), where the fly is head-fixed but still able to walk, flap its wing or in my case, susceptible to odor and taste stimuli, LFM is ideal to study neuronal activity on a large scale.

However, the technique still has some drawbacks. Even though, the setup is relatively cost-efficient, it is not yet commercially available, which means it has to be custom-built. This can be an advantage, in terms of flexibility to investigate different research questions and to optimize the setup, however it requires some training and fundamental knowledge of the different components and it can impact reproducibility of results among different labs or even among members in the same team. It is therefore imperative to implement some reliable protocols. We have already done that by creating an extensive manual of the mounting and head dissection of the fly (Woller et al. 2021). Nevertheless, it can take months of practice to master this first step. For this work, a particularly difficult part was to fix the proboscis of the fly in an extended position. In the end, this was achieved by pulling the proboscis out, with a mouth pipette, which had to be positioned with a micromanipulator. Then glue was applied carefully to the base of the proboscis.

Although the preparation of flies and the setup of the LFM can be tedious, the amount and quality of data that can be obtained from it, is worth it. After some time, it should be possible for anyone to achieve reproducible results. However, it is still to elaborate to use it as an additional method in other projects that focus for example on behavior.

Establishing the experimental protocol

There were instances where I prioritized a practical over a more sophisticated solution. For example, I simply positioned a glass capillary vertically under fly, sealed the top and filled it with a drop of taste solution. Then I moved the capillary towards the fly's head, while monitoring the it via two cameras, until the drop touched the labella. I left it there for 5 seconds and then moved the drop downwards again. This was sufficient to elicit reproducible calcium responses. In the beginning, I had to exclude some flies because, because I brought the drop to close and the solution would flood the whole head due to the capillary force. On the other hand, I encountered the problem, that the drop would evaporate, before I could finish the experiment. I thought about using low melting agarose as base instead of water, which would even have mimicked the tactile sensation of food and seems to be relevant (Oh et al. 2021; Jeong et al. 2016; Sánchez-Alcañiz et al. 2017). However, I decided against it because the "window of opportunity" (i.e. where the agarose is still liquid or already solid) when working at room temperature is relatively small. After some practice, I managed to consistently present the taste substance as described. This meant, I had to review the video recordings afterwards and note down the timeframe when the droplet touched the labella. Therefore, the microscope camera had to trigger the other video cameras, in order to synchronize the frame rate. Other relevant publications also rely on manual application of the taste stimuli, with slightly different setups (e.g. Münch et al, 2022). It would have been desirable to automate the taste presentation by using some type of remote-controlled actuators. However, it would have been a considerable amount of effort to set this up, even for someone with a background in electrical engineering. This probably would also have made the combination of odor and taste cleaner. Here, I basically had to trust my own response time, to deliver the odor stimulus via a manual trigger. I estimated there would be a delay of approximately 0.5 seconds (Dickerson et al. 2016; Jain et al. 2015). Actually, this is reflected nicely in the time series (Figure 7), where the signal in the taste responsive regions starts ramping sooner than in the odor regions. It would have been desirable to time-lock the odor and taste stimulus, but since I was more interested

in comparing total activation, the paradigm I used seemed sufficient. The LFM method anyways operates at higher acquisition speed (i.e. 10 Hz) than most other volumetric imaging approaches, which would not even be able to resolve a delay of 0.5 s. Anyway, given the slow nature of the calcium response that I am measuring (in comparison with electrophysiological recordings (Wei et al. 2020; Siegle et al. 2021), the delay between taste and odor presentation, introduced by the experimental procedure can be considered insignificant.

Another step of the experimental procedure that requires some practice is, how to position the focal plane in the “middle” of the sample (medial Z-position). Since, the flies express GCaMP pan-neuronally, there are almost no obvious landmarks in the tissue. I used the most posterior part of the tissue as a reference, because it contains quite a few cell bodies that exhibit strong fluorescence. Then, I lowered the objective about 50 μm down. Another reference point can be the MB peduncles, which appear as two bright spots on either hemisphere. These dense fiber tracts connect the MB calyx, which lies posterior, with the more anterior MB lobes (Aso et al. 2014). So, when you go deeper into the sample, and the peduncles disappear from the focal plane, you are probably too far anterior already.

After some time, I managed to find a good protocol that allowed me to achieve consistent results on a daily basis. Still, there were a few experiments which I would consider outliers but included anyways (see time series data in Figure A41-44). Particularly annoying was an artifact that resulted from a technical issue during the recording. I realized that the frame rate would drop below the constant 10 Hz for a few frames which resulted in the sharp single spikes of signal. I believe this was due to a bug in the camera software, because when I stopped the program and restarted the camera, the problem would not appear again and I could proceed with the experiment. Sometimes I only noticed this issue after the experiment was finished. Since the spikes appear randomly and not during the stimulus phase (except for one single case, Figure A42 B), I chose to include these recordings anyway. Since I was able to produce a satisfying number of replicates these artifacts would average out.

Although being quite time consuming, the processing of the light field data follows a relatively simple and standardized protocol. However, the registration of the recording to an anatomical template bears some difficulties. Here, I used a projected image from the ICA components as landmarks for the alignment, which was done by hand in FIJI. More components meant more landmarks. Hence, the registration was more difficult for the taste-only experiments, since there were much less components (Figure 26 B). Since the position of the brain under the microscope was not always exactly the same, this had to be done for every fly. It would have been more elegant to label some landmarks in the sample with another, activity-independent fluorophore (e.g. RFP) and apply some form automated registration (Creamer et al. 2022).

However, this would have meant to express another transgene in the flies and to install a second channel for red fluorescence in the LFM, as well as implementing some computational models that do not seem trivial. This only makes sense, if there was a desire to turn whole brain imaging into a high throughput method with a strong need for motion correction. In this case, the spatial resolution is anyways quite low, so there is no need for a perfect alignment, since I am not able to resolve fine differences between neighboring neuropils. Therefore, I have decided to average the signal for large macroscopic structures in the brain. The spatial resolution (3.5-12 μm laterally and from 6-35 μm axially, measured for a 20x 1.0 NA objective, Aimon et al. 2019) could have been improved slightly by using a 40x 0.8 NA objective, however, this would have meant losing some parts of the image, like the lateral areas of the OL.

While these technical considerations are important, it is crucial to keep things as consistent as possible in whatever works best in the end. Even though some of the steps described here could be improved, the data that was acquired turned out to be relatively robust. To account for the inevitable inter-individual variability, I managed to obtain a decent number of replicates, which is thankfully easy when working with *Drosophila*.

Conclusion and outlook

This work has shown that it is possible to record neural activity of the entire fruit fly brain while exposing the animal to chemosensory cues. Responses evoked by odor stimulation differed from those elicited by taste stimuli not only spatially but also in signal intensity. I could demonstrate that responses to those food-related senses were modulated by hunger according to the valence of the stimuli and can be explained by the behavioral changes that are observed in starved flies. There is evidence that other internal states like mating state, protein-deprivation or pathogen infection also influence fly behavior based on changes in sensory circuits (Hussain et al. 2016a; Boehm et al. 2022; Kobler et al. 2020; Corrales-Carvajal et al. 2016). It would be interesting to test whether global brain activity is also altered in those cases.

Furthermore, I managed to give different combinations of odor and taste which led to unexpected interactions in cases of conflicting sensory information. Hereby, it might be interesting to use the same substance for bimodal stimulation, especially considering biologically relevant food cues like over-ripe banana. These represent a blend of different odor and taste molecules (Schubert et al. 2014) and therefore might lead to differential activation in the brain compared with the more artificial combinations used here.

Flies have a good capacity for performing olfactory learning tasks (Busto et al. 2010). I only tested quasi naïve flies. Even though the underlying circuits are well studied, it would be interesting to know whether global activity changes in flies that are exposed to a known stimulus or one that was previously paired with an unconditioned stimulus.

My results showed that it is possible to obtain information about specific neuron types or even single neurons with functional relevance from relatively low-resolution images by using computational means of data analysis. If these methods can be improved further and implemented into a more streamlined pipeline, LFM would be a very attractive tool to study

neuronal activity under certain paradigms and match the results with our detailed knowledge of anatomical connectivity in the fly brain.

One functional component was implied to be involved in integrating odor and taste cues. Further research is needed to confirm that the candidate neurons which overlap with this component are actually involved in processing bimodal chemosensory information, how they are connected into the circuit and what their function is. Then this could be the first evidence of the neurophysiological mechanisms behind multisensory integration in the fly.

Publication bibliography

- Abuin, Liliane; Bargeton, Benoîte; Ulbrich, Maximilian H.; Isacoff, Ehud Y.; Kellenberger, Stephan; Benton, Richard (2011): Functional architecture of olfactory ionotropic glutamate receptors. In *Neuron* 69 (1), pp. 44–60. DOI: 10.1016/j.neuron.2010.11.042.
- Adams, M. D.; Celniker, S. E.; Holt, R. A.; Evans, C. A.; Gocayne, J. D.; Amanatides, P. G. et al. (2000): The genome sequence of *Drosophila melanogaster*. In *Science (New York, N.Y.)* 287 (5461), pp. 2185–2195. DOI: 10.1126/science.287.5461.2185.
- Ai, Minrong; Min, Soohong; Grosjean, Yael; Leblanc, Charlotte; Bell, Rati; Benton, Richard; Suh, Greg S. B. (2010): Acid sensing by the *Drosophila* olfactory system. In *Nature* 468 (7324), pp. 691–695. DOI: 10.1038/nature09537.
- Aimon, Sophie; Cheng, Karen Y.; Gjorgjieva, Julijana; Grunwald Kadow, Ilona C. (2022): Walking elicits global brain activity in *Drosophila*.
- Aimon, Sophie; Cheng, Karen Y.; Gjorgjieva, Julijana; Grunwald Kadow, Ilona C. (2023): Global change in brain state during spontaneous and forced walk in *Drosophila* is composed of combined activity patterns of different neuron classes. In *eLife* 12. DOI: 10.7554/eLife.85202.
- Aimon, Sophie; Kadow, Ilona C. Grunwald (2019): Studying complex brain dynamics using *Drosophila*. In *Journal of neurogenetics*, pp. 1–7. DOI: 10.1080/01677063.2019.1706092.
- Aimon, Sophie; Katsuki, Takeo; Jia, Tongqiu; Grosenick, Logan; Broxton, Michael; Deisseroth, Karl et al. (2019): Fast near-whole-brain imaging in adult *Drosophila* during responses to stimuli and behavior. In *PLOS Biology* 17 (2), e2006732. DOI: 10.1371/journal.pbio.2006732.
- Akerboom, Jasper; Rivera, Jonathan D. Vélez; Guilbe, María M. Rodríguez; Malavé, Elisa C. Alfaro; Hernandez, Hector H.; Tian, Lin et al. (2009): Crystal structures of the GCaMP calcium sensor reveal the mechanism of fluorescence signal change and aid rational design. In *The Journal of biological chemistry* 284 (10), pp. 6455–6464. DOI: 10.1074/jbc.M807657200.
- Amrein, Hubert; Thorne, Natasha (2005): Gustatory perception and behavior in *Drosophila melanogaster*. In *Current Biology* 15 (17), R673-84. DOI: 10.1016/j.cub.2005.08.021.
- Aponte, Yexica; Atasoy, Deniz; Sternson, Scott M. (2011): AGRP neurons are sufficient to orchestrate feeding behavior rapidly and without training. In *Nat Neurosci* 14 (3), pp. 351–355. DOI: 10.1038/nn.2739.
- Apostolopoulou, Anthi A.; Mazija, Lorena; Wüst, Alexander; Thum, Andreas Stephan (2014): The neuronal and molecular basis of quinine-dependent bitter taste signaling in *Drosophila* larvae. In *Front. Behav. Neurosci.* 8, p. 6. DOI: 10.3389/fnbeh.2014.00006.
- Araneda, R. C.; Kini, A. D.; Firestein, S. (2000): The molecular receptive range of an odorant receptor. In *Nature neuroscience* 3 (12), pp. 1248–1255. DOI: 10.1038/81774.
- Aso, Yoshinori; Hattori, Daisuke; Yu, Yang; Johnston, Rebecca M.; Iyer, Nirmala A.; Ngo, Teri-T B. et al. (2014a): The neuronal architecture of the mushroom body provides a logic for associative learning. In *eLife* 3, e04577. DOI: 10.7554/eLife.04577.
- Aso, Yoshinori; Rubin, Gerald M. (2016): Dopaminergic neurons write and update memories with cell-type-specific rules. In *eLife* 5. DOI: 10.7554/eLife.16135.
- Aso, Yoshinori; Sitaraman, Divya; Ichinose, Toshiharu; Kaun, Karla R.; Vogt, Katrin; Belliart-Guérin, Ghislain et al. (2014b): Mushroom body output neurons encode valence and guide memory-based action selection in *Drosophila*. In *eLife* 3, e04580. DOI: 10.7554/eLife.04580.
- Bai, Lu; Zhang, Zhenkun; Ye, Lichen; Cong, Lin; Zhao, Yuchen; Zhang, Tianlei et al. (2022): Volumetric Imaging of Neural Activity by Light Field Microscopy. In *Neuroscience bulletin* 38 (12), pp. 1559–1568. DOI: 10.1007/s12264-022-00923-9.

- Baker, P. F.; Hodgkin, A. L.; Ridgway, E. B. (1971): Depolarization and calcium entry in squid giant axons. In *The Journal of physiology* 218 (3), pp. 709–755. DOI: 10.1113/jphysiol.1971.sp009641.
- Barnum, George; Hong, Elizabeth J. (2022): Olfactory coding. In *Current biology : CB* 32 (23), R1296-R1301. DOI: 10.1016/j.cub.2022.10.067.
- Barrows, William Morton (1907): The reactions of the Pomace fly, *Drosophila ampelophila* loew, to odorous substances. In *J. Exp. Zool.* 4 (4), pp. 515–537. DOI: 10.1002/jez.1400040403.
- Bausenwein, B.; Dittrich, A. P.; Fischbach, K. F. (1992): The optic lobe of *Drosophila melanogaster*. II. Sorting of retinotopic pathways in the medulla. In *Cell and tissue research* 267 (1), pp. 17–28. DOI: 10.1007/BF00318687.
- Benton, Richard; Vannice, Kirsten S.; Gomez-Diaz, Carolina; Vosshall, Leslie B. (2009): Variant ionotropic glutamate receptors as chemosensory receptors in *Drosophila*. In *Cell* 136 (1), pp. 149–162. DOI: 10.1016/j.cell.2008.12.001.
- Bernstein, Jacob G.; Garrity, Paul A.; Boyden, Edward S. (2012): Optogenetics and thermogenetics: technologies for controlling the activity of targeted cells within intact neural circuits. In *Current Opinion in Neurobiology* 22 (1), pp. 61–71. DOI: 10.1016/j.conb.2011.10.023.
- Besnard, Philippe; Passilly-Degrace, Patricia; Khan, Naim A. (2016): Taste of Fat: A Sixth Taste Modality? In *Physiological reviews* 96 (1), pp. 151–176. DOI: 10.1152/physrev.00002.2015.
- Bevan, S.; Szolcsányi, J. (1990): Sensory neuron-specific actions of capsaicin: mechanisms and applications. In *Trends in pharmacological sciences* 11 (8), pp. 330–333. DOI: 10.1016/0165-6147(90)90237-3.
- Binder, Marc D. (2009): Encyclopedia of neuroscience. Heidelberg: Springer-Verlag.
- Blankenship, Meredith L.; Grigorova, Maria; Katz, Donald B.; Maier, Joost X. (2019): Retronasal Odor Perception Requires Taste Cortex, but Orthonasal Does Not. In *Current biology : CB* 29 (1), 62-69.e3. DOI: 10.1016/j.cub.2018.11.011.
- Boccaccio, Anna; Menini, Anna; Pifferi, Simone (2021): The cyclic AMP signaling pathway in the rodent main olfactory system. In *Cell Tissue Res* 383 (1), pp. 429–443. DOI: 10.1007/s00441-020-03391-7.
- Boehm, Ariane C.; Friedrich, Anja B.; Hunt, Sydney; Bandow, Paul; Siju, K. P.; Backer, Jean Francois de et al. (2022): A dopamine-gated learning circuit underpins reproductive state-dependent odor preference in *Drosophila* females. In *eLife* 11. DOI: 10.7554/eLife.77643.
- Bogovic, John A.; Otsuna, Hideo; Heinrich, Larissa; Ito, Masayoshi; Jeter, Jennifer; Meissner, Geoffrey et al. (2020): An unbiased template of the *Drosophila* brain and ventral nerve cord. In *PLoS ONE* 15 (12), e0236495. DOI: 10.1371/journal.pone.0236495.
- Bräcker, Lasse B.; Siju, K. P.; Varela, Nélia; Aso, Yoshinori; Zhang, Mo; Hein, Irina et al. (2013): Essential Role of the Mushroom Body in Context-Dependent CO₂ Avoidance in *Drosophila*. In *Current Biology* 23 (13), pp. 1228–1234. DOI: 10.1016/j.cub.2013.05.029.
- Brand, A. H.; Perrimon, N. (1993): Targeted gene expression as a means of altering cell fates and generating dominant phenotypes. In *Development* 118 (2), pp. 401–415. DOI: 10.1242/dev.118.2.401.
- Breer, H.; Boekhoff, I.; Tareilus, E. (1990): Rapid kinetics of second messenger formation in olfactory transduction. In *Nature* 345 (6270), pp. 65–68. DOI: 10.1038/345065a0.
- Broadie, K.; Prokop, A.; Bellen, H. J.; O'Kane, C. J.; Schulze, K. L.; Sweeney, S. T. (1995): Syntaxin and synaptobrevin function downstream of vesicle docking in *Drosophila*. In *Neuron* 15 (3), pp. 663–673. DOI: 10.1016/0896-6273(95)90154-x.
- Broxton, Michael; Grosenick, Logan; Yang, Samuel; Cohen, Noy; Andalman, Aaron; Deisseroth, Karl; Levoy, Marc (2013): Wave optics theory and 3-D deconvolution for the light field microscope. In *Opt. Express, OE* 21 (21), pp. 25418–25439. DOI: 10.1364/OE.21.025418.

- Budick, Seth A.; Dickinson, Michael H. (2006): Free-flight responses of *Drosophila melanogaster* to attractive odors. In *Journal of Experimental Biology* 209 (Pt 15), pp. 3001–3017. DOI: 10.1242/jeb.02305.
- Budick, Seth A.; Reiser, Michael B.; Dickinson, Michael H. (2007): The role of visual and mechanosensory cues in structuring forward flight in *Drosophila melanogaster*. In *Journal of Experimental Biology* 210 (Pt 23), pp. 4092–4103. DOI: 10.1242/jeb.006502.
- Buettner, A.; Beer, A.; Hannig, C.; Settles, M. (2001): Observation of the swallowing process by application of videofluoroscopy and real-time magnetic resonance imaging-consequences for retronasal aroma stimulation. In *Chem Senses* 26 (9), pp. 1211–1219. DOI: 10.1093/chemse/26.9.1211.
- Bullmore, Ed; Sporns, Olaf (2009): Complex brain networks: graph theoretical analysis of structural and functional systems. In *Nature reviews. Neuroscience* 10 (3), pp. 186–198. DOI: 10.1038/nrn2575.
- Burdach, K. J.; Doty, R. L. (1987): The effects of mouth movements, swallowing, and spitting on retronasal odor perception. In *Physiology & behavior* 41 (4), pp. 353–356. DOI: 10.1016/0031-9384(87)90400-8.
- Busto, Germain U.; Cervantes-Sandoval, Isaac; Davis, Ronald L. (2010): Olfactory learning in *Drosophila*. In *Physiology (Bethesda, Md.)* 25 (6), pp. 338–346. DOI: 10.1152/physiol.00026.2010.
- Cameron, Peter; Hiroi, Makoto; Ngai, John; Scott, Kristin (2010): The molecular basis for water taste in *Drosophila*. In *Nature* 465 (7294), pp. 91–95. DOI: 10.1038/nature09011.
- Caterina, M. J.; Schumacher, M. A.; Tominaga, M.; Rosen, T. A.; Levine, J. D.; Julius, D. (1997): The capsaicin receptor: a heat-activated ion channel in the pain pathway. In *Nature* 389 (6653), pp. 816–824. DOI: 10.1038/39807.
- Chandrashekar, Jayaram; Hoon, Mark A.; Ryba, Nicholas J. P.; Zuker, Charles S. (2006): The receptors and cells for mammalian taste. In *Nature* 444 (7117), pp. 288–294. DOI: 10.1038/nature05401.
- Chen, Yiming; Essner, Rachel A.; Kosar, Seher; Miller, Oliver H.; Lin, Yen-Chu; Mesgarzadeh, Sheyda; Knight, Zachary A. (2019a): Sustained NPY signaling enables AgRP neurons to drive feeding. In *eLife* 8. DOI: 10.7554/eLife.46348.
- Chen, Yiming; Lin, Yen-Chu; Kuo, Tzu-Wei; Knight, Zachary A. (2015): Sensory detection of food rapidly modulates arcuate feeding circuits. In *Cell* 160 (5), pp. 829–841. DOI: 10.1016/j.cell.2015.01.033.
- Chen, Yiming; Lin, Yen-Chu; Zimmerman, Christopher A.; Essner, Rachel A.; Knight, Zachary A. (2016): Hunger neurons drive feeding through a sustained, positive reinforcement signal. In *eLife* 5. DOI: 10.7554/eLife.18640.
- Chen, Yu-Chieh David; Park, Scarlet Jinhong; Joseph, Ryan Matthew; Ja, William W.; Dahanukar, Anupama Arun (2019b): Combinatorial Pharyngeal Taste Coding for Feeding Avoidance in Adult *Drosophila*. In *Cell reports* 29 (4), 961-973.e4. DOI: 10.1016/j.celrep.2019.09.036.
- Chiang, Ann-Shyn; Lin, Chih-Yung; Chuang, Chao-Chun; Chang, Hsiu-Ming; Hsieh, Chang-Huain; Yeh, Chang-Wei et al. (2011): Three-dimensional reconstruction of brain-wide wiring networks in *Drosophila* at single-cell resolution. In *Current biology : CB* 21 (1), pp. 1–11. DOI: 10.1016/j.cub.2010.11.056.
- Claßen, Gerbera; Scholz, Henrike (2018): Octopamine Shifts the Behavioral Response From Indecision to Approach or Aversion in *Drosophila melanogaster*. In *Front. Behav. Neurosci.* 12, p. 131. DOI: 10.3389/fnbeh.2018.00131.
- Clyne, P. J.; Warr, C. G.; Freeman, M. R.; Lessing, D.; Kim, J.; Carlson, J. R. (1999): A novel family of divergent seven-transmembrane proteins: candidate odorant receptors in *Drosophila*. In *Neuron* 22 (2), pp. 327–338. DOI: 10.1016/S0896-6273(00)81093-4.
- Corrales-Carvajal, Verónica María; Faisal, Aldo A.; Ribeiro, Carlos (2016): Internal states drive nutrient homeostasis by modulating exploration-exploitation trade-off. In *eLife* 5. DOI: 10.7554/eLife.19920.

- Costa, Marta; Manton, James D.; Ostrovsky, Aaron D.; Prohaska, Steffen; Jefferis, Gregory S. X. E. (2016): NBLAST: Rapid, Sensitive Comparison of Neuronal Structure and Construction of Neuron Family Databases. In *Neuron* 91 (2), pp. 293–311. DOI: 10.1016/j.neuron.2016.06.012.
- Couto, Africa; Alenius, Mattias; Dickson, Barry J. (2005): Molecular, anatomical, and functional organization of the *Drosophila* olfactory system. In *Current Biology* 15 (17), pp. 1535–1547. DOI: 10.1016/j.cub.2005.07.034.
- Creamer, Matthew S.; Chen, Kevin S.; Leifer, Andrew M.; Pillow, Jonathan W. (2022): Correcting motion induced fluorescence artifacts in two-channel neural imaging. In *PLoS computational biology* 18 (9), e1010421. DOI: 10.1371/journal.pcbi.1010421.
- Currier, Timothy A.; Matheson, Andrew M.; Nagel, Katherine I. (2020): Encoding and control of orientation to airflow by a set of *Drosophila* fan-shaped body neurons. In *eLife* 9. DOI: 10.7554/eLife.61510.
- Dacks, Andrew M.; Green, David S.; Root, Cory M.; Nighorn, Alan J.; Wang, Jing W. (2009): Serotonin modulates olfactory processing in the antennal lobe of *Drosophila*. In *Journal of neurogenetics* 23 (4), pp. 366–377. DOI: 10.3109/01677060903085722.
- Dahanukar, Anupama; Lei, Ya-Ting; Kwon, Jae Young; Carlson, John R. (2007): Two Gr genes underlie sugar reception in *Drosophila*. In *Neuron* 56 (3), pp. 503–516. DOI: 10.1016/j.neuron.2007.10.024.
- Dalton, P.; Doolittle, N.; Nagata, H.; Breslin, P. A. (2000): The merging of the senses: integration of subthreshold taste and smell. In *Nature neuroscience* 3 (5), pp. 431–432. DOI: 10.1038/74797.
- Dana, Hod; Sun, Yi; Mohar, Boaz; Hulse, Brad K.; Kerlin, Aaron M.; Hasseman, Jeremy P. et al. (2019): High-performance calcium sensors for imaging activity in neuronal populations and microcompartments. In *Nat Methods* 16 (7), pp. 649–657. DOI: 10.1038/s41592-019-0435-6.
- Das Chakraborty, Sudeshna; Chang, Hetan; Hansson, Bill S.; Sachse, Silke (2022): Higher-order olfactory neurons in the lateral horn support odor valence and odor identity coding in *Drosophila*. In *eLife* 11. DOI: 10.7554/eLife.74637.
- Das Chakraborty, Sudeshna; Sachse, Silke (2021): Olfactory processing in the lateral horn of *Drosophila*. In *Cell Tissue Res* 383 (1), pp. 113–123. DOI: 10.1007/s00441-020-03392-6.
- Davis, Fred P.; Nern, Aljoscha; Picard, Serge; Reiser, Michael B.; Rubin, Gerald M.; Eddy, Sean R.; Henry, Gilbert L. (2020): A genetic, genomic, and computational resource for exploring neural circuit function. In *eLife* 9. DOI: 10.7554/eLife.50901.
- Demattè, M. Luisa; Pojer, Nicola; Endrizzi, Isabella; Corollaro, Maria Laura; Betta, Emanuela; Aprea, Eugenio et al. (2014): Effects of the sound of the bite on apple perceived crispness and hardness. In *Food Quality and Preference* 38, pp. 58–64. DOI: 10.1016/j.foodqual.2014.05.009.
- Deng, Fei; Wan, Jinxia; Li, Guochuan; Dong, Hui; Xia, Xiju; Wang, Yipan et al. (2023): Dual-color GRAB sensors for monitoring spatiotemporal serotonin release in vivo.
- Dethier, V. G. (1976): The hungry fly: A physiological study of the behavior associated with feeding. Available online at <https://psycnet.apa.org/record/1976-27370-000>.
- Devineni, Anita V.; Sun, Bei; Zhukovskaya, Anna; Axel, Richard (2019): Acetic acid activates distinct taste pathways in *Drosophila* to elicit opposing, state-dependent feeding responses. In *eLife* 8. DOI: 10.7554/eLife.47677.
- Dickerson, Anne E.; Reistetter, Timothy A.; Burhans, Stacey; Apple, Katie (2016): Typical Brake Reaction Times Across the Life Span. In *Occupational therapy in health care* 30 (2), pp. 115–123. DOI: 10.3109/07380577.2015.1059971.
- Dolan, Michael-John; Belliard-Guérin, Ghislain; Bates, Alexander Shakeel; Frechter, Shahar; Lampin-Saint-Amaux, Aurélie; Aso, Yoshinori et al. (2018): Communication from Learned to Innate Olfactory Processing Centers Is Required for Memory Retrieval in *Drosophila*. In *Neuron* 100 (3), 651–668.e8. DOI: 10.1016/j.neuron.2018.08.037.

- Dolan, Michael-John; Frechter, Shahar; Bates, Alexander Shakeel; Dan, Chuntao; Huoviala, Paavo; Roberts, Ruairí Jv et al. (2019): Neurogenetic dissection of the *Drosophila* lateral horn reveals major outputs, diverse behavioural functions, and interactions with the mushroom body. In *eLife* 8. DOI: 10.7554/eLife.43079.
- Dorkenwald, Sven; Matsliah, Arie; Sterling, Amy R.; Schlegel, Philipp; Yu, Szi-Chieh; McKellar, Claire E. et al. (2023): Neuronal wiring diagram of an adult brain. In *bioRxiv : the preprint server for biology*. DOI: 10.1101/2023.06.27.546656.
- Døving, K. B.; Trotier, D. (1998): Structure and function of the vomeronasal organ. In *Journal of Experimental Biology* 201 (Pt 21), pp. 2913–2925. DOI: 10.1242/jeb.201.21.2913.
- Elmqvist, J. K.; Elias, C. F.; Saper, C. B. (1999): From lesions to leptin: hypothalamic control of food intake and body weight. In *Neuron* 22 (2), pp. 221–232. DOI: 10.1016/s0896-6273(00)81084-3.
- Engert, Stefanie; Sterne, Gabriella R.; Bock, Davi D.; Scott, Kristin (2022): *Drosophila* gustatory projections are segregated by taste modality and connectivity. In *eLife* 11. DOI: 10.7554/eLife.78110.
- Enjin, Anders; Zaharieva, Emanuela E.; Frank, Dominic D.; Mansourian, Suzan; Suh, Greg S. B.; Gallio, Marco; Stensmyr, Marcus C. (2016): Humidity Sensing in *Drosophila*. In *Current biology : CB* 26 (10), pp. 1352–1358. DOI: 10.1016/j.cub.2016.03.049.
- Faini, Giulia; Tanese, Dimitrii; Molinier, Clément; Telliez, Cécile; Hamdani, Massilia; Blot, Francois et al. (2023): Ultrafast light targeting for high-throughput precise control of neuronal networks. In *Nat Commun* 14 (1), p. 1888. DOI: 10.1038/s41467-023-37416-w.
- Feng, Jiesi; Zhang, Changmei; Lischinsky, Julieta E.; Jing, Miao; Zhou, Jingheng; Wang, Huan et al. (2019): A Genetically Encoded Fluorescent Sensor for Rapid and Specific In Vivo Detection of Norepinephrine. In *Neuron* 102 (4), 745-761.e8. DOI: 10.1016/j.neuron.2019.02.037.
- Finger, Thomas E. (2005): Cell types and lineages in taste buds. In *Chem Senses* 30 Suppl 1, i54-5. DOI: 10.1093/chemse/bjh110.
- Fişek, Mehmet; Wilson, Rachel I. (2014): Stereotyped connectivity and computations in higher-order olfactory neurons. In *Nature neuroscience* 17 (2), pp. 280–288. DOI: 10.1038/nn.3613.
- Fishilevich, Elane; Vosshall, Leslie B. (2005): Genetic and functional subdivision of the *Drosophila* antennal lobe. In *Current Biology* 15 (17), pp. 1548–1553. DOI: 10.1016/j.cub.2005.07.066.
- Flavell, Steven W.; Gordus, Andrew (2022): Dynamic functional connectivity in the static connectome of *Caenorhabditis elegans*. In *Current Opinion in Neurobiology* 73, p.102515. DOI: 10.1016/j.conb.2021.12.002.
- Fleischer, Joerg; Breer, Heinz; Strotmann, Joerg (2009): Mammalian olfactory receptors. In *Front. Cell. Neurosci.* 3, p. 9. DOI: 10.3389/neuro.03.009.2009.
- Frank, Sabine; Kullmann, Stephanie; Veit, Ralf (2013): Food related processes in the insular cortex. In *Front. Hum. Neurosci.* 7, p. 499. DOI: 10.3389/fnhum.2013.00499.
- Frechter, Shahar; Bates, Alexander Shakeel; Tootoonian, Sina; Dolan, Michael-John; Manton, James; Jamasb, Arian Rokkum et al. (2019): Functional and anatomical specificity in a higher olfactory centre. In *eLife* 8. DOI: 10.7554/eLife.44590.
- Friston, K. J.; Buechel, C.; Fink, G. R.; Morris, J.; Rolls, E.; Dolan, R. J. (1997): Psychophysiological and modulatory interactions in neuroimaging. In *NeuroImage* 6 (3), pp. 218–229. DOI: 10.1006/nimg.1997.0291.
- Fu, Ou; Iwai, Yuu; Narukawa, Masataka; Ishikawa, Ayako W.; Ishii, Kentaro K.; Murata, Ken et al. (2019): Hypothalamic neuronal circuits regulating hunger-induced taste modification. In *Nat Commun* 10 (1), p. 4560. DOI: 10.1038/s41467-019-12478-x.
- Fujii, Shinsuke; Yavuz, Ahmet; Slone, Jesse; Jagge, Christopher; Song, Xiangyu; Amrein, Hubert (2015): *Drosophila* Sugar Receptors in Sweet Taste Perception, Olfaction, and Internal Nutrient Sensing. In *Current Biology* 25 (5), pp. 621–627. DOI: 10.1016/j.cub.2014.12.058.

- Gadziola, Marie A.; Tylicki, Kate A.; Christian, Diana L.; Wesson, Daniel W. (2015): The olfactory tubercle encodes odor valence in behaving mice. In *J. Neurosci.* 35 (11), pp. 4515–4527. DOI: 10.1523/JNEUROSCI.4750-14.2015.
- Ganguly, Anindya; Pang, Lisa; Duong, Vi-Khoi; Lee, Angelina; Schoniger, Hanni; Varady, Erika; Dahanukar, Anupama (2017): A Molecular and Cellular Context-Dependent Role for Ir76b in Detection of Amino Acid Taste. In *Cell reports* 18 (3), pp. 737–750. DOI: 10.1016/j.celrep.2016.12.071.
- Gendre, Nanaë; Lüer, Karin; Friche, Sandrine; Grillenzoni, Nicola; Ramaekers, Ariane; Technau, Gerhard M.; Stocker, Reinhard F. (2004): Integration of complex larval chemosensory organs into the adult nervous system of *Drosophila*. In *Development* 131 (1), pp. 83–92. DOI: 10.1242/dev.00879.
- Gibbons, Jonathan R.; Sadiq, Nazia M. (2023): StatPearls. Neuroanatomy, Neural Taste Pathway. Treasure Island (FL).
- Grabe, Veit; Baschwitz, Amelie; Dweck, Hany K. M.; Lavista-Llanos, Sofia; Hansson, Bill S.; Sachse, Silke (2016): Elucidating the Neuronal Architecture of Olfactory Glomeruli in the *Drosophila* Antennal Lobe. In *Cell reports* 16 (12), pp. 3401–3413. DOI: 10.1016/j.celrep.2016.08.063.
- Hanci, Deniz; Altun, Huseyin (2016): Hunger state affects both olfactory abilities and gustatory sensitivity. In *European archives of oto-rhino-laryngology : official journal of the European Federation of Oto-Rhino-Laryngological Societies (EUFOS) : affiliated with the German Society for Oto-Rhino-Laryngology - Head and Neck Surgery* 273 (7), pp. 1637–1641. DOI: 10.1007/s00405-015-3589-6.
- Harris, David T.; Kallman, Benjamin R.; Mullaney, Brendan C.; Scott, Kristin (2015): Representations of taste modality in the *Drosophila* brain. In *Neuron* 86 (6), pp. 1449–1460. DOI: 10.1016/j.neuron.2015.05.026.
- Heisenberg, M.; Borst, A.; Wagner, S.; Byers, D. (1985): *Drosophila* mushroom body mutants are deficient in olfactory learning. In *Journal of neurogenetics* 2 (1), pp. 1–30. DOI: 10.3109/01677068509100140.
- Hiroi, Makoto; Tanimura, Teiichi; Marion-Poll, Frédéric (2008): Hedonic taste in *Drosophila* revealed by olfactory receptors expressed in taste neurons. In *PLoS ONE* 3 (7), e2610. DOI: 10.1371/journal.pone.0002610.
- Hu, Wantong; Peng, Yiqing; Sun, Jiameng; Zhang, Fang; Zhang, Xuchen; Wang, Lianzhang et al. (2018): Fan-Shaped Body Neurons in the *Drosophila* Brain Regulate Both Innate and Conditioned Nociceptive Avoidance. In *Cell reports* 24 (6), pp. 1573–1584. DOI: 10.1016/j.celrep.2018.07.028.
- Hussain, Ashiq; Üçpınar, Habibe K.; Zhang, Mo; Loschek, Laura F.; Kadow, Ilona C. Grunwald (2016a): Neuropeptides Modulate Female Chemosensory Processing upon Mating in *Drosophila*. In *PLoS Biology* 14 (5), e1002455. DOI: 10.1371/journal.pbio.1002455.
- Hussain, Ashiq; Zhang, Mo; Üçpınar, Habibe K.; Svensson, Thomas; Quillery, Elsa; Gompel, Nicolas et al. (2016b): Ionotropic Chemosensory Receptors Mediate the Taste and Smell of Polyamines. In *PLoS Biology* 14 (5), e1002454. DOI: 10.1371/journal.pbio.1002454.
- Inagaki, Hidehiko K.; Panse, Ketaki M.; Anderson, David J. (2014): Independent, reciprocal neuromodulatory control of sweet and bitter taste sensitivity during starvation in *Drosophila*. In *Neuron* 84 (4), pp. 806–820. DOI: 10.1016/j.neuron.2014.09.032.
- Iravani, Behzad; Schaefer, Martin; Wilson, Donald A.; Arshamian, Artin; Lundström, Johan N. (2021): The human olfactory bulb processes odor valence representation and cues motor avoidance behavior. In *Proceedings of the National Academy of Sciences of the United States of America* 118 (42). DOI: 10.1073/pnas.2101209118.
- Ito, Kei; Shinomiya, Kazunori; Ito, Masayoshi; Armstrong, J. Douglas; Boyan, George; Hartenstein, Volker et al. (2014): A systematic nomenclature for the insect brain. In *Neuron* 81 (4), pp. 755–765. DOI: 10.1016/j.neuron.2013.12.017.
- Itskov, Pavel M.; Moreira, José-Maria; Vinnik, Ekaterina; Lopes, Gonçalo; Safarik, Steve; Dickinson, Michael H.; Ribeiro, Carlos (2014): Automated monitoring and quantitative analysis of feeding behaviour in *Drosophila*. In *Nat Commun* 5 (1), p. 4560. DOI: 10.1038/ncomms5560.

- Jain, Aditya; Bansal, Ramta; Kumar, Avnish; Singh, K. D. (2015): A comparative study of visual and auditory reaction times on the basis of gender and physical activity levels of medical first year students. In *International journal of applied & basic medical research* 5 (2), pp. 124–127. DOI: 10.4103/2229-516X.157168.
- Jefferis, Gregory S. X. E. (2005): Insect olfaction: a map of smell in the brain. In *Current Biology* 15 (17), R668-70. DOI: 10.1016/j.cub.2005.08.033.
- Jefferis, Gregory S. X. E.; Potter, Christopher J.; Chan, Alexander M.; Marin, Elizabeth C.; Rohlfsing, Torsten; Maurer, Calvin R.; Luo, Liqun (2007): Comprehensive maps of *Drosophila* higher olfactory centers: spatially segregated fruit and pheromone representation. In *Cell* 128 (6), pp. 1187–1203. DOI: 10.1016/j.cell.2007.01.040.
- Jelen, Meghan; Musso, Pierre-Yves; Junca, Pierre; Gordon, Michael D. (2021): Optogenetic induction of appetitive and aversive taste memories in *Drosophila*.
- Jenett, Arnim; Rubin, Gerald M.; Ngo, Teri-T B.; Shepherd, David; Murphy, Christine; Dionne, Heather et al. (2012): A GAL4-driver line resource for *Drosophila* neurobiology. In *Cell reports* 2 (4), pp. 991–1001. DOI: 10.1016/j.celrep.2012.09.011.
- Jeong, Yong Taek; Oh, Soo Min; Shim, Jaewon; Seo, Jeong Taeg; Kwon, Jae Young; Moon, Seok Jun (2016): Mechanosensory neurons control sweet sensing in *Drosophila*. In *Nat Commun* 7, p. 12872. DOI: 10.1038/ncomms12872.
- Jiao, Yuchen; Moon, Seok Jun; Wang, Xiaoyue; Ren, Qiuting; Montell, Craig (2008): Gr64f is required in combination with other gustatory receptors for sugar detection in *Drosophila*. In *Current Biology* 18 (22), pp. 1797–1801. DOI: 10.1016/j.cub.2008.10.009.
- Jing, Miao; Zhang, Peng; Wang, Guangfu; Feng, Jiesi; Mesik, Lukas; Zeng, Jianzhi et al. (2018): A genetically encoded fluorescent acetylcholine indicator for in vitro and in vivo studies. In *Nat Biotechnol* 36 (8), pp. 726–737. DOI: 10.1038/nbt.4184.
- Jung, Seung-Hye; Hueston, Catherine; Bhandawat, Vikas (2015): Odor-identity dependent motor programs underlie behavioral responses to odors. In *eLife* 4. DOI: 10.7554/eLife.11092.
- Kain, Pinky; Dahanukar, Anupama (2015): Secondary taste neurons that convey sweet taste and starvation in the *Drosophila* brain. In *Neuron* 85 (4), pp. 819–832. DOI: 10.1016/j.neuron.2015.01.005.
- Kang, Kyeongjin; Panzano, Vincent C.; Chang, Elaine C.; Ni, Lina; Dainis, Alexandra M.; Jenkins, Adam M. et al. (2011): Modulation of TRPA1 thermal sensitivity enables sensory discrimination in *Drosophila*. In *Nature* 481 (7379), pp. 76–80. DOI: 10.1038/nature10715.
- Kato, Yoshiaki S.; Tomita, Jun; Kume, Kazuhiko (2022): Interneurons of fan-shaped body promote arousal in *Drosophila*. In *PLoS ONE* 17 (11), e0277918. DOI: 10.1371/journal.pone.0277918.
- Kim, Heesoo; Kirkhart, Colleen; Scott, Kristin (2017a): Long-range projection neurons in the taste circuit of *Drosophila*. In *eLife* 6, p. 13819. DOI: 10.7554/eLife.23386.
- Kim, Susy M.; Su, Chih-Ying; Wang, Jing W. (2017b): Neuromodulation of Innate Behaviors in *Drosophila*. In *Annual review of neuroscience* 40, pp. 327–348. DOI: 10.1146/annurev-neuro-072116-031558.
- Kinnamon, Sue C. (2009): Umami taste transduction mechanisms. In *The American journal of clinical nutrition* 90 (3), 753S-755S. DOI: 10.3945/ajcn.2009.27462K.
- Kirkhart, Colleen; Scott, Kristin (2015): Gustatory Learning and Processing in the *Drosophila* Mushroom Bodies. In *J. Neurosci.* 35 (15), pp. 5950–5958. DOI: 10.1523/JNEUROSCI.3930-14.2015.
- Kleene, Steven J. (2008): The electrochemical basis of odor transduction in vertebrate olfactory cilia. In *Chem Senses* 33 (9), pp. 839–859. DOI: 10.1093/chemse/bjn048.
- Ko, Kang I.; Root, Cory M.; Lindsay, Scott A.; Zaninovich, Orel A.; Shepherd, Andrew K.; Wasserman, Steven A. et al. (2015): Starvation promotes concerted modulation of appetitive olfactory behavior via parallel neuromodulatory circuits. In *eLife* 4. DOI: 10.7554/eLife.08298.

Kobler, Johanna M.; Rodriguez Jimenez, Francisco J.; Petcu, Irina; Grunwald Kadow, Ilona C. (2020): Immune Receptor Signaling and the Mushroom Body Mediate Post-ingestion Pathogen Avoidance. In *Current biology : CB* 30 (23), 4693-4709.e3. DOI: 10.1016/j.cub.2020.09.022.

Landayan, Dan; Wang, Brian P.; Zhou, Jennifer; Wolf, Fred W. (2021): Thirst interneurons that promote water seeking and limit feeding behavior in *Drosophila*. In *eLife* 10. DOI: 10.7554/eLife.66286.

LeDue, Emily E.; Mann, Kevin; Koch, Ellen; Chu, Bonnie; Dakin, Roslyn; Gordon, Michael D. (2016): Starvation-Induced Depotentiation of Bitter Taste in *Drosophila*. In *Current biology : CB* 26 (21), pp. 2854–2861. DOI: 10.1016/j.cub.2016.08.028.

Levitsky, David A.; Barre, Laura; Michael, John Jeshurun; Zhong, Yingyi; He, Yitong; Mizia, Alyse; Kaila, Sahib (2022): The Rise and Fall of Physiological Theories of the Control of Human Eating Behavior. In *Frontiers in nutrition* 9, p. 826334. DOI: 10.3389/fnut.2022.826334.

Levoy, Marc; Ng, Ren; Adams, Andrew; Footer, Matthew; Horowitz, Mark (2006): Light field microscopy. In *ACM Trans. Graph.* 25 (3), pp. 924–934. DOI: 10.1145/1141911.1141976.

Lewis, Laurence P. C.; Siju, K. P.; Aso, Yoshinori; Friedrich, Anja B.; Bulteel, Alexander J. B.; Rubin, Gerald M.; Grunwald Kadow, Ilona C. (2015): A Higher Brain Circuit for Immediate Integration of Conflicting Sensory Information in *Drosophila*. In *Current biology : CB* 25 (17), pp. 2203–2214. DOI: 10.1016/j.cub.2015.07.015.

Li, Songling; Li, Bingxue; Gao, Li; Wang, Jingwen; Yan, Zhiqiang (2022): Humidity response in *Drosophila* olfactory sensory neurons requires the mechanosensitive channel TMEM63. In *Nat Commun* 13 (1), p. 3814. DOI: 10.1038/s41467-022-31253-z.

Liman, Emily R. (2020): Salty Taste: From Transduction to Transmitter Release, Hold the Calcium. In *Neuron* 106 (5), pp. 709–711. DOI: 10.1016/j.neuron.2020.05.012.

Liman, Emily R.; Kinnamon, Sue C. (2021): Sour taste: receptors, cells and circuits. In *Current opinion in physiology* 20, pp. 8–15. DOI: 10.1016/j.cophys.2020.12.006.

Limbania, Daniela; Turner, Grace Lynn; Wasserman, Sara M. (2023): Dehydrated *Drosophila melanogaster* track a water plume in tethered flight. In *iScience* 26 (3), p. 106266. DOI: 10.1016/j.isci.2023.106266.

Lin, Suwei; Oswald, David; Chandra, Vikram; Talbot, Clifford; Huetteroth, Wolf; Waddell, Scott (2014): Neural correlates of water reward in thirsty *Drosophila*. In *Nat Neurosci* 17 (11), pp. 1536–1542. DOI: 10.1038/nn.3827.

Lin, Suwei; Senapati, Bhagyashree; Tsao, Chang-Hui (2019): Neural basis of hunger-driven behaviour in *Drosophila*. In *Open biology* 9 (3), p. 180259. DOI: 10.1098/rsob.180259.

Livneh, Yoav; Ramesh, Rohan N.; Burgess, Christian R.; Levandowski, Kirsten M.; Madara, Joseph C.; Fenselau, Henning et al. (2017): Homeostatic circuits selectively gate food cue responses in insular cortex. In *Nature* 546 (7660), pp. 611–616. DOI: 10.1038/nature22375.

Livneh, Yoav; Sugden, Arthur U.; Madara, Joseph C.; Essner, Rachel A.; Flores, Vanessa I.; Sugden, Lauren A. et al. (2020): Estimation of Current and Future Physiological States in Insular Cortex. In *Neuron* 105 (6), 1094-1111.e10. DOI: 10.1016/j.neuron.2019.12.027.

Machado, Cleiton F.; Reis-Silva, Thiago M.; Lyra, Cassandra S.; Felicio, Luciano F.; Malnic, Bettina (2018): Buried Food-seeking Test for the Assessment of Olfactory Detection in Mice. In *Bio-protocol* 8 (12), e2897. DOI: 10.21769/BioProtoc.2897.

Maier, Joost X.; Wachowiak, Matt; Katz, Donald B. (2012): Chemosensory convergence on primary olfactory cortex. In *J. Neurosci.* 32 (48), pp. 17037–17047. DOI: 10.1523/JNEUROSCI.3540-12.2012.

Mamiya, Akira; Beshel, Jennifer; Xu, Chunsu; Zhong, Yi (2008): Neural representations of airflow in *Drosophila* mushroom body. In *PLoS ONE* 3 (12), e4063. DOI: 10.1371/journal.pone.0004063.

Mann, Kevin; Gallen, Courtney L.; Clandinin, Thomas R. (2017): Whole-Brain Calcium Imaging Reveals an Intrinsic Functional Network in *Drosophila*. In *Current biology : CB* 27 (15), 2389-2396.e4. DOI: 10.1016/j.cub.2017.06.076.

- Marella, Sunanda; Fischler, Walter; Kong, Priscilla; Asgarian, Sam; Rueckert, Erroll; Scott, Kristin (2006): Imaging taste responses in the fly brain reveals a functional map of taste category and behavior. In *Neuron* 49 (2), pp. 285–295. DOI: 10.1016/j.neuron.2005.11.037.
- Marella, Sunanda; Mann, Kevin; Scott, Kristin (2012): Dopaminergic modulation of sucrose acceptance behavior in *Drosophila*. In *Neuron* 73 (5), pp. 941–950. DOI: 10.1016/j.neuron.2011.12.032.
- Marin, Elizabeth C.; Jefferis, Gregory S. X. E.; Komiyama, Takaki; Zhu, Haitao; Luo, Liqun (2002): Representation of the glomerular olfactory map in the *Drosophila* brain. In *Cell* 109 (2), pp. 243–255. DOI: 10.1016/S0092-8674(02)00700-6.
- Masek, Pavel; Worden, Kurtresha; Aso, Yoshinori; Rubin, Gerald M.; Keene, Alex C. (2015): A dopamine-modulated neural circuit regulating aversive taste memory in *Drosophila*. In *Current biology : CB* 25 (11), pp. 1535–1541. DOI: 10.1016/j.cub.2015.04.027.
- Masse, Nicolas Y.; Turner, Glenn C.; Jefferis, Gregory S. X. E. (2009): Olfactory information processing in *Drosophila*. In *Current biology : CB* 19 (16), R700-13. DOI: 10.1016/j.cub.2009.06.026.
- Matheson, Andrew M. M.; Lanz, Aaron J.; Medina, Ashley M.; Licata, Al M.; Currier, Timothy A.; Syed, Mubarak H.; Nagel, Katherine I. (2022): A neural circuit for wind-guided olfactory navigation. In *Nat Commun* 13 (1), p. 4613. DOI: 10.1038/s41467-022-32247-7.
- McRaven, Christopher; Tanese, Dimitrii; Zhang, Lixia; Yang, Chao-Tsung; Ahrens, Misha B.; Emiliani, Valentina; Koyama, Minoru (2020): High-throughput cellular-resolution synaptic connectivity mapping in vivo with concurrent two-photon optogenetics and volumetric Ca²⁺ imaging.
- Miranda, Maria Isabel (2012): Taste and odor recognition memory: the emotional flavor of life. In *Reviews in the neurosciences* 23 (5-6), pp. 481–499. DOI: 10.1515/revneuro-2012-0064.
- Miyamoto, Tetsuya; Slone, Jesse; Song, Xiangyu; Amrein, Hubert (2012): A fructose receptor functions as a nutrient sensor in the *Drosophila* brain. In *Cell* 151 (5), pp. 1113–1125. DOI: 10.1016/j.cell.2012.10.024.
- Miyazaki, Takaaki; Ito, Kei (2010): Neural architecture of the primary gustatory center of *Drosophila melanogaster* visualized with GAL4 and LexA enhancer-trap systems. In *The Journal of comparative neurology* 518 (20), pp. 4147–4181. DOI: 10.1002/cne.22433.
- Molitor, Elena von; Riedel, Katja; Krohn, Michael; Hafner, Mathias; Rudolf, Rüdiger; Cesetti, Tiziana (2021): Sweet Taste Is Complex: Signaling Cascades and Circuits Involved in Sweet Sensation. In *Front. Hum. Neurosci.* 15, p. 667709. DOI: 10.3389/fnhum.2021.667709.
- Mollo, Ernesto; Boero, Ferdinando; Peñuelas, Josep; Fontana, Angelo; Garson, Mary J.; Roussis, Vassilios et al. (2022): Taste and Smell: A Unifying Chemosensory Theory. In *The Quarterly Review of Biology* 97 (2), pp. 69–94. DOI: 10.1086/720097.
- Mombaerts, P. (1999): Seven-transmembrane proteins as odorant and chemosensory receptors. In *Science (New York, N. Y.)* 286 (5440), pp. 707–711. DOI: 10.1126/science.286.5440.707.
- Moreira, José-Maria; Itskov, Pavel M.; Goldschmidt, Dennis; Baltazar, Celia; Steck, Kathrin; Tastekin, Ibrahim et al. (2019): optoPAD, a closed-loop optogenetics system to study the circuit basis of feeding behaviors. In *eLife* 8. DOI: 10.7554/eLife.43924.
- Münch, Daniel; Goldschmidt, Dennis; Ribeiro, Carlos (2022): The neuronal logic of how internal states control food choice. In *Nature* 607 (7920), pp. 747–755. DOI: 10.1038/s41586-022-04909-5.
- Murthy, Venkatesh N. (2011): Olfactory maps in the brain. In *Annual review of neuroscience* 34, pp. 233–258. DOI: 10.1146/annurev-neuro-061010-113738.
- Namiki, Shigehiro; Dickinson, Michael H.; Wong, Allan M.; Korff, Wyatt; Card, Gwyneth M. (2018): The functional organization of descending sensory-motor pathways in *Drosophila*. In *eLife* 7. DOI: 10.7554/eLife.34272.
- Nayak, Shubha V.; Singh, R.Naresh (1983): Sensilla on the tarsal segments and mouthparts of adult *Drosophila melanogaster meigen* (Diptera : *Drosophilidae*). In *International Journal of Insect Morphology and Embryology* 12 (5-6), pp. 273–291. DOI: 10.1016/0020-7322(83)90023-5.

- Nei, Masatoshi; Niimura, Yoshihito; Nozawa, Masafumi (2008): The evolution of animal chemosensory receptor gene repertoires: roles of chance and necessity. In *Nat Rev Genet* 9 (12), pp. 951–963. DOI: 10.1038/nrg2480.
- Nelson, G.; Hoon, M. A.; Chandrashekar, J.; Zhang, Y.; Ryba, N. J.; Zuker, C. S. (2001): Mammalian sweet taste receptors. In *Cell* 106 (3), pp. 381–390. DOI: 10.1016/S0092-8674(01)00451-2.
- Niswender, Kevin D.; Schwartz, Michael W. (2003): Insulin and leptin revisited: adiposity signals with overlapping physiological and intracellular signaling capabilities. In *Frontiers in neuroendocrinology* 24 (1), pp. 1–10. DOI: 10.1016/s0091-3022(02)00105-x.
- Oh, Soo Min; Jeong, Kyunghwa; Seo, Jeong Taeg; Moon, Seok Jun (2021): Multisensory interactions regulate feeding behavior in *Drosophila*. In *Proceedings of the National Academy of Sciences of the United States of America* 118 (7). DOI: 10.1073/pnas.2004523118.
- Pan, Yufeng; Zhou, Yanqiong; Guo, Chao; Gong, Haiyun; Gong, Zhefeng; Liu, Li (2009): Differential roles of the fan-shaped body and the ellipsoid body in *Drosophila* visual pattern memory. In *Learning & memory (Cold Spring Harbor, N.Y.)* 16 (5), pp. 289–295. DOI: 10.1101/lm.1331809.
- Patella, Paola; Wilson, Rachel I. (2018): Functional Maps of Mechanosensory Features in the *Drosophila* Brain. In *Current biology : CB* 28 (8), 1189-1203.e5. DOI: 10.1016/j.cub.2018.02.074.
- Perisse, Emmanuel; Oswald, David; Barnstedt, Oliver; Talbot, Clifford B.; Huetteroth, Wolf; Waddell, Scott (2016): Aversive Learning and Appetitive Motivation Toggle Feed-Forward Inhibition in the *Drosophila* Mushroom Body. In *Neuron* 90 (5), pp. 1086–1099. DOI: 10.1016/j.neuron.2016.04.034.
- Randi, Francesco; Sharma, Anuj K.; Dvali, Sophie; Leifer, Andrew M. (2022): Neural signal propagation atlas of *C. elegans*. Available online at <https://arxiv.org/pdf/2208.04790>.
- Robertson, Hugh M.; Warr, Coral G.; Carlson, John R. (2003): Molecular evolution of the insect chemoreceptor gene superfamily in *Drosophila melanogaster*. In *Proceedings of the National Academy of Sciences of the United States of America* 100 Suppl 2 (Suppl 2), pp. 14537–14542. DOI: 10.1073/pnas.2335847100.
- Rolls, Edmund T. (2006): Brain mechanisms underlying flavour and appetite. In *Philosophical transactions of the Royal Society of London. Series B, Biological sciences* 361 (1471), pp. 1123–1136. DOI: 10.1098/rstb.2006.1852.
- Rolls, Edmund T. (2012): Taste, olfactory and food texture reward processing in the brain and the control of appetite. In *The Proceedings of the Nutrition Society* 71 (4), pp. 488–501. DOI: 10.1017/S0029665112000821.
- Rolls, Edmund T. (2019): Taste and smell processing in the brain. In *Handbook of clinical neurology* 164, pp. 97–118. DOI: 10.1016/B978-0-444-63855-7.00007-1.
- Root, Cory M.; Ko, Kang I.; Jafari, Amir; Wang, Jing W. (2011): Presynaptic facilitation by neuropeptide signaling mediates odor-driven food search. In *Cell* 145 (1), pp. 133–144. DOI: 10.1016/j.cell.2011.02.008.
- Roudnitzky, Natacha; Bult, Johannes H. F.; Wijk, Rene A. de; Reden, Jens; Schuster, Benno; Hummel, Thomas (2011): Investigation of interactions between texture and ortho- and retronasal olfactory stimuli using psychophysical and electrophysiological approaches. In *Behavioural brain research* 216 (1), pp. 109–115. DOI: 10.1016/j.bbr.2010.07.019.
- Rozin, P. (1982): "Taste-smell confusions" and the duality of the olfactory sense. In *Perception & psychophysics* 31 (4), pp. 397–401. DOI: 10.3758/BF03202667.
- Rubinov, Mikail; Sporns, Olaf (2010): Complex network measures of brain connectivity: uses and interpretations. In *NeuroImage* 52 (3), pp. 1059–1069. DOI: 10.1016/j.neuroimage.2009.10.003.
- Samuelsen, Chad L.; Fontanini, Alfredo (2017): Processing of Intraoral Olfactory and Gustatory Signals in the Gustatory Cortex of Awake Rats. In *J. Neurosci.* 37 (2), pp. 244–257. DOI: 10.1523/JNEUROSCI.1926-16.2016.

- Sánchez-Alcañiz, Juan Antonio; Zappia, Giovanna; Marion-Poll, Frédéric; Benton, Richard (2017): A mechanosensory receptor required for food texture detection in *Drosophila*. In *Nat Commun* 8, p. 14192. DOI: 10.1038/ncomms14192.
- Sato, Koji; Pellegrino, Maurizio; Nakagawa, Takao; Nakagawa, Tatsuro; Vosshall, Leslie B.; Touhara, Kazushige (2008): Insect olfactory receptors are heteromeric ligand-gated ion channels. In *Nature* 452 (7190), pp. 1002–1006. DOI: 10.1038/nature06850.
- Sayin, Sercan; Boehm, Ariane C.; Kobler, Johanna M.; Backer, Jean-François de; Grunwald Kadow, Ilona C. (2018): Internal State Dependent Odor Processing and Perception—The Role of Neuromodulation in the Fly Olfactory System. In *Front. Cell. Neurosci.* 12, p. 11. DOI: 10.3389/fncel.2018.00011.
- Scheffer, Louis K.; Xu, C. Shan; Januszewski, Michal; Lu, Zhiyuan; Takemura, Shin-Ya; Hayworth, Kenneth J. et al. (2020): A connectome and analysis of the adult *Drosophila* central brain. In *eLife* 9. DOI: 10.7554/eLife.57443.
- Scheidler, Nicole H.; Liu, Cheng; Hamby, Kelly A.; Zalom, Frank G.; Syed, Zainulabeuddin (2015): Volatile codes: Correlation of olfactory signals and reception in *Drosophila*-yeast chemical communication. In *Sci Rep* 5 (1), p. 14059. DOI: 10.1038/srep14059.
- Schubert, Marco; Hansson, Bill S.; Sachse, Silke (2014): The banana code-natural blend processing in the olfactory circuitry of *Drosophila melanogaster*. In *Frontiers in physiology* 5, p. 59. DOI: 10.3389/fphys.2014.00059.
- Schultzhaus, Janna N.; Saleem, Sehresh; Iftikhar, Hina; Carney, Ginger E. (2017): The role of the *Drosophila* lateral horn in olfactory information processing and behavioral response. In *Journal of Insect Physiology* 98, pp. 29–37. DOI: 10.1016/j.jinsphys.2016.11.007.
- Schwartz, G. J. (2000): The role of gastrointestinal vagal afferents in the control of food intake: current prospects. In *Nutrition (Burbank, Los Angeles County, Calif.)* 16 (10), pp. 866–873. DOI: 10.1016/S0899-9007(00)00464-0.
- Scott, J. W.; McBride, R. L.; Schneider, S. P. (1980): The organization of projections from the olfactory bulb to the piriform cortex and olfactory tubercle in the rat. In *The Journal of comparative neurology* 194 (3), pp. 519–534. DOI: 10.1002/cne.901940304.
- Scott, K.; Brady, R.; Cravchik, A.; Morozov, P.; Rzhetsky, A.; Zuker, C.; Axel, R. (2001): A chemosensory gene family encoding candidate gustatory and olfactory receptors in *Drosophila*. In *Cell* 104 (5), pp. 661–673. DOI: 10.1016/S0092-8674(01)00263-X.
- Seki, Yoichi; Rybak, Jürgen; Wicher, Dieter; Sachse, Silke; Hansson, Bill S. (2010): Physiological and morphological characterization of local interneurons in the *Drosophila* antennal lobe. In *Journal of neurophysiology* 104 (2), pp. 1007–1019. DOI: 10.1152/jn.00249.2010.
- Semmelhack, Julia L.; Wang, Jing W. (2009): Select *Drosophila* glomeruli mediate innate olfactory attraction and aversion. In *Nature* 459 (7244), pp. 218–223. DOI: 10.1038/nature07983.
- Shanbhag, S. R.; Hekmat-Safe, D.; Kim, M. S.; Park, S. K.; Carlson, J. R.; Pikielny, C. et al. (2001): Expression mosaic of odorant-binding proteins in *Drosophila* olfactory organs. In *Microscopy research and technique* 55 (5), pp. 297–306. DOI: 10.1002/jemt.1179.
- Shanbhag, S.R; Müller, B.; Steinbrecht, R.A (1999): Atlas of olfactory organs of *Drosophila melanogaster*. In *International Journal of Insect Morphology and Embryology* 28 (4), pp. 377–397. DOI: 10.1016/S0020-7322(99)00039-2.
- Shepherd, Gordon M. (2004): The human sense of smell: are we better than we think? In *PLOS Biology* 2 (5), E146. DOI: 10.1371/journal.pbio.0020146.
- Shiraiwa, Takashi (2008): Multimodal chemosensory integration through the maxillary palp in *Drosophila*. In *PLoS ONE* 3 (5), e2191. DOI: 10.1371/journal.pone.0002191.
- Shiraiwa, Takashi; Carlson, John R. (2007): Proboscis extension response (PER) assay in *Drosophila*. In *JoVE (Journal of Visualized Experiments)* (3), p. 193. DOI: 10.3791/193.

- Shiu, Philip K.; Sterne, Gabriella R.; Engert, Stefanie; Dickson, Barry J.; Scott, Kristin (2022): Taste quality and hunger interactions in a feeding sensorimotor circuit. In *eLife* 11. DOI: 10.7554/eLife.79887.
- Siegle, Joshua H.; Ledochowitsch, Peter; Jia, Xiaoxuan; Millman, Daniel J.; Ocker, Gabriel K.; Caldejon, Shiella et al. (2021): Reconciling functional differences in populations of neurons recorded with two-photon imaging and electrophysiology. In *eLife Sciences Publications, Ltd*, 7/16/2021. Available online at <https://elifesciences.org/articles/69068>, checked on 5/16/2023.
- Siju, K. P.; Štih, Vilim; Aimon, Sophie; Gjorgjieva, Julijana; Portugues, Ruben; Kadow, Ilona C. Grunwald (2020): Valence and State-Dependent Population Coding in Dopaminergic Neurons in the Fly Mushroom Body. In *Current Biology* 0 (0). DOI: 10.1016/j.cub.2020.04.037.
- Small, Dana M.; Gerber, Johannes C.; Mak, Y. Erica; Hummel, Thomas (2005): Differential neural responses evoked by orthonasal versus retronasal odorant perception in humans. In *Neuron* 47 (4), pp. 593–605. DOI: 10.1016/j.neuron.2005.07.022.
- Small, Dana M.; Prescott, John (2005): Odor/taste integration and the perception of flavor. In *Experimental brain research* 166 (3-4), pp. 345–357. DOI: 10.1007/s00221-005-2376-9.
- Snell, Nathaniel J.; Fisher, John D.; Hartmann, Griffin G.; Zolyomi, Bence; Talay, Mustafa; Barnea, Gilad (2022): Complex representation of taste quality by second-order gustatory neurons in *Drosophila*. In *Current biology : CB* 32 (17), 3758-3772.e4. DOI: 10.1016/j.cub.2022.07.048.
- Spence, Charles (2015): Multisensory flavor perception. In *Cell* 161 (1), pp. 24–35. DOI: 10.1016/j.cell.2015.03.007.
- St Johnston, D.; Nüsslein-Volhard, C. (1992): The origin of pattern and polarity in the *Drosophila* embryo. In *Cell* 68 (2), pp. 201–219. DOI: 10.1016/0092-8674(92)90466-p.
- Sterne, Gabriella R.; Otsuna, Hideo; Dickson, Barry J.; Scott, Kristin (2021): Classification and genetic targeting of cell types in the primary taste and premotor center of the adult *Drosophila* brain. In *eLife* 10. DOI: 10.7554/eLife.71679.
- Stocker, R. F. (1994): The organization of the chemosensory system in *Drosophila melanogaster*: a review. In *Cell and tissue research* 275 (1), pp. 3–26. DOI: 10.1007/BF00305372.
- Stocker, R. F.; Lienhard, M. C.; Borst, A.; Fischbach, K. F. (1990): Neuronal architecture of the antennal lobe in *Drosophila melanogaster*. In *Cell and tissue research* 262 (1), pp. 9–34. DOI: 10.1007/BF00327741.
- Stocker, Reinhard F. (2009): The olfactory pathway of adult and larval *Drosophila*: conservation or adaptation to stage-specific needs? In *Annals of the New York Academy of Sciences* 1170, pp. 482–486. DOI: 10.1111/j.1749-6632.2009.03896.x.
- Störtkuhl, Klemens F.; Kettler, Raffael; Fischer, Sven; Hovemann, Bernhard T. (2005): An increased receptive field of olfactory receptor Or43a in the antennal lobe of *Drosophila* reduces benzaldehyde-driven avoidance behavior. In *Chem Senses* 30 (1), pp. 81–87. DOI: 10.1093/chemse/bji003.
- Stoyanov, George S.; Matev, Boyko K.; Valchanov, Petar; Sapundzhiev, Nikolay; Young, John R. (2018): The Human Vomeronasal (Jacobson's) Organ: A Short Review of Current Conceptions, With an English Translation of Potiquet's Original Text. In *Cureus* 10 (5), e2643. DOI: 10.7759/cureus.2643.
- Strube-Bloss, Martin F.; Grabe, Veit; Hansson, Bill S.; Sachse, Silke (2017): Calcium imaging revealed no modulatory effect on odor-evoked responses of the *Drosophila* antennal lobe by two populations of inhibitory local interneurons. In *Sci Rep* 7 (1), p. 7854. DOI: 10.1038/s41598-017-08090-y.
- Strutz, Antonia; Soelter, Jan; Baschwitz, Amelie; Farhan, Abu; Grabe, Veit; Rybak, Jürgen et al. (2014): Decoding odor quality and intensity in the *Drosophila* brain. In *eLife* 3, e04147. DOI: 10.7554/eLife.04147.
- Suh, Greg S. B.; Wong, Allan M.; Hergarden, Anne C.; Wang, Jing W.; Simon, Anne F.; Benzer, Seymour et al. (2004): A single population of olfactory sensory neurons mediates an innate avoidance behaviour in *Drosophila*. In *Nature* 431 (7010), pp. 854–859. DOI: 10.1038/nature02980.

- Sun, Fangmiao; Zeng, Jianzhi; Jing, Miao; Zhou, Jingheng; Feng, Jiesi; Owen, Scott F. et al. (2018): A Genetically Encoded Fluorescent Sensor Enables Rapid and Specific Detection of Dopamine in Flies, Fish, and Mice. In *Cell* 174 (2), 481-496.e19. DOI: 10.1016/j.cell.2018.06.042.
- T. H. Morgan; A. H. Sturtevant; H. J. Muller; C. B. Bridges. (1915): The mechanism of Mendelian heredity. New York: Henry Holt and Company.
- Talay, Mustafa; Richman, Ethan B.; Snell, Nathaniel J.; Hartmann, Griffin G.; Fisher, John D.; Sorkaç, Altar et al. (2017): Transsynaptic Mapping of Second-Order Taste Neurons in Flies by trans-Tango. In *Neuron* 96 (4), 783-795.e4. DOI: 10.1016/j.neuron.2017.10.011.
- Tanaka, Nobuaki K.; Awasaki, Takeshi; Shimada, Takashi; Ito, Kei (2004): Integration of chemosensory pathways in the *Drosophila* second-order olfactory centers. In *Current Biology* 14 (6), pp. 449–457. DOI: 10.1016/j.cub.2004.03.006.
- Tank, D. W.; Sugimori, M.; Connor, J. A.; Llinás, R. R. (1988): Spatially resolved calcium dynamics of mammalian Purkinje cells in cerebellar slice. In *Science (New York, N.Y.)* 242 (4879), pp. 773–777. DOI: 10.1126/science.2847315.
- Thorne, Natasha; Chromey, Caroline; Bray, Steve; Amrein, Hubert (2004): Taste perception and coding in *Drosophila*. In *Current Biology* 14 (12), pp. 1065–1079. DOI: 10.1016/j.cub.2004.05.019.
- Tian, Lin; Hires, S. Andrew; Mao, Tianyi; Huber, Daniel; Chiappe, M. Eugenia; Chalasani, Sreekanth H. et al. (2009): Imaging neural activity in worms, flies and mice with improved GCaMP calcium indicators. In *Nat Methods* 6 (12), pp. 875–881. DOI: 10.1038/nmeth.1398.
- Tomita, Jun; Ban, Gosuke; Kato, Yoshiaki S.; Kume, Kazuhiko (2021): Protocerebral Bridge Neurons That Regulate Sleep in *Drosophila melanogaster*. In *Frontiers in neuroscience* 15, p. 647117. DOI: 10.3389/fnins.2021.647117.
- Tsao, Chang-Hui; Chen, Chien-Chun; Lin, Chen-Han; Yang, Hao-Yu; Lin, Suewei (2018): *Drosophila* mushroom bodies integrate hunger and satiety signals to control innate food-seeking behavior. In *eLife* 7. DOI: 10.7554/eLife.35264.
- van Breugel, Floris; Dickinson, Michael H. (2014): Plume-tracking behavior of flying *Drosophila* emerges from a set of distinct sensory-motor reflexes. In *Current biology : CB* 24 (3), pp. 274–286. DOI: 10.1016/j.cub.2013.12.023.
- Varela, Nélia; Gaspar, Miguel; Dias, Sophie; Vasconcelos, Maria Luísa (2019): Avoidance response to CO₂ in the lateral horn. In *PLOS Biology* 17 (1), e2006749. DOI: 10.1371/journal.pbio.2006749.
- Veldhuizen, Maria G.; Nachtigal, Danielle; Teulings, Lynsey; Gitelman, Darren R.; Small, Dana M. (2010): The insular taste cortex contributes to odor quality coding. In *Front. Hum. Neurosci.* 4, p. 58. DOI: 10.3389/fnhum.2010.00058.
- Vosshall, Leslie B.; Stocker, Reinhard F. (2007): Molecular architecture of smell and taste in *Drosophila*. In *Annual review of neuroscience* 30, pp. 505–533. DOI: 10.1146/annurev.neuro.30.051606.094306.
- Wang, Qi; Shui, Bo; Kotlikoff, Michael I.; Sonderrmann, Holger (2008): Structural basis for calcium sensing by GCaMP2. In *Structure (London, England: 1993)* 16 (12), pp. 1817–1827. DOI: 10.1016/j.str.2008.10.008.
- Wang, Zuoren; Singhvi, Aakanksha; Kong, Priscilla; Scott, Kristin (2004): Taste Representations in the *Drosophila* Brain. In *Cell* 117 (7), pp. 981–991. DOI: 10.1016/j.cell.2004.06.011.
- Wei, Ziqiang; Lin, Bei-Jung; Chen, Tsai-Wen; Daie, Kayvon; Svoboda, Karel; Druckmann, Shaul (2020): A comparison of neuronal population dynamics measured with calcium imaging and electrophysiology. In *PLOS Computational Biology* 16 (9), e1008198. DOI: 10.1371/journal.pcbi.1008198.
- Weiss, Linnea A.; Dahanukar, Anupama; Kwon, Jae Young; Banerjee, Diya; Carlson, John R. (2011): The molecular and cellular basis of bitter taste in *Drosophila*. In *Neuron* 69 (2), pp. 258–272. DOI: 10.1016/j.neuron.2011.01.001.

- White, J. G.; Southgate, E.; Thomson, J. N.; Brenner, S. (1986): The structure of the nervous system of the nematode *Caenorhabditis elegans*. In *Philosophical transactions of the Royal Society of London. Series B, Biological sciences* 314 (1165), pp. 1–340. DOI: 10.1098/rstb.1986.0056.
- Wicher, Dieter; Schäfer, Ronny; Bauernfeind, René; Stensmyr, Marcus C.; Heller, Regine; Heinemann, Stefan H.; Hansson, Bill S. (2008): Drosophila odorant receptors are both ligand-gated and cyclic-nucleotide-activated cation channels. In *Nature* 452 (7190), pp. 1007–1011. DOI: 10.1038/nature06861.
- Wolff, Tanya; Rubin, Gerald M. (2018): Neuroarchitecture of the Drosophila central complex: A catalog of nodulus and asymmetrical body neurons and a revision of the protocerebral bridge catalog. In *The Journal of comparative neurology* 526 (16), pp. 2585–2611. DOI: 10.1002/cne.24512.
- Woller, Alexandra; Bandow, Paul; Aimon, Sophie; Grunwald Kadow, Ilona C. (2021): Preparing Adult Drosophila melanogaster for Whole Brain Imaging during Behavior and Stimuli Responses. In *JoVE (Journal of Visualized Experiments)* (170), e61876. DOI: 10.3791/61876.
- Wong, Allan M.; Wang, Jing W.; Axel, Richard (2002): Spatial representation of the glomerular map in the Drosophila protocerebrum. In *Cell* 109 (2), pp. 229–241. DOI: 10.1016/S0092-8674(02)00707-9.
- Yang, Weijian; Yuste, Rafael (2017): In vivo imaging of neural activity. In *Nat Methods* 14 (4), pp. 349–359. DOI: 10.1038/nmeth.4230.
- Yao, Zepeng; Scott, Kristin (2022): Serotonergic neurons translate taste detection into internal nutrient regulation. In *Neuron* 110 (6), 1036-1050.e7. DOI: 10.1016/j.neuron.2021.12.028.
- Yapici, Nilay; Cohn, Raphael; Schusterreiter, Christian; Ruta, Vanessa; Vosshall, Leslie B. (2016): A Taste Circuit that Regulates Ingestion by Integrating Food and Hunger Signals. In *Cell* 165 (3), pp. 715–729. DOI: 10.1016/j.cell.2016.02.061.
- Youn, Hyesoo; Kirkhart, Colleen; Chia, Justine; Scott, Kristin (2018): A subset of octopaminergic neurons that promotes feeding initiation in Drosophila melanogaster. In *PLoS ONE* 13 (6), e0198362. DOI: 10.1371/journal.pone.0198362.
- Zampini, Massimiliano; Sanabria, Daniel; Phillips, Nicola; Spence, Charles (2007): The multisensory perception of flavor: Assessing the influence of color cues on flavor discrimination responses. In *Food Quality and Preference* 18 (7), pp. 975–984. DOI: 10.1016/j.foodqual.2007.04.001.
- Zhang, Yali V.; Ni, Jinfei; Montell, Craig (2013): The molecular basis for attractive salt-taste coding in Drosophila. In *Science (New York, N.Y.)* 340 (6138), pp. 1334–1338. DOI: 10.1126/science.1234133.
- Zheng, Zhihao; Lauritzen, J. Scott; Perlman, Eric; Robinson, Camenzind G.; Nichols, Matthew; Milkie, Daniel et al. (2018): A Complete Electron Microscopy Volume of the Brain of Adult Drosophila melanogaster. In *Cell* 174 (3), 730-743.e22. DOI: 10.1016/j.cell.2018.06.019.
- Zhu, Junwei; Park, Kye-Chung; Baker, Thomas C. (2003): Identification of odors from overripe mango that attract vinegar flies, Drosophila melanogaster. In *J Chem Ecol* 29 (4), pp. 899–909. DOI: 10.1023/A:1022931816351.
- Zhu, Yan (2013): The Drosophila visual system: From neural circuits to behavior. In *Cell adhesion & migration* 7 (4), pp. 333–344. DOI: 10.4161/cam.25521.

Appendix

List of appendix figures

Figure A1	Classification models predicting stimulus type from AL alone	123
Figure A2	Classification models predicting stimulus type from GNG alone	124
Figure A3	Linear discriminant classification model predicts internal state and valence from odor data	125
Figure A4	Linear discriminant classification model predicts internal state and valence from taste data	126
Figure A5	Linear discriminant classification model fails to predict internal state and valence from multisensory data	127
Figure A6	Neural network classification model fails to predict internal state from multisensory data sets	128
Figure A7	Linear discriminant classification model predicts valence from multisensory data sets	129
Figure A8	Brain-wide correlation during resting phase (20 percent threshold)	130
Figure A9	Brain-wide correlation during stimulus phase (20 percent threshold)	131
Figure A10	Correlation ratio and connectivity change between rest and stim (20 percent threshold)	132
Figure A11	Individual time series for the odor responses in fed flies	133
Figure A12	Individual time series for the odor responses in starved flies	134
Figure A13	Individual time series for the taste responses in fed flies	135
Figure A14	Individual time series for the taste responses in starved flies	136
Figure A15	Individual time series for the taste + odor responses to matching valence in fed flies	137
Figure A16	Individual time series for the taste + odor responses to conflicting valence in fed flies	138
Figure A17	Individual time series for the taste + odor responses to matching valence in starved flies	139
Figure A18	Individual time series for the taste + odor responses to conflicting valence in starved flies	140
Figure A11.2	Average time series for the odor responses in fed flies	141
Figure A12.2	Average time series for the odor responses in starved flies	142
Figure A13.2	Average time series for the taste responses in fed flies	143
Figure A14.2	Average time series for the taste responses in starved flies	144
Figure A15.2	Average time series for the taste + odor responses to matching valence in fed flies	145
Figure A16.2	Average time series for the taste + odor responses to conflicting valence in fed flies	146
Figure A17.2	Average time series for the taste + odor responses to matching valence in starved flies	147
Figure A18.2	Average time series for the taste + odor responses to conflicting valence in starved flies	178
Figure A19 – A31	Average time series for functional components during the first stimulus	149-161

Figure A32	Classification models predicting the stimulus type with a reduced set of responses	162
Figure A33	Brain-wide correlation before and during odor stimulation	163
Figure A34	Brain-wide correlation before and during taste stimulation	164
Figure A35	Brain-wide correlation before and during multisensory stimulation	165
Figure A36	Correlation ratio and connectivity change between rest and stimulus phase	166
Figure A37	Brain-wide correlation before and during odor stimulation (20 percent threshold)	167
Figure A38	Brain-wide correlation before and during taste stimulation (20 percent threshold)	168
Figure A39	Brain-wide correlation before and during multisensory stimulation (20 percent threshold)	169
Figure A40	Correlation ratio and connectivity change between rest and stimulus phase (20 percent threshold)	170
Figure A41	Two atypical recordings, from two starved flies, stimulated with sucrose	171
Figure A42	Two atypical recordings, from two fed flies, stimulated with benzaldehyde and quinine	172
Figure A43	Two atypical recordings, from two flies, stimulated with benzaldehyde and quinine	173
Figure A44	Two atypical recordings, from the same starved fly	174

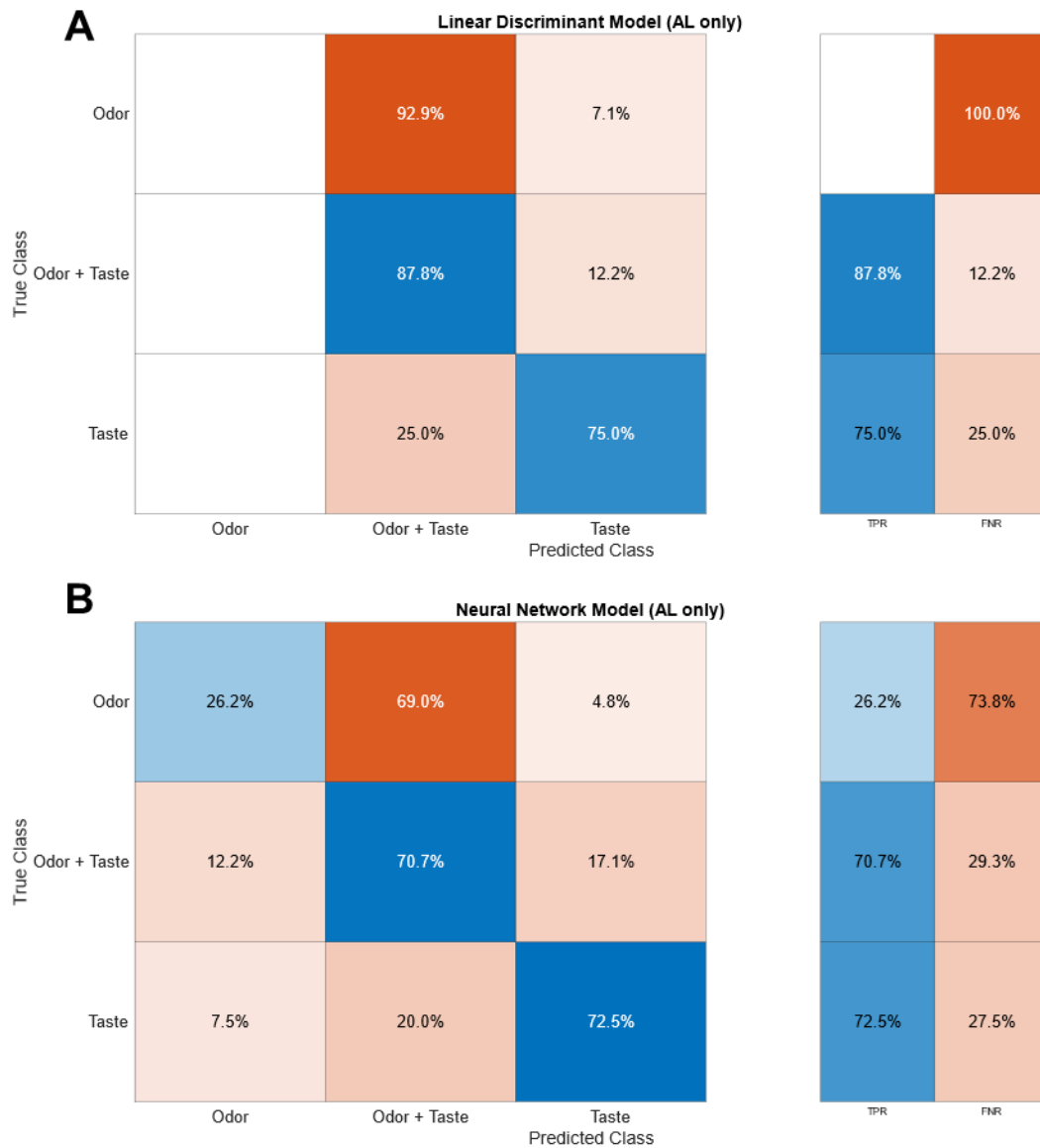


Figure A1: Classification models predicting stimulus type from AL alone

Confusion matrices for (A) the linear discriminant model and (B) the neural network model predicting the stimulus type from a dataset containing only responses of the AL. TPR=true positive rate, FNR=false negative rate.

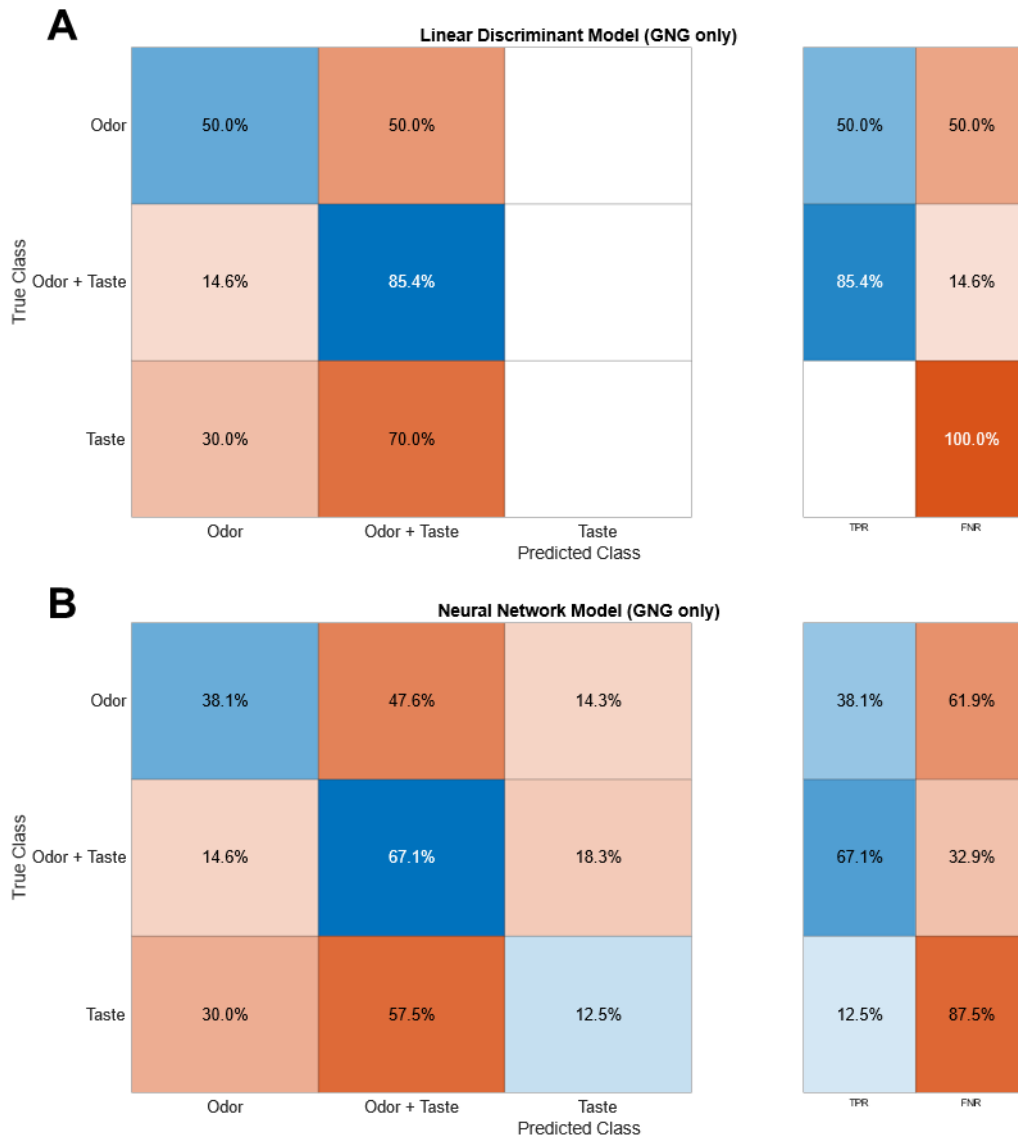


Figure A2: Classification models predicting stimulus type from GNG alone

Confusion matrices for (A) the linear discriminant model and (B) the neural network model predicting the stimulus type from a dataset containing only responses of the GNG. TPR=true positive rate, FNR=false negative rate.

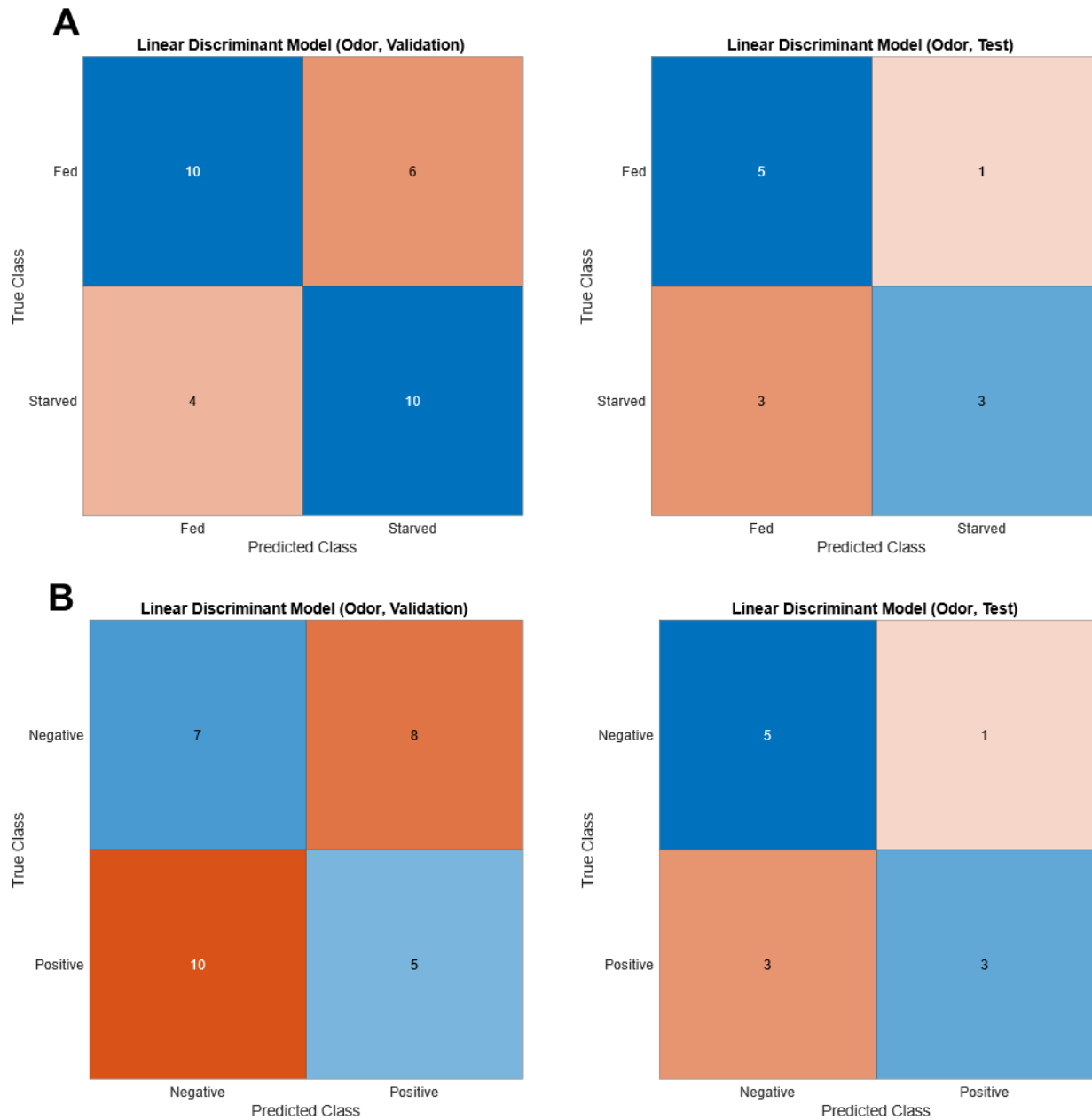


Figure A3 Linear discriminant classification model predicts internal state and valence from odor data

A Confusion matrices for the linear discriminant model (LDM) predicting the internal state of the flies from the odor data set. Left: Model validation for the training dataset (70% of all odor observations). Right: Model performance on the test dataset (30% of all odor observations). B Confusion matrices for the linear discriminant model (LDM) predicting the valence of the stimulus from the odor data set. Left: Model validation for the training dataset (70% of all odor observations). Right: Model performance on the test dataset (30% of all odor observations). Numbers indicate total observations.

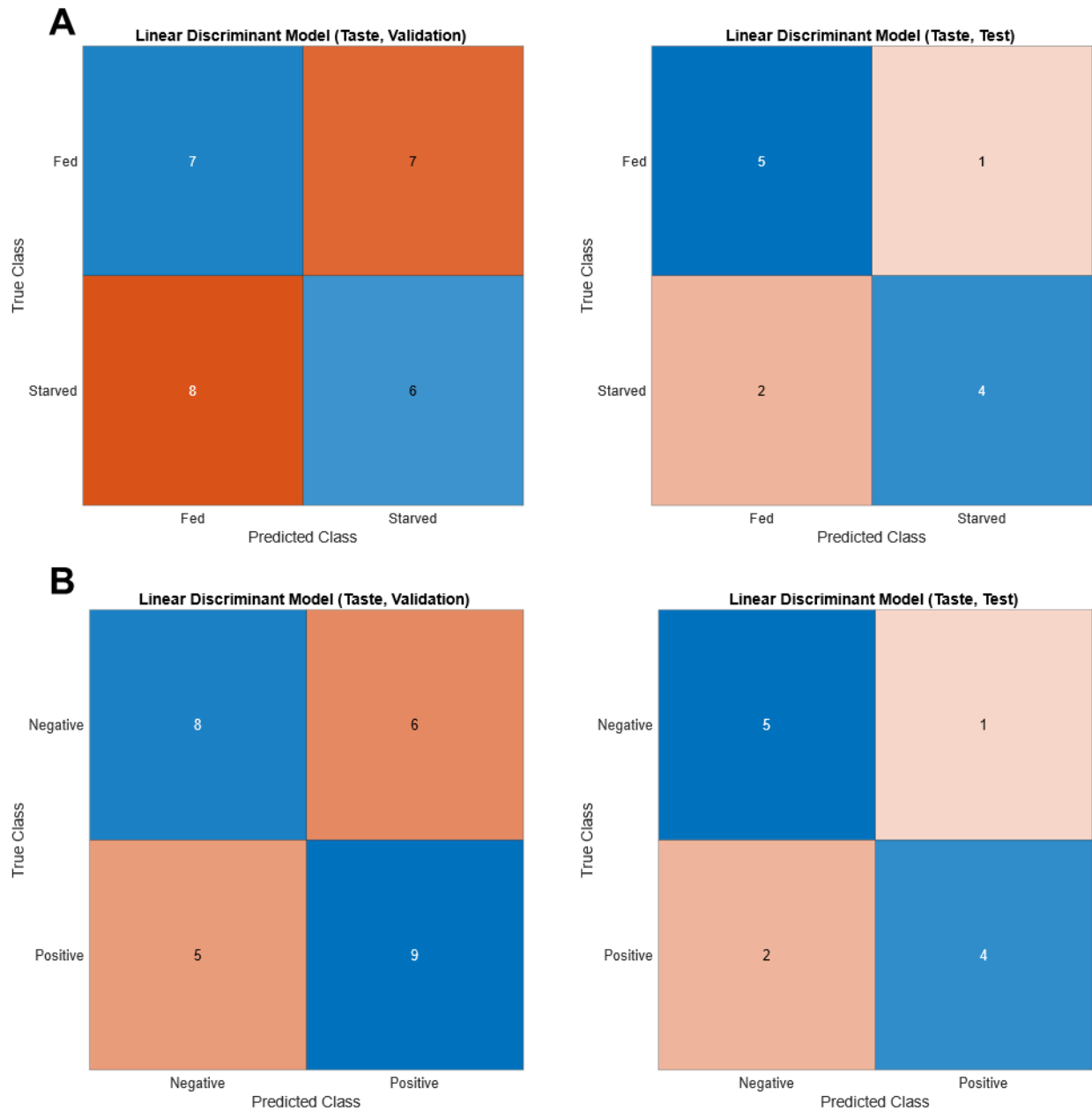


Figure A4: Linear discriminant classification model predicts internal state and valence from taste data

A Confusion matrices for the linear discriminant model (LDM) predicting the internal state of the flies from the taste data set. Left: Model validation for the training dataset (70% of all taste observations). Right: Model performance on the test dataset (30% of all taste observations). B Confusion matrices for the linear discriminant model (LDM) predicting the valence of the stimulus from the taste data set. Left: Model validation for the training dataset (70% of all taste observations). Right: Model performance on the test dataset (30% of all taste observations). Numbers indicate total observations.

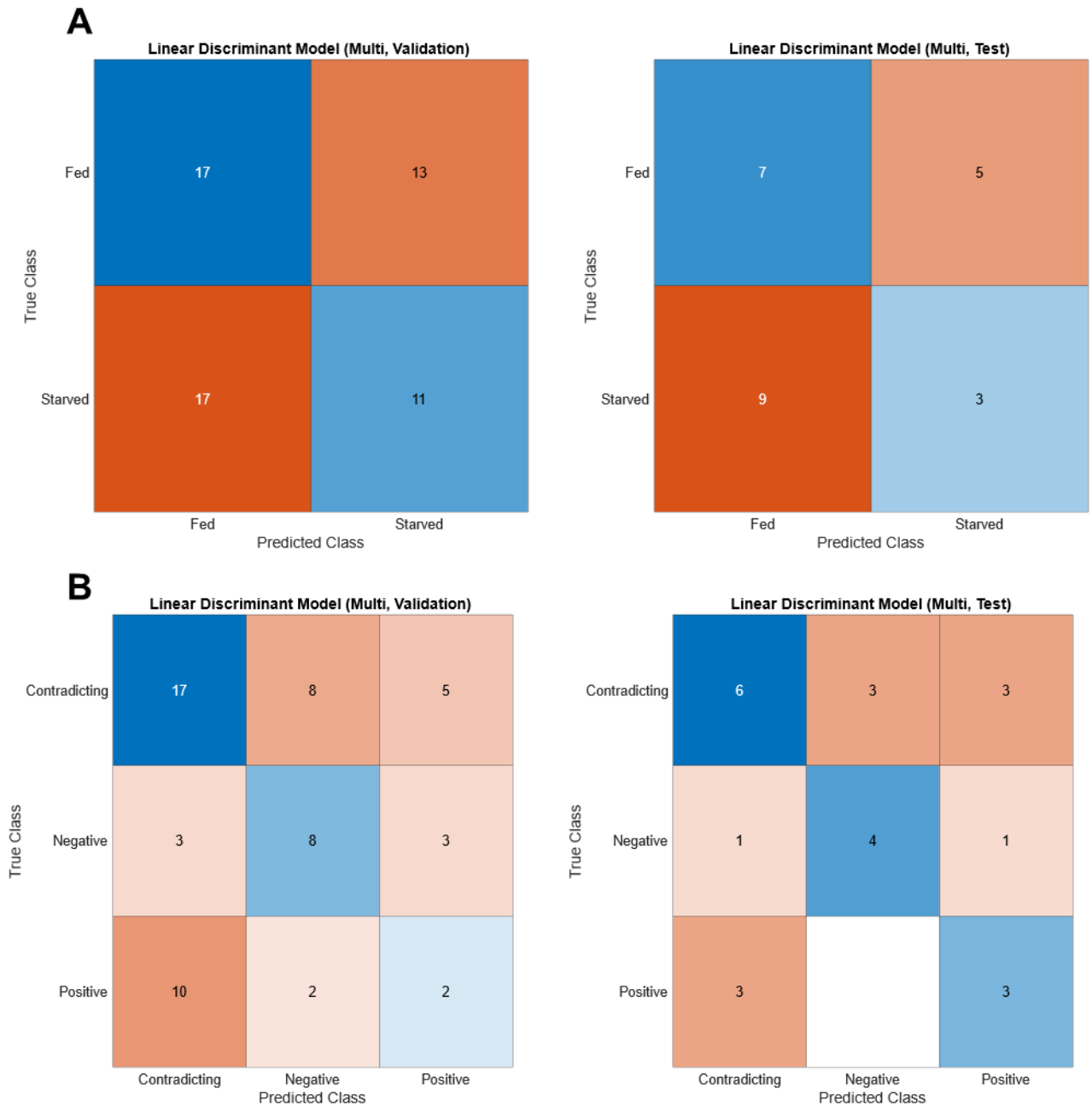


Figure A5: Linear discriminant classification model fails to predict internal state and valence from multisensory data

A Confusion matrices for linear discriminant model (LDM) predicting the internal state of the flies from the multisensory data set. Left: Model validation for the training dataset (70% of all multisensory observations). Right: Model performance on the test dataset (30% of all multisensory observations). B Confusion matrices for the linear discriminant model (LDM) predicting the valence of the stimulus from the multisensory data set. Left: Model validation for the training dataset (70% of all multisensory observations). Right: Model performance on the test dataset (30% of all multisensory observations). Numbers indicate total observations.

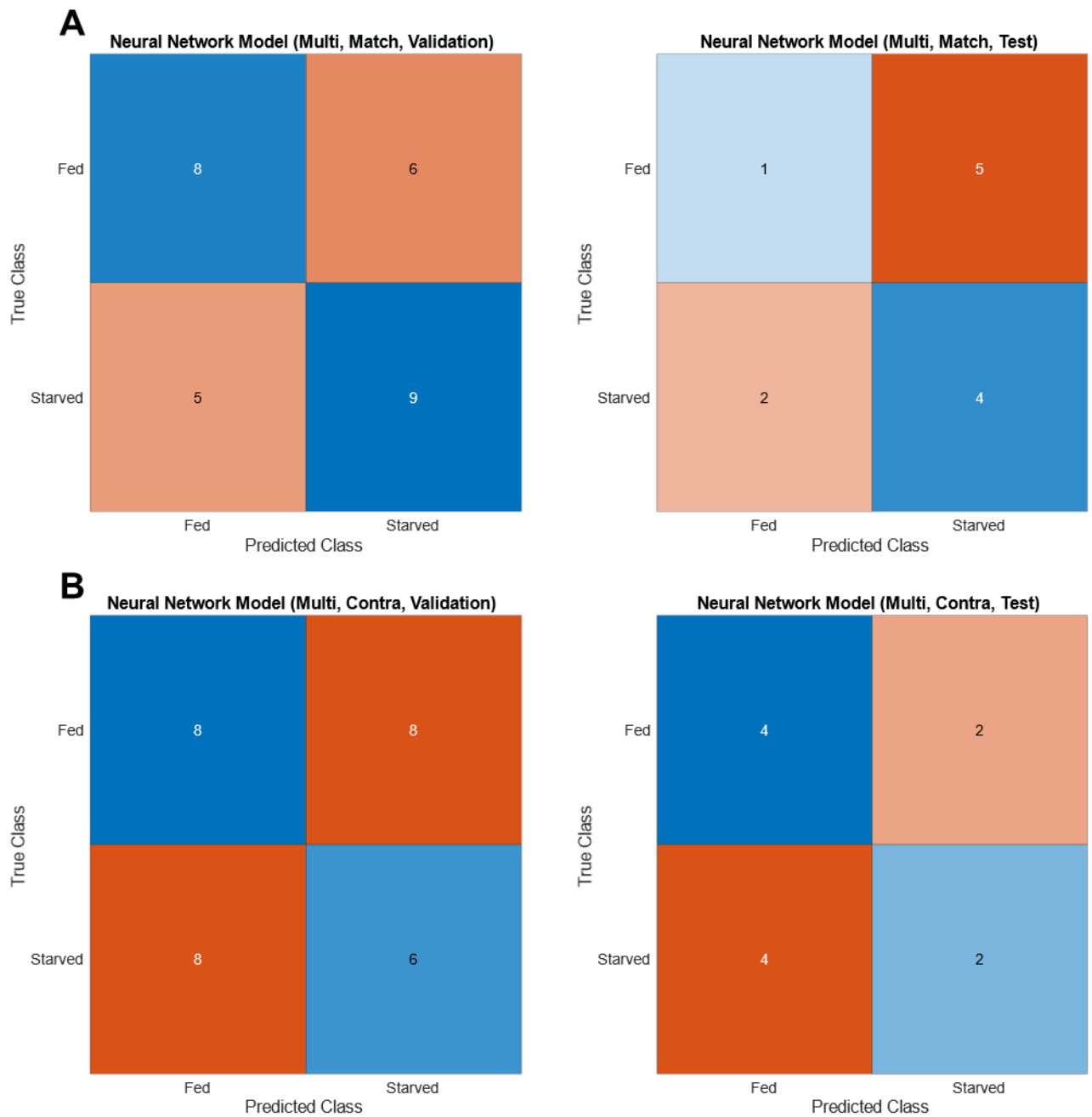


Figure A6: Neural network classification model fails to predict internal state from multisensory data sets

A Confusion matrices for the neural network model (NNM) predicting the internal state of the animals from the multisensory data with stimuli of matching valence. Left: Model validation for the training dataset (70% of all multisensory observations). Right: Model performance on the test dataset (30% of all multisensory observations). B Confusion matrices for the neural network model (NNM) predicting the internal state of the animals from the multisensory data with stimuli of contradicting valence . Left: Model validation for the training dataset (70% of all multisensory observations). Right: Model performance on the test dataset (30% of all multisensory observations). Numbers indicate total observations.

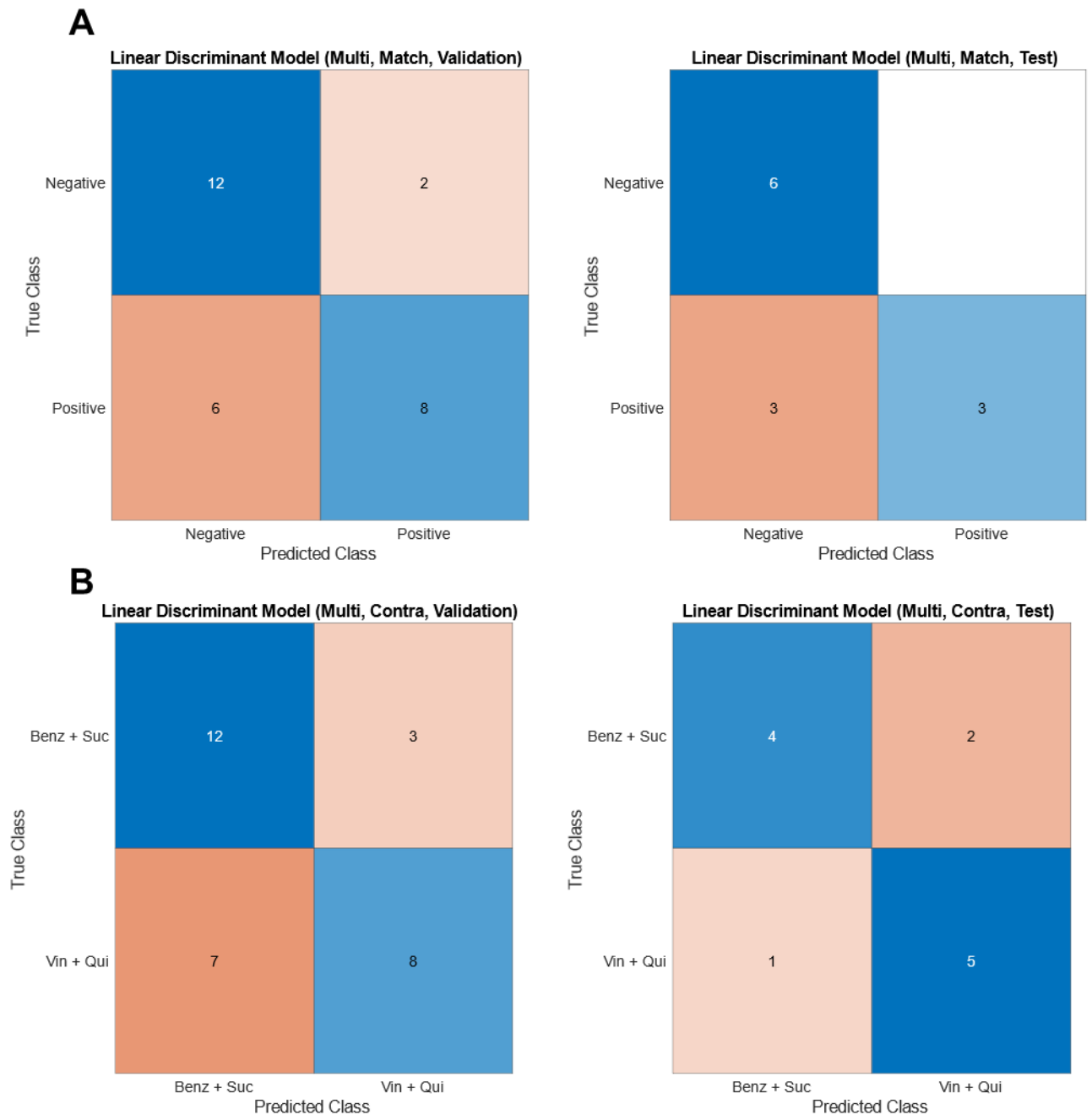


Figure A7: Linear discriminant classification model predicts valence from multisensory data sets

A Confusion matrices for the linear discriminant model (LDM) predicting valence of the stimulus pair from the multisensory data with stimuli of matching valence (Positive: Vinegar + Sucrose, negative: Benzaldehyde + Quinine). Left: Model validation for the training dataset (70% of all multisensory observations). Right: Model performance on the test dataset (30% of all multisensory observations). B Confusion matrices for the linear discriminant model (LDM) predicting the valence of the stimulus from the multisensory data with stimuli of contradicting valence. Left: Model validation for the training dataset (70% of all multisensory observations). Right: Model performance on the test dataset (30% of all multisensory observations). Numbers indicate total observations.

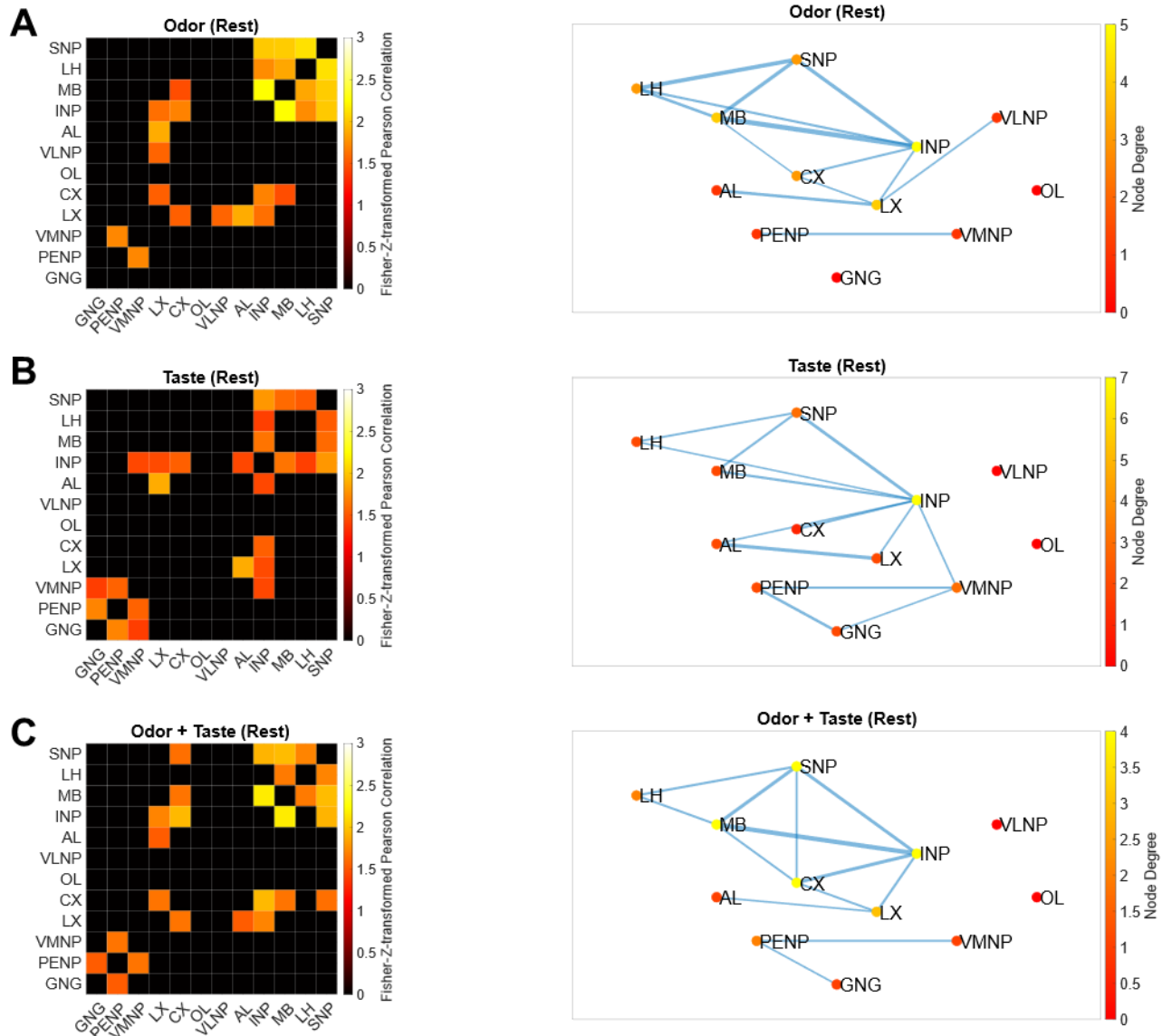


Figure A8: Brain-wide correlation during resting phase (20 percent threshold)

A Adjacency matrix and resulting graph of the activity correlation of the odor group. B Adjacency matrix and resulting graph of the activity correlation of the taste group. C Adjacency matrix and resulting graph of the activity correlation of the multisensory group. Data for fed and starved groups was pooled. The resting phase was defined as the first 25 seconds of every recording before the first stimulus was applied. Correlation was thresholded proportionally to retain only 20 percent of the strongest connections. The width of the edges (blue lines) scales proportionally with weight of the connection between the nodes.

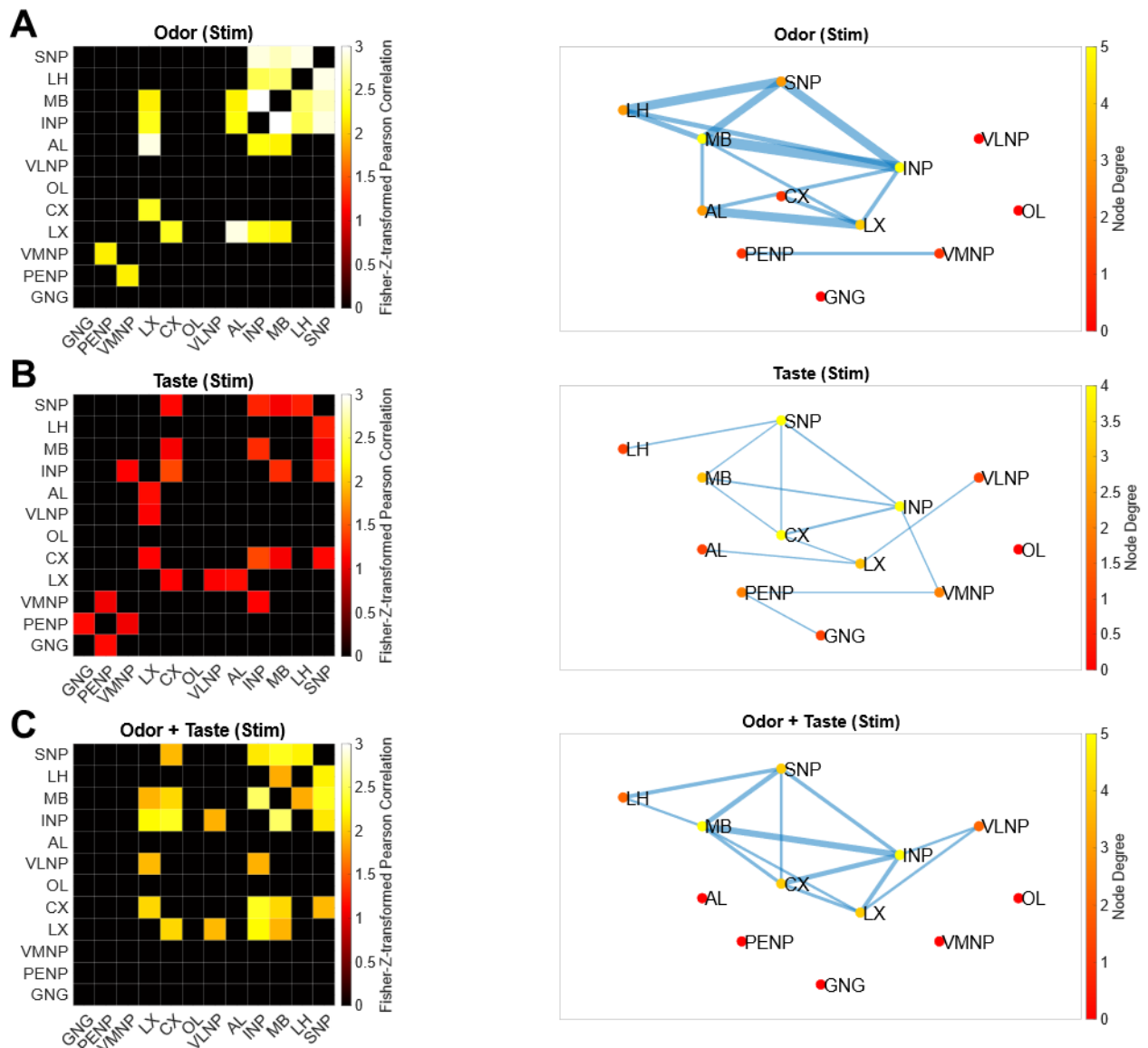


Figure A9: Brain-wide correlation during stimulus phase (20 percent threshold)

A Adjacency matrix and resulting graph of the activity correlation of the odor group. B Adjacency matrix and resulting graph of the activity correlation of the taste group. C Adjacency matrix and resulting graph of the activity correlation of the multisensory group. Data for fed and starved groups was pooled. The stimulus phase was defined as the first 15 seconds after the onset of the first stimulus. Correlation was thresholded proportionally to retain only 20 percent of the strongest connections. The width of the edges (blue lines) scales proportionally with weight of the connection between the nodes.

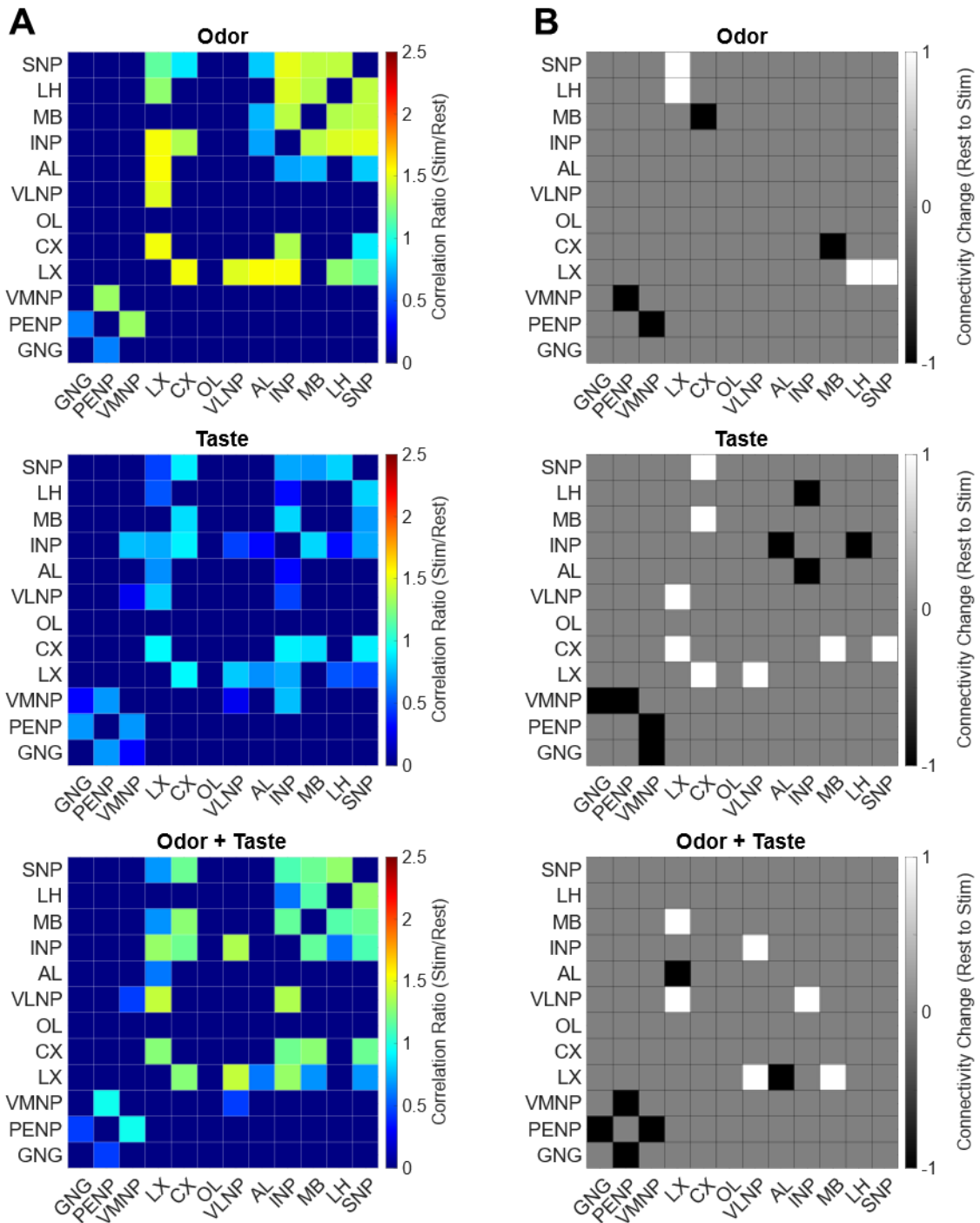


Figure A10: Correlation ratio and connectivity change between rest and stim (20 percent threshold)

A Correlation ratio matrices for the all stimulus groups. Correlation ratio was calculated by dividing the correlation during stim with the correlation during rest. Correlation was thresholded proportionally to retain only 20 percent of the strongest connections. B Connectivity matrices for all stimulus groups. Connectivity change was calculated by subtracting the binary connectivity during rest from the binary connectivity during stim. Black: connection is lost, white: connection is gained, grey: connection remains unchanged.

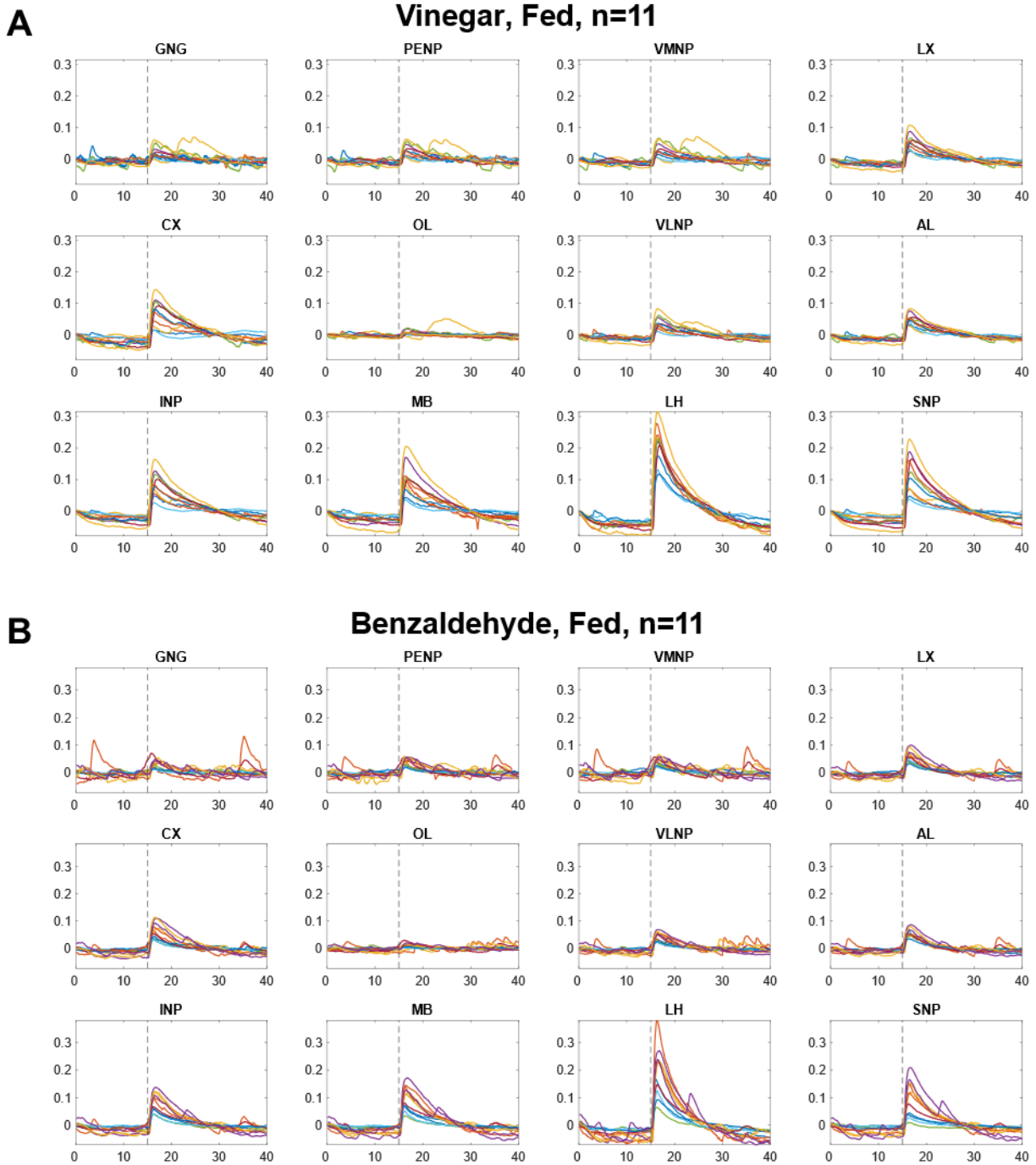
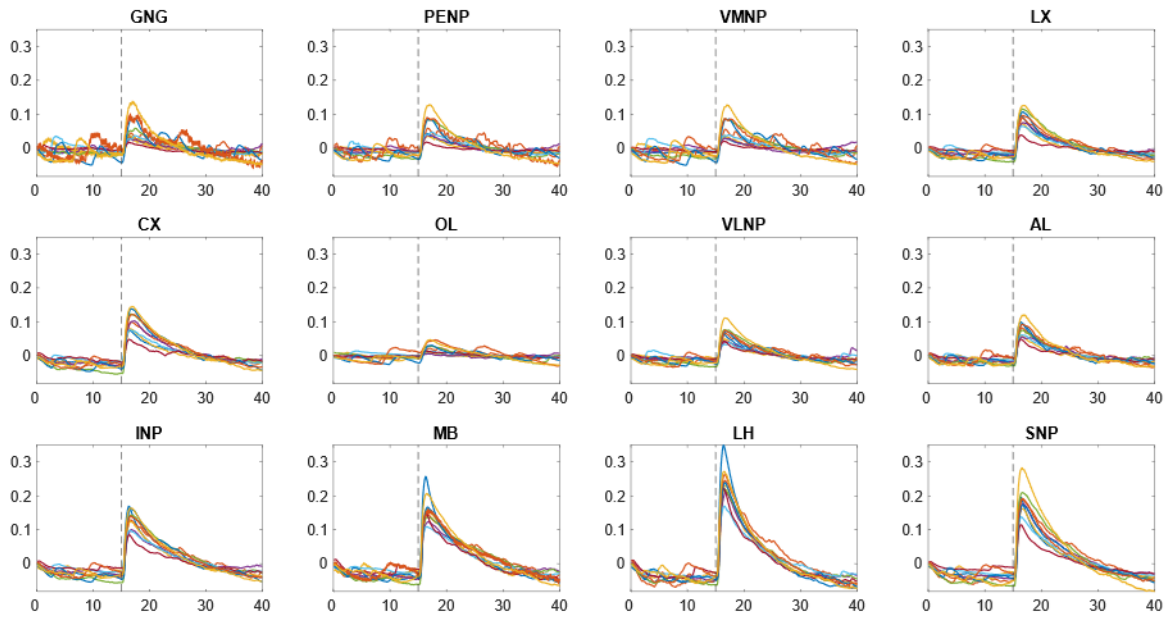
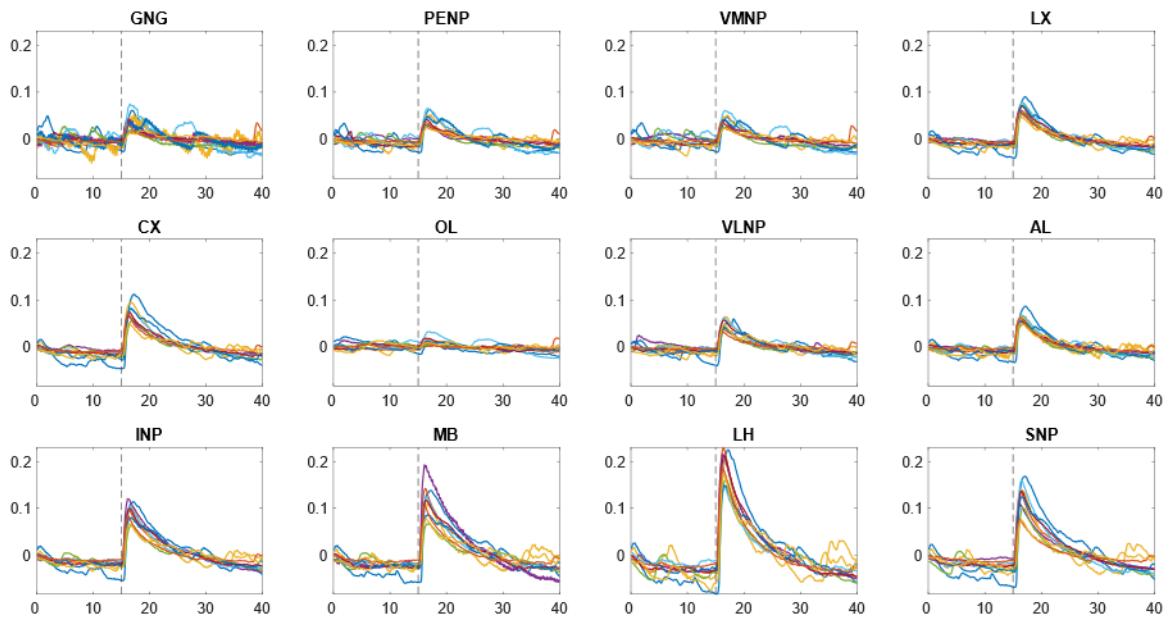


Figure A11: Individual time series for the odor responses in fed flies

A Individual dF/F time series for the first vinegar stimulation. B Individual dF/F for the first benzaldehyde stimulation. Y-axis: dF/F , X-axis: time (s). Every colored line is the response of one fly. Dashed vertical line at 15 seconds indicates stimulus onset.

A**Vinegar, Starved, n=10****B****Benzaldehyde, Starved, n=10****Figure A12: Individual time series for the odor responses in starved flies**

A Individual dF/F time series for the first vinegar stimulation. B Individual dF/F for the first benzaldehyde stimulation. Y-axis: dF/F , X-axis: time (s). Every colored line is the response of one fly. Dashed vertical line at 15 seconds indicates stimulus onset.

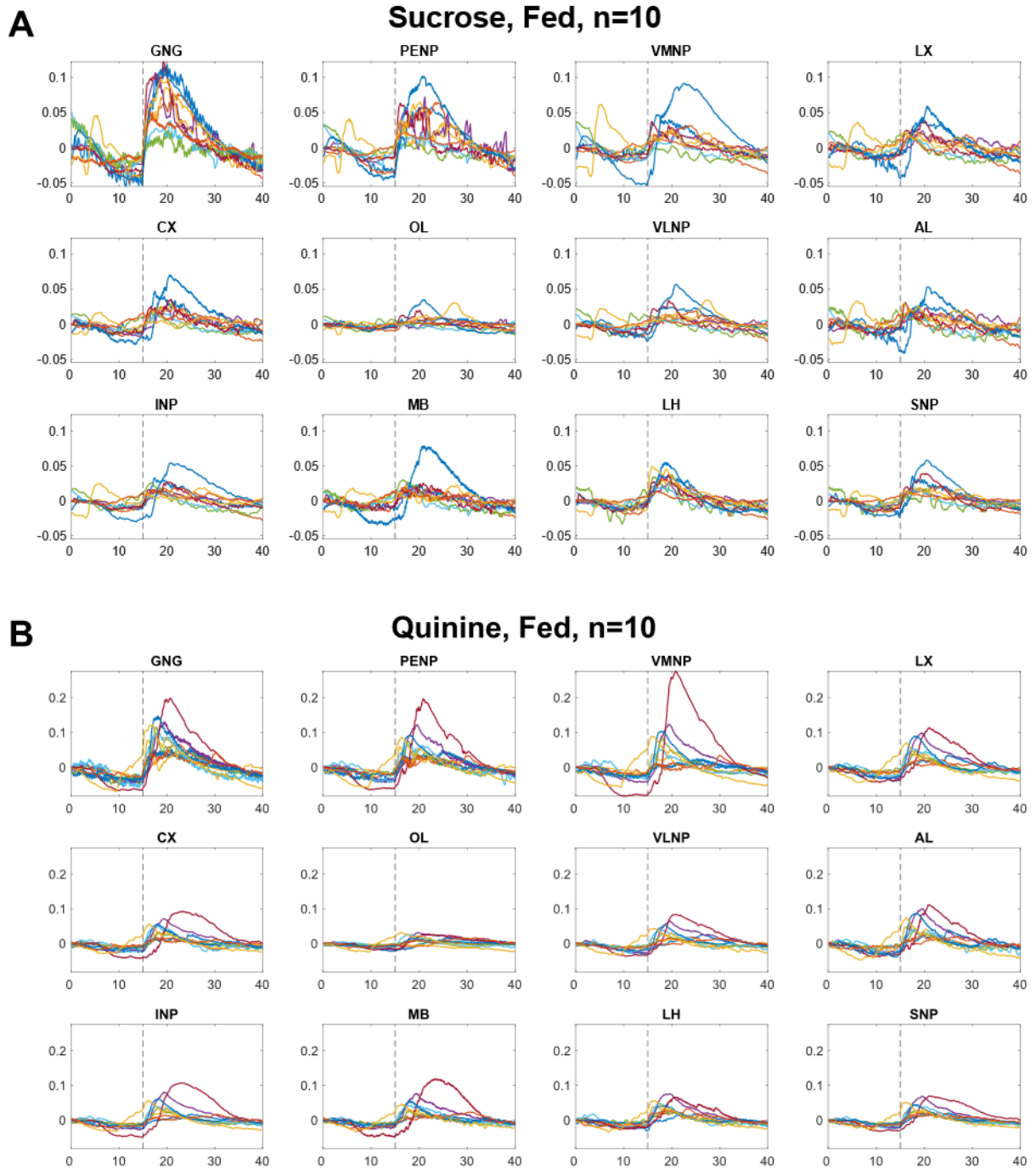


Figure A13: Individual time series for the taste responses in fed flies

A Individual dF/F time series for the first sucrose stimulation. B Individual dF/F for the first quinine stimulation. Y-axis: dF/F , X-axis: time (s). Every colored line is the response of one fly. Dashed vertical line at 15 seconds indicates stimulus onset.

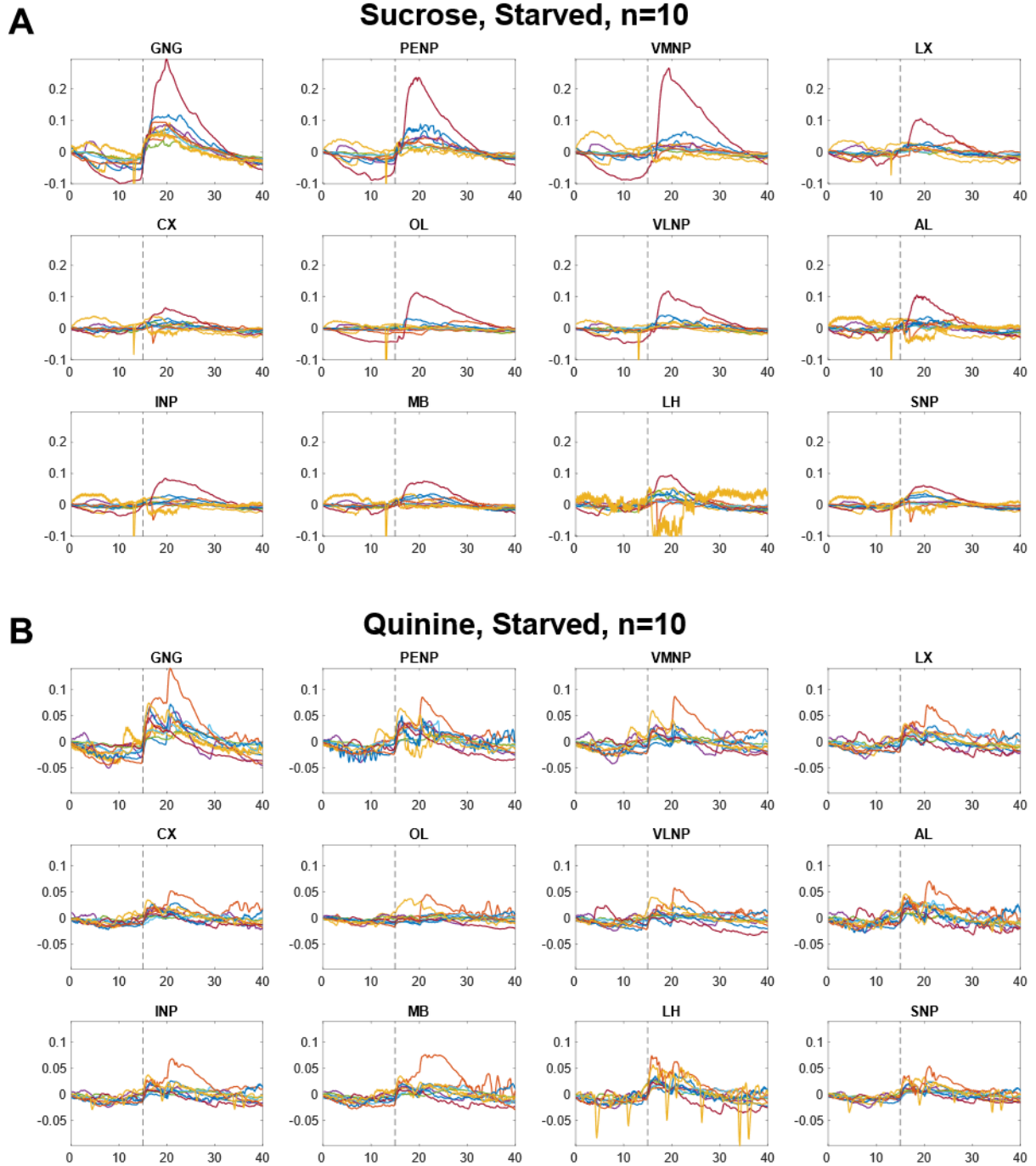


Figure A14: Individual time series for the taste responses in starved flies

A Individual dF/F time series for the first sucrose stimulation. B Individual dF/F for the first quinine stimulation. Y-axis: dF/F , X-axis: time (s). Every colored line is the response of one fly. Dashed vertical line at 15 seconds indicates stimulus onset.

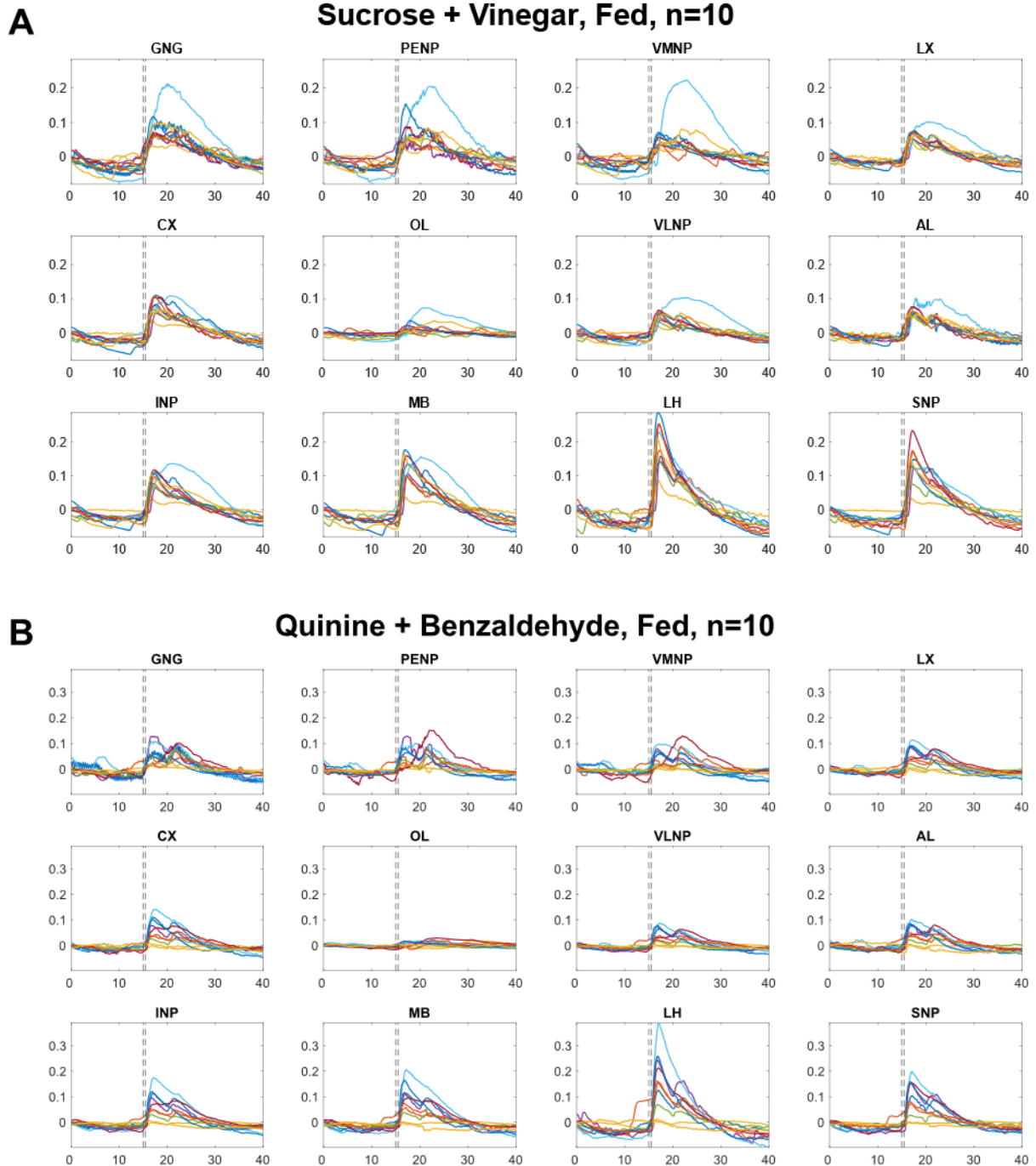


Figure A15: Individual time series for the taste + odor responses to matching valence in fed flies
 A Individual dF/F time series for the first sucrose + vinegar stimulation. B Individual dF/F for the first quinine + benzaldehyde stimulation. Y-axis: dF/F, X-axis: time (s). Every colored line is the response of one fly. Dashed vertical line at 15 seconds indicates taste onset. Second dashed line at 15.5 seconds indicates estimated odor onset.

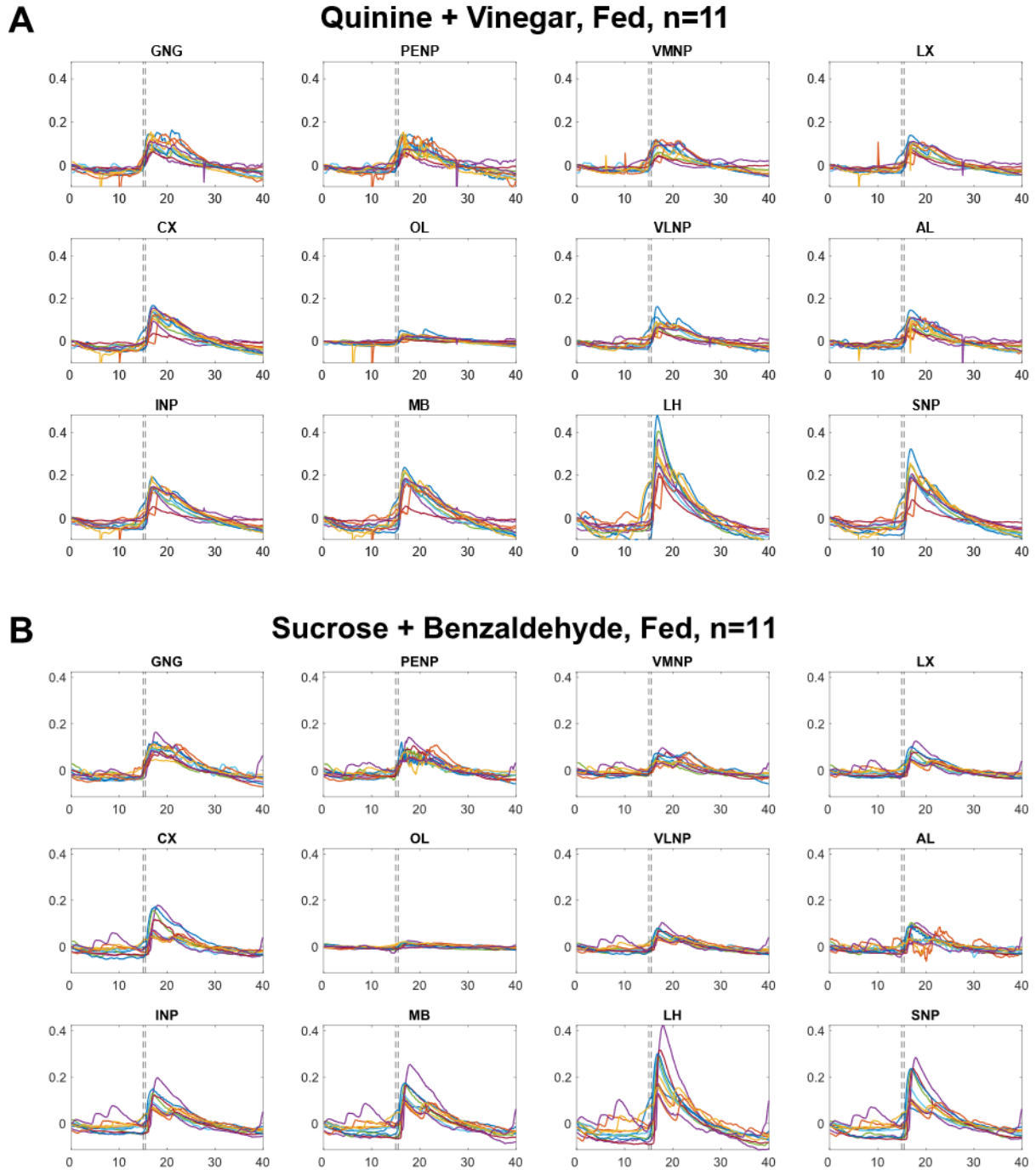


Figure A16: Individual time series for the taste + odor responses to conflicting valence in fed flies

A Individual dF/F time series for the first quinine + vinegar stimulation. B Individual dF/F for the first sucrose + benzaldehyde stimulation. Y-axis: dF/F, X-axis: time (s). Every colored line is the response of one fly. Dashed vertical line at 15 seconds indicates taste onset. Second dashed line at 15.5 seconds indicates estimated odor onset.

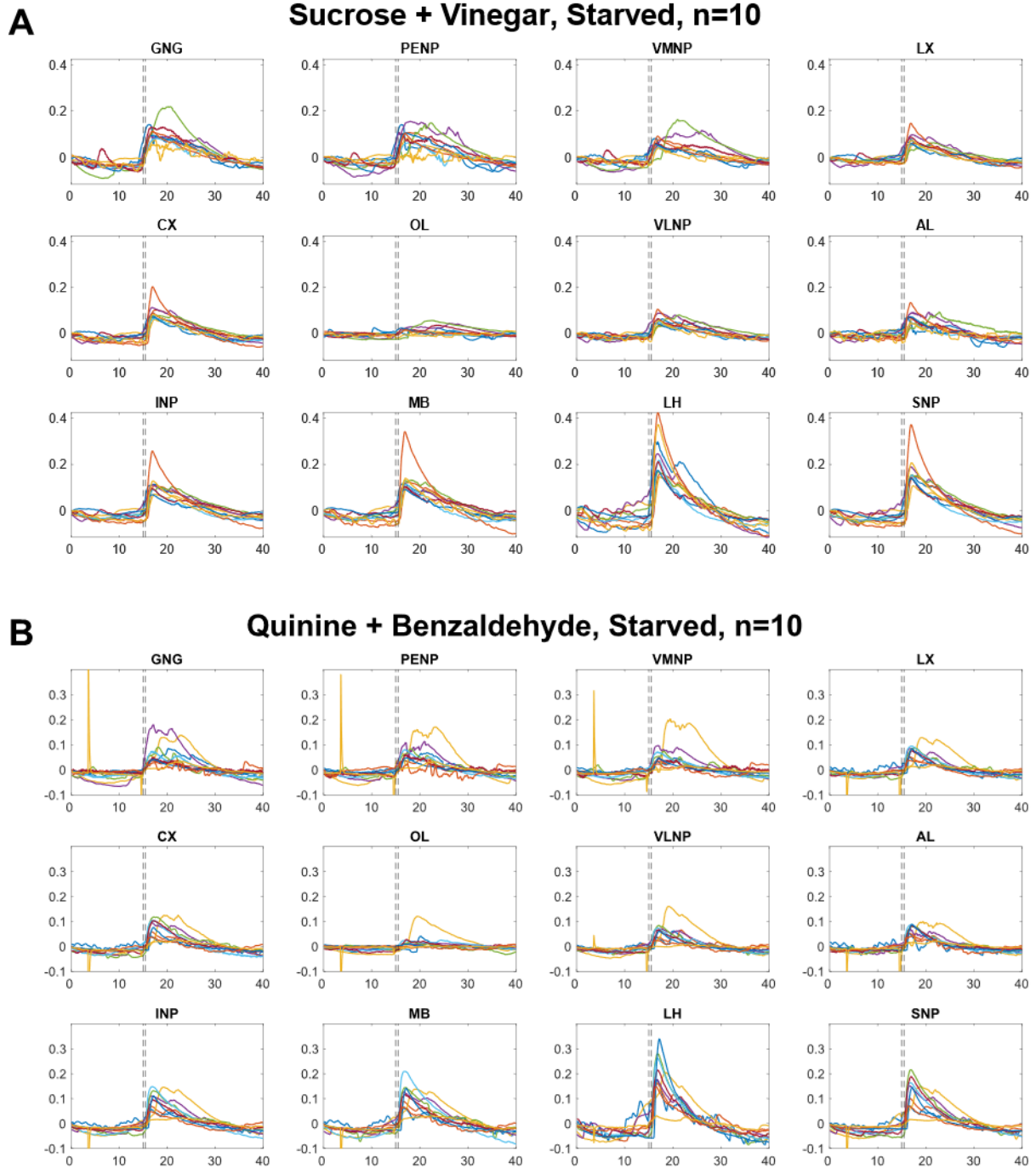


Figure A17: Individual time series for the taste + odor responses to matching valence in starved flies

A Individual dF/F time series for the first sucrose + vinegar stimulation. B Individual dF/F for the first quinine + benzaldehyde stimulation. Y-axis: dF/F, X-axis: time (s). Every colored line is the response of one fly. Dashed vertical line at 15 seconds indicates taste onset. Second dashed line at 15.5 seconds indicates estimated odor onset.

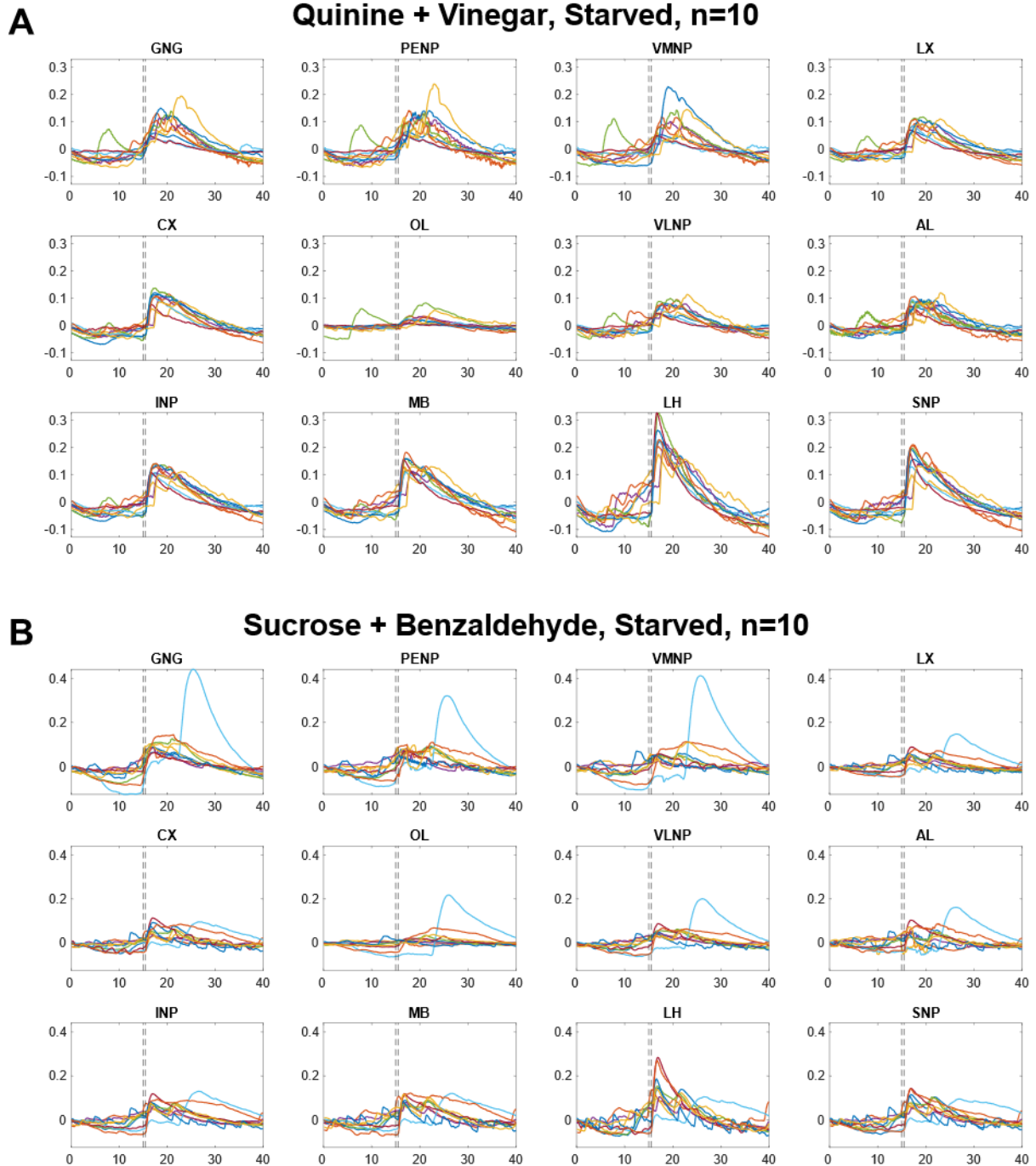


Figure A18: Individual time series for the taste + odor responses to conflicting valence in starved flies

A Individual dF/F time series for the first quinine + vinegar stimulation. B Individual dF/F for the first sucrose + benzaldehyde stimulation. Y-axis: dF/F, X-axis: time (s). Every colored line is the response of one fly. Dashed vertical line at 15 seconds indicates taste onset. Second dashed line at 15.5 seconds indicates estimated odor onset.

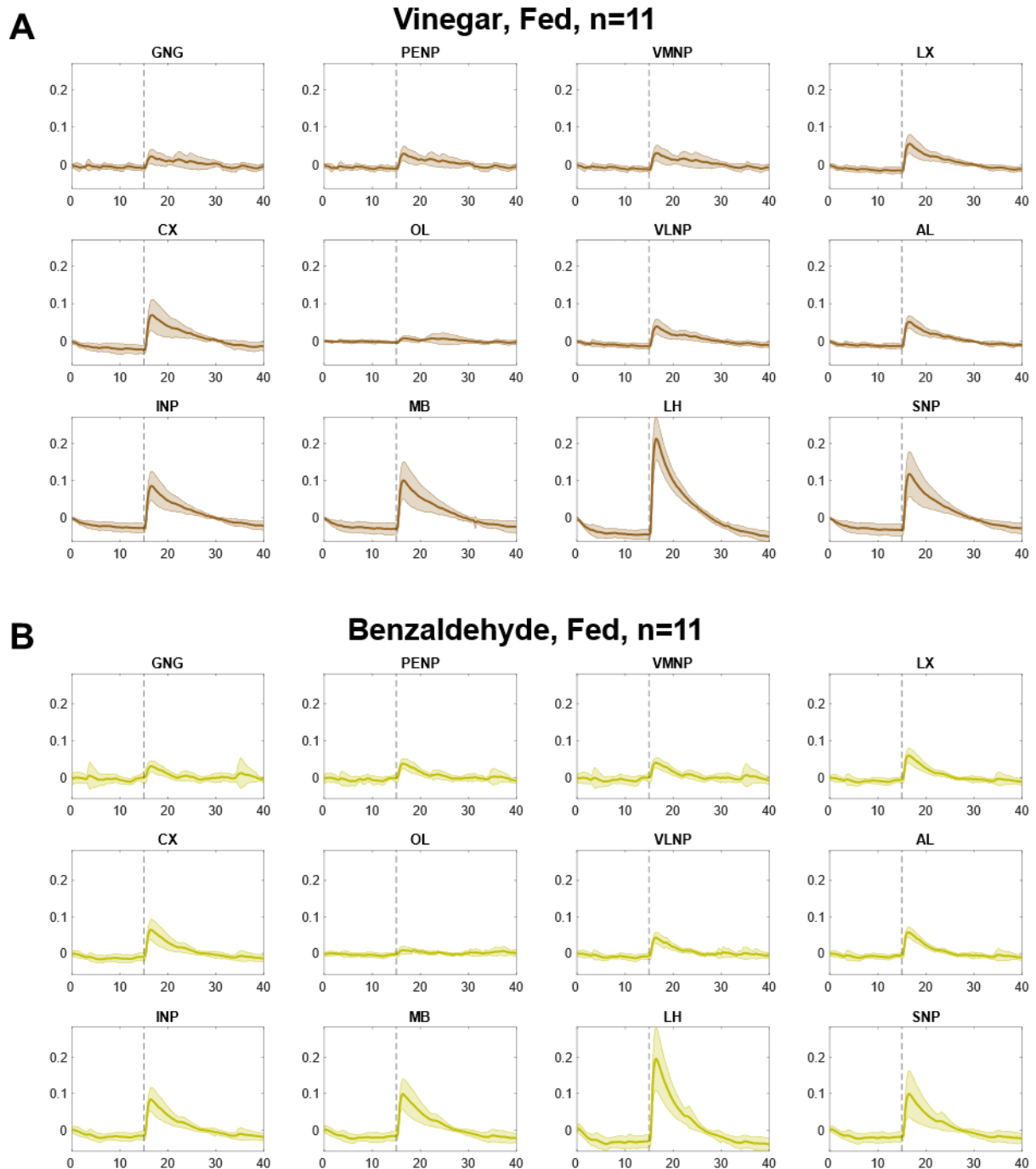


Figure A11.2: Average time series for the odor responses in fed flies

A Average dF/F time series for the first vinegar stimulation. B Average dF/F for the first benzaldehyde stimulation. Y-axis: dF/F , X-axis: time (s). Solid line indicates average time series across individuals. Shaded area indicates standard deviation. Dashed vertical line at 15 seconds indicates stimulus onset.

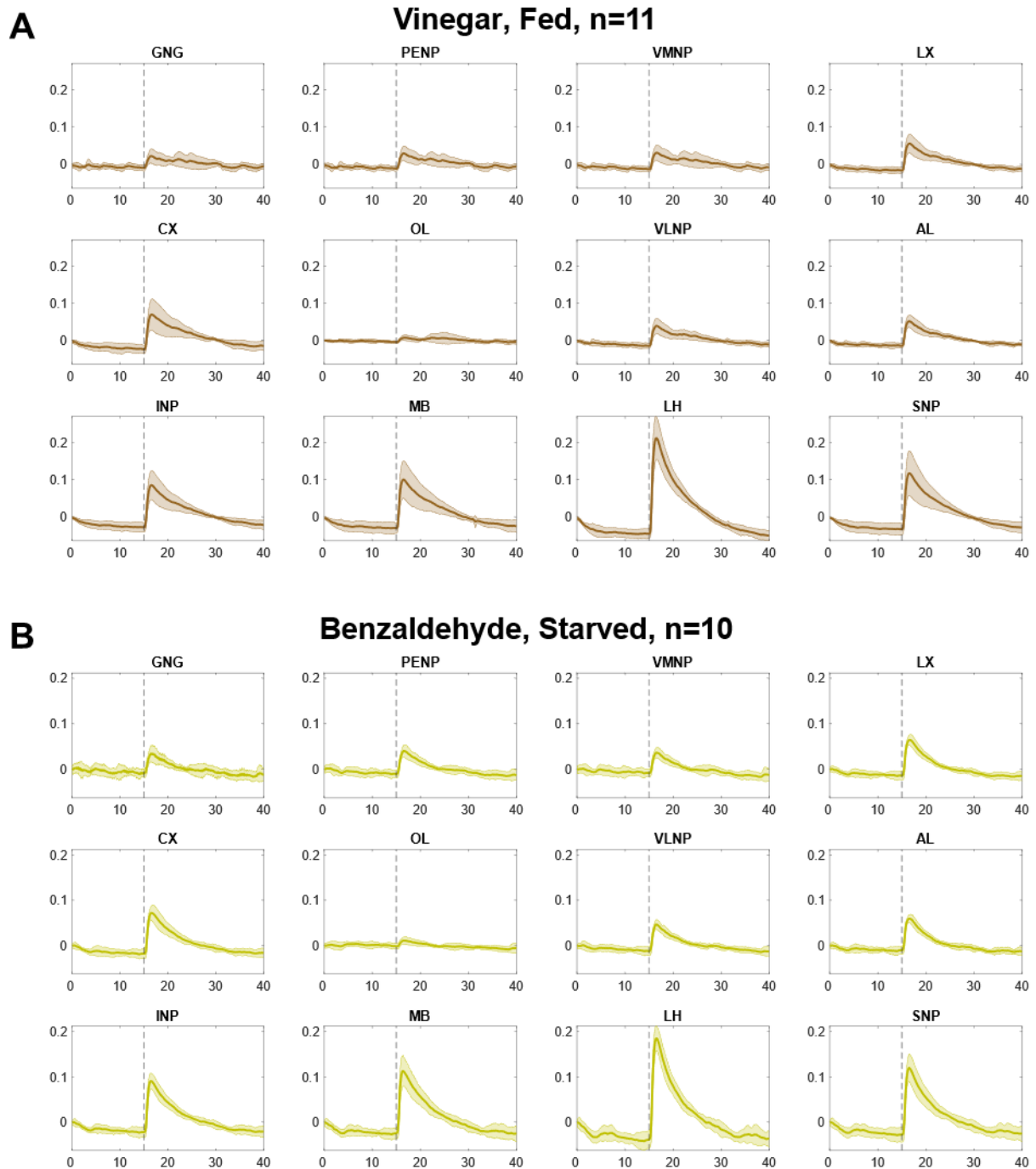


Figure A12.2: Average time series for the odor responses in starved flies

A Average dF/F time series for the first vinegar stimulation. B Average dF/F for the first benzaldehyde stimulation. Y-axis: dF/F, X-axis: time (s). Solid line indicates average time series across individuals. Shaded area indicates standard deviation. Dashed vertical line at 15 seconds indicates stimulus onset.

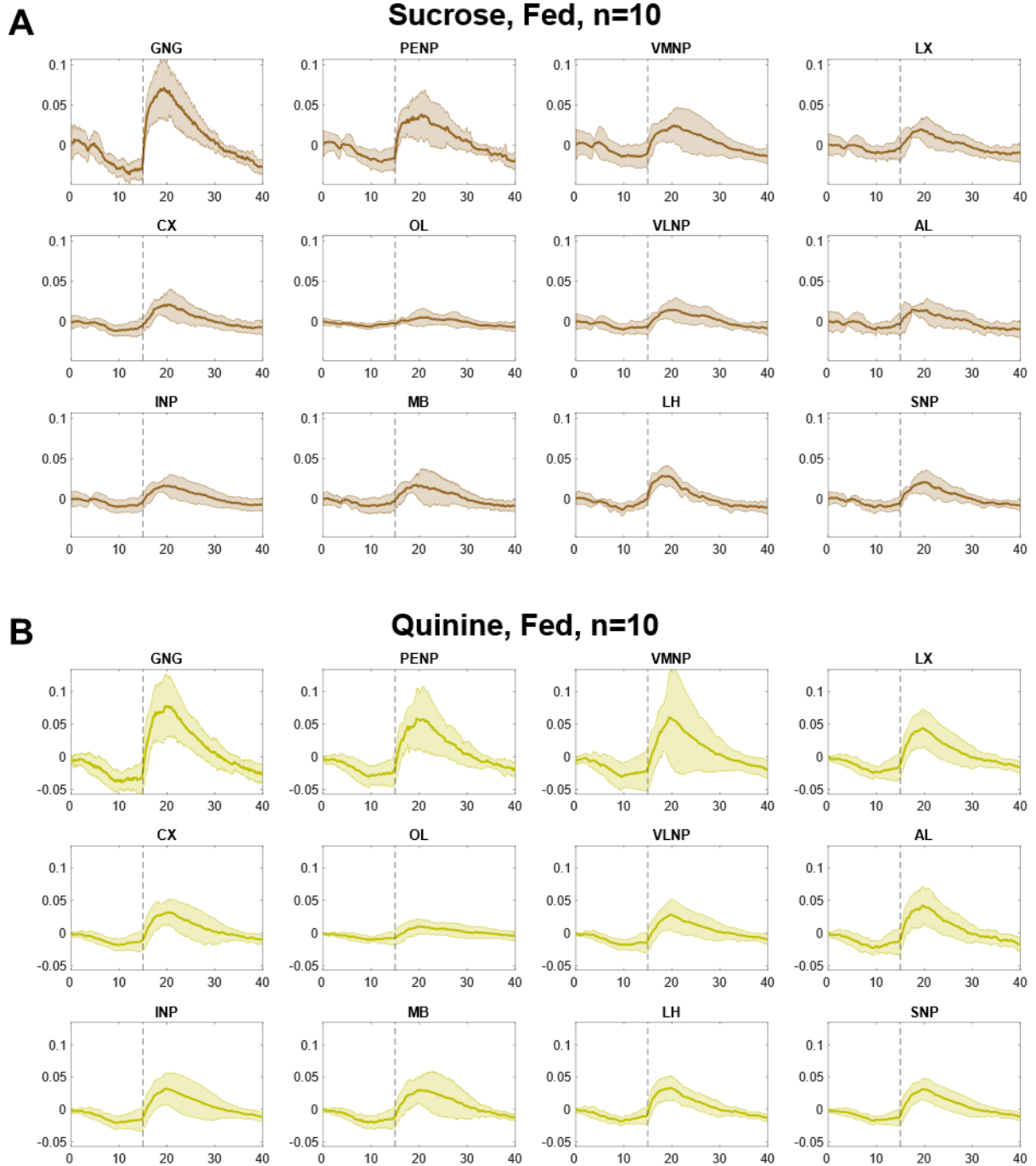


Figure A13.2: Average time series for the taste responses in fed flies

A Average dF/F time series for the first sucrose stimulation. B Average dF/F for the first quinine stimulation. Y-axis: dF/F , X-axis: time (s). Solid line indicates average time series across individuals. Shaded area indicates standard deviation. Dashed vertical line at 15 seconds indicates stimulus onset.

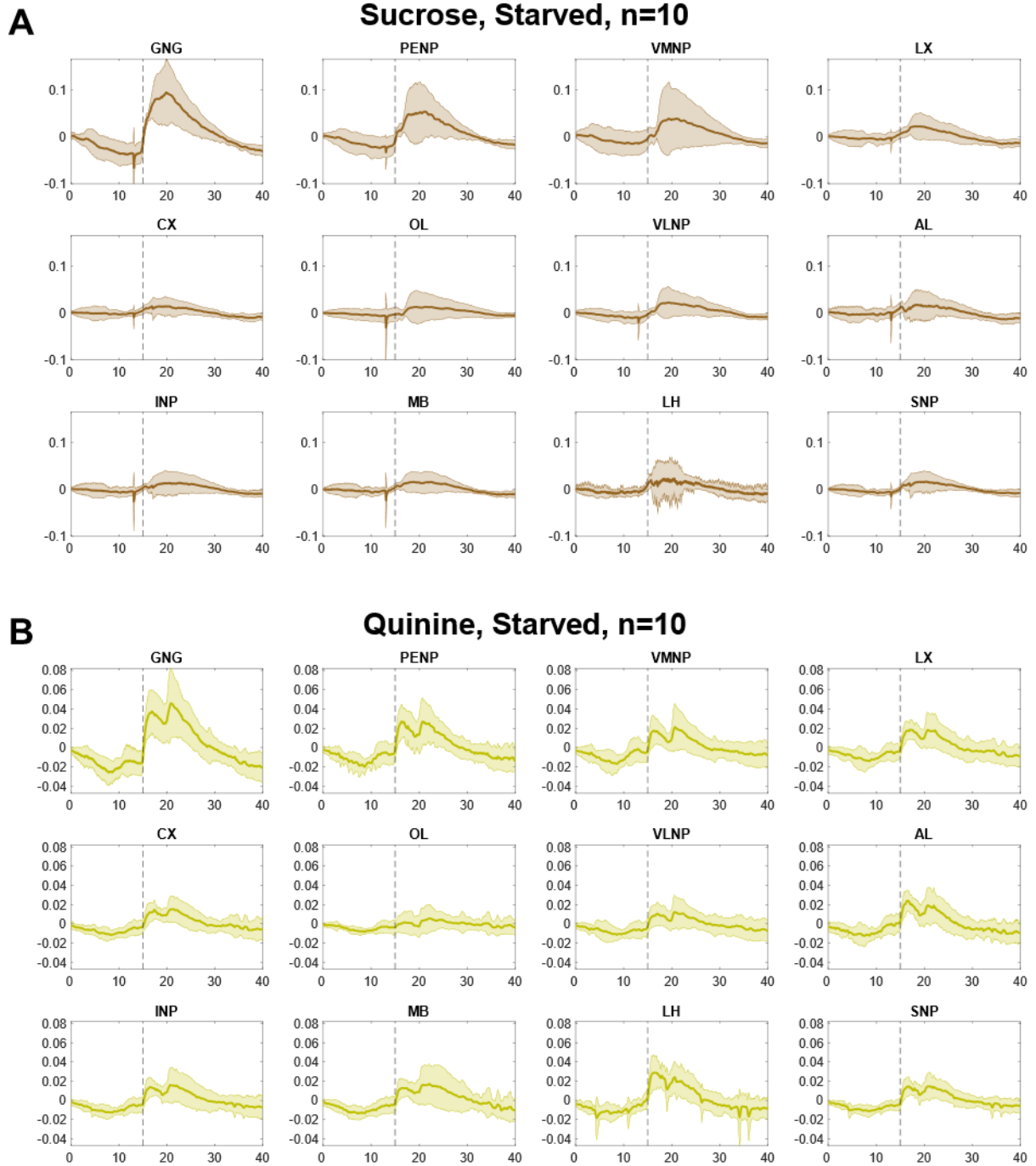


Figure A14.2: Average time series for the taste responses in starved flies

A Average dF/F time series for the first sucrose stimulation. B Average dF/F for the first quinine stimulation. Y-axis: dF/F , X-axis: time (s). Solid line indicates average time series across individuals. Shaded area indicates standard deviation. Dashed vertical line at 15 seconds indicates stimulus onset.

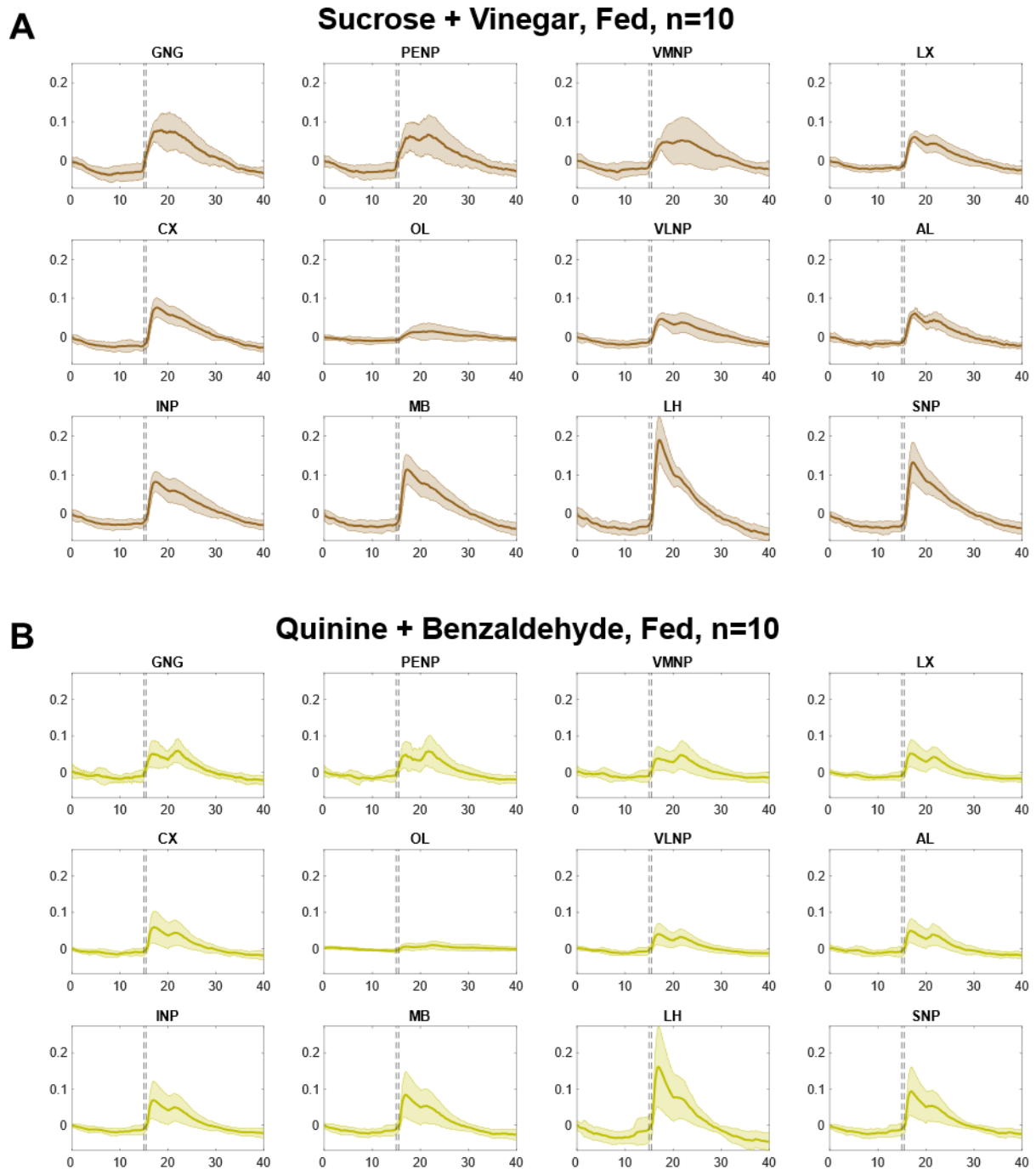


Figure A15.2: Average time series for the taste + odor responses to matching valence in fed flies
 A Average dF/F time series for the first sucrose + vinegar stimulation. B Average dF/F for the first quinine + benzaldehyde stimulation. Y-axis: dF/F , X-axis: time (s). Solid line indicates average time series across individuals. Shaded area indicates standard deviation. Dashed vertical line at 15 seconds indicates taste onset. Second dashed line at 15.5 seconds indicates estimated odor onset.

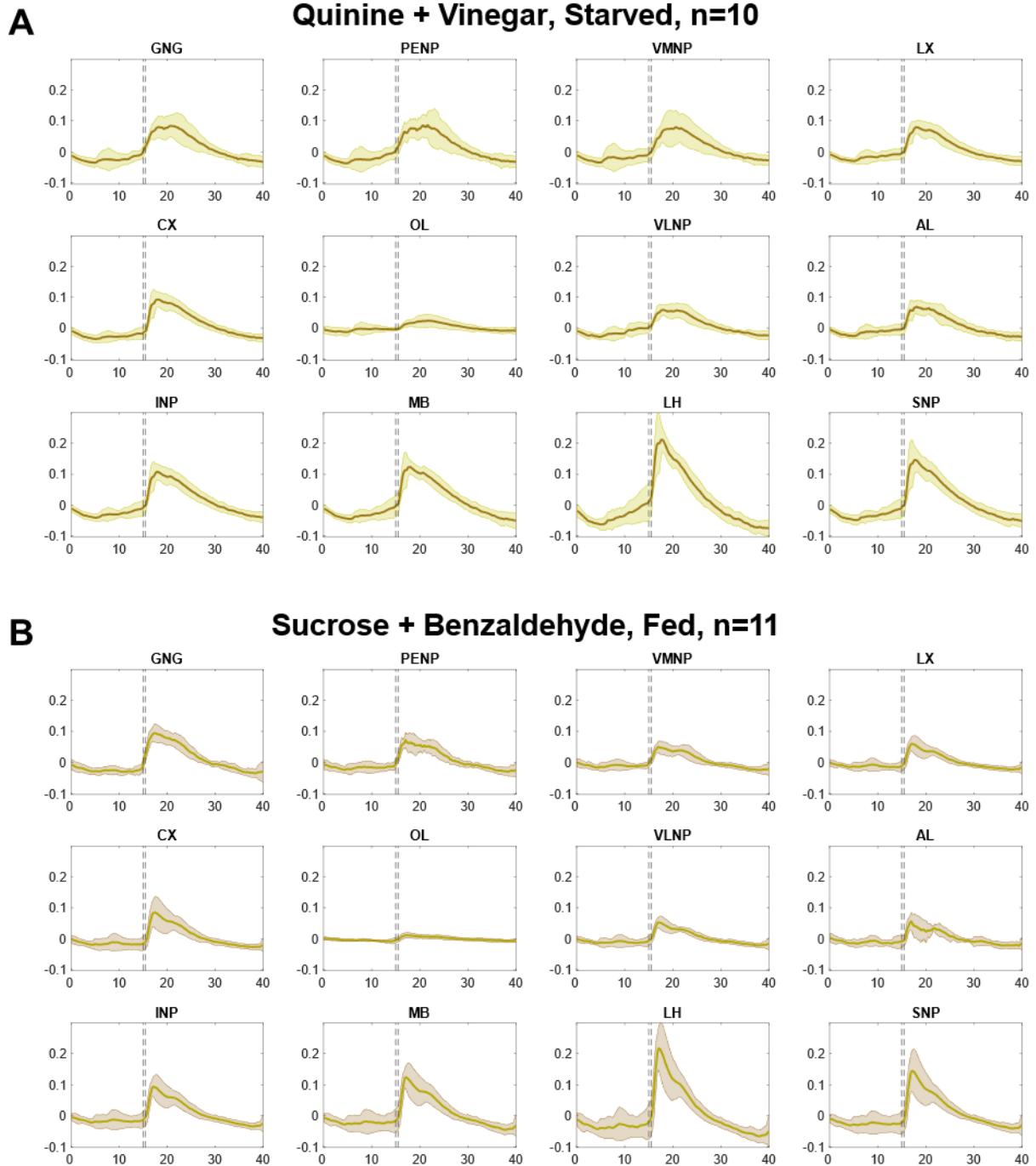


Figure A16.2: Average time series for the taste + odor responses to conflicting valence in fed flies

A Average dF/F time series for the first quinine + vinegar stimulation. B Average dF/F for the first sucrose + benzaldehyde stimulation. Y-axis: dF/F , X-axis: time (s). Solid line indicates average time series across individuals. Shaded area indicates standard deviation. Dashed vertical line at 15 seconds indicates taste onset. Second dashed line at 15.5 seconds indicates estimated odor onset.

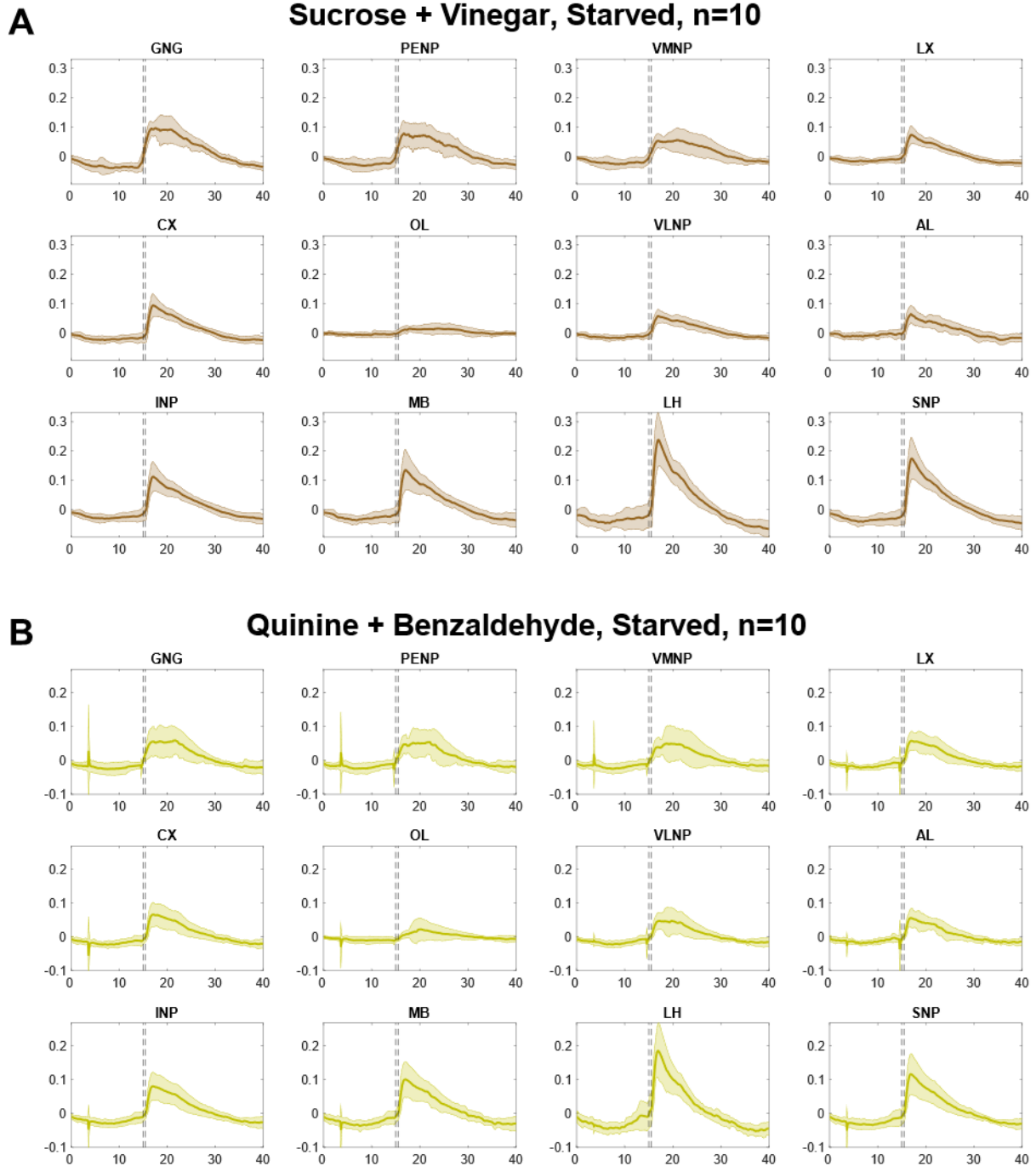


Figure A17.2: Average time series for the taste + odor responses to matching valence in starved flies

A Average dF/F time series for the first sucrose + vinegar stimulation. B Average dF/F for the first quinine + benzaldehyde stimulation. Y-axis: dF/F, X-axis: time (s). Solid line indicates average time series across individuals. Shaded area indicates standard deviation. Dashed vertical line at 15 seconds indicates taste onset. Second dashed line at 15.5 seconds indicates estimated odor onset.

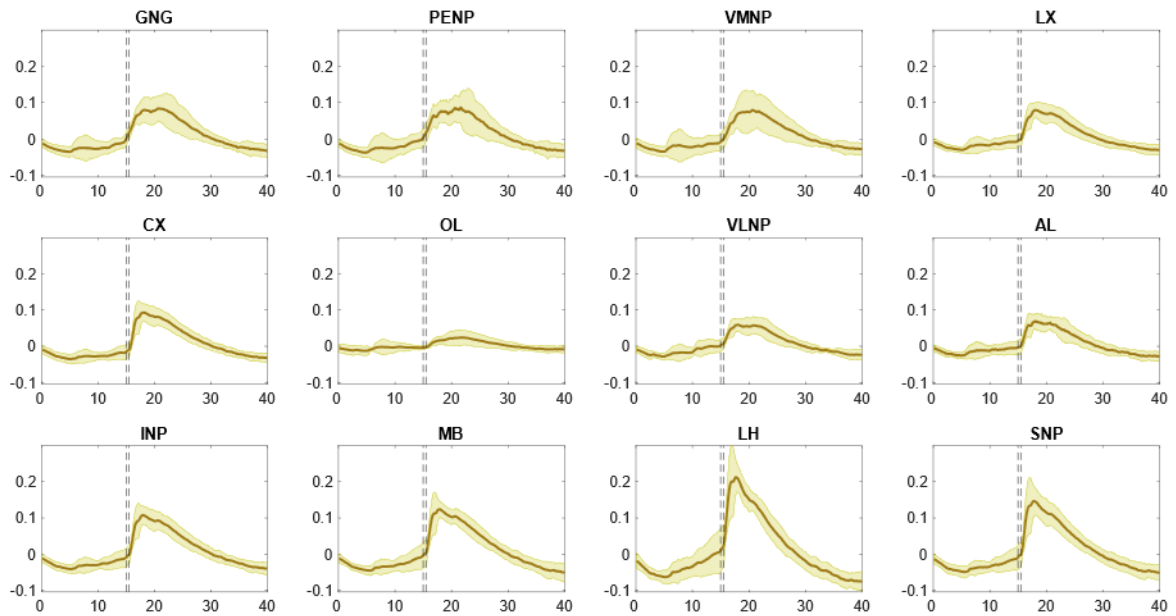
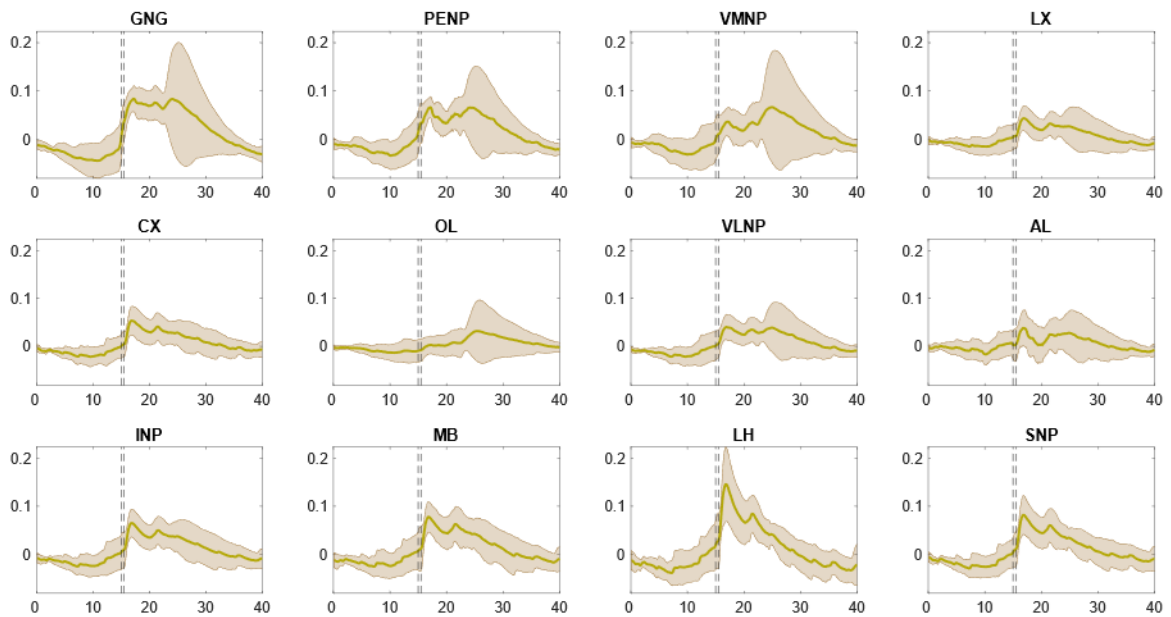
A**Quinine + Vinegar, Starved, n=10****B****Sucrose + Benzaldehyde, Starved, n=10**

Figure A18.2: Average time series for the taste + odor responses to conflicting valence in starved flies

A Average dF/F time series for the first quinine + vinegar stimulation. B Average dF/F for the first sucrose + benzaldehyde stimulation. Y-axis: dF/F, X-axis: time (s). Solid line indicates average time series across individuals. Shaded area indicates standard deviation. Dashed vertical line at 15 seconds indicates taste onset. Second dashed line at 15.5 seconds indicates estimated odor onset.

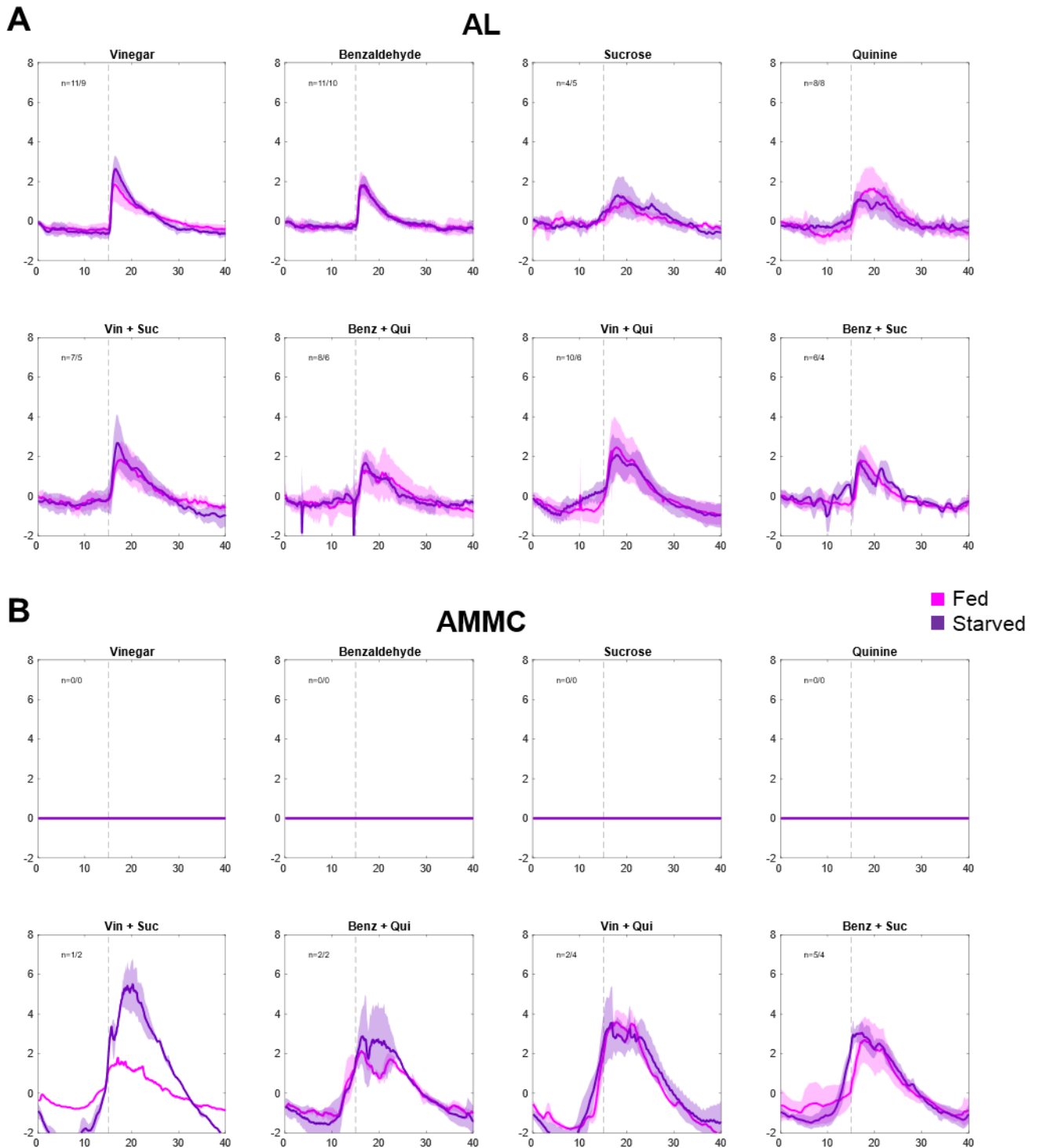


Figure A19: Average time series for functional components during the first stimulus
 A Average dF/F time series for AL. B Average dF/F time series for AMMC. Y-axis: dF/F, X-axis: time (s). Solid line indicates average time series across individuals. Shaded area indicates standard deviation. Dashed vertical line at 15 seconds indicates stimulus onset.

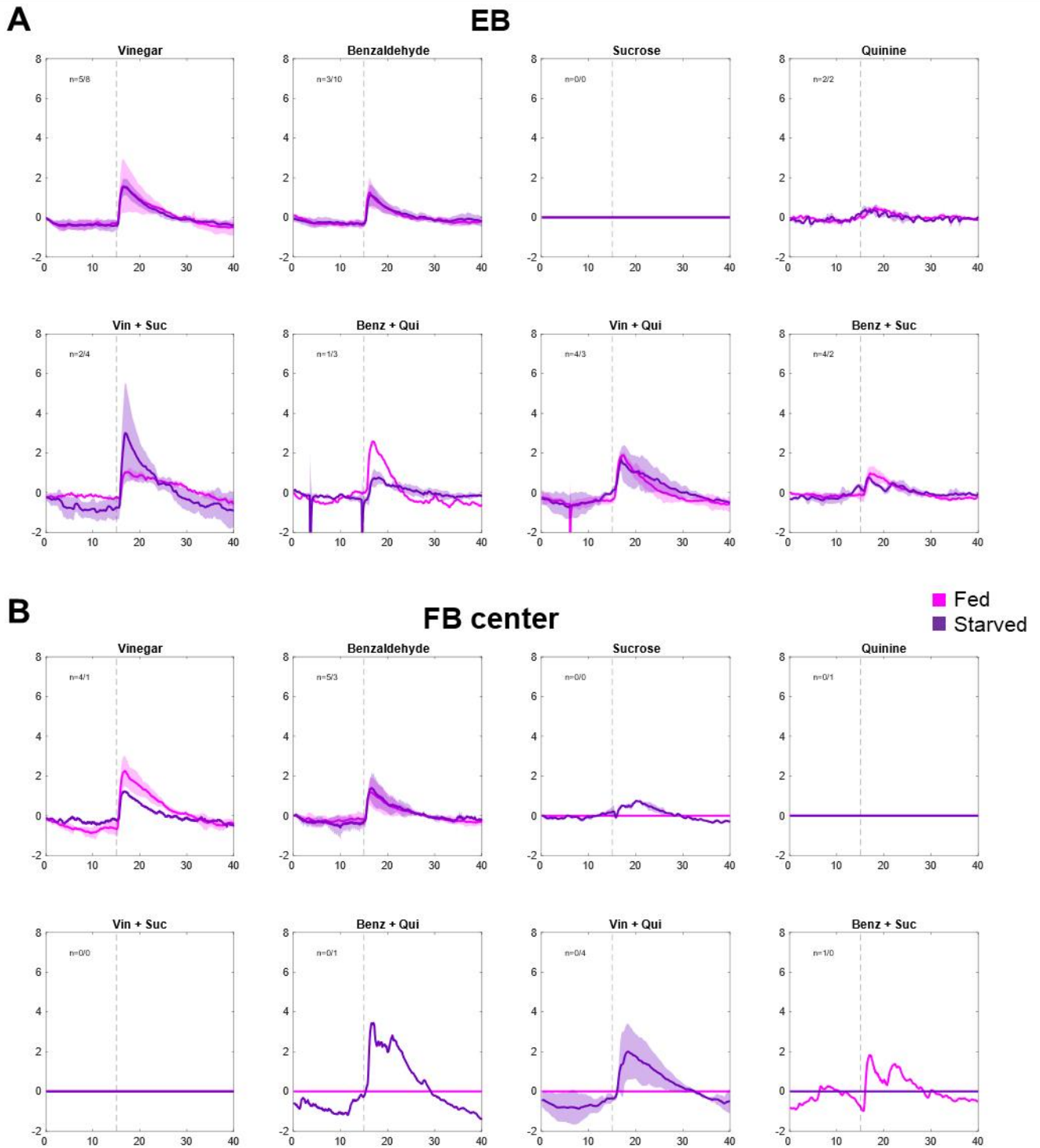


Figure A20: Average time series for functional components during the first stimulus

A Average dF/F time series for EB. B Average dF/F time series for FB center. Y-axis: dF/F, X-axis: time (s). Solid line indicates average time series across individuals. Shaded area indicates standard deviation. Dashed vertical line at 15 seconds indicates stimulus onset.

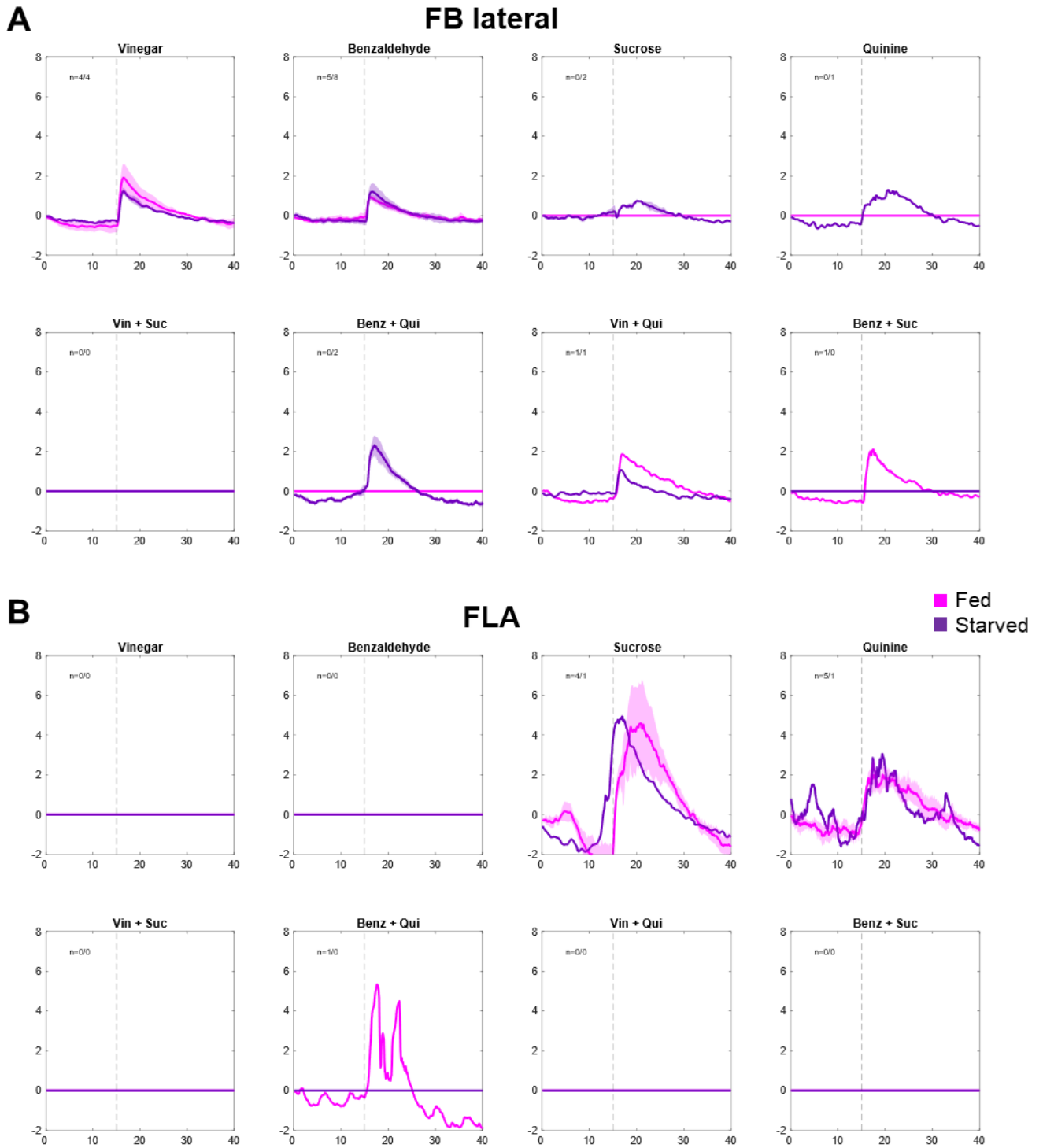


Figure A21: Average time series for functional components during the first stimulus

A Average dF/F time series for FB lateral. B Average dF/F time series for FLA. Y-axis: dF/F, X-axis: time (s). Solid line indicates average time series across individuals. Shaded area indicates standard deviation. Dashed vertical line at 15 seconds indicates stimulus onset.

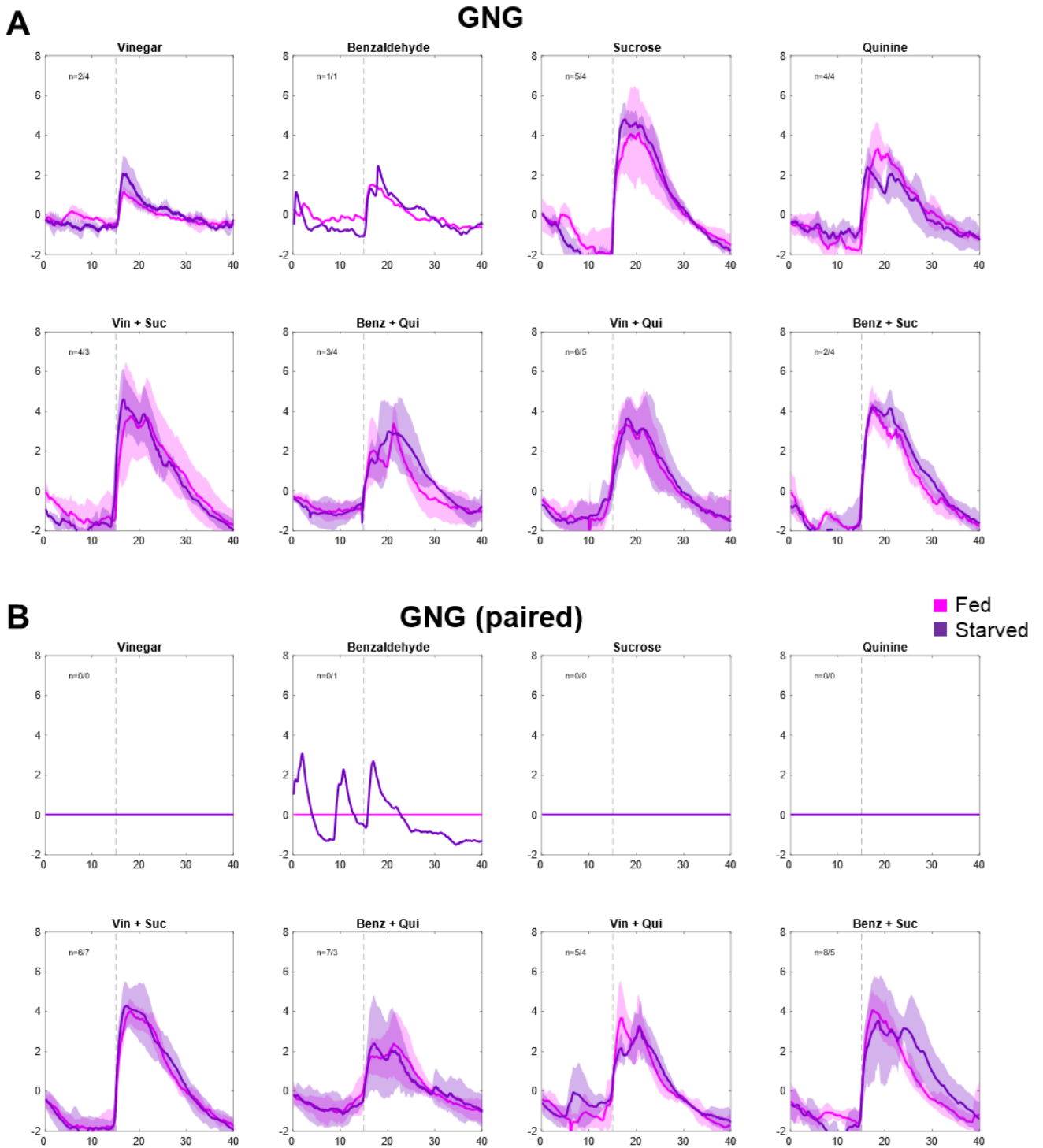


Figure A22: Average time series for functional components during the first stimulus
 A Average dF/F time series for GNG. B Average dF/F time series for GNG (paired). Y-axis: dF/F, X-axis: time (s). Solid line indicates average time series across individuals. Shaded area indicates standard deviation. Dashed vertical line at 15 seconds indicates stimulus onset.

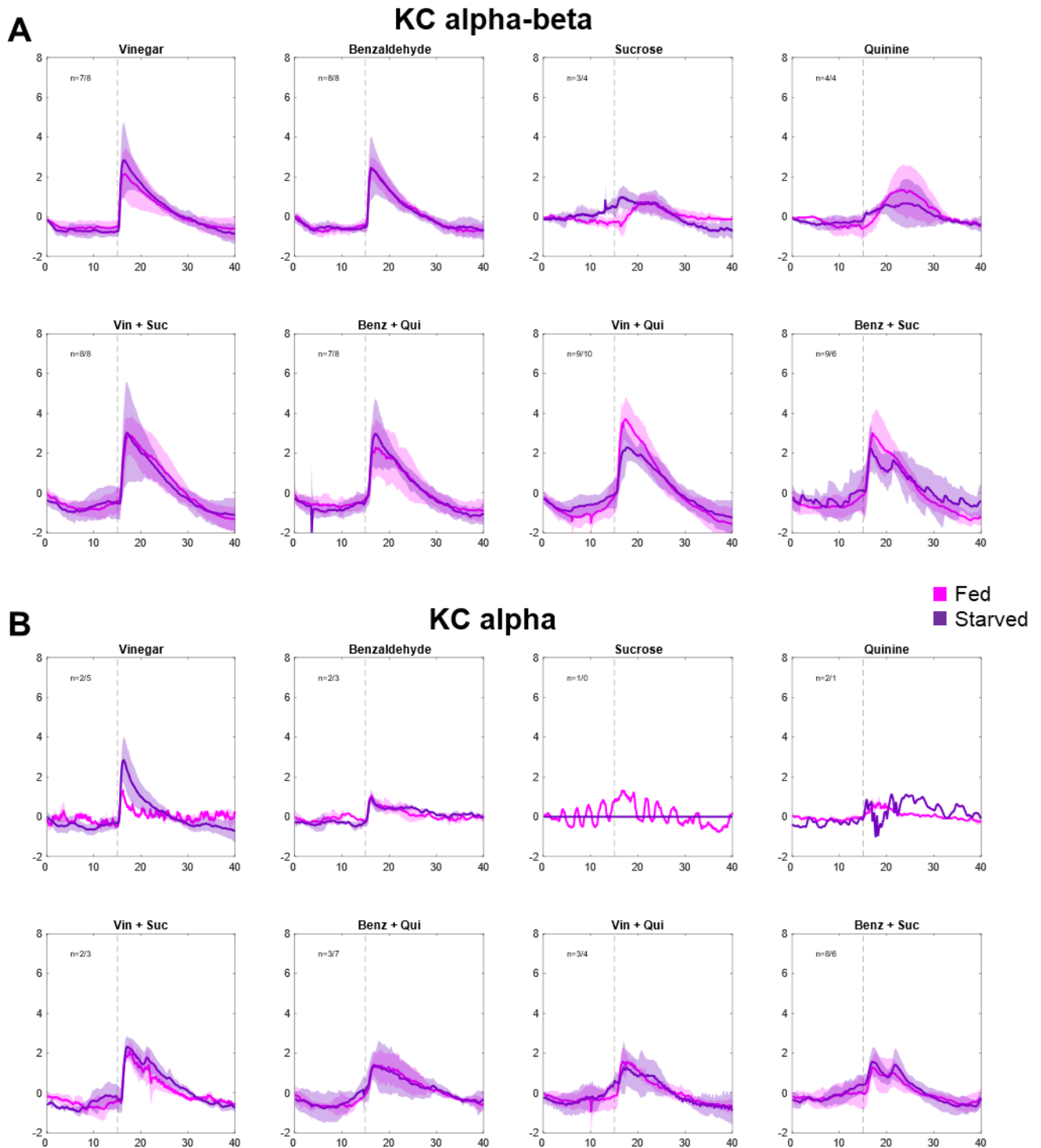


Figure A23: Average time series for functional components during the first stimulus

A Average dF/F time series for KC alpha-beta. B Average dF/F time series for KC alpha. Y-axis: dF/F, X-axis: time (s). Solid line indicates average time series across individuals. Shaded area indicates standard deviation. Dashed vertical line at 15 seconds indicates stimulus onset.

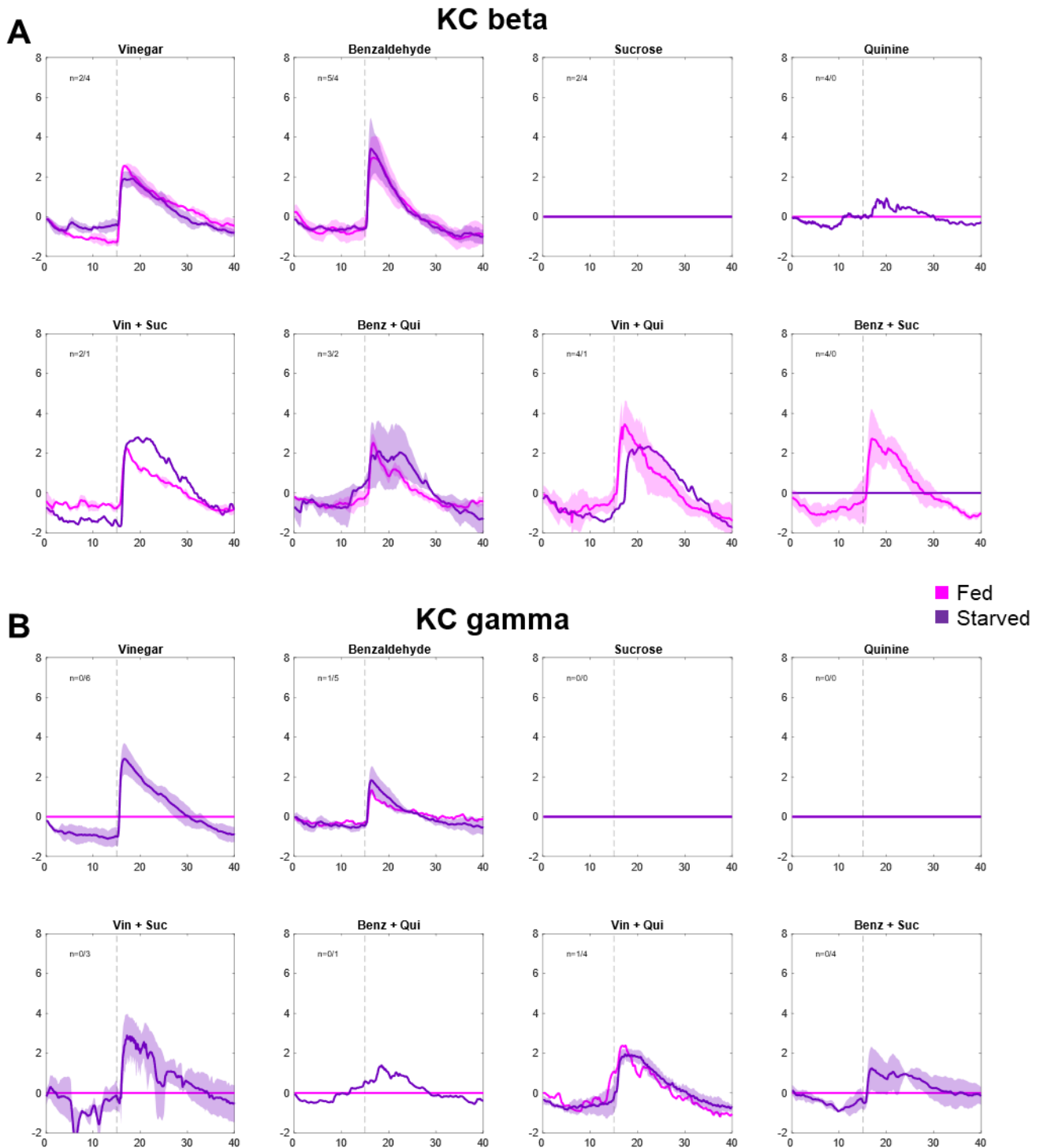


Figure A24: Average time series for functional components during the first stimulus

A Average dF/F time series for KC beta. B Average dF/F time series for KC gamma. Y-axis: dF/F, X-axis: time (s). Solid line indicates average time series across individuals. Shaded area indicates standard deviation. Dashed vertical line at 15 seconds indicates stimulus onset.

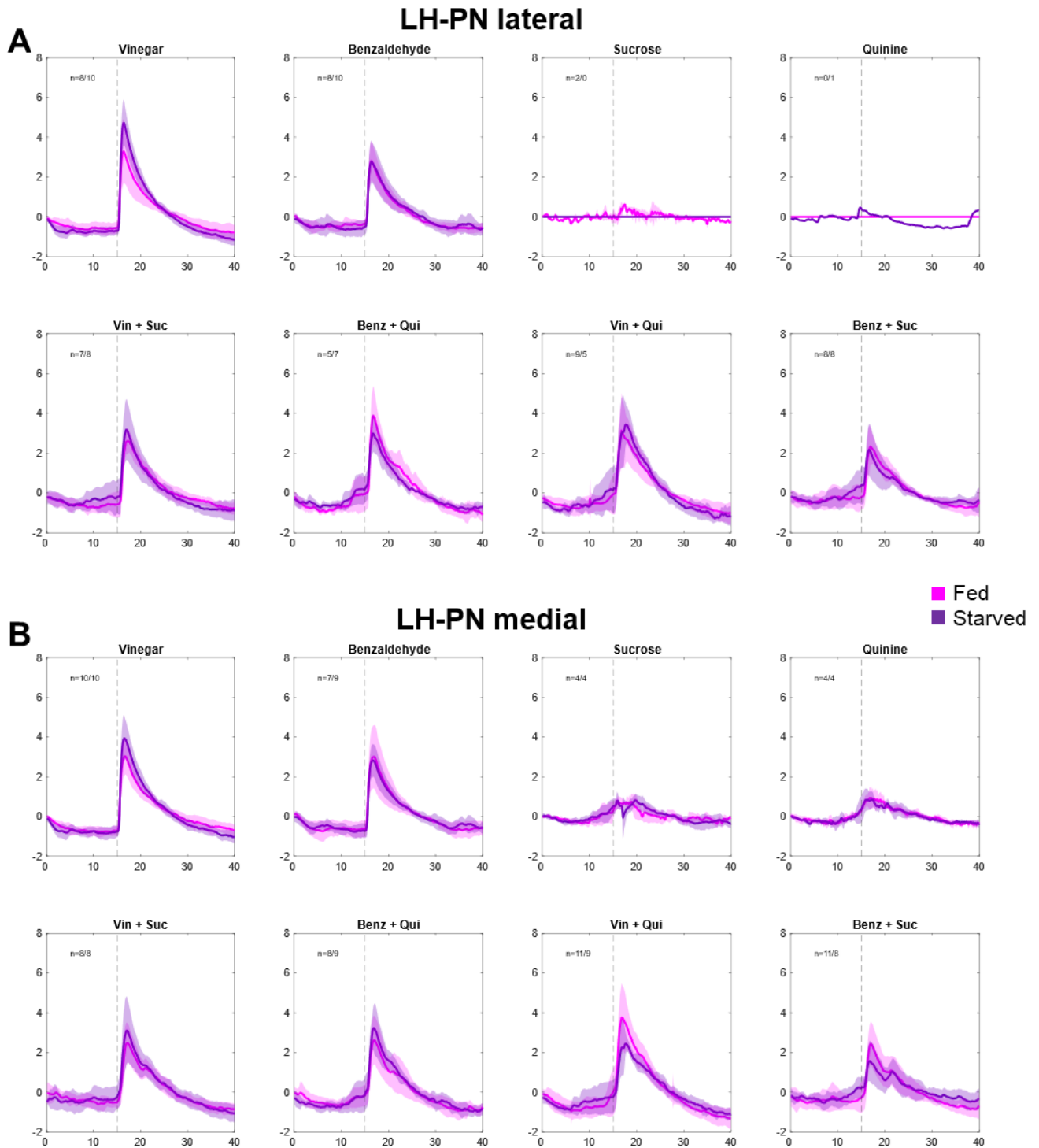


Figure A25: Average time series for functional components during the first stimulus

A Average dF/F time series for LH-PN lateral. B Average dF/F time series for LH-PN medial. Y-axis: dF/F, X-axis: time (s). Solid line indicates average time series across individuals. Shaded area indicates standard deviation. Dashed vertical line at 15 seconds indicates stimulus onset.

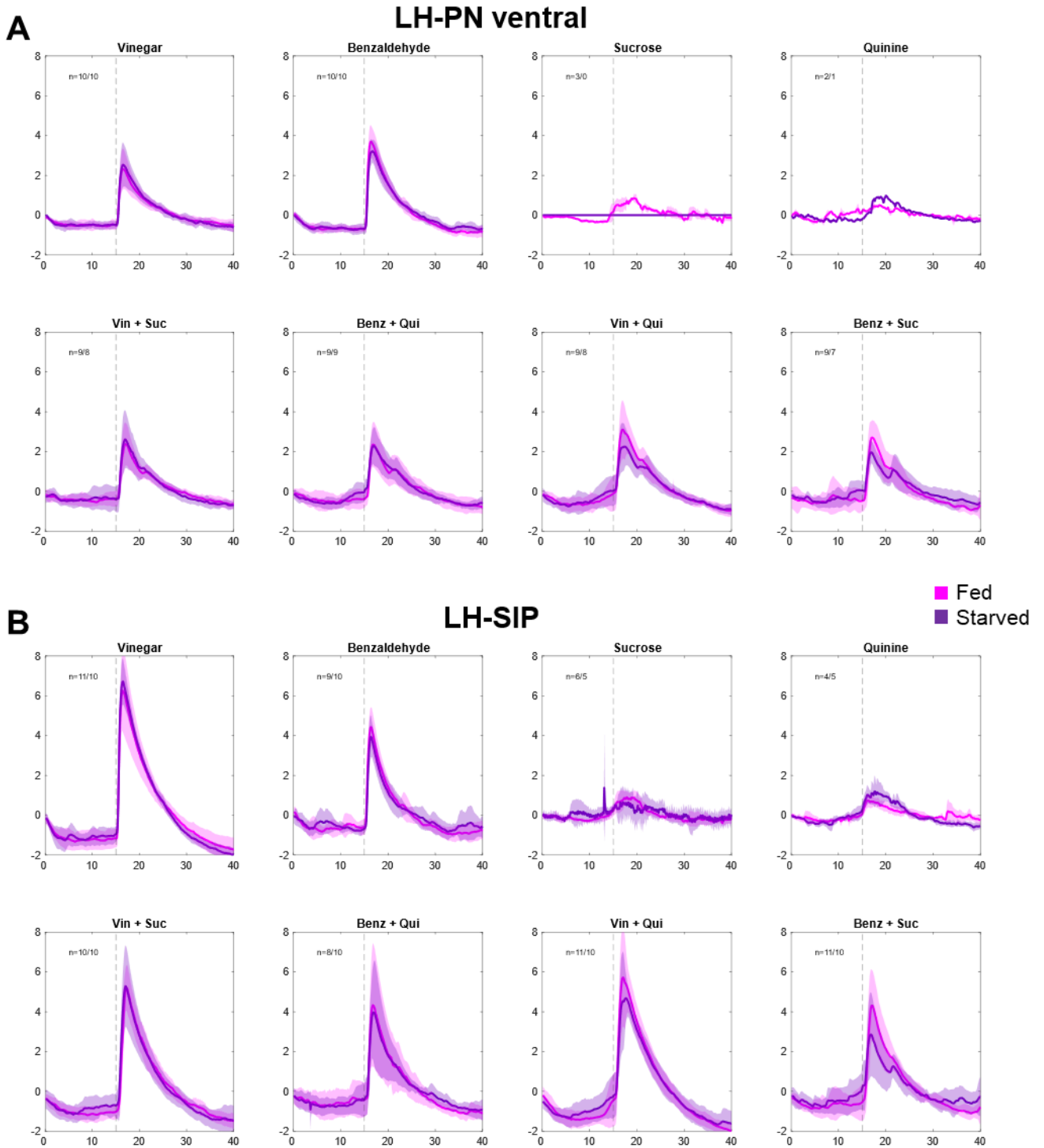


Figure A26: Average time series for functional components during the first stimulus

A Average dF/F time series for LH-PN ventral. B Average dF/F time series for LH-SIP. Y-axis: dF/F, X-axis: time (s). Solid line indicates average time series across individuals. Shaded area indicates standard deviation. Dashed vertical line at 15 seconds indicates stimulus onset.

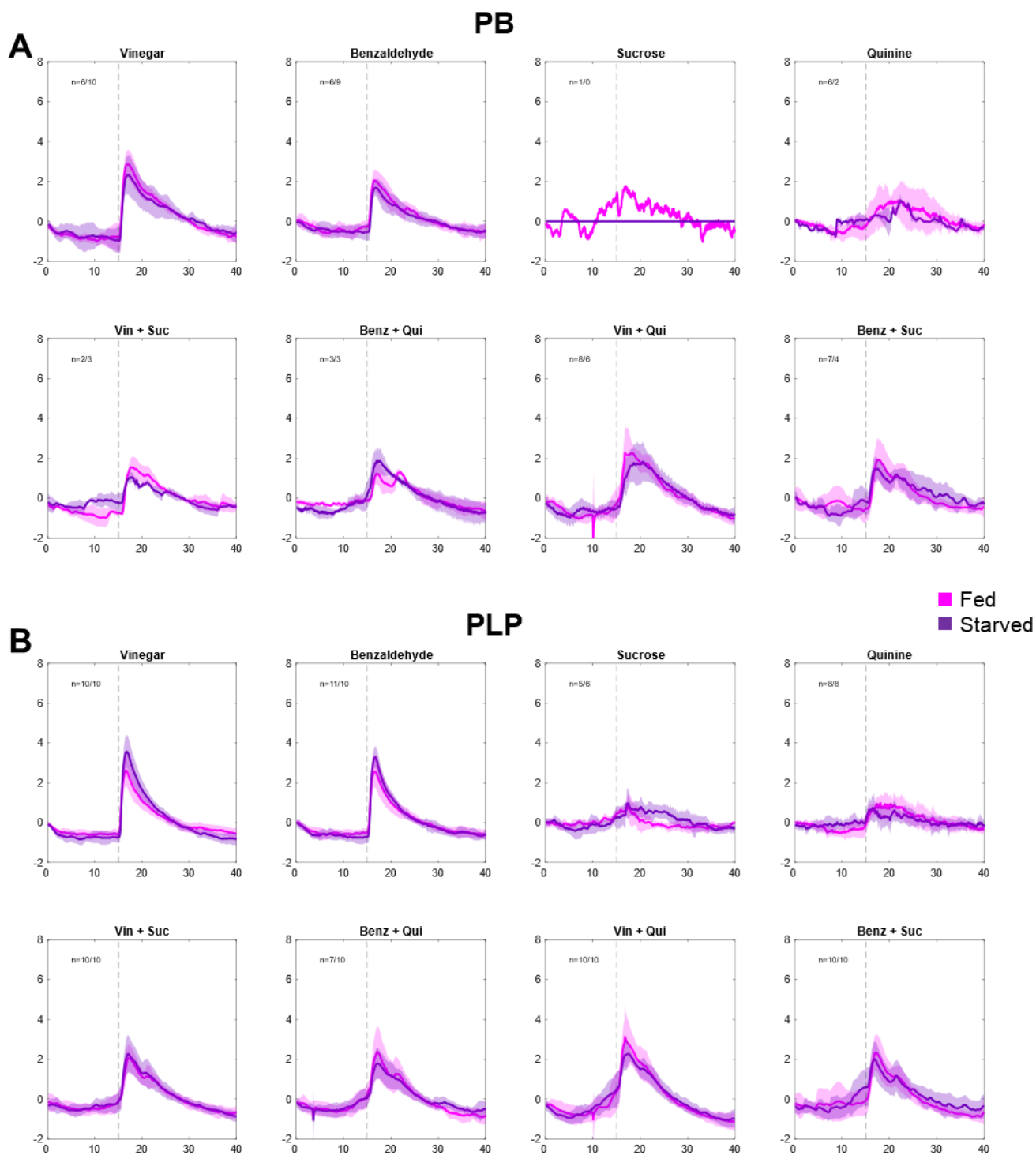


Figure A27: Average time series for functional components during the first stimulus

A Average dF/F time series for PB. B Average dF/F time series for PLP. Y-axis: dF/F, X-axis: time (s). Solid line indicates average time series across individuals. Shaded area indicates standard deviation. Dashed vertical line at 15 seconds indicates stimulus onset.

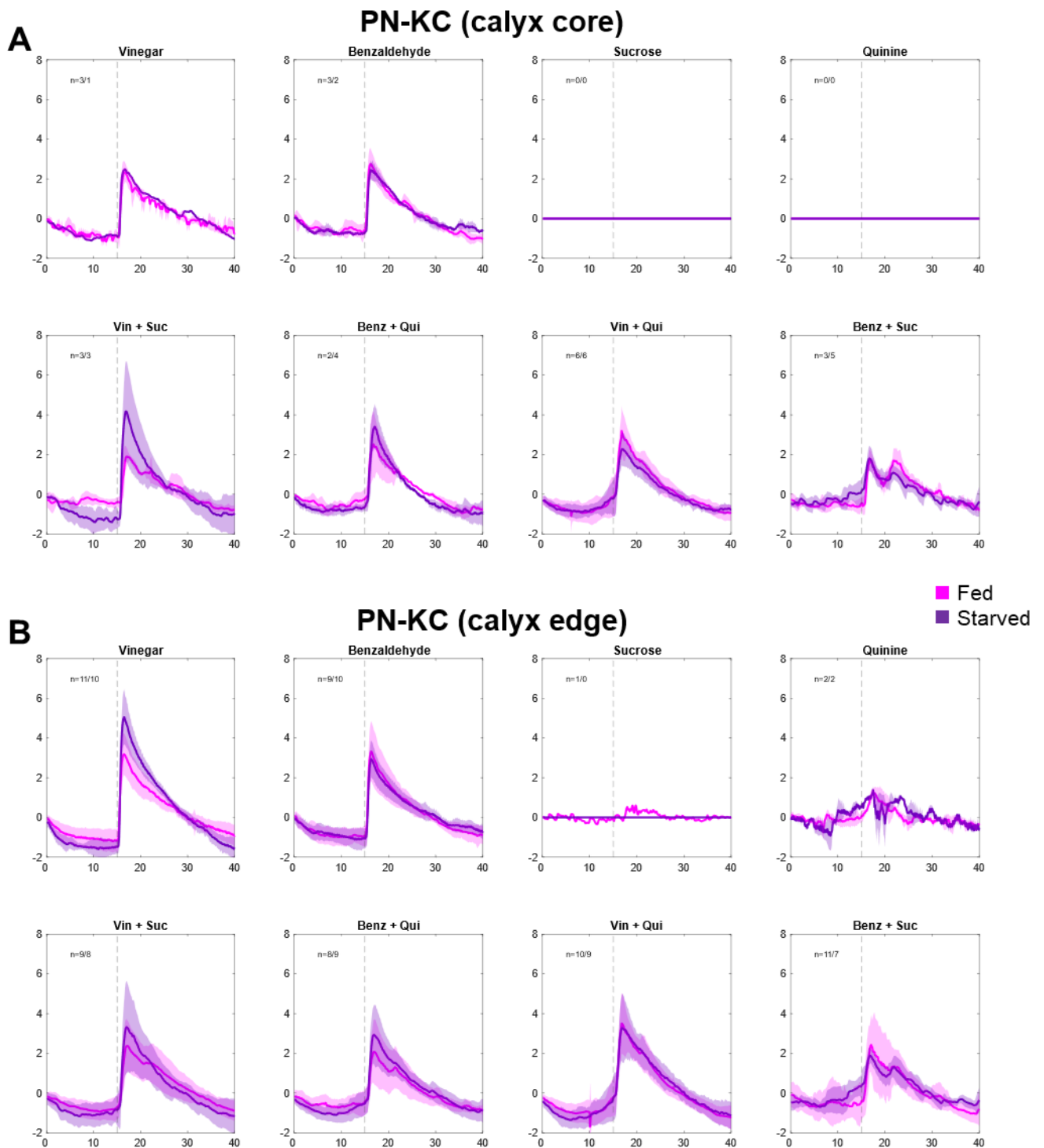


Figure A28: Average time series for functional components during the first stimulus

A Average dF/F time series for PN-KC (calyx core). B Average dF/F time series for PN-KC (calyx edge). Y-axis: dF/F, X-axis: time (s). Solid line indicates average time series across individuals. Shaded area indicates standard deviation. Dashed vertical line at 15 seconds indicates stimulus onset.

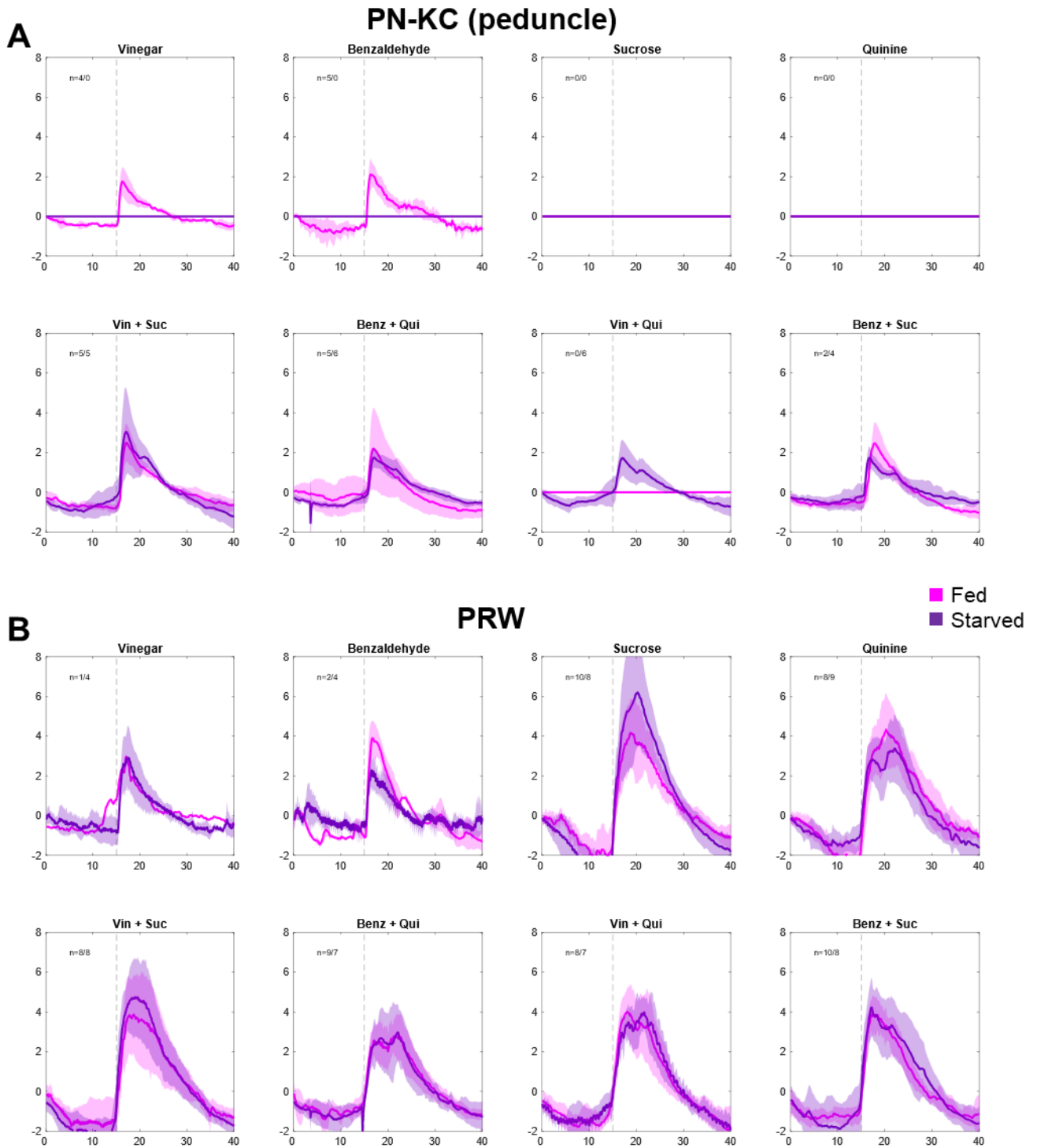


Figure A29: Average time series for functional components during the first stimulus

A Average dF/F time series for PN-KC (peduncle). B Average dF/F time series for PRW. Y-axis: dF/F, X-axis: time (s). Solid line indicates average time series across individuals. Shaded area indicates standard deviation. Dashed vertical line at 15 seconds indicates stimulus onset.

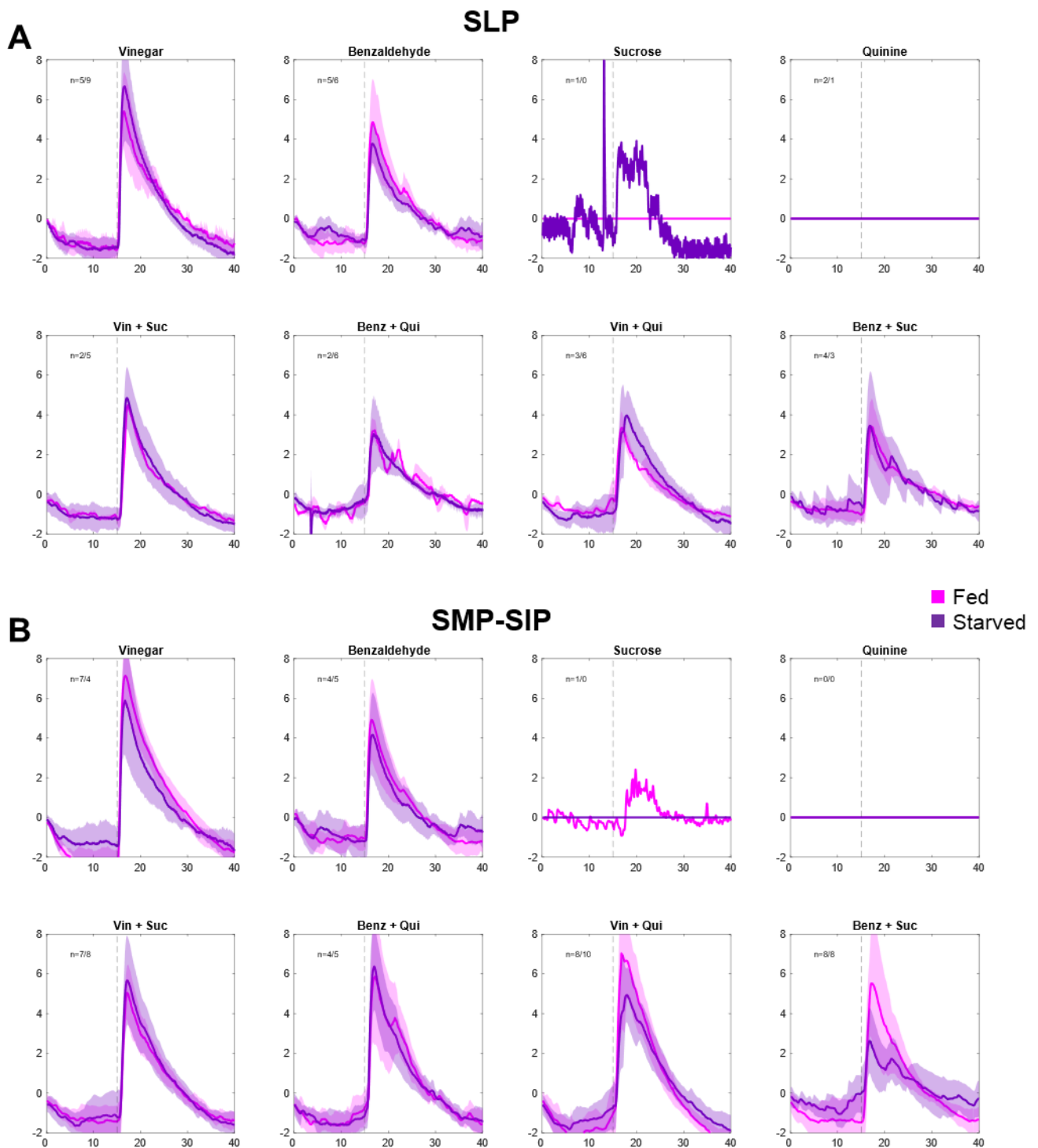


Figure A30: Average time series for functional components during the first stimulus

A Average dF/F time series for SLP. B Average dF/F time series for SMP-SIP. Y-axis: dF/F, X-axis: time (s). Solid line indicates average time series across individuals. Shaded area indicates standard deviation. Dashed vertical line at 15 seconds indicates stimulus onset.

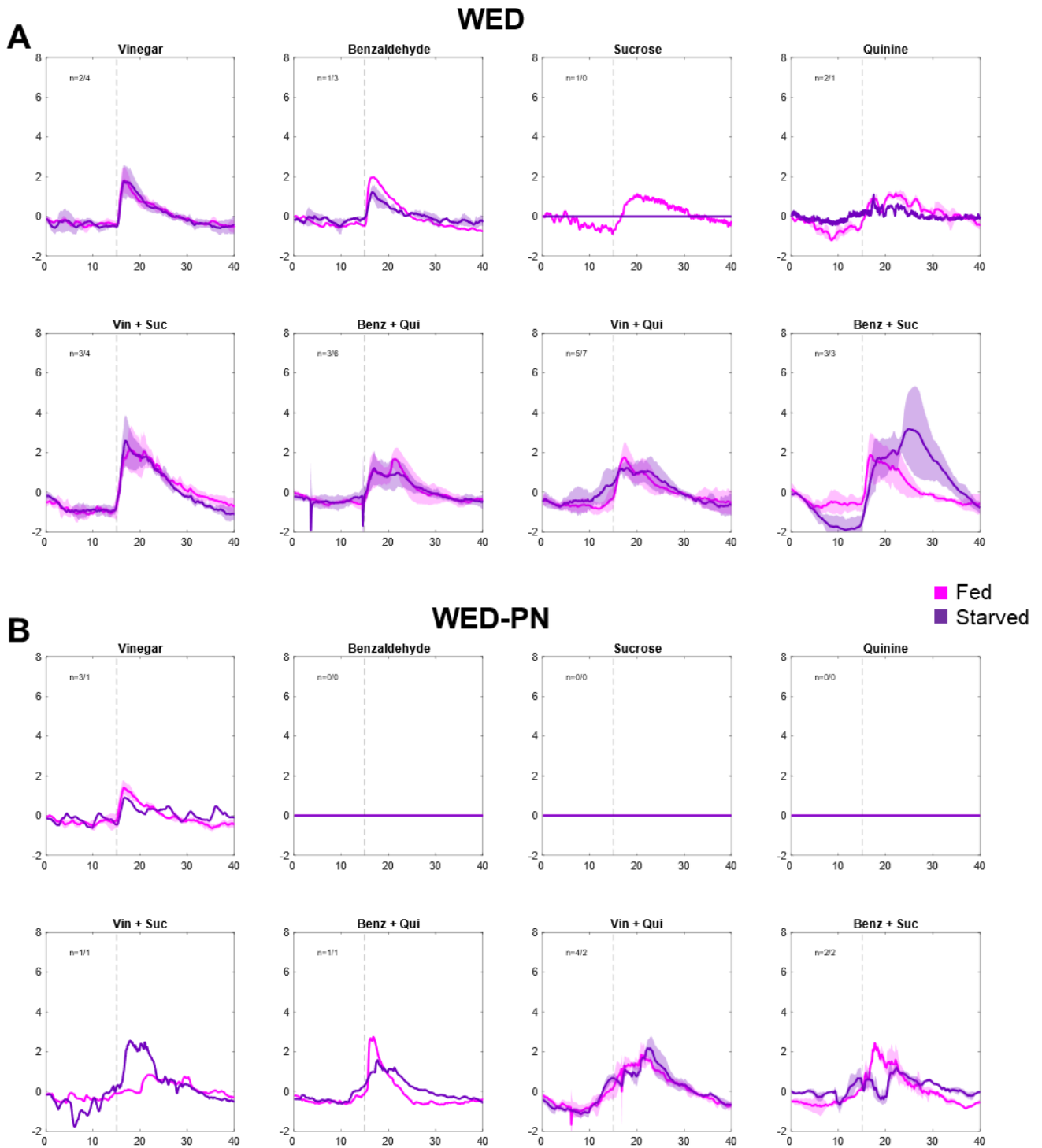


Figure A31: Average time series for functional components during the first stimulus

A Average dF/F time series for WED. B Average dF/F time series for WED-PN. Y-axis: dF/F, X-axis: time (s). Solid line indicates average time series across individuals. Shaded area indicates standard deviation. Dashed vertical line at 15 seconds indicates stimulus onset.

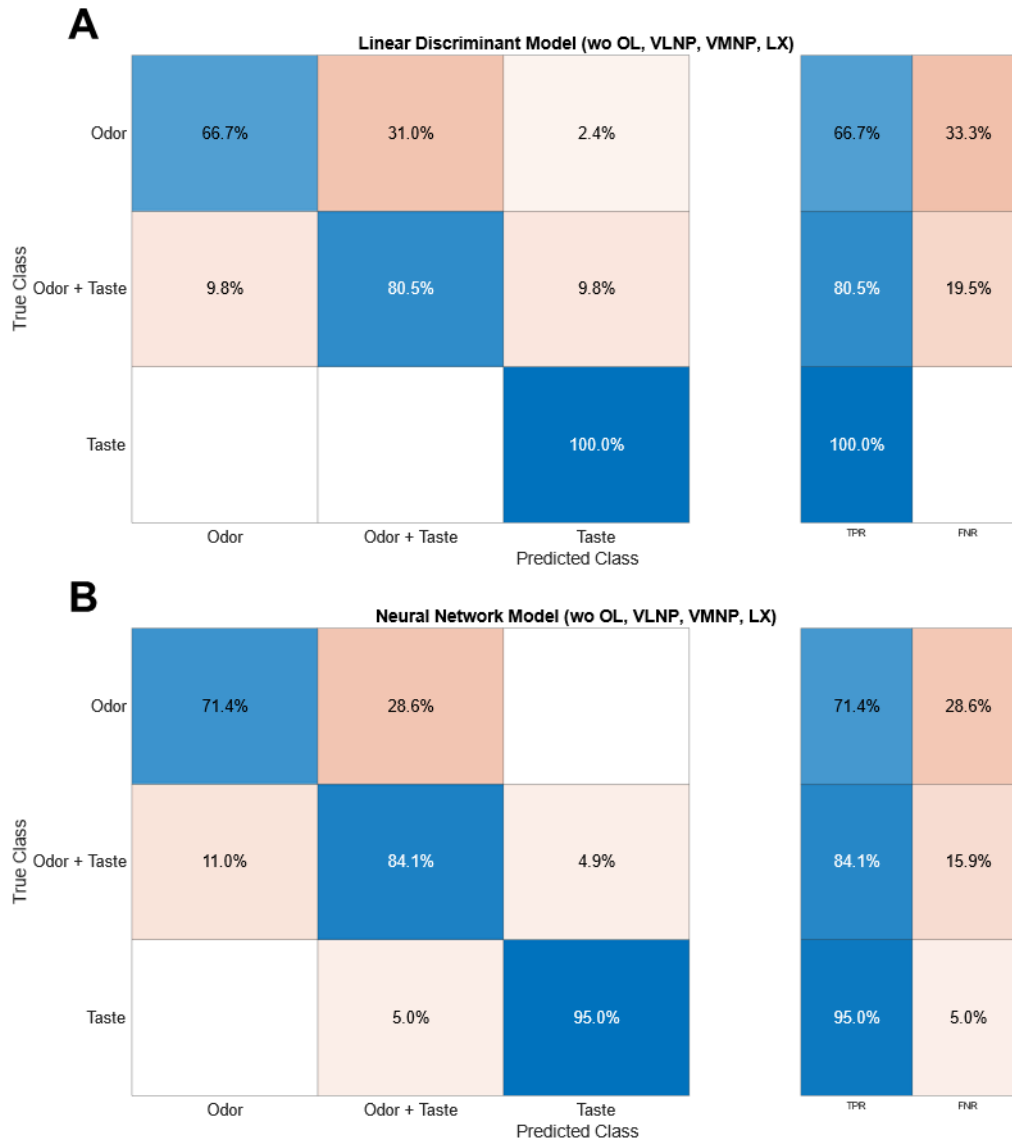


Figure A32: Classification models predicting the stimulus type with a reduced set of responses
 Confusion matrices for (A) the linear discriminant model and (B) the neural network model predicting the stimulus type from a dataset where NNM responses from the OL, VLNP, VMNP and LX were excluded to improve performance. TPR=true positive rate, FNR=false negative rate.

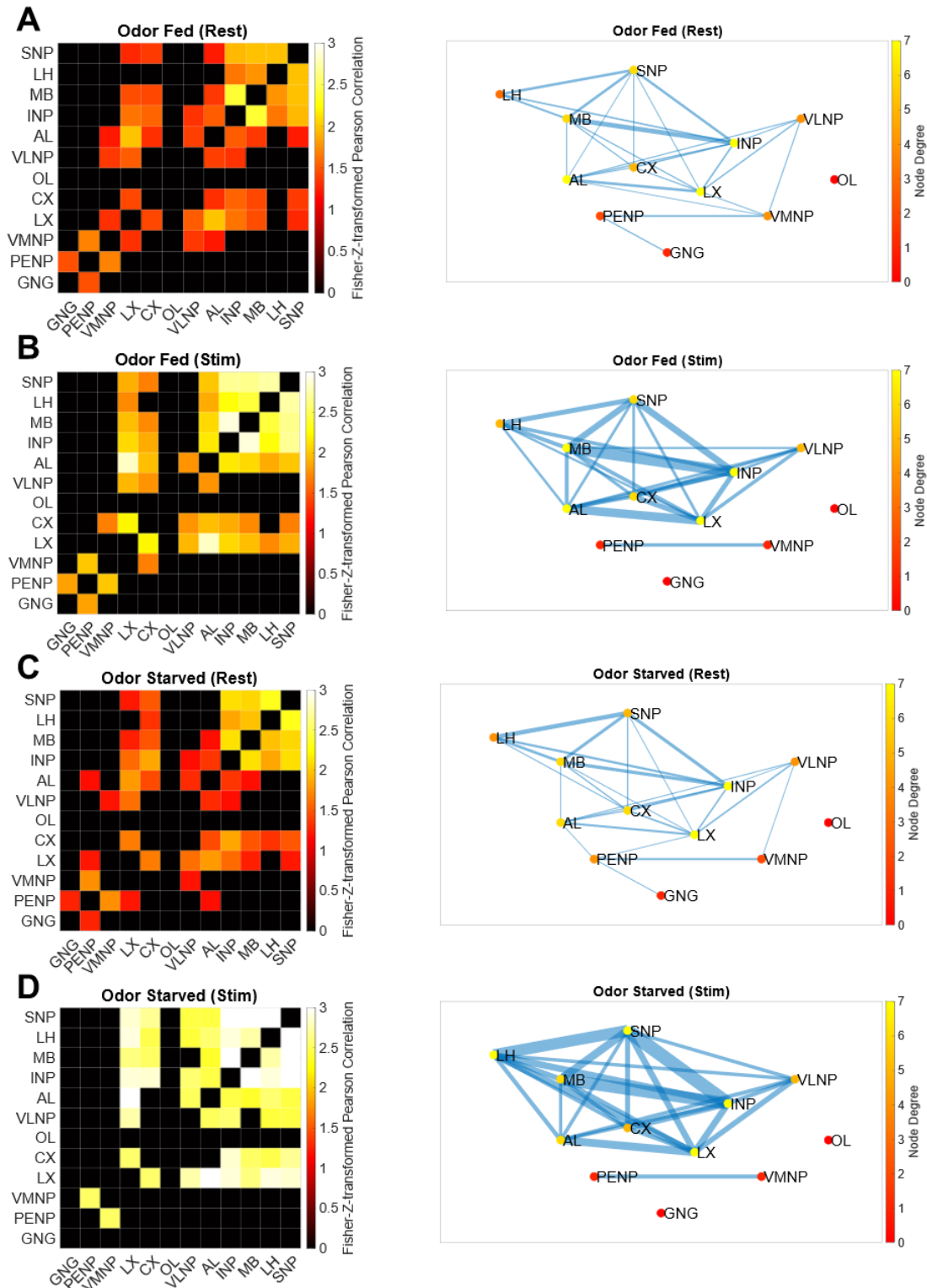


Figure A33: Brain-wide correlation before and during odor stimulation

Adjacency matrix and resulting graph of the activity correlation for the fed group during (A) resting and (B) stimulus phase. Adjacency matrix and resulting graph of the activity correlation for the starved group during (C) resting and (D) stimulus phase. The resting phase was defined as the first 25 seconds of every recording before the first stimulus was applied. The stimulus phase was defined as the first 15 seconds after the onset of the first stimulus. Correlation was thresholded proportionally to retain only 40 percent of the strongest connections. The width of the edges (blue lines) scales proportionally with weight of the connection between the nodes.

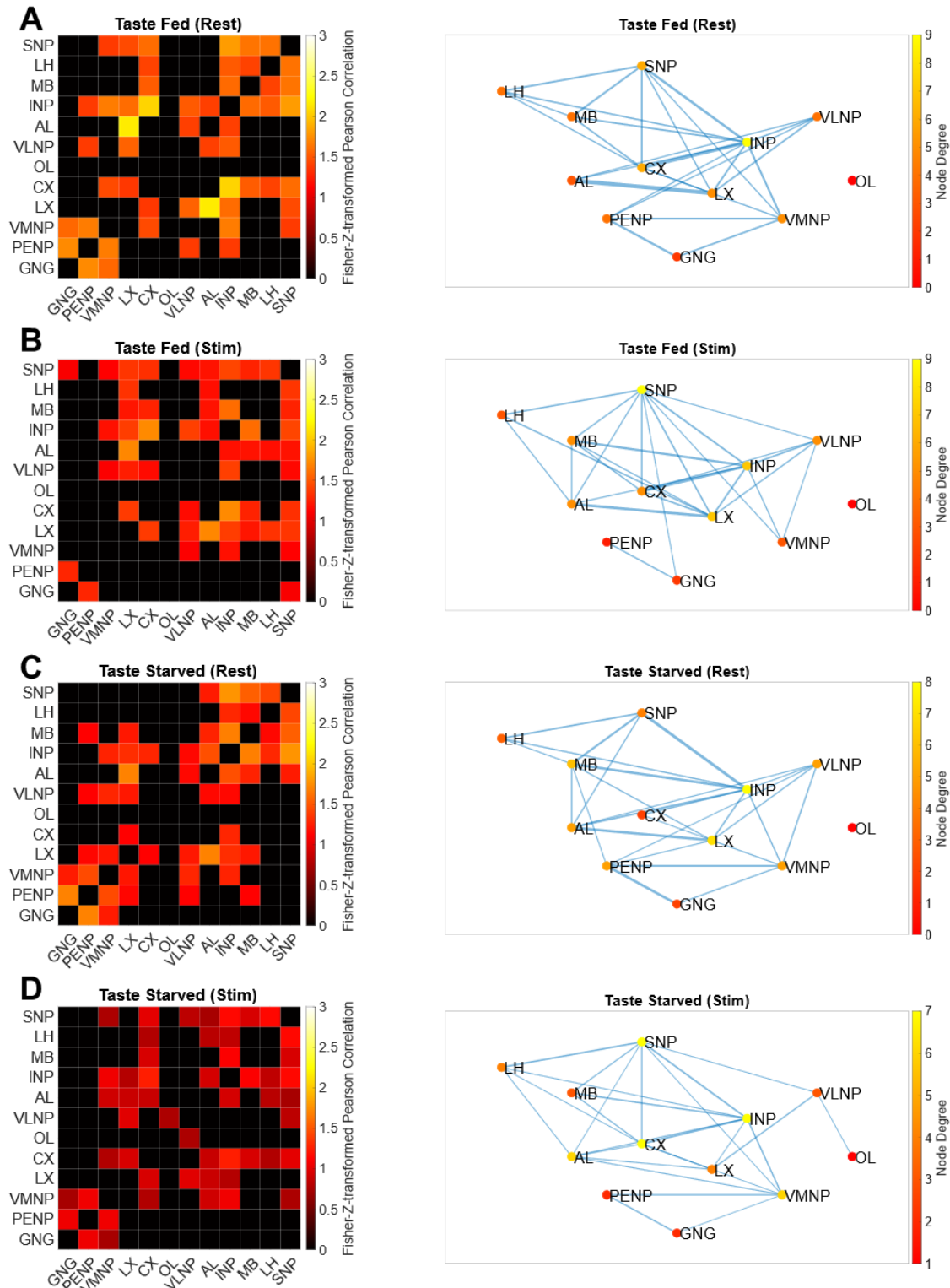


Figure A34: Brain-wide correlation before and during taste stimulation

Adjacency matrix and resulting graph of the activity correlation for the fed group during (A) resting and (B) stimulus phase. Adjacency matrix and resulting graph of the activity correlation for the starved group during (C) resting and (D) stimulus phase. The resting phase was defined as the first 25 seconds of every recording before the first stimulus was applied. The stimulus phase was defined as the first 15 seconds after the onset of the first stimulus. Correlation was thresholded proportionally to retain only 40 percent of the strongest connections. The width of the edges (blue lines) scales proportionally with weight of the connection between the nodes.

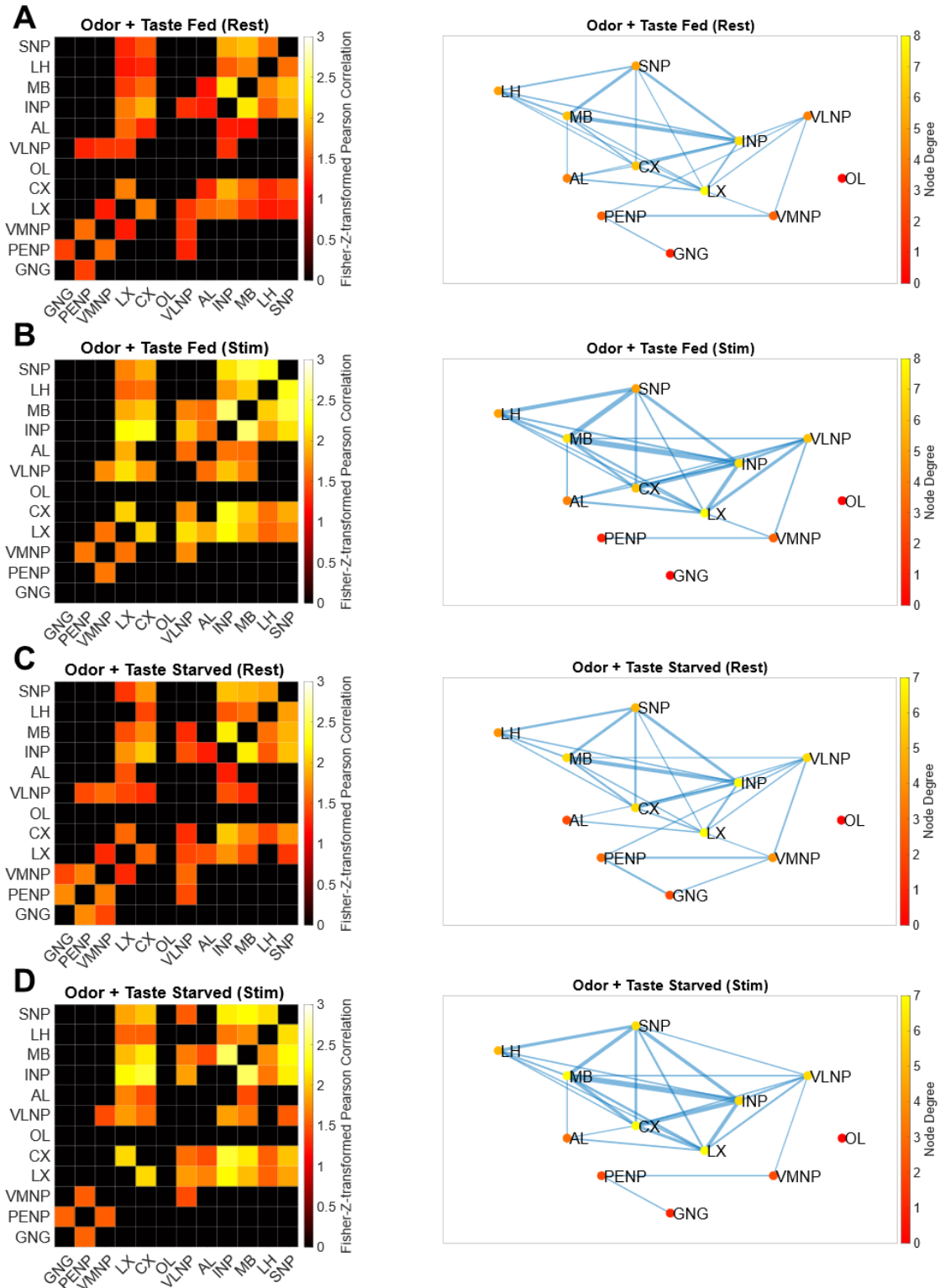


Figure A35: Brain-wide correlation before and during multisensory stimulation

Adjacency matrix and resulting graph of the activity correlation for the fed group during (A) resting and (B) stimulus phase. Adjacency matrix and resulting graph of the activity correlation for the starved group during (C) resting and (D) stimulus phase. The resting phase was defined as the first 25 seconds of every recording before the first stimulus was applied. The stimulus phase was defined as the first 15 seconds after the onset of the first stimulus. Correlation was thresholded proportionally to retain only 40 percent of the strongest connections. The width of the edges (blue lines) scales proportionally with weight of the connection between the nodes.

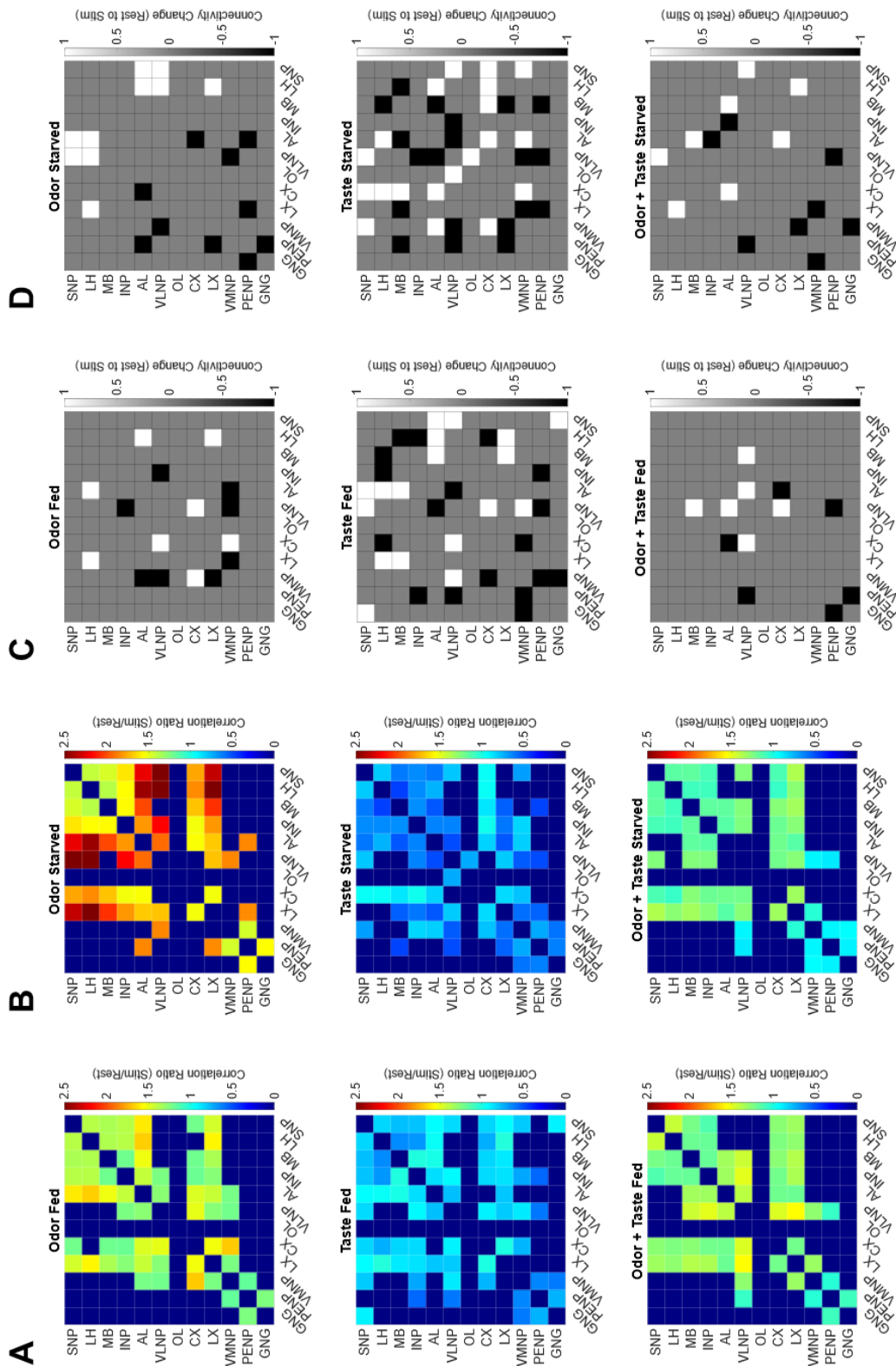


Figure A36: Correlation ratio and connectivity change between rest and stimulus phase

A Correlation ratio matrices for the fed groups. B Correlation ratio matrices for the starved groups. Correlation ratio was calculated by dividing the correlation during stim with the correlation during rest. Correlation was thresholded proportionally to retain only 40 percent of the strongest connections. C Connectivity matrices for the fed groups. D Connectivity matrices for the starved groups. Connectivity change was calculated by subtracting the binary connectivity during rest from the binary connectivity during stim.

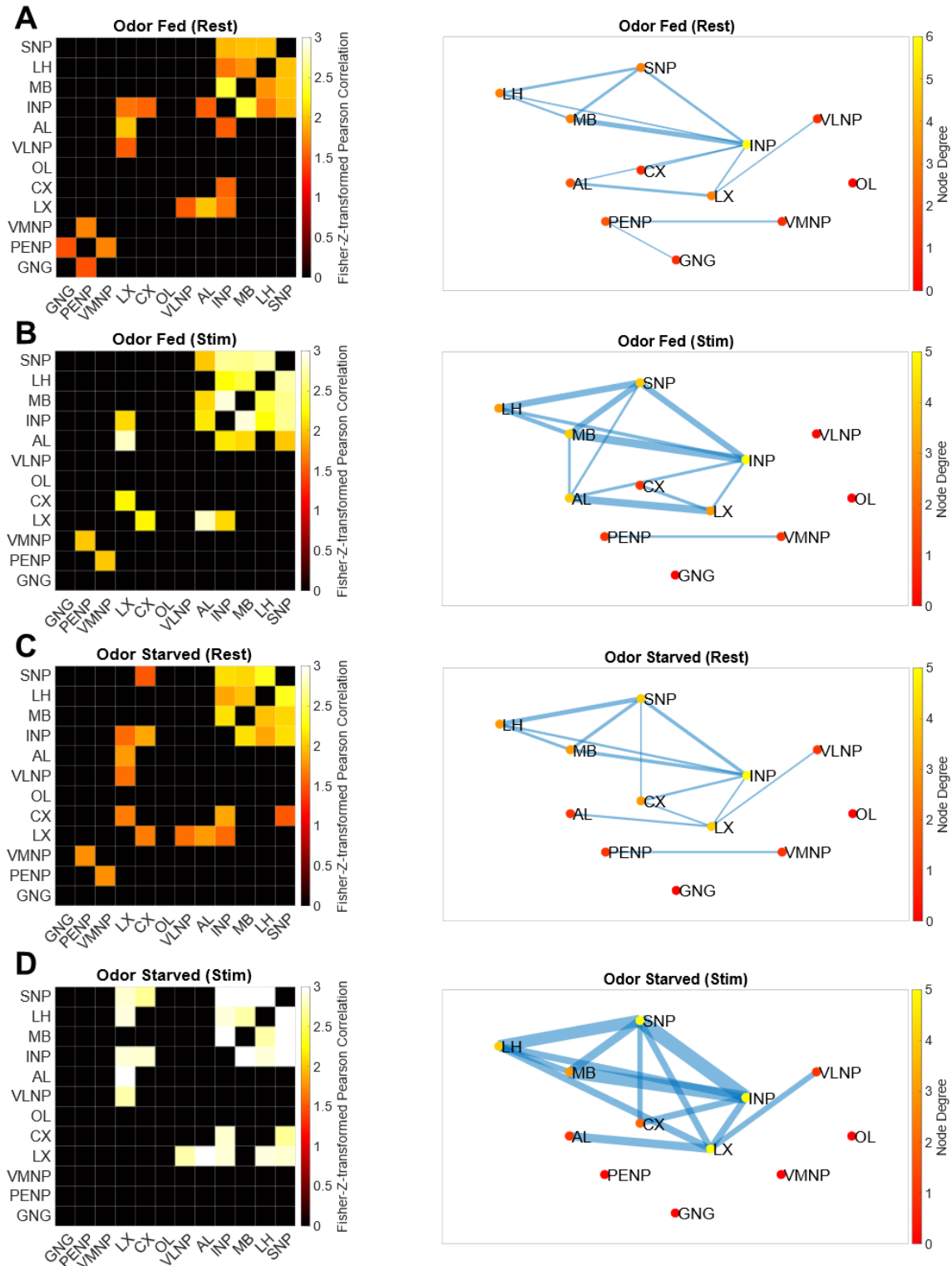


Figure A37: Brain-wide correlation before and during odor stimulation (20 percent threshold)

Adjacency matrix and resulting graph of the activity correlation for the fed group during (A) resting and (B) stimulus phase. Adjacency matrix and resulting graph of the activity correlation for the starved group during (C) resting and (D) stimulus phase. The resting phase was defined as the first 25 seconds of every recording before the first stimulus was applied. The stimulus phase was defined as the first 15 seconds after the onset of the first stimulus. Correlation was thresholded proportionally to retain only 20 percent of the strongest connections. The width of the edges (blue lines) scales proportionally with weight of the connection between the nodes.

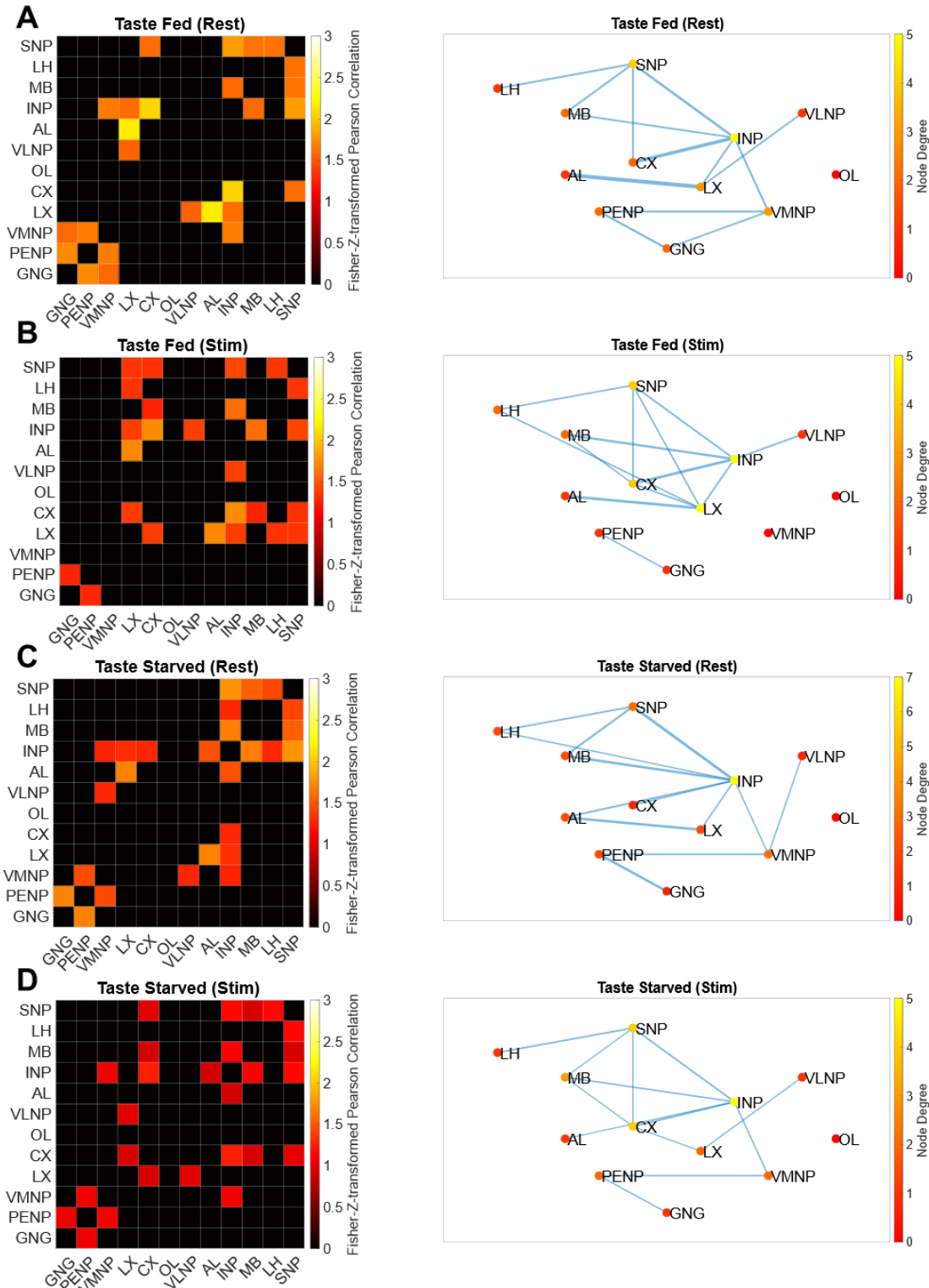


Figure A38: Brain-wide correlation before and during taste stimulation (20 percent threshold)
 Adjacency matrix and resulting graph of the activity correlation for the fed group during (A) resting and (B) stimulus phase. Adjacency matrix and resulting graph of the activity correlation for the starved group during (C) resting and (D) stimulus phase. The resting phase was defined as the first 25 seconds of every recording before the first stimulus was applied. The stimulus phase was defined as the first 15 seconds after the onset of the first stimulus. Correlation was thresholded proportionally to retain only 20 percent of the strongest connections. The width of the edges (blue lines) scales proportionally with weight of the connection between the nodes.

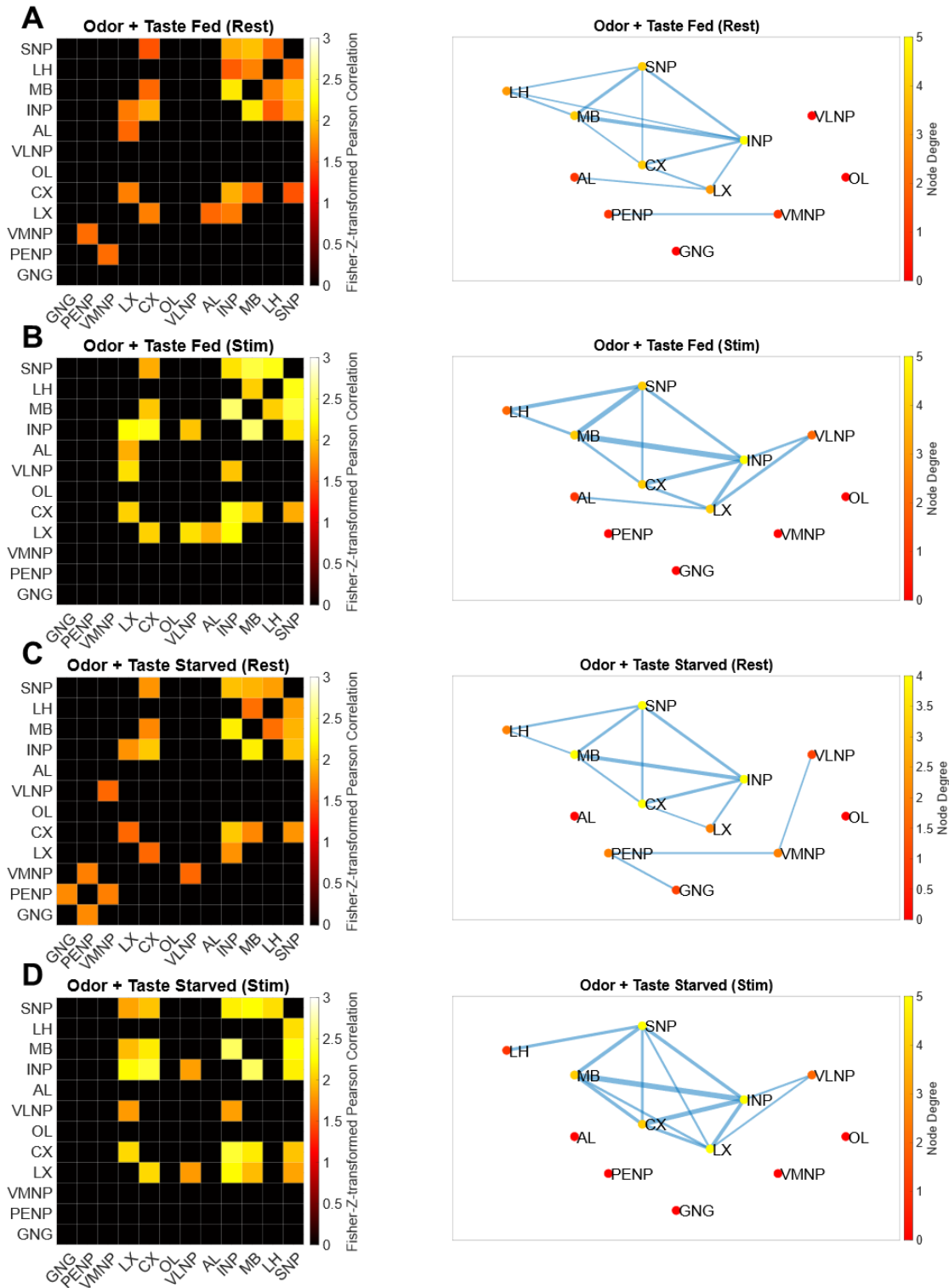


Figure A39 Brain-wide correlation before and during multisensory stimulation (20 percent threshold)

Adjacency matrix and resulting graph of the activity correlation for the fed group during (A) resting and (B) stimulus phase. Adjacency matrix and resulting graph of the activity correlation for the starved group during (C) resting and (D) stimulus phase. The resting phase was defined as the first 25 seconds of every recording before the first stimulus was applied. The stimulus phase was defined as the first 15 seconds after the onset of the first stimulus. Correlation was thresholded proportionally to retain only 20 percent of the strongest connections. The width of the edges (blue lines) scales proportionally with weight of the connection between the nodes.

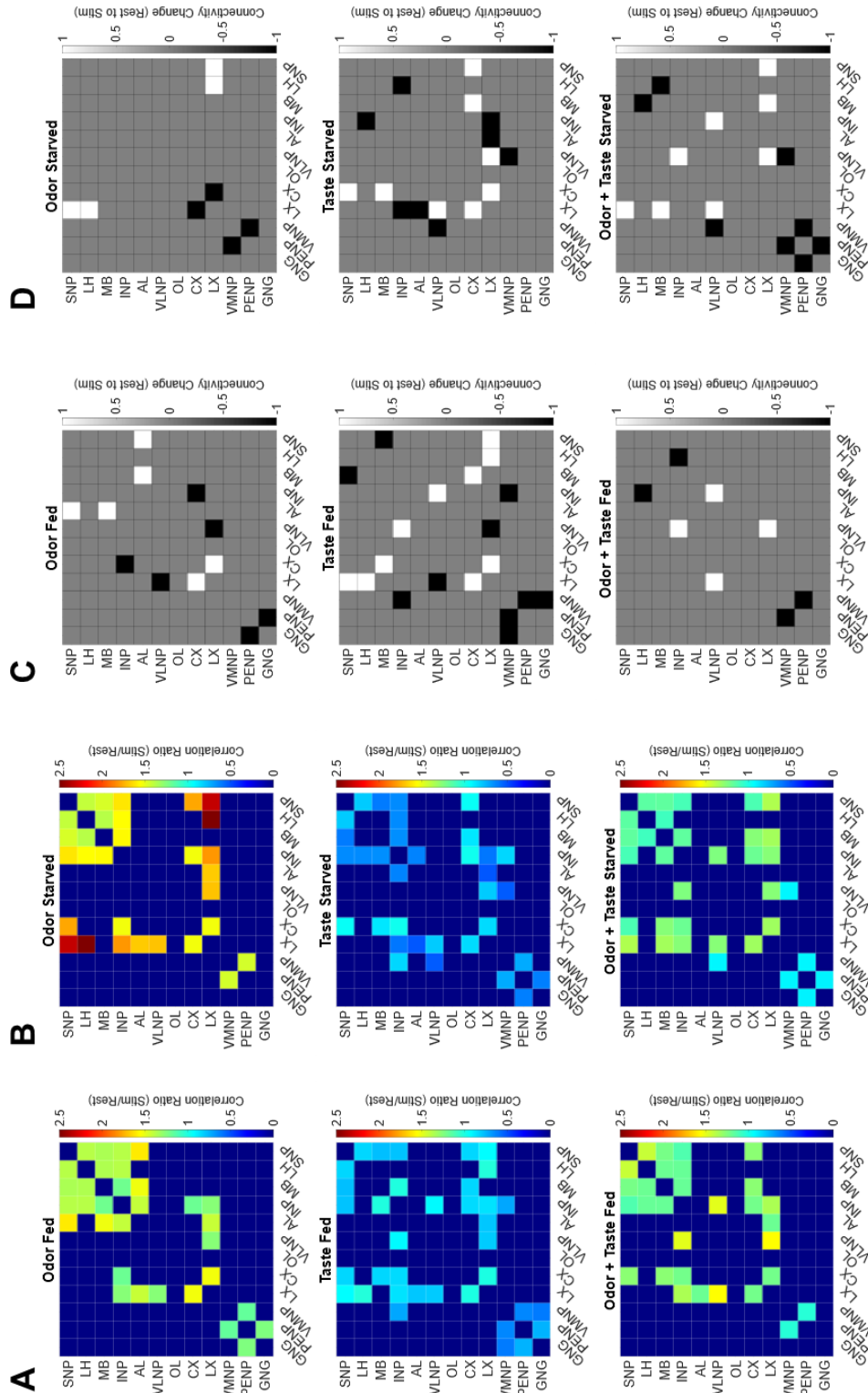


Figure A40: Correlation ratio and connectivity change between rest and stimulus phase (20 percent threshold)

A Correlation ratio matrices for the fed groups. B Correlation ratio matrices for the starved groups. Correlation ratio was calculated by dividing the correlation during stim with the correlation during rest. Correlation was thresholded proportionally to retain only 20 percent of the strongest connections. C Connectivity matrices for the fed groups. D Connectivity matrices for the starved groups. Connectivity change was calculated by subtracting the binary connectivity during rest from the binary connectivity during stim.

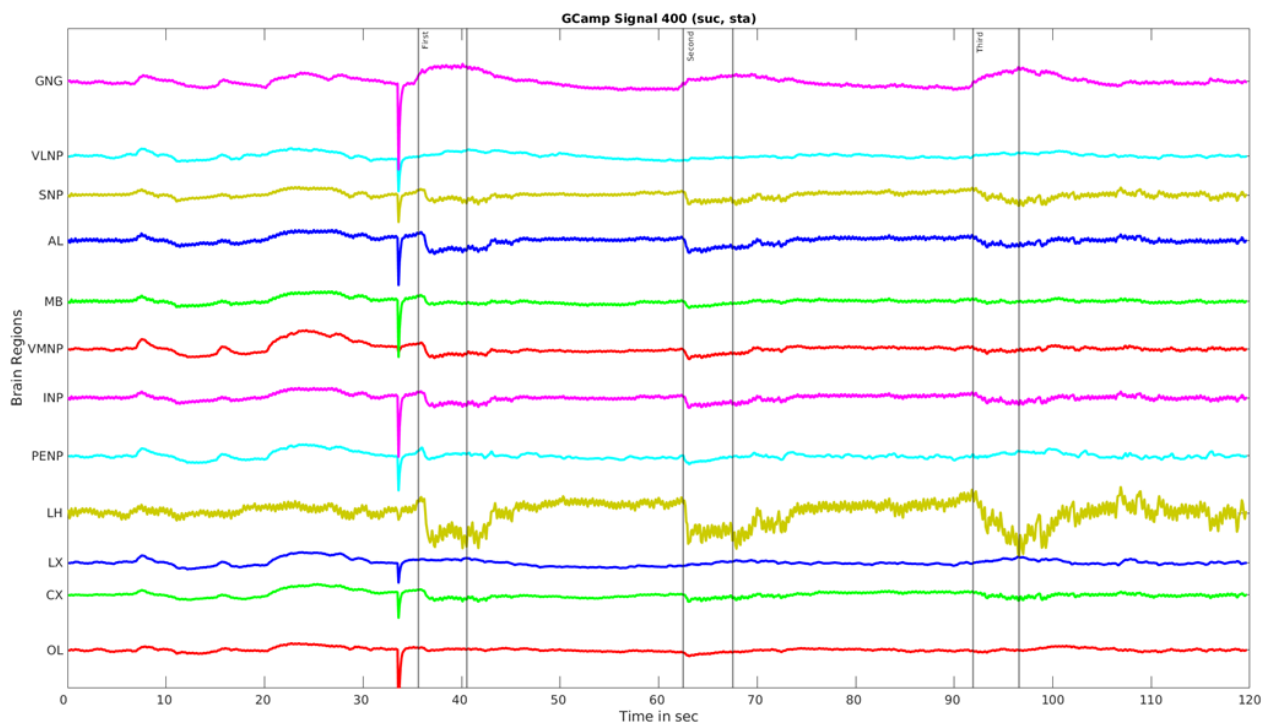
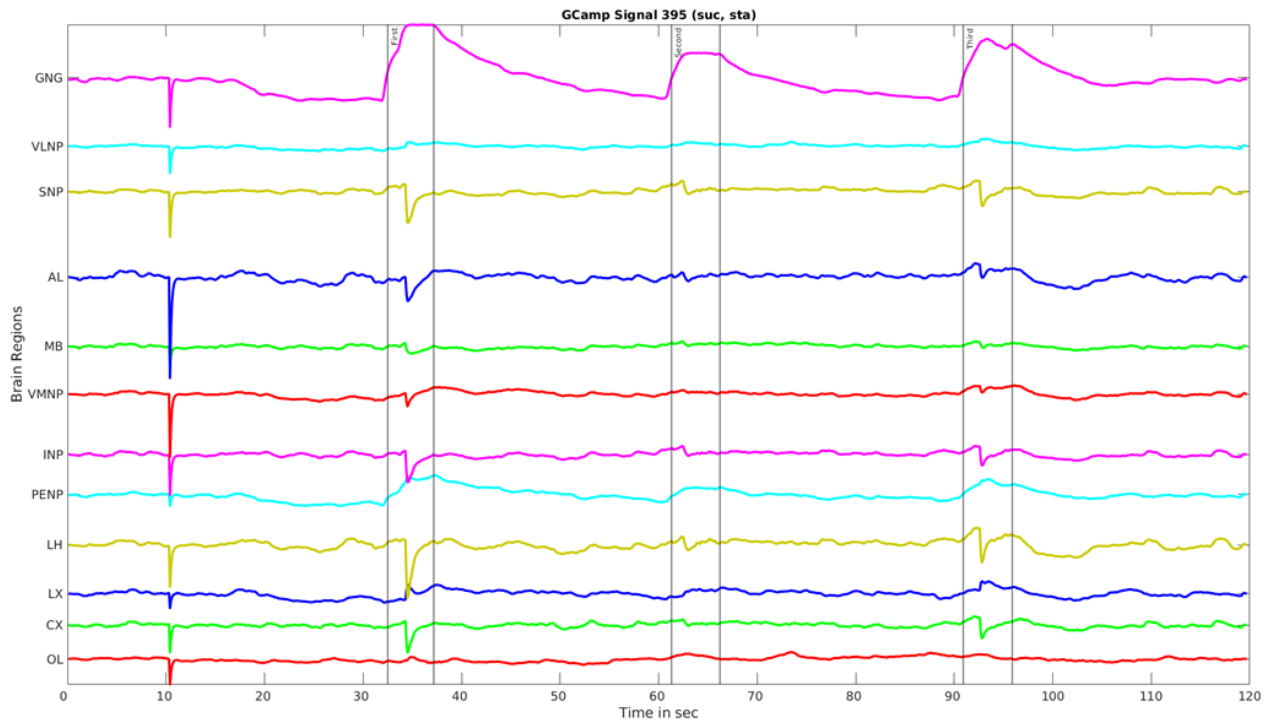


Figure A41: Two atypical recordings, from two starved flies, stimulated with sucrose

A Time series data for recording 395. Framerate artifact at 11 sec. Still included because of good GNG response, even though there are negative peaks in other regions. B Time series data for recording 400. Framerate artifact at 33 sec. Still included because of good GNG response. Appears small because it is shown relative to the maximum, which is the artifact in this case. Black vertical lines indicate on and offset of the stimulus.

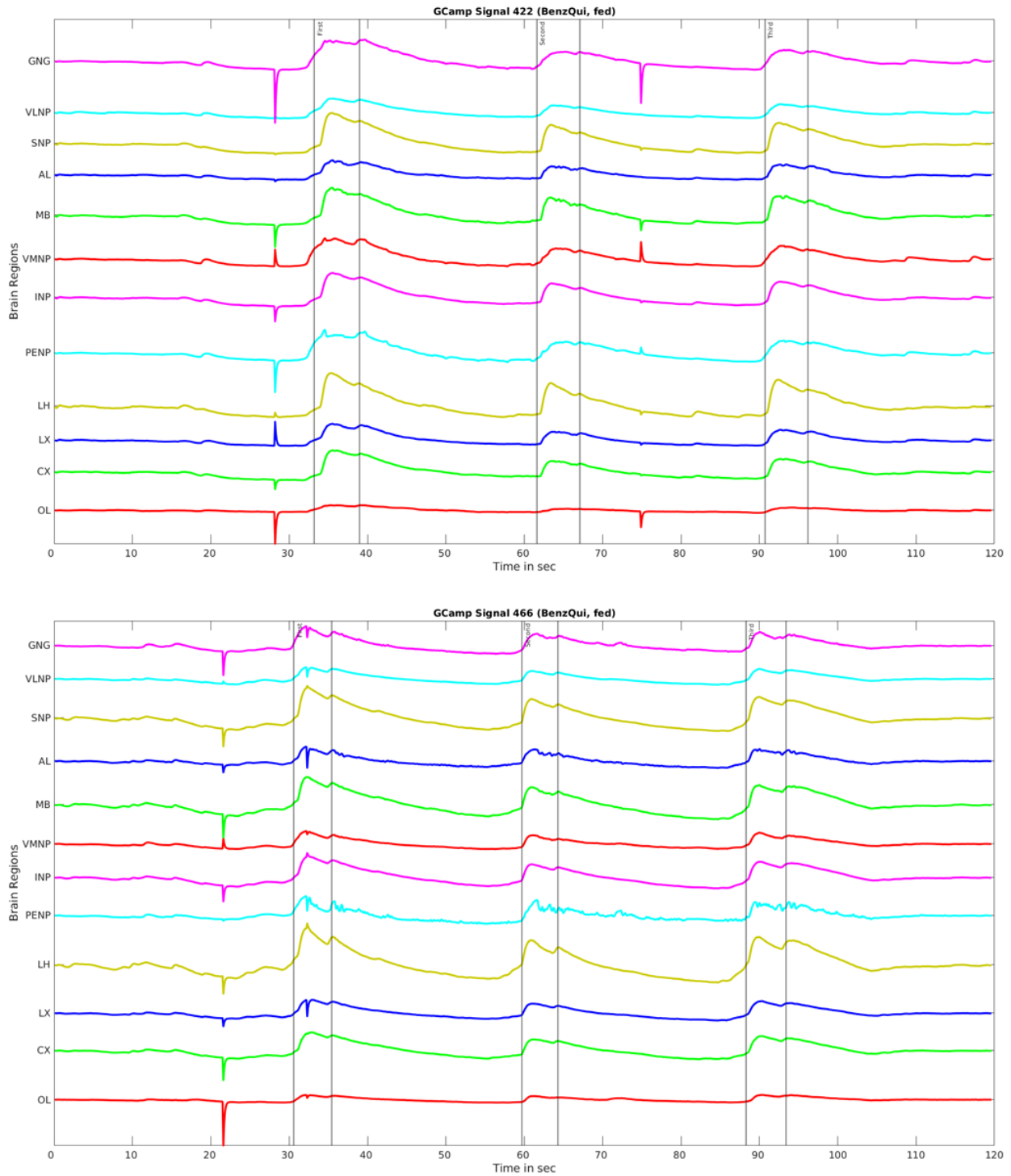


Figure A42: Two atypical recordings, from two fed flies, stimulated with benzaldehyde and quinine

A Time series data for recording 422. Framerate artifact at 28 and 75 sec. Still included because of good responses. B Time series data for recording 466. Frame rate artifact at 21 and 32 sec. Still included because of good response at second and third trial. Black vertical lines indicate on and offset of the stimulus.

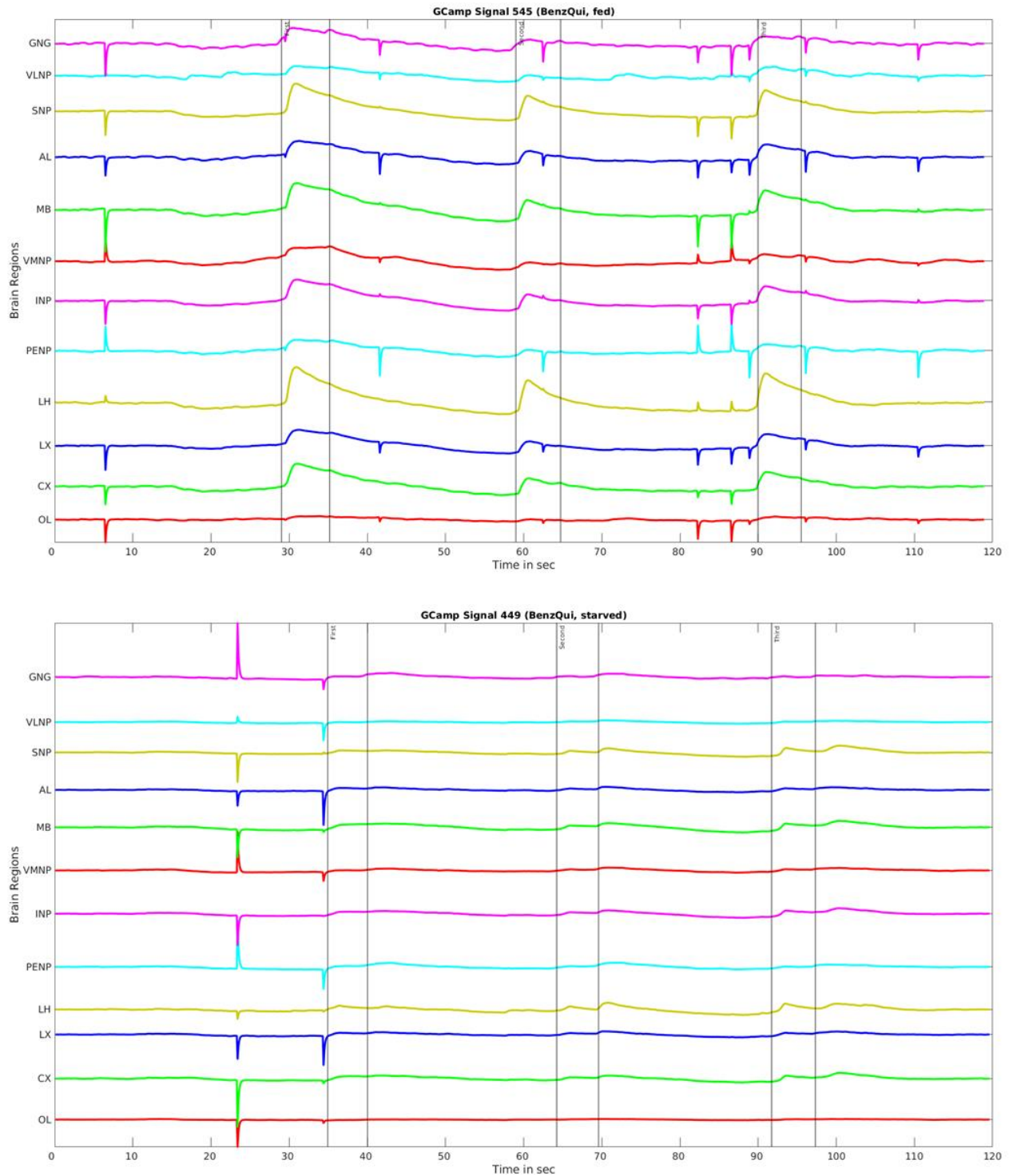


Figure A43: Two atypical recordings, from two flies, stimulated with benzaldehyde and quinine
 A Time series data for recording 545 (fed). Multiple framerate artifacts. Still included because of good responses. B Time series data for recording 449 (starved). Frame rate artifact at 23 and 34 sec. Still included because of good responses. Appear small because they are shown relative to the maximum, which is the artifact in this case. Black vertical lines indicate on and offset of the stimulus.

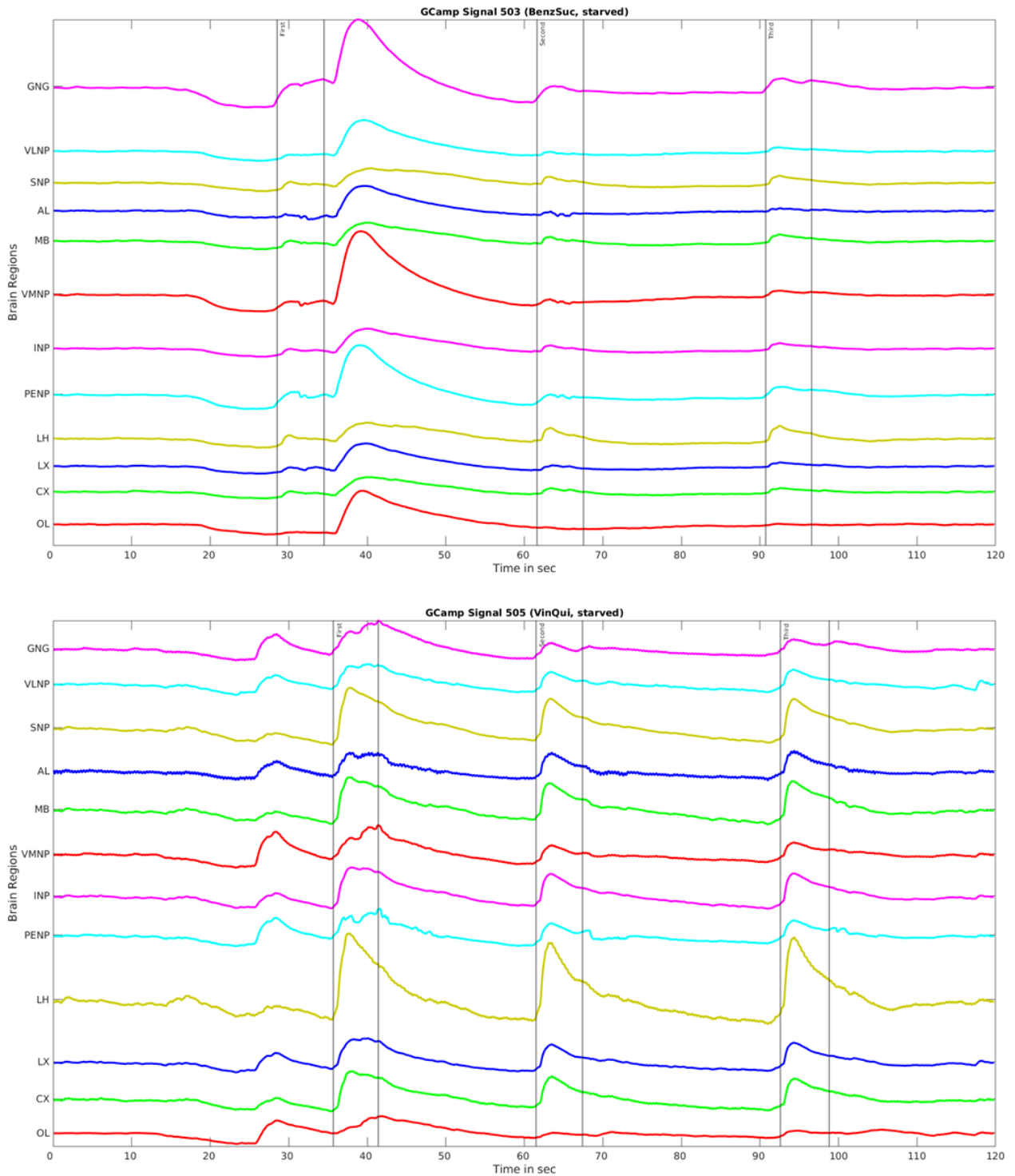


Figure A44: Two atypical recordings, from the same starved fly

A Time series data for recording 503 (benzaldehyde + sucrose). Strong signal, peaking at 39 sec. Included, because outside the stimulus time. B Time series data for recording 505 (vinegar + quinine). Strong signal, peaking at 29 sec. Included, because outside the stimulus time. Both show good responses to the stimulus. The unspecific response shows activation of the OL therefore it might be caused by a visual stimulus. Black vertical lines indicate on and offset of the stimulus.

List of appendix tables

Table A1	3-way ANOVA on odor responses	176
Table A2	3-way ANOVA on taste responses	176
Table A3	3-way ANOVA on multisensory responses in fed flies	177
Table A4	3-way ANOVA on multisensory responses in starved flies	177
Table A5	Results of 3-way ANOVA with multiple comparison on peak odor responses	178-180
Table A6	Results of 3-way ANOVA with multiple comparison on peak taste responses	180-182
Table A7	Results of 3-way ANOVA with multiple comparison on peak multisensory responses in fed flies	182-184
Table A8	Results of 3-way ANOVA with multiple comparison on peak multisensory responses in starved flies	184-186
Table A9	Functional components and neurons with similar morphology	187-188

Table A4 3-way ANOVA on odor responses

ANOVA table	SS	DF	MS	F (DFn, DFd)
Region	0,9575	11	0,08704	F (11, 209) = 145,0
Vinegar v Benz	0,01178	1	0,01178	F (1, 19) = 3,945
Fed v Starved	0,04272	1	0,04272	F (1, 19) = 5,107
Region x Vinegar v Benz	0,005821	11	0,0005292	F (11, 209) = 3,139
Region x Fed v Starved	0,01278	11	0,001162	F (11, 209) = 1,936
Vinegar v Benz x Fed v Starved	0,01291	1	0,01291	F (1, 19) = 4,325
Region x Vinegar v Benz x Fed v Starved	0,002152	11	0,0001956	F (11, 209) = 1,160
Subject	0,1589	19	0,008366	
Subject x Region	0,1254	209	0,0006002	
Subject x Vinegar v Benz	0,05673	19	0,002986	
Residual	0,03524	209	0,0001686	

Table A5 3-way ANOVA on taste responses

ANOVA table	SS	DF	MS	F (DFn, DFd)
Region	0,04968	11	0,004516	F (11, 198) = 50,14
Sucrose vs Quinine	0,0002302	1	0,0002302	F (1, 18) = 0,2117
Fed vs Starved	0,002625	1	0,002625	F (1, 18) = 1,426
Region x Sucrose vs Quinine	0,002957	11	0,0002688	F (11, 198) = 5,733
Region x Fed vs Starved	0,001759	11	0,0001599	F (11, 198) = 1,776
Sucrose vs Quinine x Fed vs Starved	0,003481	1	0,003481	F (1, 18) = 3,201
Region x Sucrose vs Quinine x Fed vs Starved	0,001863	11	0,0001694	F (11, 198) = 3,614
Subject	0,03313	18	0,001841	
Subject x Region	0,01783	198	9,006e-005	
Subject x Sucrose vs Quinine	0,01958	18	0,001088	
Residual	0,009282	198	4,688e-005	

Table A6 3-way ANOVA on multisensory responses in fed flies

ANOVA table	SS	DF	MS	F (DFn, DFd)
Region	0,2160	11	0,01964	F (11, 209) = 95,69
Matching vs Conflicting	0,04131	1	0,04131	F (1, 19) = 8,395
Vinegar v Benzaldehyde	0,01589	1	0,01589	F (1, 19) = 6,562
Region x Matching vs Conflicting	0,01256	11	0,001142	F (11, 209) = 5,564
Region x Vinegar v Benzaldehyde	0,002019	11	0,0001836	F (11, 209) = 1,925
Matching vs Conflicting x Vinegar v Benzaldehyde	0,008966	1	0,008966	F (1, 19) = 3,702
Region x Matching vs Conflicting x Vinegar v Benzaldehyde	0,001724	11	0,0001568	F (11, 209) = 1,644
Subject	0,09350	19	0,004921	
Subject x Region	0,04289	209	0,0002052	
Subject x Vinegar v Benzaldehyde	0,04601	19	0,002422	
Residual	0,01993	209	9,535e-005	

Table A7 3-way ANOVA on multisensory responses in starved flies

ANOVA table	SS	DF	MS	F (DFn, DFd)
Region	0,1884	11	0,01712	F (11, 198) = 65,88
Matching v Conflicting	0,004981	1	0,004981	F (1, 18) = 1,061
Vinegar v Benzaldehyde	0,02606	1	0,02606	F (1, 18) = 9,664
Region x Matching v Conflicting	0,0005615	11	5,105e-005	F (11, 198) = 0,1964
Region x Vinegar v Benzaldehyde	0,008309	11	0,0007554	F (11, 198) = 3,870
Matching v Conflicting x Vinegar v Benzaldehyde	0,002294	1	0,002294	F (1, 18) = 0,8508
Region x Matching v Conflicting x Vinegar v Benzaldehyde	0,002992	11	0,0002720	F (11, 198) = 1,394
Subject	0,08452	18	0,004696	
Subject x Region	0,05146	198	0,0002599	
Subject x Vinegar v Benzaldehyde	0,04854	18	0,002697	
Residual	0,03865	198	0,0001952	

Table A8 Results of 3-way ANOVA with multiple comparison on peak odor responses

Tukey's multiple comparisons test	Predicted (LS) mean diff,	95,00% CI of diff,	Summary	Adjusted P Value
OL:Vin Fed vs. OL:Vin Starved	-0,007924	-0,05816 to 0,04231	ns	>0,9999
OL:Vin Fed vs. OL:Benz Fed	0,0002865	-0,03423 to 0,03481	ns	>0,9999
OL:Vin Fed vs. OL:Benz Starved	-0,0005519	-0,05079 to 0,04969	ns	>0,9999
OL:Vin Starved vs. OL:Benz Fed	0,008210	-0,04203 to 0,05845	ns	>0,9999
OL:Vin Starved vs. OL:Benz Starved	0,007372	-0,02883 to 0,04358	ns	>0,9999
OL:Benz Fed vs. OL:Benz Starved	-0,0008384	-0,05108 to 0,04940	ns	>0,9999
CX:Vin Fed vs. CX:Vin Starved	-0,02430	-0,07454 to 0,02593	ns	0,9993
CX:Vin Fed vs. CX:Benz Fed	0,003473	-0,03105 to 0,03799	ns	>0,9999
CX:Vin Fed vs. CX:Benz Starved	-0,009458	-0,05969 to 0,04078	ns	>0,9999
CX:Vin Starved vs. CX:Benz Fed	0,02778	-0,02246 to 0,07801	ns	0,9895
CX:Vin Starved vs. CX:Benz Starved	0,01485	-0,02136 to 0,05105	ns	>0,9999
CX:Benz Fed vs. CX:Benz Starved	-0,01293	-0,06317 to 0,03731	ns	>0,9999
LX:Vin Fed vs. LX:Vin Starved	-0,02691	-0,07715 to 0,02333	ns	0,9941
LX:Vin Fed vs. LX:Benz Fed	-0,003765	-0,03828 to 0,03075	ns	>0,9999
LX:Vin Fed vs. LX:Benz Starved	-0,01257	-0,06281 to 0,03767	ns	>0,9999
LX:Vin Starved vs. LX:Benz Fed	0,02314	-0,02709 to 0,07338	ns	0,9998
LX:Vin Starved vs. LX:Benz Starved	0,01434	-0,02186 to 0,05054	ns	>0,9999
LX:Benz Fed vs. LX:Benz Starved	-0,008804	-0,05904 to 0,04143	ns	>0,9999
LH:Vin Fed vs. LH:Vin Starved	-0,02941	-0,07965 to 0,02083	ns	0,9733
LH:Vin Fed vs. LH:Benz Fed	0,003778	-0,03074 to 0,03830	ns	>0,9999
LH:Vin Fed vs. LH:Benz Starved	0,007132	-0,04310 to 0,05737	ns	>0,9999
LH:Vin Starved vs. LH:Benz Fed	0,03319	-0,01705 to 0,08342	ns	0,8697
LH:Vin Starved vs. LH:Benz Starved	0,03654	0,0003370 to 0,07275	*	0,0441
LH:Benz Fed vs. LH:Benz Starved	0,003355	-0,04688 to 0,05359	ns	>0,9999
PENP:Vin Fed vs. PENP:Vin Starved	-0,02495	-0,07519 to 0,02528	ns	0,9987
PENP:Vin Fed vs. PENP:Benz Fed	-0,004295	-0,03881 to 0,03022	ns	>0,9999
PENP:Vin Fed vs. PENP:Benz Starved	-0,009930	-0,06017 to 0,04031	ns	>0,9999
PENP:Vin Starved vs. PENP:Benz Fed	0,02066	-0,02958 to 0,07090	ns	>0,9999
PENP:Vin Starved vs. PENP:Benz Starved	0,01503	-0,02118 to 0,05123	ns	>0,9999
PENP:Benz Fed vs. PENP:Benz Starved	-0,005635	-0,05587 to 0,04460	ns	>0,9999
INP:Vin Fed vs. INP:Vin Starved	-0,03900	-0,08923 to 0,01124	ns	0,5181
INP:Vin Fed vs. INP:Benz Fed	-0,001131	-0,03565 to 0,03339	ns	>0,9999

INP:Vin Fed vs. INP:Benz Starved	-0,01379	-0,06403 to 0,03645	ns	>0,9999
INP:Vin Starved vs. INP:Benz Fed	0,03786	-0,01237 to 0,08810	ns	0,5957
INP:Vin Starved vs. INP:Benz Starved	0,02520	-0,01100 to 0,06141	ns	0,7629
INP:Benz Fed vs. INP:Benz Starved	-0,01266	-0,06290 to 0,03758	ns	>0,9999
VMNP:Vin Fed vs. VMNP:Vin Starved	-0,01920	-0,06944 to 0,03104	ns	>0,9999
VMNP:Vin Fed vs. VMNP:Benz Fed	-0,002965	-0,03748 to 0,03155	ns	>0,9999
VMNP:Vin Fed vs. VMNP:Benz Starved	-0,003554	-0,05379 to 0,04668	ns	>0,9999
VMNP:Vin Starved vs. VMNP:Benz Fed	0,01623	-0,03400 to 0,06647	ns	>0,9999
VMNP:Vin Starved vs. VMNP:Benz Starved	0,01564	-0,02056 to 0,05185	ns	>0,9999
VMNP:Benz Fed vs. VMNP:Benz Starved	-0,0005895	-0,05083 to 0,04965	ns	>0,9999
MB:Vin Fed vs. MB:Vin Starved	-0,05330	-0,1035 to -0,003067	*	0,0206
MB:Vin Fed vs. MB:Benz Fed	-0,001972	-0,03649 to 0,03255	ns	>0,9999
MB:Vin Fed vs. MB:Benz Starved	-0,02185	-0,07208 to 0,02839	ns	>0,9999
MB:Vin Starved vs. MB:Benz Fed	0,05133	0,001095 to 0,1016	*	0,0368
MB:Vin Starved vs. MB:Benz Starved	0,03146	-0,004749 to 0,06766	ns	0,2327
MB:Benz Fed vs. MB:Benz Starved	-0,01988	-0,07011 to 0,03036	ns	>0,9999
AL:Vin Fed vs. AL:Vin Starved	-0,02144	-0,07167 to 0,02880	ns	>0,9999
AL:Vin Fed vs. AL:Benz Fed	-0,005999	-0,04052 to 0,02852	ns	>0,9999
AL:Vin Fed vs. AL:Benz Starved	-0,009695	-0,05993 to 0,04054	ns	>0,9999
AL:Vin Starved vs. AL:Benz Fed	0,01544	-0,03480 to 0,06568	ns	>0,9999
AL:Vin Starved vs. AL:Benz Starved	0,01174	-0,02446 to 0,04795	ns	>0,9999
AL:Benz Fed vs. AL:Benz Starved	-0,003696	-0,05393 to 0,04654	ns	>0,9999
SNP:Vin Fed vs. SNP:Vin Starved	-0,05448	-0,1047 to -0,004242	*	0,0143
SNP:Vin Fed vs. SNP:Benz Fed	0,01034	-0,02418 to 0,04486	ns	>0,9999
SNP:Vin Fed vs. SNP:Benz Starved	-0,01398	-0,06422 to 0,03625	ns	>0,9999
SNP:Vin Starved vs. SNP:Benz Fed	0,06482	0,01458 to 0,1151	***	0,0004
SNP:Vin Starved vs. SNP:Benz Starved	0,04049	0,004291 to 0,07670	**	0,0087
SNP:Benz Fed vs. SNP:Benz Starved	-0,02432	-0,07456 to 0,02592	ns	0,9993
VLNP:Vin Fed vs. VLNP:Vin Starved	-0,01729	-0,06753 to 0,03294	ns	>0,9999
VLNP:Vin Fed vs. VLNP:Benz Fed	-0,001153	-0,03567 to 0,03337	ns	>0,9999
VLNP:Vin Fed vs. VLNP:Benz Starved	-0,007079	-0,05732 to 0,04316	ns	>0,9999
VLNP:Vin Starved vs. VLNP:Benz Fed	0,01614	-0,03410 to 0,06638	ns	>0,9999
VLNP:Vin Starved vs. VLNP:Benz Starved	0,01021	-0,02599 to 0,04642	ns	>0,9999
VLNP:Benz Fed vs. VLNP:Benz Starved	-0,005925	-0,05616 to 0,04431	ns	>0,9999
GNG:Vin Fed vs. GNG:Vin Starved	-0,02464	-0,07488 to 0,02560	ns	0,9990

GNG:Vin Fed vs. GNG:Benz Fed	-0,002059	-0,03658 to 0,03246	ns	>0,9999
GNG:Vin Fed vs. GNG:Benz Starved	-0,009734	-0,05997 to 0,04050	ns	>0,9999
GNG:Vin Starved vs. GNG:Benz Fed	0,02258	-0,02765 to 0,07282	ns	0,9999
GNG:Vin Starved vs. GNG:Benz Starved	0,01491	-0,02130 to 0,05111	ns	>0,9999
GNG:Benz Fed vs. GNG:Benz Starved	-0,007675	-0,05791 to 0,04256	ns	>0,9999

Table A9 Results of 3-way ANOVA with multiple comparison on peak taste responses

Tukey's multiple comparisons test	Mean Diff,	95,00% CI of diff,	Summary	Adjusted P Value
OL:Sucrose Fed vs. OL:Sucrose Starved	-0,002689	-0,02703 to 0,02165	ns	>0,9999
OL:Sucrose Fed vs. OL:Quinine Fed	-0,003143	-0,02400 to 0,01771	ns	>0,9999
OL:Sucrose Fed vs. OL:Quinine Starved	-1,509e-005	-0,02435 to 0,02432	ns	>0,9999
OL:Sucrose Starved vs. OL:Quinine Fed	-0,0004536	-0,02479 to 0,02389	ns	>0,9999
OL:Sucrose Starved vs. OL:Quinine Starved	0,002674	-0,01818 to 0,02353	ns	>0,9999
OL:Quinine Fed vs. OL:Quinine Starved	0,003128	-0,02121 to 0,02747	ns	>0,9999
CX:Sucrose Fed vs. CX:Sucrose Starved	0,003847	-0,02049 to 0,02819	ns	>0,9999
CX:Sucrose Fed vs. CX:Quinine Fed	-0,004842	-0,02569 to 0,01601	ns	>0,9999
CX:Sucrose Fed vs. CX:Quinine Starved	0,005750	-0,01859 to 0,03009	ns	>0,9999
CX:Sucrose Starved vs. CX:Quinine Fed	-0,008689	-0,03303 to 0,01565	ns	>0,9999
CX:Sucrose Starved vs. CX:Quinine Starved	0,001903	-0,01895 to 0,02276	ns	>0,9999
CX:Quinine Fed vs. CX:Quinine Starved	0,01059	-0,01375 to 0,03493	ns	>0,9999
LX:Sucrose Fed vs. LX:Sucrose Starved	0,0003581	-0,02398 to 0,02470	ns	>0,9999
LX:Sucrose Fed vs. LX:Quinine Fed	-0,01267	-0,03353 to 0,008179	ns	0,9446
LX:Sucrose Fed vs. LX:Quinine Starved	0,0004189	-0,02392 to 0,02476	ns	>0,9999
LX:Sucrose Starved vs. LX:Quinine Fed	-0,01303	-0,03737 to 0,01131	ns	0,9941
LX:Sucrose Starved vs. LX:Quinine Starved	6,078e-005	-0,02079 to 0,02091	ns	>0,9999
LX:Quinine Fed vs. LX:Quinine Starved	0,01309	-0,01125 to 0,03743	ns	0,9935
LH:Sucrose Fed vs. LH:Sucrose Starved	-0,003949	-0,02829 to 0,02039	ns	>0,9999
LH:Sucrose Fed vs. LH:Quinine Fed	7,226e-005	-0,02078 to 0,02093	ns	>0,9999
LH:Sucrose Fed vs. LH:Quinine Starved	-0,005072	-0,02941 to 0,01927	ns	>0,9999
LH:Sucrose Starved vs. LH:Quinine Fed	0,004021	-0,02032 to 0,02836	ns	>0,9999
LH:Sucrose Starved vs. LH:Quinine Starved	-0,001123	-0,02198 to 0,01973	ns	>0,9999
LH:Quinine Fed vs. LH:Quinine Starved	-0,005144	-0,02948 to 0,01920	ns	>0,9999
PENP:Sucrose Fed vs. PENP:Sucrose Starved	-0,001507	-0,02585 to 0,02283	ns	>0,9999

PENP:Sucrose Fed vs. PENP:Quinine Fed	-0,008591	-0,02944 to 0,01226	ns	>0,9999
PENP:Sucrose Fed vs. PENP:Quinine Starved	0,009898	-0,01444 to 0,03424	ns	>0,9999
PENP:Sucrose Starved vs. PENP:Quinine Fed	-0,007084	-0,03142 to 0,01726	ns	>0,9999
PENP:Sucrose Starved vs. PENP:Quinine Starved	0,01140	-0,009449 to 0,03226	ns	0,9886
PENP:Quinine Fed vs. PENP:Quinine Starved	0,01849	-0,005851 to 0,04283	ns	0,5745
INP:Sucrose Fed vs. INP:Sucrose Starved	0,001357	-0,02298 to 0,02570	ns	>0,9999
INP:Sucrose Fed vs. INP:Quinine Fed	-0,006630	-0,02748 to 0,01422	ns	>0,9999
INP:Sucrose Fed vs. INP:Quinine Starved	0,001287	-0,02305 to 0,02563	ns	>0,9999
INP:Sucrose Starved vs. INP:Quinine Fed	-0,007987	-0,03233 to 0,01635	ns	>0,9999
INP:Sucrose Starved vs. INP:Quinine Starved	-6,959e-005	-0,02092 to 0,02078	ns	>0,9999
INP:Quinine Fed vs. INP:Quinine Starved	0,007917	-0,01642 to 0,03226	ns	>0,9999
VMNP:Sucrose Fed vs. VMNP:Sucrose Starved	-0,002924	-0,02726 to 0,02142	ns	>0,9999
VMNP:Sucrose Fed vs. VMNP:Quinine Fed	-0,01742	-0,03828 to 0,003431	ns	0,3163
VMNP:Sucrose Fed vs. VMNP:Quinine Starved	0,002486	-0,02185 to 0,02682	ns	>0,9999
VMNP:Sucrose Starved vs. VMNP:Quinine Fed	-0,01450	-0,03884 to 0,009841	ns	0,9649
VMNP:Sucrose Starved vs. VMNP:Quinine Starved	0,005409	-0,01544 to 0,02626	ns	>0,9999
VMNP:Quinine Fed vs. VMNP:Quinine Starved	0,01991	-0,004432 to 0,04425	ns	0,3798
MB:Sucrose Fed vs. MB:Sucrose Starved	0,004533	-0,01981 to 0,02887	ns	>0,9999
MB:Sucrose Fed vs. MB:Quinine Fed	-0,004055	-0,02491 to 0,01680	ns	>0,9999
MB:Sucrose Fed vs. MB:Quinine Starved	0,004994	-0,01934 to 0,02933	ns	>0,9999
MB:Sucrose Starved vs. MB:Quinine Fed	-0,008588	-0,03293 to 0,01575	ns	>0,9999
MB:Sucrose Starved vs. MB:Quinine Starved	0,0004612	-0,02039 to 0,02131	ns	>0,9999
MB:Quinine Fed vs. MB:Quinine Starved	0,009049	-0,01529 to 0,03339	ns	>0,9999
AL:Sucrose Fed vs. AL:Sucrose Starved	-0,002094	-0,02643 to 0,02225	ns	>0,9999
AL:Sucrose Fed vs. AL:Quinine Fed	-0,01253	-0,03339 to 0,008320	ns	0,9523
AL:Sucrose Fed vs. AL:Quinine Starved	-0,002401	-0,02674 to 0,02194	ns	>0,9999
AL:Sucrose Starved vs. AL:Quinine Fed	-0,01044	-0,03478 to 0,01390	ns	>0,9999
AL:Sucrose Starved vs. AL:Quinine Starved	-0,0003072	-0,02116 to 0,02055	ns	>0,9999
AL:Quinine Fed vs. AL:Quinine Starved	0,01013	-0,01421 to 0,03447	ns	>0,9999
SNP:Sucrose Fed vs. SNP:Sucrose Starved	0,001141	-0,02320 to 0,02548	ns	>0,9999
SNP:Sucrose Fed vs. SNP:Quinine Fed	-0,004018	-0,02487 to 0,01684	ns	>0,9999
SNP:Sucrose Fed vs. SNP:Quinine Starved	0,001633	-0,02271 to 0,02597	ns	>0,9999

SNP:Sucrose Starved vs. SNP:Quinine Fed	-0,005158	-0,02950 to 0,01918	ns	>0,9999
SNP:Sucrose Starved vs. SNP:Quinine Starved	0,0004920	-0,02036 to 0,02135	ns	>0,9999
VLNP:Sucrose Fed vs. VLNP:Sucrose Starved	-0,002483	-0,02682 to 0,02186	ns	>0,9999
VLNP:Sucrose Fed vs. VLNP:Quinine Fed	-0,007555	-0,02841 to 0,01330	ns	>0,9999
VLNP:Sucrose Fed vs. VLNP:Quinine Starved	-0,001281	-0,02562 to 0,02306	ns	>0,9999
VLNP:Sucrose Starved vs. VLNP:Quinine Fed	-0,005072	-0,02941 to 0,01927	ns	>0,9999
VLNP:Sucrose Starved vs. VLNP:Quinine Starved	0,001202	-0,01965 to 0,02206	ns	>0,9999
VLNP:Quinine Fed vs. VLNP:Quinine Starved	0,006274	-0,01807 to 0,03061	ns	>0,9999
GNG:Sucrose Fed vs. GNG:Sucrose Starved	-0,004093	-0,02843 to 0,02025	ns	>0,9999
GNG:Sucrose Fed vs. GNG:Quinine Fed	0,0001362	-0,02072 to 0,02099	ns	>0,9999
GNG:Sucrose Fed vs. GNG:Quinine Starved	0,02181	-0,002530 to 0,04615	ns	0,1804
GNG:Sucrose Starved vs. GNG:Quinine Fed	0,004229	-0,02011 to 0,02857	ns	>0,9999
GNG:Sucrose Starved vs. GNG:Quinine Starved	0,02590	0,005049 to 0,04676	**	0,0011
GNG:Quinine Fed vs. GNG:Quinine Starved	0,02167	-0,002666 to 0,04601	ns	0,1916

Table A10 Results of 3-way ANOVA with multiple comparison on peak multisensory responses in fed flies

Tukey's multiple comparisons test	Predicted (LS) mean diff,	95,00% CI of diff,	Summary	Adjusted P Value
OL:VinSuc vs. OL:BenzQui	0,002395	-0,04714 to 0,05193	ns	>0,9999
OL:VinSuc vs. OL:VinQui	-0,01254	-0,07837 to 0,05329	ns	>0,9999
OL:VinSuc vs. OL:BenzSuc	-0,0007358	-0,06656 to 0,06509	ns	>0,9999
OL:BenzQui vs. OL:VinQui	-0,01493	-0,08076 to 0,05090	ns	>0,9999
OL:BenzQui vs. OL:BenzSuc	-0,003131	-0,06896 to 0,06270	ns	>0,9999
OL:VinQui vs. OL:BenzSuc	0,01180	-0,03543 to 0,05903	ns	>0,9999
CX:VinSuc vs. CX:BenzQui	0,01587	-0,03366 to 0,06541	ns	>0,9999
CX:VinSuc vs. CX:VinQui	-0,04130	-0,1071 to 0,02453	ns	0,9293
CX:VinSuc vs. CX:BenzSuc	-0,005541	-0,07137 to 0,06029	ns	>0,9999
CX:BenzQui vs. CX:VinQui	-0,05717	-0,1230 to 0,008658	ns	0,2406
CX:BenzQui vs. CX:BenzSuc	-0,02142	-0,08724 to 0,04441	ns	>0,9999
CX:VinQui vs. CX:BenzSuc	0,03576	-0,01148 to 0,08299	ns	0,5669
LX:VinSuc vs. LX:BenzQui	0,009471	-0,04007 to 0,05901	ns	>0,9999
LX:VinSuc vs. LX:VinQui	-0,02974	-0,09557 to 0,03608	ns	0,9999
LX:VinSuc vs. LX:BenzSuc	-0,0008326	-0,06666 to 0,06500	ns	>0,9999

LX:BenZQui vs. LX:VinQui	-0,03922	-0,1050 to 0,02661	ns	0,9652
LX:BenZQui vs. LX:BenZSuc	-0,01030	-0,07613 to 0,05552	ns	>0,9999
LX:VinQui vs. LX:BenZSuc	0,02891	-0,01832 to 0,07614	ns	0,9402
LH:VinSuc vs. LH:BenZQui	0,02439	-0,02515 to 0,07393	ns	0,9985
LH:VinSuc vs. LH:VinQui	-0,08865	-0,1545 to -0,02282	***	0,0001
LH:VinSuc vs. LH:BenZSuc	-0,03647	-0,1023 to 0,02936	ns	0,9892
LH:BenZQui vs. LH:VinQui	-0,1130	-0,1789 to -0,04721	****	<0,0001
LH:BenZQui vs. LH:BenZSuc	-0,06085	-0,1267 to 0,004974	ns	0,1312
LH:VinQui vs. LH:BenZSuc	0,05219	0,004954 to 0,09942	*	0,0108
PENP:VinSuc vs. PENP:BenZQui	0,009778	-0,03976 to 0,05932	ns	>0,9999
PENP:VinSuc vs. PENP:VinQui	-0,03303	-0,09886 to 0,03280	ns	0,9984
PENP:VinSuc vs. PENP:BenZSuc	-0,01352	-0,07935 to 0,05231	ns	>0,9999
PENP:BenZQui vs. PENP:VinQui	-0,04281	-0,1086 to 0,02302	ns	0,8906
PENP:BenZQui vs. PENP:BenZSuc	-0,02330	-0,08913 to 0,04253	ns	>0,9999
PENP:VinQui vs. PENP:BenZSuc	0,01951	-0,02772 to 0,06674	ns	>0,9999
INP:VinSuc vs. INP:BenZQui	0,01244	-0,03710 to 0,06198	ns	>0,9999
INP:VinSuc vs. INP:VinQui	-0,04894	-0,1148 to 0,01689	ns	0,6311
INP:VinSuc vs. INP:BenZSuc	-0,01313	-0,07895 to 0,05270	ns	>0,9999
INP:BenZQui vs. INP:VinQui	-0,06137	-0,1272 to 0,004455	ns	0,1195
INP:BenZQui vs. INP:BenZSuc	-0,02556	-0,09139 to 0,04026	ns	>0,9999
INP:VinQui vs. INP:BenZSuc	0,03581	-0,01142 to 0,08304	ns	0,5630
VMNP:VinSuc vs. VMNP:BenZQui	0,002278	-0,04726 to 0,05182	ns	>0,9999
VMNP:VinSuc vs. VMNP:VinQui	-0,03176	-0,09759 to 0,03407	ns	0,9993
VMNP:VinSuc vs. VMNP:BenZSuc	-0,004941	-0,07077 to 0,06089	ns	>0,9999
VMNP:BenZQui vs. VMNP:VinQui	-0,03404	-0,09987 to 0,03179	ns	0,9970
VMNP:BenZQui vs. VMNP:BenZSuc	-0,007219	-0,07305 to 0,05861	ns	>0,9999
VMNP:VinQui vs. VMNP:BenZSuc	0,02682	-0,02041 to 0,07405	ns	0,9796
MB:VinSuc vs. MB:BenZQui	0,02659	-0,02294 to 0,07613	ns	0,9920
MB:VinSuc vs. MB:VinQui	-0,05343	-0,1193 to 0,01240	ns	0,4003
MB:VinSuc vs. MB:BenZSuc	-0,01350	-0,07933 to 0,05233	ns	>0,9999
MB:BenZQui vs. MB:VinQui	-0,08002	-0,1459 to -0,01420	**	0,0015
MB:BenZQui vs. MB:BenZSuc	-0,04009	-0,1059 to 0,02574	ns	0,9523
MB:VinQui vs. MB:BenZSuc	0,03993	-0,007300 to 0,08716	ns	0,2904
AL:VinSuc vs. AL:BenZQui	0,009980	-0,03956 to 0,05952	ns	>0,9999
AL:VinSuc vs. AL:VinQui	-0,03129	-0,09711 to 0,03454	ns	0,9995

AL:VinSuc vs. AL:BenzSuc	2,999e-005	-0,06580 to 0,06586	ns	>0,9999
AL:BenzQui vs. AL:VinQui	-0,04127	-0,1071 to 0,02456	ns	0,9299
AL:BenzQui vs. AL:BenzSuc	-0,009950	-0,07578 to 0,05588	ns	>0,9999
AL:VinQui vs. AL:BenzSuc	0,03132	-0,01592 to 0,07855	ns	0,8497
SNP:VinSuc vs. SNP:BenzQui	0,03764	-0,01190 to 0,08718	ns	0,5574
SNP:VinSuc vs. SNP:VinQui	-0,06425	-0,1301 to 0,001581	ns	0,0691
SNP:VinSuc vs. SNP:BenzSuc	-0,009137	-0,07497 to 0,05669	ns	>0,9999
SNP:BenzQui vs. SNP:VinQui	-0,1019	-0,1677 to -0,03606	****	<0,0001
SNP:BenzQui vs. SNP:BenzSuc	-0,04678	-0,1126 to 0,01905	ns	0,7379
SNP:VinQui vs. SNP:BenzSuc	0,05511	0,007878 to 0,1023	**	0,0040
VLNP:VinSuc vs. VLNP:BenzQui	0,002398	-0,04714 to 0,05194	ns	>0,9999
VLNP:VinSuc vs. VLNP:VinQui	-0,03136	-0,09719 to 0,03447	ns	0,9995
VLNP:VinSuc vs. VLNP:BenzSuc	-0,01041	-0,07624 to 0,05542	ns	>0,9999
VLNP:BenzQui vs. VLNP:VinQui	-0,03376	-0,09959 to 0,03207	ns	0,9975
VLNP:BenzQui vs. VLNP:BenzSuc	-0,01281	-0,07864 to 0,05302	ns	>0,9999
VLNP:VinQui vs. VLNP:BenzSuc	0,02095	-0,02628 to 0,06818	ns	0,9999
GNG:VinSuc vs. GNG:BenzQui	0,01895	-0,03059 to 0,06849	ns	>0,9999
GNG:VinSuc vs. GNG:VinQui	-0,02015	-0,08598 to 0,04568	ns	>0,9999
GNG:VinSuc vs. GNG:BenzSuc	-0,01631	-0,08214 to 0,04951	ns	>0,9999
GNG:BenzQui vs. GNG:VinQui	-0,03910	-0,1049 to 0,02673	ns	0,9667
GNG:BenzQui vs. GNG:BenzSuc	-0,03527	-0,1011 to 0,03056	ns	0,9941
GNG:VinQui vs. GNG:BenzSuc	0,003835	-0,04340 to 0,05107	ns	>0,9999

Table A11 Results of 3-way ANOVA with multiple comparison on peak multisensory responses in starved flies

Tukey's multiple comparisons test	Mean Diff,	95,00% CI of diff,	Summary	Adjusted P Value
OL:VinSuc vs. OL:BenzQui	0,0009923	-0,04866 to 0,05064	ns	>0,9999
OL:VinSuc vs. OL:VinQui	-0,001428	-0,06725 to 0,06440	ns	>0,9999
OL:VinSuc vs. OL:BenzSuc	0,007966	-0,05786 to 0,07379	ns	>0,9999
OL:BenzQui vs. OL:VinQui	-0,002420	-0,06824 to 0,06340	ns	>0,9999
OL:BenzQui vs. OL:BenzSuc	0,006973	-0,05885 to 0,07280	ns	>0,9999
OL:VinQui vs. OL:BenzSuc	0,009393	-0,04026 to 0,05904	ns	>0,9999
CX:VinSuc vs. CX:BenzQui	0,02797	-0,02168 to 0,07761	ns	0,9816
CX:VinSuc vs. CX:VinQui	-0,001108	-0,06693 to 0,06471	ns	>0,9999
CX:VinSuc vs. CX:BenzSuc	0,03601	-0,02981 to 0,1018	ns	0,9912

CX:BenZQui vs. CX:VinQui	-0,02907	-0,09490 to 0,03675	ns	>0,9999
CX:BenZQui vs. CX:BenZSuc	0,008049	-0,05777 to 0,07387	ns	>0,9999
CX:VinQui vs. CX:BenZSuc	0,03712	-0,01253 to 0,08677	ns	0,5964
LX:VinSuc vs. LX:BenZQui	0,01448	-0,03517 to 0,06412	ns	>0,9999
LX:VinSuc vs. LX:VinQui	-0,005522	-0,07134 to 0,06030	ns	>0,9999
LX:VinSuc vs. LX:BenZSuc	0,03008	-0,03574 to 0,09590	ns	0,9998
LX:BenZQui vs. LX:VinQui	-0,02000	-0,08582 to 0,04583	ns	>0,9999
LX:BenZQui vs. LX:BenZSuc	0,01560	-0,05022 to 0,08143	ns	>0,9999
LX:VinQui vs. LX:BenZSuc	0,03560	-0,01405 to 0,08525	ns	0,6973
LH:VinSuc vs. LH:BenZQui	0,04644	-0,003211 to 0,09609	ns	0,1130
LH:VinSuc vs. LH:VinQui	0,001746	-0,06408 to 0,06757	ns	>0,9999
LH:VinSuc vs. LH:BenZSuc	0,08962	0,02380 to 0,1554	****	<0,0001
LH:BenZQui vs. LH:VinQui	-0,04469	-0,1105 to 0,02113	ns	0,8259
LH:BenZQui vs. LH:BenZSuc	0,04318	-0,02264 to 0,1090	ns	0,8785
LH:VinQui vs. LH:BenZSuc	0,08788	0,03823 to 0,1375	****	<0,0001
PENP:VinSuc vs. PENP:BenZQui	0,02067	-0,02898 to 0,07031	ns	>0,9999
PENP:VinSuc vs. PENP:VinQui	0,0001617	-0,06566 to 0,06598	ns	>0,9999
PENP:VinSuc vs. PENP:BenZSuc	0,01997	-0,04585 to 0,08579	ns	>0,9999
PENP:BenZQui vs. PENP:VinQui	-0,02050	-0,08633 to 0,04532	ns	>0,9999
PENP:BenZQui vs. PENP:BenZSuc	-0,0006954	-0,06652 to 0,06513	ns	>0,9999
PENP:VinQui vs. PENP:BenZSuc	0,01981	-0,02984 to 0,06946	ns	>0,9999
INP:VinSuc vs. INP:BenZQui	0,03089	-0,01875 to 0,08054	ns	0,9252
INP:VinSuc vs. INP:VinQui	0,003761	-0,06206 to 0,06958	ns	>0,9999
INP:VinSuc vs. INP:BenZSuc	0,04845	-0,01737 to 0,1143	ns	0,6547
INP:BenZQui vs. INP:VinQui	-0,02713	-0,09296 to 0,03869	ns	>0,9999
INP:BenZQui vs. INP:BenZSuc	0,01756	-0,04827 to 0,08338	ns	>0,9999
INP:VinQui vs. INP:BenZSuc	0,04469	-0,004959 to 0,09434	ns	0,1681
VMNP:VinSuc vs. VMNP:BenZQui	0,01187	-0,03778 to 0,06152	ns	>0,9999
VMNP:VinSuc vs. VMNP:VinQui	-0,007509	-0,07333 to 0,05831	ns	>0,9999
VMNP:VinSuc vs. VMNP:BenZSuc	0,02281	-0,04301 to 0,08863	ns	>0,9999
VMNP:BenZQui vs. VMNP:VinQui	-0,01938	-0,08520 to 0,04645	ns	>0,9999
VMNP:BenZQui vs. VMNP:BenZSuc	0,01094	-0,05488 to 0,07676	ns	>0,9999
VMNP:VinQui vs. VMNP:BenZSuc	0,03032	-0,01933 to 0,07997	ns	0,9410
MB:VinSuc vs. MB:BenZQui	0,03626	-0,01339 to 0,08591	ns	0,6543
MB:VinSuc vs. MB:VinQui	0,005305	-0,06052 to 0,07113	ns	>0,9999

MB:VinSuc vs. MB:BenzSuc	0,05992	-0,005906 to 0,1257	ns	0,1542
MB:BenzQui vs. MB:VinQui	-0,03096	-0,09678 to 0,03487	ns	0,9996
MB:BenzQui vs. MB:BenzSuc	0,02366	-0,04217 to 0,08948	ns	>0,9999
MB:VinQui vs. MB:BenzSuc	0,05461	0,004963 to 0,1043	*	0,0117
AL:VinSuc vs. AL:BenzQui	0,008856	-0,04079 to 0,05850	ns	>0,9999
AL:VinSuc vs. AL:VinQui	-0,01028	-0,07610 to 0,05554	ns	>0,9999
AL:VinSuc vs. AL:BenzSuc	0,02516	-0,04066 to 0,09099	ns	>0,9999
AL:BenzQui vs. AL:VinQui	-0,01914	-0,08496 to 0,04669	ns	>0,9999
AL:BenzQui vs. AL:BenzSuc	0,01631	-0,04951 to 0,08213	ns	>0,9999
AL:VinQui vs. AL:BenzSuc	0,03544	-0,01421 to 0,08509	ns	0,7074
SNP:VinSuc vs. SNP:BenzQui	0,05879	0,009138 to 0,1084	**	0,0030
SNP:VinSuc vs. SNP:VinQui	0,01282	-0,05300 to 0,07864	ns	>0,9999
SNP:VinSuc vs. SNP:BenzSuc	0,08685	0,02103 to 0,1527	***	0,0002
SNP:BenzQui vs. SNP:VinQui	-0,04597	-0,1118 to 0,01986	ns	0,7734
SNP:BenzQui vs. SNP:BenzSuc	0,02806	-0,03776 to 0,09388	ns	>0,9999
SNP:VinQui vs. SNP:BenzSuc	0,07403	0,02438 to 0,1237	****	<0,0001
VLNP:VinSuc vs. VLNP:BenzQui	0,005346	-0,04430 to 0,05499	ns	>0,9999
VLNP:VinSuc vs. VLNP:VinQui	-0,002124	-0,06795 to 0,06370	ns	>0,9999
VLNP:VinSuc vs. VLNP:BenzSuc	0,01862	-0,04720 to 0,08444	ns	>0,9999
VLNP:BenzQui vs. VLNP:VinQui	-0,007470	-0,07329 to 0,05835	ns	>0,9999
VLNP:BenzQui vs. VLNP:BenzSuc	0,01327	-0,05255 to 0,07910	ns	>0,9999
VLNP:VinQui vs. VLNP:BenzSuc	0,02074	-0,02891 to 0,07039	ns	>0,9999
GNG:VinSuc vs. GNG:BenzQui	0,02937	-0,02028 to 0,07902	ns	0,9617
GNG:VinSuc vs. GNG:VinQui	0,01505	-0,05078 to 0,08087	ns	>0,9999
GNG:VinSuc vs. GNG:BenzSuc	0,01812	-0,04770 to 0,08395	ns	>0,9999
GNG:BenzQui vs. GNG:VinQui	-0,01432	-0,08014 to 0,05150	ns	>0,9999
GNG:BenzQui vs. GNG:BenzSuc	-0,01124	-0,07707 to 0,05458	ns	>0,9999
GNG:VinQui vs. GNG:BenzSuc	0,003075	-0,04657 to 0,05272	ns	>0,9999

Table A12 Functional components and neurons with similar morphology

Component	FlyCircuit	Virtual Fly Brain	Reference
AL	VGlut-F-400797		Chiang et al. 2011
	Gad1-F-500358		Chiang et al. 2011
	Trh-F-500186		Chiang et al. 2011
	5-HT1B-F-500007		Chiang et al. 2011
	and many more...		
		R70E03	(Jenett et al. 2012)
		R51B02	Jenett et al. 2012
		R24C12	Jenett et al. 2012
		R14B06	Jenett et al. 2012
AMMC	Gad1-F-300185		Chiang et al. 2011
	TH-F-000025		Chiang et al. 2011
	VGlut-F-000062		Chiang et al. 2011
		R70G01	Jenett et al. 2012
		R71B08	Jenett et al. 2012
EB	VGlut-F-200478		Chiang et al. 2011
	Gad1-F-000625		Chiang et al. 2011
	5-HT1B-F-500002		Chiang et al. 2011
	Trh-M-200097		Chiang et al. 2011
	and many more...		
		ExR4(ring)_L (FlyEM-HB:1198330641)	Scheffer et al. 2020
		ExR6(ring)_L (FlyEM-HB:1228692168)	Scheffer et al. 2020
		R19G02L	
FB lateral	VGlut-F-300443		Chiang et al. 2011
	5HT1A-F-400022		Chiang et al. 2011
	and many more...		
		vDeltaF_C7 (FlyEM-HB:1102191106)	Scheffer et al. 2020
FB center	Tdc2-F-200060		Chiang et al. 2011
	fru-F-600135		Chiang et al. 2011
	Trh-F-500221		Chiang et al. 2011
	and some more...		
		vDeltaE_C5 (FlyEM-HB:1009051653)	Scheffer et al. 2020
FLA	VGlut-F-500173		Chiang et al. 2011
	VGlut-F-100313		Chiang et al. 2011
	Cha-F-500111		Chiang et al. 2011
	TH-F-000049		Chiang et al. 2011
	TH-M-000037		Chiang et al. 2011
	and some more...		
		R60C08	Jenett et al. 2012
GNG	TH-F-000004		Chiang et al. 2011
	TH-M-200073		Chiang et al. 2011
GNG (paired)	fru-M-300037		Chiang et al. 2011
	VGlut-F-800026		Chiang et al. 2011
	VGlut-F-000195		Chiang et al. 2011
	and some more...		

LH-SIP	Gad1-F-000703		Chiang et al. 2011
	VGlut-F-200319		Chiang et al. 2011
	Gad1-F-700589		Chiang et al. 2011
	Gad1-F-600664		Chiang et al. 2011
		R47G10 LexA	Aso et al. 2014 (1)
LH_PN lateral	Gad1-F-900076		Chiang et al. 2011
	VGlut-F-600764		Chiang et al. 2011
	Gad1-F-800565		Chiang et al. 2011
	Gad1-F-100835		Chiang et al. 2011
LH_PN_medial	Cha-F-700236		Chiang et al. 2011
	Gad1-F-700084		Chiang et al. 2011
	Gad1-F-600106		Chiang et al. 2011
	Gad1-F-500258		Chiang et al. 2011
LH_PN_ventral	Gad1-F-200366		Chiang et al. 2011
	Gad1-F-200322		Chiang et al. 2011
	Gad1-F-000540		Chiang et al. 2011
	and some more...		
alpha Kcs		MB504B	Aso et al. 2014 (2)
		MB065B	Aso et al. 2014 (2)
alpha-beta Kcs	VGlut-F-100045		Chiang et al. 2011
	Trh-F-200069		Chiang et al. 2011
	Trh-M-200129		Chiang et al. 2011
	Trh-M-100006		Chiang et al. 2011
	Trh-M-200082		Chiang et al. 2011
	Cha-F-700169		Chiang et al. 2011
	Trh-F-200003		Chiang et al. 2011
	Trh-F-200078		Chiang et al. 2011
	Trh-F-200087		Chiang et al. 2011
	Trh-M-200086		Chiang et al. 2011
	Trh-M-200105		Chiang et al. 2011
	Trh-M-100000		Chiang et al. 2011
	Trh-M-200110		Chiang et al. 2011
		MB152B	Aso et al. 2014 (2)
		MB008B	Aso et al. 2014 (2)
beta Kcs	Trh-M-200075		Chiang et al. 2011
	VGlut-F-000334		Chiang et al. 2011
		MB188B	Aso et al. 2014 (2)
gamma Kcs		MB009B	Aso et al. 2014 (2)
PN-KC (peduncle)		MB085C	Aso et al. 2014 (2)
		MB262B	Aso et al. 2014 (2)
PN-KC (calyx core)	-	-	-
PN-KC (calyx edge)	-	-	-
PB		R55G08	Jenett et al. 2012
		SS52266	(Wolff and Rubin 2018)
		SS00116	(Davis et al. 2020)
	Cha-F-300305		Chiang et al. 2011

Curriculum vitae

Paul Bandow

Professional experience

01/2020 – today

PhD candidate, Institute for Physiology II, University of Bonn, Prof. Dr. Grunwald Kadow (formerly Professorship for neuronal control and metabolism, TU München, 01/2020 – 01/2022)

- Neurophysiology of smell and taste (*D. melanogaster*)
- Project management, literature research, conducting experiments, statistics
- Collaborative work inside an international, English-speaking team
- Scientific writing, presenting results in front of experts in the field
- Teaching of pre-medical students (lectures, practicals, seminars)
- Planning and coordination of weekly team meetings
- Work with transgenic model organism (BIO S1), molecular genetics
- Wide-field microscopy, in-vivo experiments, Calcium-imaging
- Image processing and data analysis in MATLAB, Python, ImageJ, MS Excel, Prism

10/2016 – 06/2017

Basketball instructor, University Sports Center Munich (ZHS München)

- Conducting exercises and drills, coaching of beginners, refereeing games

10/2014- 03/2016

Shelf service, for CMC, at Edeka, Allershausen

- Stocking up shelves after business hours, sorting items for expiry date

Education

10/2020 – today

Graduate student, Graduate School of Systemic Neuroscience, LMU Munich

10/2016 – 11/2019

M. Sc. Biology, TU Munich, Grade 1,3 (very good)

10/2013 – 04/2017

B. Sc. Biology, TU Munich, Grade 1,9 (good)

10/2012 – 09/2013

Studium Naturale, TU Munich (Orientation study for life sciences)

07/2003 – 06/2012

High school, Ernst-Ludwig Schule, Bad Nauheim, Abitur 2,1 (good)

Scholarship

05/2015 – 05/2018

TUM Junge Akademie, Active member, group: Food Security

- Self-organized project work in a small team
- Conducting polls, interviewing experts, writing a report, presenting results

International Experience

07/2017 – 11/2017

Exchange semester (TUMexchange), University of Queensland, Brisbane, Australia

- Participating in lectures, seminars and field trips
- Writing reports and protocols, taking final exams

Internships and lab experience

09/2018

Lab practical Chair for livestock biotechnology, TU Munich

- Cell culture, mammalian cells, sterile bench work, cloning

04/2017- 05/2017

Lab internship Chair of Zoology, TU Munich

- Creating topographic maps of retinal ganglion cells (*Gallus spec.*)

- Immunohistochemistry, confocal microscopy

09/2016

Lab practical Chair of Virology, TU Munich

- RT-PCR, FACS, gel electrophoresis, cloning

10/2015- 11/2015

Lab internship Chair of Genetics, TU Munich

- Analysis of secondary metabolites (*A. thaliana*)
- HPLC, PCR, gel electrophoresis

Publications as Coauthor

09/2022

Boehm et al, A dopamine-gated learning circuit underpins reproductive state-dependent odor preference in *Drosophila* females, eLife

04/2021

Woller et al, Preparing Adult *Drosophila melanogaster* for Whole Brain Imaging during Behavior and Stimuli Responses, JOVE

Computer skills

MATLAB, Beginner

Python, Basics

ImageJ, Advanced

Adobe Illustrator, Basics

MS Office, Advanced

GraphPad Prism, Advanced

Language skills

German, Native

English, fluent, C1 (Council of Europe Level)

French, Basics

List of publications

Preparing Adult *Drosophila melanogaster* for Whole Brain Imaging during Behavior and Stimuli Responses

Alexandra Woller, Paul Bandow, Sophie Aimon, Ilona C. Grunwald Kadow

April 27 2021 J. Vis. Exp. (170), e61876, doi:10.3791/61876

A dopamine-gated learning circuit underpins reproductive state-dependent odor preference in *Drosophila* females

Ariane C Boehm, Anja B Friedrich, Sydney Hunt, Paul Bandow, KP Siju, Jean Francois De Backer, Julia Claussen, Marie Helen Link, Thomas F Hofmann, Corinna Dawid, Ilona C Grunwald Kadow

Sep 21, 2022 eLife, doi: 10.7554/eLife.77643

Declaration of author contributions

I designed and carried out all experiments for this dissertation.

Sophie Aimon designed and built the LFM imaging setup. I modified it by adding the odor and taste delivery systems.

Fly preparation for imaging was carried out by me, as described in the publication by Woller et al. (2021), where I contributed as a co-author.

The first steps of image data processing (i.e. deconvolution, movement correction, calculating dF/F , spatial PCA/ICA and template registration) were performed with code written by Sophie Aimon. All other steps of data processing and analysis were carried out by me, either with code written in MATLAB, MS Excel or GraphPad Prism.

Subhadarshini Parhi contributed a python-based GUI that I used to sort the spatial components.

Author _____

Supervisor _____